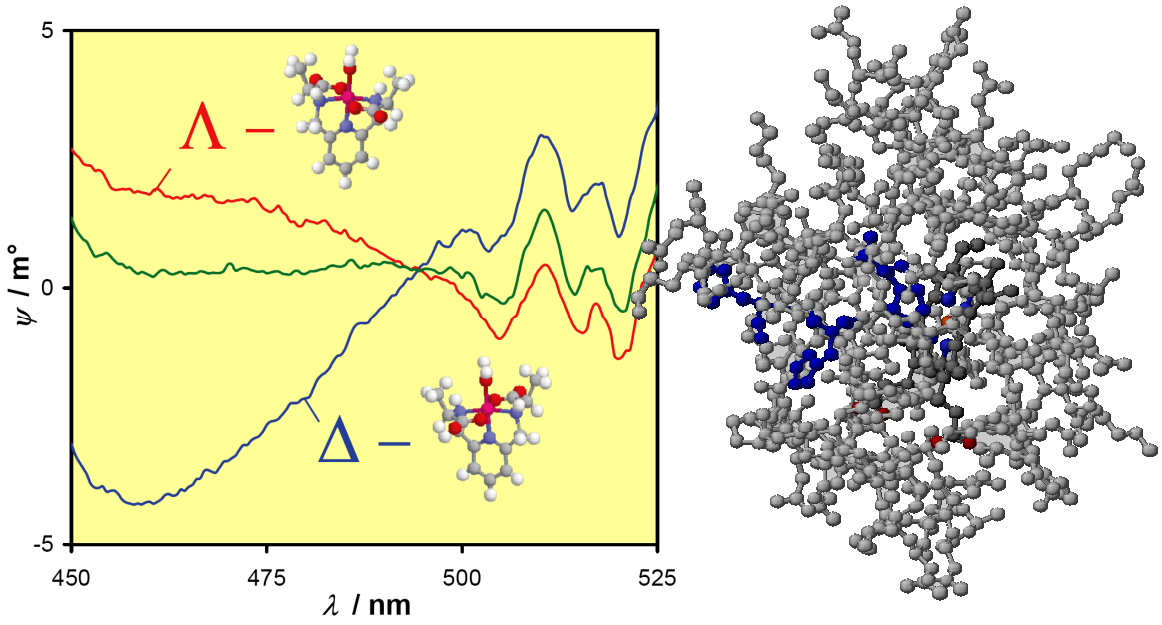

Optically Active Metal Complexes as Probes for Enantioselective Electron-Transfer Reactions Involving Cytochrome *c*

Thèse présentée à la Faculté des Sciences

Institut de Chimie

Université de Neuchâtel

Pour l'obtention du grade de Docteur ès Sciences

Par

Ulrich Scholten

Acceptée sur proposition du jury :

Prof. Klaus Bernauer, directeur de thèse

Prof. Robert Deschenaux, rapporteur

Prof. Peter Belser (Université de Fribourg), rapporteur

Soutenue le 28 janvier 2005

Université de Neuchâtel unine

Optically Active Metal Complexes as Probes for Enantioselective Electron-Transfer Reactions Involving Cytochrome *c*

Thèse présentée à la Faculté des Sciences

Institut de Chimie

Université de Neuchâtel

Pour l'obtention du grade de Docteur ès Sciences

Par

Ulrich Scholten

Acceptée sur proposition du jury :

Prof. Klaus Bernauer, directeur de thèse

Prof. Robert Deschenaux, rapporteur

Prof. Peter Belser (Université de Fribourg), rapporteur

Soutenue le 28 janvier 2005

This thesis is also available as electronic document on the website of the Université de Neuchâtel: www.unine.ch

Printed in Switzerland by / Imprimé en Suisse par

Imprimerie Saint Paul, Fribourg

"You are worthy, our Lord and God, to receive glory and honour and power, for you created all things, and by your will they were created and have their being."

The Bible (NIV), Revelation 4: 11

Im Andenken an Herrn Dr. Werner Seelentag, meinen Chemielehrer am Dietrich-Bonhoeffer-Gymnasium in Bergisch Gladbach, der mit seiner begeisternden Art womöglich den Weg zu dieser Arbeit gebahnt hat.

Université de Neuchâtel

IMPRIMATUR POUR LA THESE

Optically Active Metal Complexes as Probes for Enantioselective Electron-Transfer Reactions Involving Cytochrome *c*

Ulrich SCHOLTEN

UNIVERSITE DE NEUCHATEL

FACULTE DES SCIENCES

La Faculté des sciences de l'Université de Neuchâtel,
sur le rapport des membres du jury

MM. K. Bernauer (directeur de thèse),
R. Deschenaux
et P. Belser (Fribourg)

autorise l'impression de la présente thèse.

Neuchâtel, le 22 février 2006

Le doyen :

J.-P. Derendinger

Faculté des Sciences
■ Rue Emile-Argand 11 ■ CP 158 ■ CH-2009 Neuchâtel
■ Téléphone : +41 32 718 21 00 ■ Fax : +41 32 718 21 03 ■ E-mail : secretariat.sciences@unine.ch ■ www.unine.ch

RÉSUMÉ (FRENCH SUMMARY)

English summary: see chapter 6.1 (p. 136).
Deutsche Zusammenfassung: siehe Kapitel 6.3 (p. 138).
Riassunto in italiano: vedi capitolo 6.4 (p. 140).

Mots clé en français : cytochrome *c*, complexes de cobalt(II), complexes de chrome(II), énantiosélectivité, cinétique, dichroïsme circulaire.

Keywords in English: cytochrome *c*, cobalt(II) complexes, chromium(II) complexes, enantioselectivity, kinetics, circular dichroism.

Le but de ce travail est d'étudier quelques complexes de cobalt(III) et chrome (III) par rapport à leurs structures et leurs propriétés d'oxydoréduction ainsi que l'emploi de composés correspondants de cobalt(II) et de chrome(II) comme sondes chirales dans des réactions de transfert d'électrons avec le cytochrome *c*.

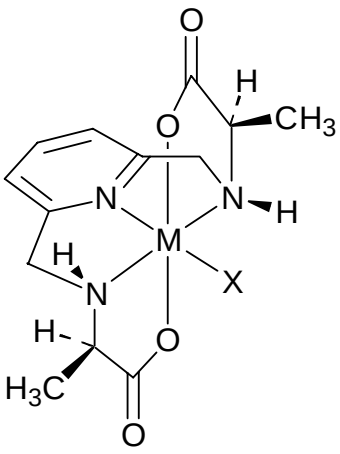

Δ-[M((*R*,*R*)-alamp)X]

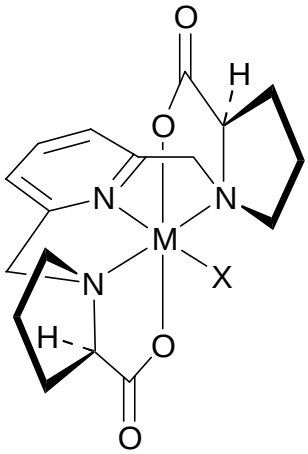

Δ-[M((*R*,*R*)-promp)X]

[Co^{II}(alamp)H_2O] et [Co^{II}(promp)H_2O] ont été employés dans la réduction du ferricytochrome *c*. Les constantes de vitesse sont de trois à quatre ordres de grandeur inférieures à celles des réductions avec les complexes analogues de fer(II), ce qui est principalement dû à des entropies de réaction plus négatives. Les composés correspondants de cobalt(III) des deux énantiomères du [Co^{II}(alamp)] sont partiellement attachés à la protéine pendant le transfert d'électrons, ce qui montre que ce dernier a suivi, au moins en partie, un mécanisme de sphère interne, l'imidazole de His 26 ou His 33 étant utilisé comme ligand pontant. Aucune fixation

covalente de l'entité $[Co^{III}(promp)]$ n'a été observée dans les conditions de réaction choisies. Alors que la stéréosélectivité de la réaction globale est assez faible pour les deux composés, $[Co^{II}(alamp)H_2O]$ et $[Co^{II}(promp)H_2O]$, elle est – avec un rapport k_{RR}/k_{SS} de 2.9 pour $[Co^{II}(alamp)H_2O]$ – relativement élevée pour la partie de la réaction qui s'est déroulée selon un mécanisme de sphère interne. Comme la stéréosélectivité globale résulte de celles des deux parties, sphère interne et sphère externe, les deux mécanismes semblent présenter des stéréosélectivités significatives mais opposées.

Le nouveau complexe $[Cr^{III}(S,S\text{-promp})H_2O]^+$ montre une activité électrochimique à un potentiel inférieur à 1.0 V vs. SHE à pH 7, très probablement dû à une décomposition catalytique de l'eau. La brève existence de l'espèce de chrome(II) correspondante a été démontrée par un échange de ligand consécutif à un transfert d'électrons. Dans la réduction du ferricytochrome *c* par le zinc, le $[Cr^{III}(promp)H_2O]^+$ déploie une activité catalytique remarquable par le biais d'un intermédiaire de chrome(II) qui est formé à la surface métallique. Toutefois, aucune espèce de chrome(III) ne semble être fixée à la protéine conjointement au transfert d'électrons.

Le nouveau complexe $[Co^{III}(S,S\text{-b3amp})H_2O]^+$ contient deux cycles de chélation d'aminocarboxylate à six atomes. L'existence d'au moins trois diastéréoisomères, dont deux symétriques et un non symétrique, et l'équilibre d'isomérisation en milieu basique entre deux parmi eux ont été montrés par des analyses spectrophotométriques et spectropolarimétriques. A cause de l'existence de cet équilibre d'isomérisation, nous pensons que les complexes avec le nouveau ligand b3amp ne conviennent pas à l'analyse des interactions stéréochimiques lors des réactions de transfert d'électrons. Pour cette raison-là, la partie du projet dans laquelle ces types de complexes auraient été utilisés pour la reconnaissance chirale dans les réactions de transfert d'électrons a été abandonnée.

La combinaison de la spectrophotométrie et du dichroïsme circulaire s'est avérée une nouvelle fois comme un outil performant et essentiel pour l'étude des structures de complexes optiquement actifs en solution ainsi que de la cinétique et des mécanismes réactionnels.

TABLE OF CONTENTS / TABLE DES MATIÈRES

CHAPTER 3: REDUCTION OF CYTOCHROME *C* BY OPTICALLY ACTIVE COBALT(II) COMPLEXES

CHAPTER 4: CYTOCHROME *C* REDUCTION CATALYZED BY AN OPTICALLY ACTIVE CHROMIUM(II) COMPLEX

CHAPTER 5: STRUCTURE AND ISOMERISATION OF COBALT(III) COMPLEXES WITH A NEW BIS(β-AMINOCARBOXYLATE)PYRIDINE LIGAND

CHAPTER 6: SUMMARIES

CHAPTER 7: APPENDICES

REMERCIEMENTS (ACKNOWLEDGEMENTS)

Nombreuses sont les personnes qui ont contribué à l'aboutissement de ma thèse. Je leur exprime ma vive reconnaissance :

Ma mère m'a permis d'entreprendre des études de chimie par son soutien financier et moral.

Le professeur Klaus Bernauer, mon directeur de thèse, a parfaitement encadré ce travail. D'une part, il m'a accordé sa confiance et une grande liberté dans l'organisation de mon travail de recherche et d'enseignement. D'autre part, il a toujours été disponible pour me faire bénéficier de ses grandes compétences dans la théorie et la pratique. Ce soutien précieux, l'attitude positive et les nombreux encouragements de mon "Doktorvater" ont été déterminants dans l'achèvement de mon travail de laboratoire et de rédaction. Son dévouement dans l'enseignement, sa modestie et ses qualités humaines extraordinaires me restent un exemple brillant.

Les professeurs Robert Deschenaux et Peter Belser ont mis leur temps et leurs connaissances à ma disposition en tant qu'experts de mon jury de thèse. Leurs commentaires perspicaces et leurs critiques constructives ont amélioré la qualité de mon manuscrit.

La docteure Deirdre Hügi-Cleary a relu mon manuscrit et apporté des améliorations au texte anglais. Le professeur Raffaele Tabacchi a corrigé le résumé en italien.

Avec mes collègues (cités dans l'ordre chronologique), les docteurs Luca Verardo, Charly Nusbaumer, Fabiola Gilet Marechal, Claudia Kressl, Simona Ghizdavu Pellascio, Nathalie Guicher, Michel Pfenniger, Christophe Vichard, Michel Meyer, Fuchun Zhu, Amel Cabort et Rathinam Viswanathan, j'ai fait un bout de chemin dans le groupe de recherche du professeur Bernauer. L'entraide, la collaboration, le partage, quelques activités communes hors de l'université et l'apprentissage de la délicate chimie des relations humaines m'ont laissé de nombreux souvenirs. Je mentionne également le bon accueil que les collaborateurs du professeur Ward m'ont réservé.

Plusieurs étudiant(e)s de l'Université de Neuchâtel et de l'Ecole d'Ingénieurs et d'Architectes de Fribourg ont travaillé sur des sujets de ma thèse ou à la suite de celle-ci : Alejandro Castillejo Merchàn et Céline Diserens (travaux de diplôme); Thierry Vauthier (travail de certificat); Alexandre Vienne (travail de semestre); Dr Dilovan Çati, Dr Gilles Gasser, Luc-Alexis Leuthold, Dr Roger Mafua, Daniel Berdat, Virginie Plumez, Carine Houriet, Julie Lenoble, Ludwig Muster, Nicolas Charbonnet, Gaël Pitarella et Victoria Zampa (travaux pratiques avancés).

Pendant leur apprentissage de laborantin(e), Gaël Millet, Carlos Tardon, Tiffany Monnier et Valérie Mauron et, *last but not least*, Sabine Unternährer ont accompli avec professionnalisme un volume considérable de travail pratique pour moi.

D'autres professeurs de l'Université de Neuchâtel m'ont également soutenu de diverses manières : Le professeur Georg Süss-Fink m'a fait cadeau de chlorure de ruthénium et m'a accueilli dans ses laboratoires pendant quelques semaines pour pouvoir effectuer des synthèses à l'aide de la technique de *Schlenk*. Les professeurs Helen Stoeckli-Evans et Thomas Ward ont mis à ma disposition une place dans leurs laboratoires après la retraite du professeur Bernauer. Le professeur Peter Schürmann m'a offert quelques échantillons de ferrédoxine.

Le docteur Bernhard Pellascio de l'Université de Berne ainsi que les docteurs Guy-Marie Dubin, Christine Poliart, Camille Perret, Armelle Michel et Nicolas Mottier de l'Université de Neuchâtel ont établi les spectres de masse de mes composés. Heinz Bursian a enregistré les spectres de résonance magnétique nucléaire à haute fréquence. La professeure Helen Stoeckli-Evans ainsi que les docteures Antonia Neels, Ana Tesouro Vallina et Jessica Pacifico ont assuré le service de radiocristallographie. Inge Müller nous a instruits dans l'établissement de spectres ORD à l'Université de Fribourg. Le professeur Jean-Nicolas Aebischer nous a permis d'enregistrer des cyclovoltammogrammes sur l'instrument de l'Ecole d'Ingénieurs et d'Architectes de Fribourg.

Radoslav Sobota s'est énormément engagé dans la résolution de problèmes informatiques. Les docteurs Matthieu Fauré, Emmanuel Couché, Yann Berger et Jérôme Collot m'ont fait bénéficier de leurs compétences dans des problèmes de chimie spécifiques à leur domaine.

François Bettinelli, Maurice Binggeli et Claire Rosset ont assuré l'approvisionnement en produits chimiques au magasin et se sont toujours montrés très serviables.

Philippe Stauffer, Jean-Pierre Perret-Gentil et André Floreano ont fait tous leurs efforts pour que l'Institut de Chimie à Neuchâtel reste un endroit propre, soigné et accueillant.

L'achèvement d'une thèse de doctorat demande une grande part de persévérance. Mes frères et sœurs en Christ de l'église de Cormondrèche m'ont encouragé, encadré et réconforté dans les moments difficiles. Leur hospitalité sincère et chaleureuse a embelli mes années d'études.

Merci à vous tous!

ABBREVIATIONS AND SYMBOLS

γ	mass concentration in g·(100 mL)$^{-1}$
δ	chemical shift (NMR), bending vibration (IR)
ρ	rocking vibration
ν	stretching (valence vibration)
$\bar{\nu}$	wavenumber (IR)
$\varepsilon_{(max)}$	maximum molar extinction coefficient
$\Delta\varepsilon_{(max)}$	(maximum) molar circular dichroic absorption coefficient (= ε_L - ε_R)
$\lambda_{(max)}$	(maximum) absorption wavelength
ψ	ionic force in mol·L^{-1}
ψ	ellipticity
σ	surface
θ	temperature in °C
ϑ	bond angle
$[\theta]$	molar ellipticity
#	activation (in $\Delta^{\#}G$, $\Delta^{\#}H$ and $\Delta^{\#}S$)
A	absorption
A_L - A_R	absorption difference between left- and right hand circular polarized light
Ac	acetyl
AcOEt	acetic acid, ethyl ester (ethyl acetate)
AcOH	acetic acid
arom.	aromatic
as	asymmetric
br	broad
buim	butylimidazole
coal.	coalescing
CD	circular dichroism
c	amount concentration in mol·L^{-1}
conc.	concentrated
COSY	homonuclear correlation spectroscopy (^{1}H-^{1}H)
CPK	Molecular models according to Corey, Pauling and Kutin
CV	cyclovoltammetry
cyt *c*	cytochrome *c*
d	day(s)
d	doublet / bond length in pm / optical path length in dm
dec.	decomposition

DMSO	dimethyl sulphoxide (solvent)
dmso	dimethyl sulphoxide (coordinated ligand)
DEPT	distortionless enhancement by polarisation transfer (135° experiment)
E_{pa} / E_{pc}	anodic / cathodic peak potential
EA	elemental analysis
e.e.	enantiomeric excess
EI	electron ionisation
ESI	electron spray ionisation
Et	ethyl
EtOH	ethanol
GC	gas chromatography
h	hour(s)
HETCOR	heteronuclear correlation spectroscopy (^{13}C-^{1}H)
His	histidine
i_{pa} / i_{pc}	anodic / cathodic peak current
IR	infrared spectroscopy
^{2}J, ^{3}J, ^{4}J	geminal, vicinal, allylic coupling constant
l	optical path length in cm
Leu	leucine
m	multiplet (NMR), medium (IR)
M.p.	melting-point
Me	methyl
MeOH	methanol
M, M^+, M^-	molecular peak
M_r	relative molar mass (versus the twelfth of the mass of one mole of ^{12}C atoms)
MS	mass spectrometry
NIV	New International Version®, © 1973-1984 by International Bible Society
NMR	nuclear magnetic resonance spectroscopy
n	refractive index
neg.	negative
ORD	optical rotary dispersion
phen	1,10-phenanthroline
pos.	positive
q	quadruplet
quint.	quintuplet
r.t.	room temperature, (20±5)°C
R_f	retention factor
s	singlet (NMR), strong (IR)
sext.	sextuplet
sh	shoulder
sl.	slightly

SR	short range
SHE	standard hydrogen electrode
sym	symmetric
t	triplet
TLC	thin-layer chromatography
TMS	tetramethylsilane
Tris	tris(hydroxymethyl)aminomethane
U(eq)	equivalent isotropic displacement parameter
UV-VIS	spectrophotometry in the ultraviolet and visible domain
vs	very strong
vw	very weak
w	weak

CHAPTER 1:
INTRODUCTION

1.1 Investigation of electron-transfer reactions in biological systems

The complexity of biological systems has stimulated the curiosity of the scientific community for a long time. Whereas simple chemical equilibria could be analyzed by appropriate physical methods, biological systems were almost considered as a black box of which only the static composition, the entry and the exit flow could be studied. Since the 20th century, researchers sought to prepare model compounds to study and even to imitate biological activity.

The numerous transport chains in metabolism represent an important example. They are based on coordinated transport and transfer phenomena of molecules, ions and electrons. Electron-transfer processes often entail long pathways. The transfers generally take place between metalloproteins or even protein complexes. Fig. 1-1 shows the *X*-ray structure of a model compound prepared by Pelletier and Kraut [1], an artificial protein complex between cytochrome *c*, a haem-protein located in the respiratory chain, and cytochrome *c* peroxidase, an enzyme containing two haem-proteins that accepts two electrons from two ferricytochrome *c* molecules during the catalytic reduction of alkyl hydroperoxides by ferrocytochrome *c*. In order to facilitate the analysis of such intricate electron transfers, it is useful to replace a donor or acceptor protein by small model compounds, e.g. redox active transition metal complexes of which the structural, spectral and electrochemical properties are known. As proteins are polymers of amino-acids that exhibit definite chirality and provide chirality to the protein surface, the use of optically active model complexes may offer additional means to study the nature of the interaction and the reactivity of the protein with its neighbouring partners.

Analyses of the system can be performed by NMR spectroscopy if the complex exhibits no or only weak paramagnetism as well as by optical methods if it absorbs in a convenient spectral range. Circular dichroism is a very powerful tool to investigate selectively the chiral components of the system.

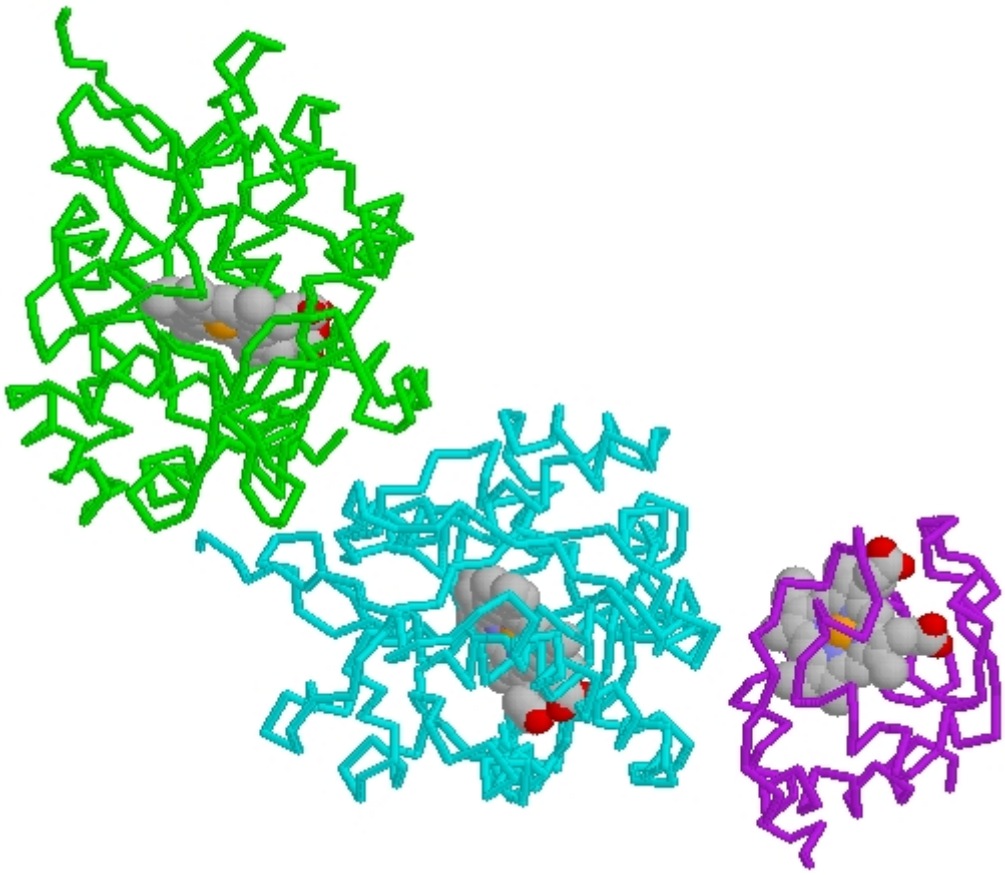

Fig. 1-1. *Crystal structure of an artificially prepared complex between two electron transfer proteins: cytochrome c peroxidase from yeast (left and central unit) and horse heart cytochrome c.* Resolution 280 pm. [1], image generated by [2].

Horse heart cytochrome *c* has a reduction potential of +260 mV at pH 7 [3] and is therefore accessible to reduction by a wide range of metal complexes in aqueous solution, for instance Fe^{II} species [4]. Covalent binding after the electron transfer can occur during reduction by metals that are inert at the oxidized state, such as the redox couples Co^{III}/Co^{II}.

Plant ferredoxins, a class of proteins located in photosystem I, contain a [2Fe2S] cluster as redox-active part and have a very low reduction potential near -400 mV at pH 8 [5]. They have been largely studied in electron-transfer reactions involving transition metal complexes [6]. In this case, the Cr^{III}/Cr^{II} couple would be a suitable candidate for a reductive binding to the metalloprotein and the Ru^{III}/Ru^{II} couple for an oxidative binding.

Chiral metal complexes can be used in electron-transfer reactions to identify chiral recognition on the protein surface and the binding-sites for inner-sphere electron-transfer reactions. The prerequisite in reactions with labile, redox active metal centres is the formation of a sin-

gle isomer of the complex showing predetermined chirality. Most of the metal complexes with the ligands presented in §1.2 meet this requirement.

1.2 Coordination of transition metals by chiral pentadentate ligands with C_2 symmetry

In octahedral complexes linear, pentadentate ligands can assume four different coordination geometries, as represented in Fig. 1-2. If the ligand is achiral three of them, the A, B and C types, are chiral and inert metal complexes can be separated into their enantiomers, whereas the D type isomer has a symmetry plane and is therefore achiral. The structures represented in Fig. 1-2 have an absolute configuration $\Delta_{(1,3)}\Delta_{(2,4)} = \Delta$ for A and $\Lambda_{(1,3)}\Delta_{(1,4)}\Lambda_{(2,4)} = \Lambda$ for C according to the ring pairing method [7]. No definite chirality can be attributed to B by this method because the only two chiral pairs with opposite chirality are present: $\Lambda_{(1,4)}\Delta_{(1,3)}$. Substitution, which can take place either on coordinating nitrogen atoms or on the carbon atoms of the backbone, introduces additional chiral centres, and therefore increases considerably the number of possible isomers. Stability differences between the isomers of coordination compounds have been extensively discussed e.g. by Corey [8a] and Bernauer [8b]. Despite the smaller angle formed by the metal ion, the conformational analysis of five- and six-membered chelate rings shows some analogy with that of the corresponding carbocyclic systems. The energy differences between axial and equatorial orientation of the substituents increase with the puckering of the ring and the size of the substituents.

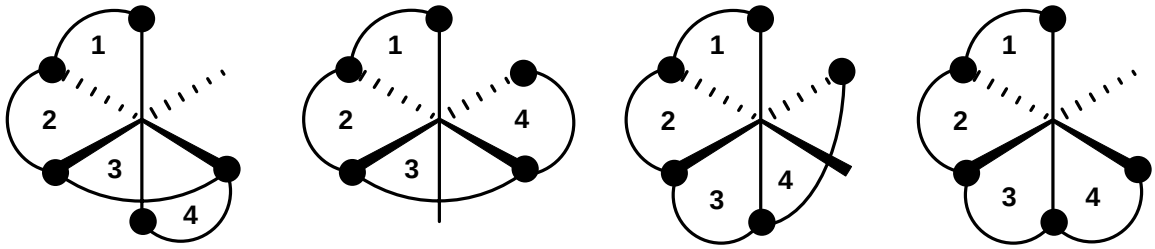

(a) (b) (c) (d)

Fig. 1-2. *Coordination modes of linear, pentadentate ligands to octahedral metal centres:* a) fac-mer-fac *("A type");* b) fac-mer-mer *("B type");* c) fac-fac-mer *("C type";*. d) fac-fac-fac *("D type")*

In complexes with ligands of the basic framework **I** and **II** presented on Table 1-1, the number of possible isomers is reduced to compounds with the geometries of type A and B. Indeed, only the meridional arrangement of the inner five-membered rings 2 and 3 is possible because of the common pyridine unit. Structures of complexes with various substituted ligands of type **I** have been studied by ^{1}H-NMR and CD measurements as well as by X-ray structural determinations.

Table 1-1. *Substitution Pattern of different type **I** and **II** ligands*

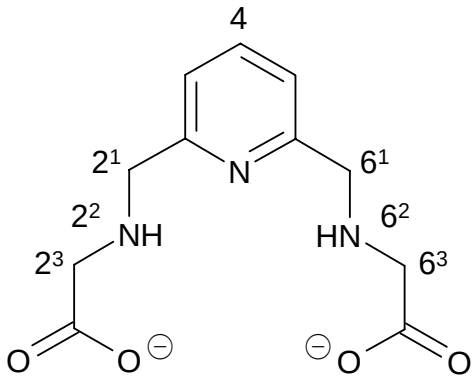

(**I**)

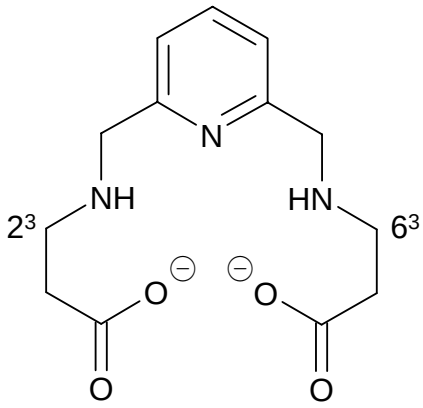

(**II**)

Ligand name	Framework type	Substituted atoms		
		$C(2^1,6^1)$	$N(2^2,6^2)$	$C(2^3,6^3)$
bamap	**I**	$-CH_3$	$-CH_3$	
alamp	**I**			$-CH_3$
sarmp	**I**		$-CH_3$	
promp	**I**		$-CH_2CH_2CH-$	
malmp	**I**		$-CH_3$	$-CH_3$
bapap	**I**	$-CH_2CH_2CH-$		
b3amp	**II**			$-CH_3$

As the two cobalt(III) complexes represented on Scheme 1-1, all the complexes analysed so far exhibit the coordination geometry of type A in Table 1-1, except the solid [Cu((*S*,*S*)-alamp] [9]. In this case, the unsymmetrical arrangement of type B is found forming a linear coordination polymer with one bridging carboxylate group completing the octahedral coordination sphere of the metal ions. In solution the complex is assumed to be of the same structure as the Co^{III} analogues.

In all compounds exhibiting the C_2 symmetric geometry (A) the *fac-mer-fac* coordination mode allows only one arrangement of the two nitrogen atoms, the chirality of which is determined by the absolute configuration of the complex, (*R*,*R*) in the complex with *Λ*-, respectively (*S*,*S*) in the complex with Δ configuration. This has been confirmed by the partial resolution of $[Co(sarmp)(H_2O)]^+$, the complex formed with the ligand substituted only at the aliphatic nitrogen atoms [10]. The configuration of $[Co(sarmp)H_2O]^+$ is quite stable, slow racemisation which implies consecutive inversion at the two nitrogen and at the cobalt centre occurs under slightly basic conditions (half life 800 min at pH = 9 at 40°C) [11]. In carbocyclic systems, the ring substituents generally prefer the equatorial position to the axial one [8]. However, five-membered chelate rings of aminocarboxylate groups are almost planar and axial and equatorial positions are energetically only slightly different. On the other hand, if the present ligand core bears respectively one methyl substituent on the *α*-carbon (as for example in alamp), each enantiomer of the ligand (with definite and identical chirality of the two asymmetric carbon atoms) can theoretically form two C_2 symmetric diastereoisomeric metal complexes locating the substituents of the α-carbon in an exo- or endo position - except the complexes with the promp ligand (see design on the right). Model considerations indicate that the steric interaction between the methylene protons next to the pyridine ring and the methyl group destabilises the *endo* position (see Scheme 1-1). Indeed, the formation of an *endo* diastereoisomer could never be observed in the synthesis of the inert cobalt(III) complexes with ligands of this type and we therefore believe that the same structure is strongly preferred in the formation of labile complexes. That means that the absolute configuration of the *α*-carbon predetermines the absolute configuration of the metal complexes.

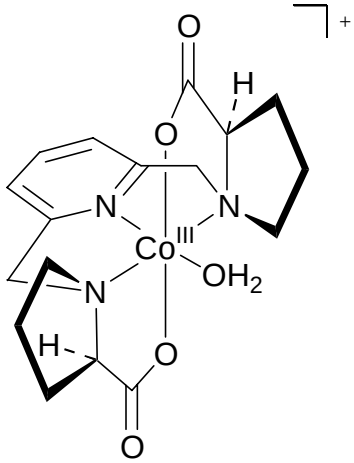

Δ-$[Co^{III}((R,R)\text{-promp})H_2O]^+$

Scheme 1-1. *Equilibrium between the two diastereoisomers of the C_2-symmetric [Co^{III}(S,S)-alampH2O]$^+$ complex.* The isomer with the methyl groups in *exo* position is strongly favoured because of two unfavourable steric interactions in the *endo* form (arrow).

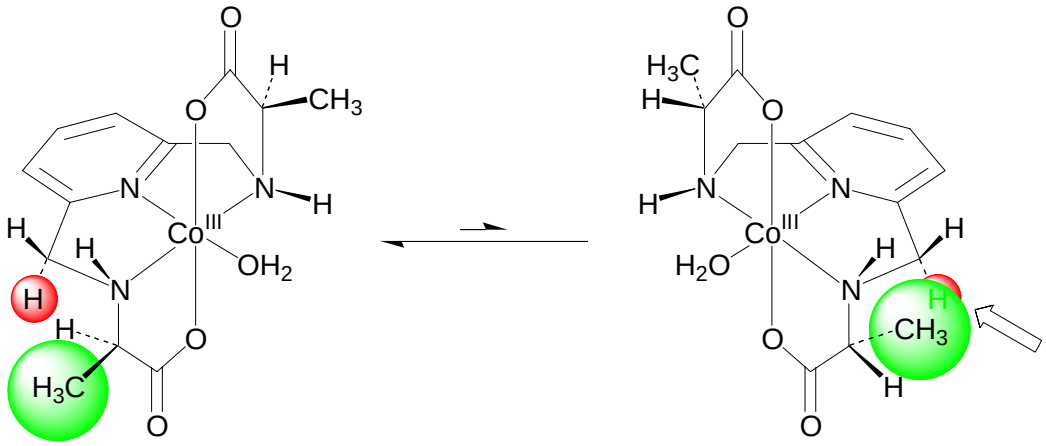

Δ-*exo*-[Co^{III}((*R*$_C$,*R*$_C$)(*S*$_N$,*S*$_N$)-alamp)H$_2$O]$^+$ Λ-*endo*-[Co^{III}((*R*$_C$,*R*$_C$)(*R*$_N$,*R*$_N$)-alamp)H$_2$O]$^+$

For bamap (the ligand with both, the carbon atoms next to the pyridine ring and the aliphatic nitrogen atoms methylated the two diasteroisomers) the racemic in which both asymmetric carbon atoms have the same absolute configuration and the meso compound in which they have opposite absolute configuration, were obtained [12]. Whereas for the racemic ligand the more favourable C_2 symmetric coordination geometry allows both methyl groups to be located in the energetically favourable staggered position, the meso compound can occur in two relatively unfavourable structures: the unsymmetrical coordination geometry (B) with both pairs of methyl groups in a staggered position or the C_2-symmetric structure with one of the two pairs of methyl groups in a quasi-eclipsed position. X-ray crystal and NMR solution analyses show that the second possibility is more favourable.

The situation is somewhat different in malmp [10] where the two neighbouring methyl groups are located at the nitrogen atoms and in the α-position of the aminocarboxylate moiety. In this case the two possibilities, both with the C_2-symmetry, are of almost equal stability. The complex with C-methyl group in the *endo* position, interacting with the methylene group near the pyridine group, and the complex with the two methyl groups in the eclipsed position (*exo)* in equilibrium are formed in an *endo*:*exo* ratio of about 2:1 at room temperature. The consequence of this situation is that, unlike the other members of this ligand family, [Co(malmp)L]$^+$ can undergo epimerisation in basic medium (all of the methyl groups pass

from the *endo* to the *exo* position and vice versa) because the change of the absolute configuration at the asymmetric carbon atom causes only small energy changes due to steric interactions of the α-C methyl groups with other parts of the complex [13].

In addition to the examples listed in Table 1-1, the ligands promp and malmp have also been prepared with a substitution by a methoxy- or a chloro-group on position 4 of the pyridine ring [13][14].

Complexes with several substituted ligands of type **I** have been thoroughly studied for their structural and reactivity behaviour. The redox properties and the stereoselectivity in electron transfer reactions have been investigated in order to unravel reaction mechanisms, mostly for cobalt and iron complexes [15] and the compounds have been used as chiral probes in electron transfer involving metalloproteins (see chapter 3 and references therein). On the other hand, ligands exhibiting framework **II** have not yet been described in the literature.

1.3 Purpose and outline of this thesis

The aim of the present work is to investigate optically active complexes of cobalt, chromium and ruthenium with some of ligands presented in §1.2 as probes for chiral recognition in electron-transfer reactions involving metalloproteins.

Chapter 2 describes all synthetic proceedings.

The kinetics, stereoselectivity and the potential covalent binding in the reduction of ferricytochrome *c* by both enantiomers of the complexes $[Co^{II}(alamp)H_2O]$ and $[Co^{II}(promp)H_2O]$ at various temperatures and pH 7.5 and 9.0 are presented in chapter 3.

Chapter 4 deals with the $[Cr^{III}(S,S\text{-promp})H_2O]^+$ ion and its catalytic effect in the reduction of ferricytochrome *c*.

In chapter 5, the equilibrium between three isomers of a cobalt(III) complex with the type **II** ligand $b3amp^{2-}$ is unravelled.

1.4 References

[1] H. Pelletier, J. Kraut, *Science* **1992**, *258*, 1748.

[2] Eric Martz, 'Protein Explorer 1.982, Program for the visualization of .pdb data files, University of Massachusetts at Amherst, United States of America, 2002.

[3] G.R. Moore, C.G.S. Eley, G. Williams, in 'Advances in Inorganic and Bioinorganic Mechanisms', Academic Press, London, 1984, Vol. 3, p. 1.

[4] a) K. Bernauer, P. Jauslin, *Chimia* **1993**, *47*, 218 and references therein; b) P. Jauslin, Ph.D. Thesis, Université de Neuchâtel, 1994.

[5] R. Cammack, K.K. Rao, C.P.Bargeron, K.G. Hutson, P.W. Andrew, L.J. Rogers, *Biochem J.* **1977**, *168*, 205.

[6] K. Bernauer, M. Monzione, P. Schürmann, V. Viette, *Helv. Chim. Acta* **1990**, *73*, 346 and references therein.

[7] *Inorg. Chem.* **1970**, *1*, 1.

[8] a) E. J.Corey, J.C. Bailar Jr, *J. Am. Chem. Soc.* **1959**, *81*, 2620; b) K. Bernauer, in 'Topics in Current Chemistry', Ed. F.L. Boschke, Springer, Berlin, 1976, Vol. 65.

[9] K. Bernauer, Université de Neuchâtel, unpublished results.

[10] K. Bernauer, H. Stoeckli-Evans, D. Hugi-Cleary, H.J. Hilgers, H. Abd-el-Khalek, J. Porret, J.J. Sauvain, *Helv. Chim. Acta* **1992**, *75*, 2327.

[11] C. Vichard, Diploma work, Université de Neuchâtel, 1997.

[12] K. Bernauer, P. Pousaz, J. Porret, A. Jeanguenat, *Helv. Chim. Acta* **1988**, *71*, 1339.

[13] C. Kressl, PhD. Thesis, Université de Neuchâtel, 1997.

[14] K. Bernauer, E. Fuchs, D. Hugi-Cleary, *Inorg. Chem. Acta* **1994**, *218*, 73.

[15] K. Bernauer, D. Hugi-Cleary, H.J. Hilgers, H. Abd-el-Khalek, N. Brügger, C. Kressl, *Inorg. Chim. Acta* **1998**, *275-276*, 1.

CHAPTER 2:
LIGAND AND COMPLEX SYNTHESES

2.1 Synthetic methods

2.1.1 Pentadentate aminocarboxylate ligands based on a 2,5-disubstituted pyridine framework

The aminocarboxylate ligands based on a 2,5-disubstituted pyridine framework are synthesised in optically pure form from 2,5-bis(chloromethyl)pyridine and an excess of the corresponding enantiomerically pure amino acid (Scheme 1-1). The unreacted amino acid is removed by column chromatography on a strongly acidic cation exchanger. 2,6- bis[3-carboxy-2-azabutyl]pyridine (H_2alamp, **1** on Scheme 2-1) was recrystallized as a neutral molecule and 2,6-bis[(2-carboxypyrrolidin-1-yl)methyl]pyridine (H_2-promp, **2**) as the hydrochloride salt. 2,6-bis[3-carboxymethyl-2-azabutyl]pyridine (H_2b3amp, **3**) could not yet be crystallised. In some syntheses, by-products with only one amino acid substitution were observed. The other methylene group on the pyridine ring was either substituted by a hydroxy- or a methoxy-group. Both side-reactions, hydrolysis and etherification with the solvent, have probably been favoured by a too low pH during the reaction. Both by-products could be removed by flash column chromatography on silica gel.

As the ligand promp crystallised with various amounts of HCl, the exact content of H_2promp in the hydrochloride salt batch was checked by measuring the ellipticity of the corresponding copper(II) complexes formed in situ with an excess of copper(II) sulphate. The molar dichroic absorption coefficient of the copper complex had been previously determined by spectropolarimetric titration.

Scheme 1-1. *Synthesis of the aminocarboxylate ligands used for complex formation.* According to [1][2][3].

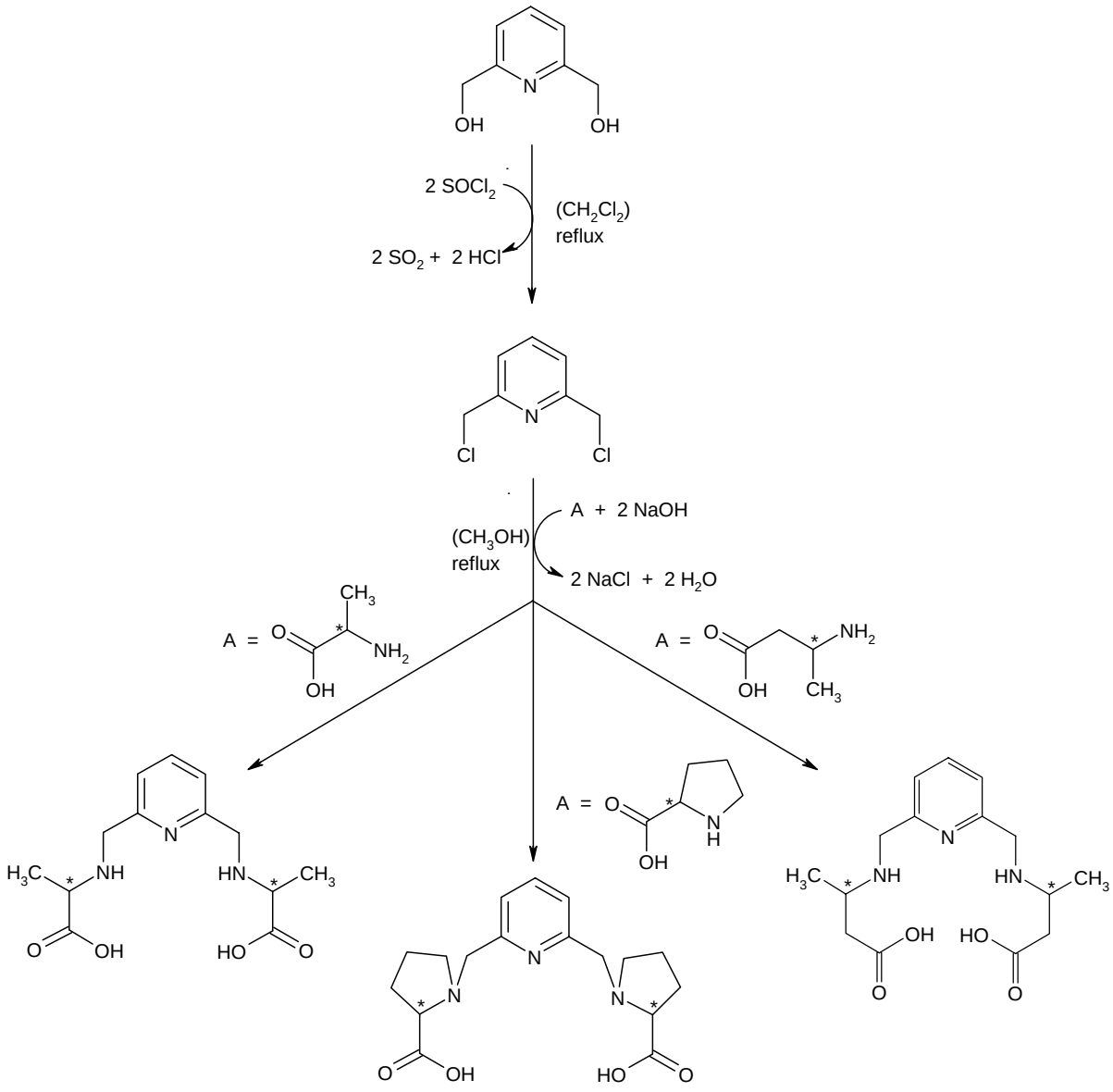

Optically pure proline and alanine were commercially available whereas both enantiomers of 3-aminobutyric acid were resolved from the racemic mixture with quinine and brucine respectively, according to 2-2.

Scheme 2-2. *Chiral separation of racemic 3-aminobutyric acid.* According to [4] and [5].

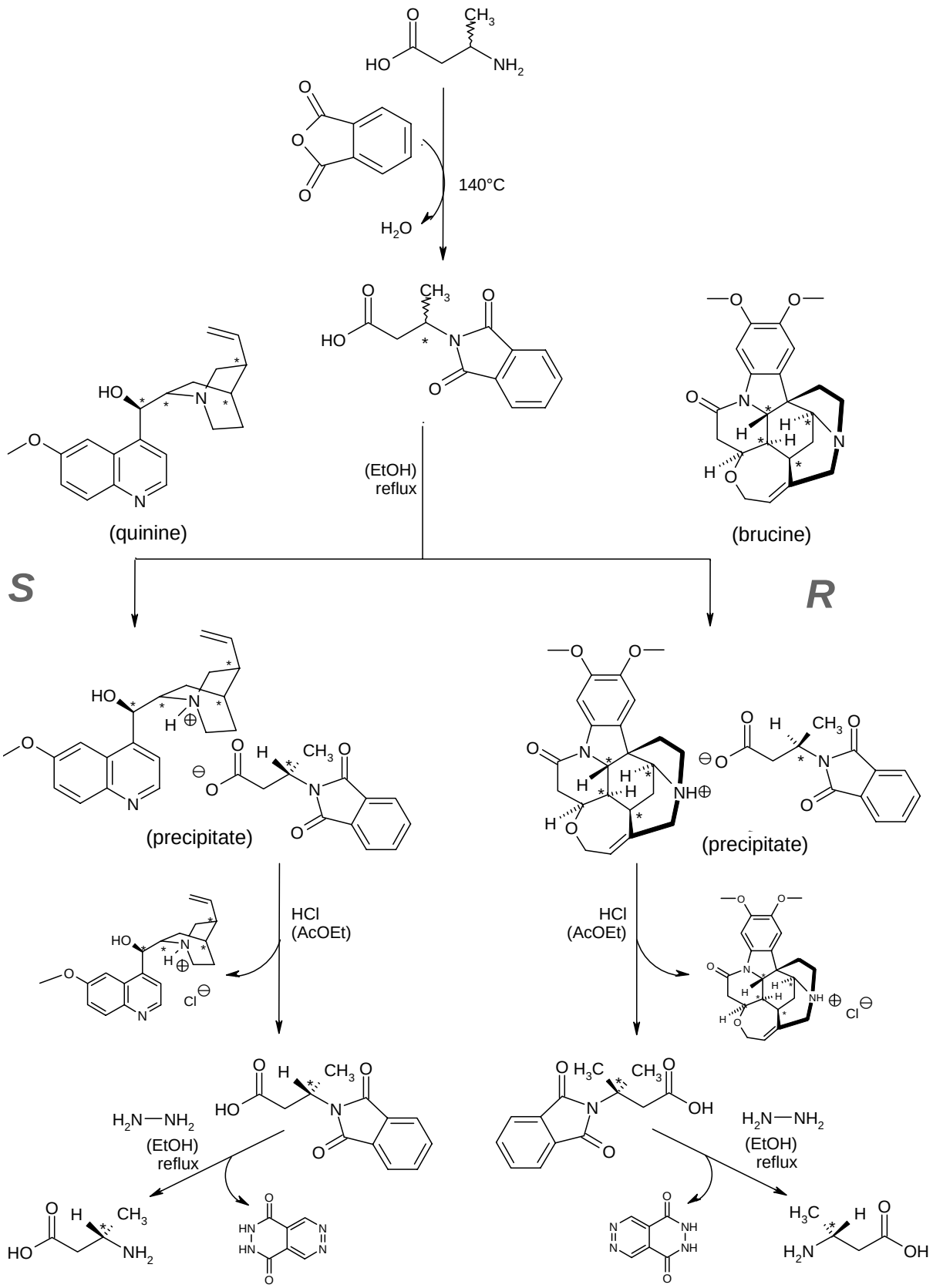

2.1.2 Preparation of transition metal complexes with aminocarboxylate ligands

Copper(II) and cobalt(II) complexes were formed at room temperature by mixing aqueous solutions of the metal salts and the ligands. In the case of the chromium(III) complex, heating was necessary. The cobalt(III) complexes have been prepared by oxidising the corresponding cobalt(II) complexes with hydrogen peroxide and air oxygen in the presence of active charcoal. Both chromium(III) and cobalt(III) complexes were purified in several steps by column chromatography on Sephadex cation exchanger and size-exclusion resins.

The preparation of an optically active ruthenium complex with H_2(*S*,*S*)-promp has first been tried by a procedure analogous to the preparation of the $[Ru^{III}(edta)]^-$ [6]: When the ligand and $[Ru^{III}Cl_5(H_2O)]^{2-}$ in aqueous solution were heated to reflux for several hours, a colour change from brownish red to dark green, as well as an emergence of a CD signal were clearly observed. Nevertheless, an analysis by ESI mass spectrometry of the crude reaction mixture revealed only the presence of the free ligand. Probably the stability of the ruthenium(III) complex is so low that aquation took place upon dilution.

A more promising procedure was the substitution of the ligand on a ruthenium(II) centre with either DMSO or acetonitrile as leaving groups (Scheme 2-3). This method is currently used for the preparation of complexes with bipyridine derivatives as ligands [7][8]. It seems that the DMSO ligand stabilises noticeably the (+II) oxidation state of ruthenium [9].

Both ruthenium complexes reacted with the H_2(*S*,*S*)-promp ligand and the CD spectra of the reaction mixtures exhibited the same pattern, those of the reaction with $[Ru^{II}Cl_2(NCCH_3)_4]$ being better resolved (Fig. 2-1). Surprisingly, in the reaction represented the CD activity increased continuously during 260 h of heating in boiling ethanol but then collapsed completely and irreversibly within 24h although no change in the solution colour was observed. Extended exposition to sunlight at r.t. of an aliquot drawn from the reaction mixture engendered also a remarkable drop of the CD activity along with a darkening of the solution colour. The colour change is also reflected by the slight bathochromic shift on the CD spectrum (Fig. 2-1).

ESI mass spectra of the reaction mixtures parting from $[Ru^{II}Cl_2(dmso)_4]$ as well as from $[Ru^{II}Cl_2(NCCH_3)_4]$ (Fig. 2-2) reveal clearly the formation of a ruthenium complex. As the

Scheme 2-3. *Methods for the preparation of a ruthenium complex with the (*S,S*)-promp*$^{2-}$ *ligand.* On the analogy of [7] and [8]. The oxidation state of the ruthenium centre in the final reaction product could not be determined unambiguously.

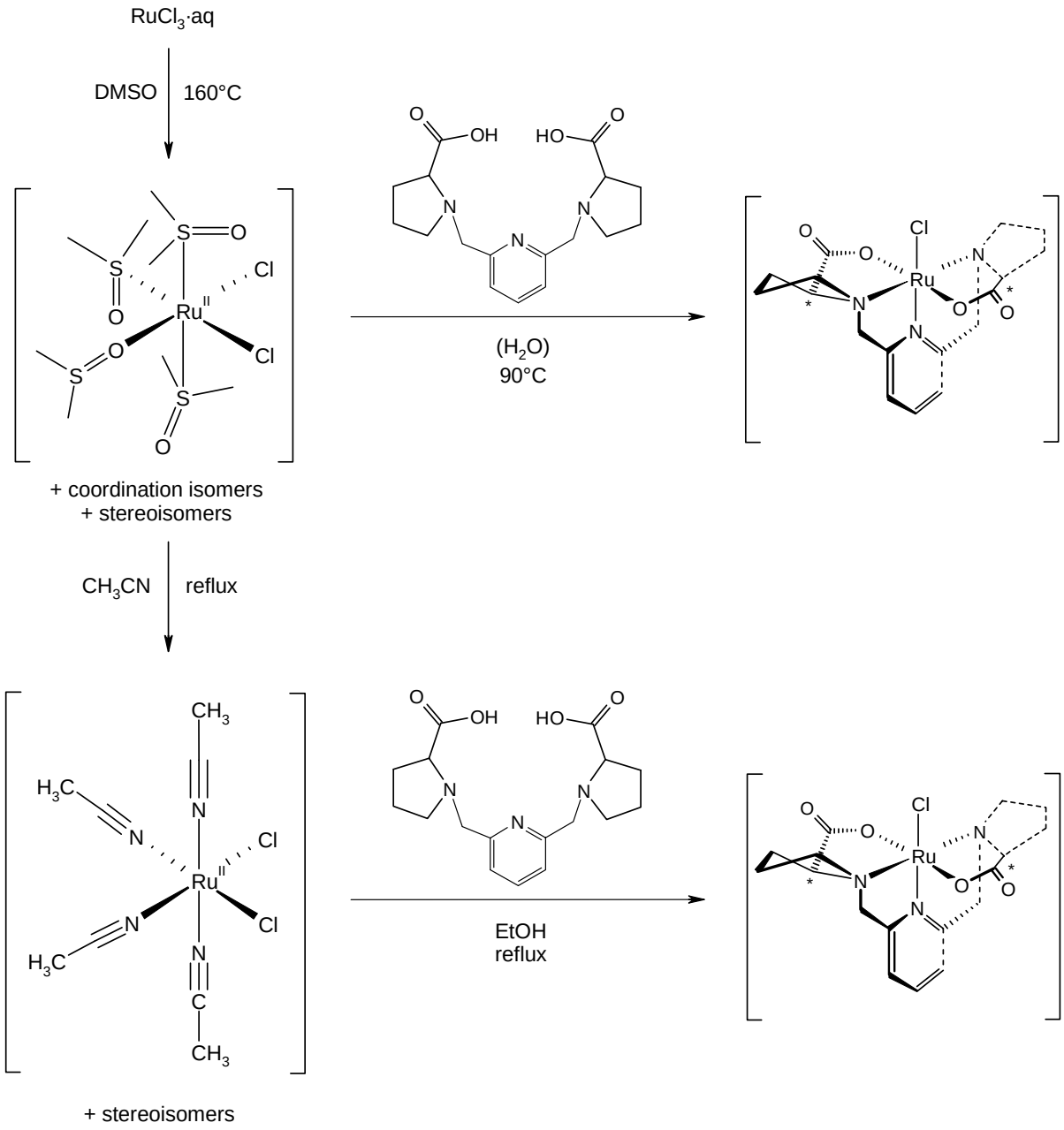

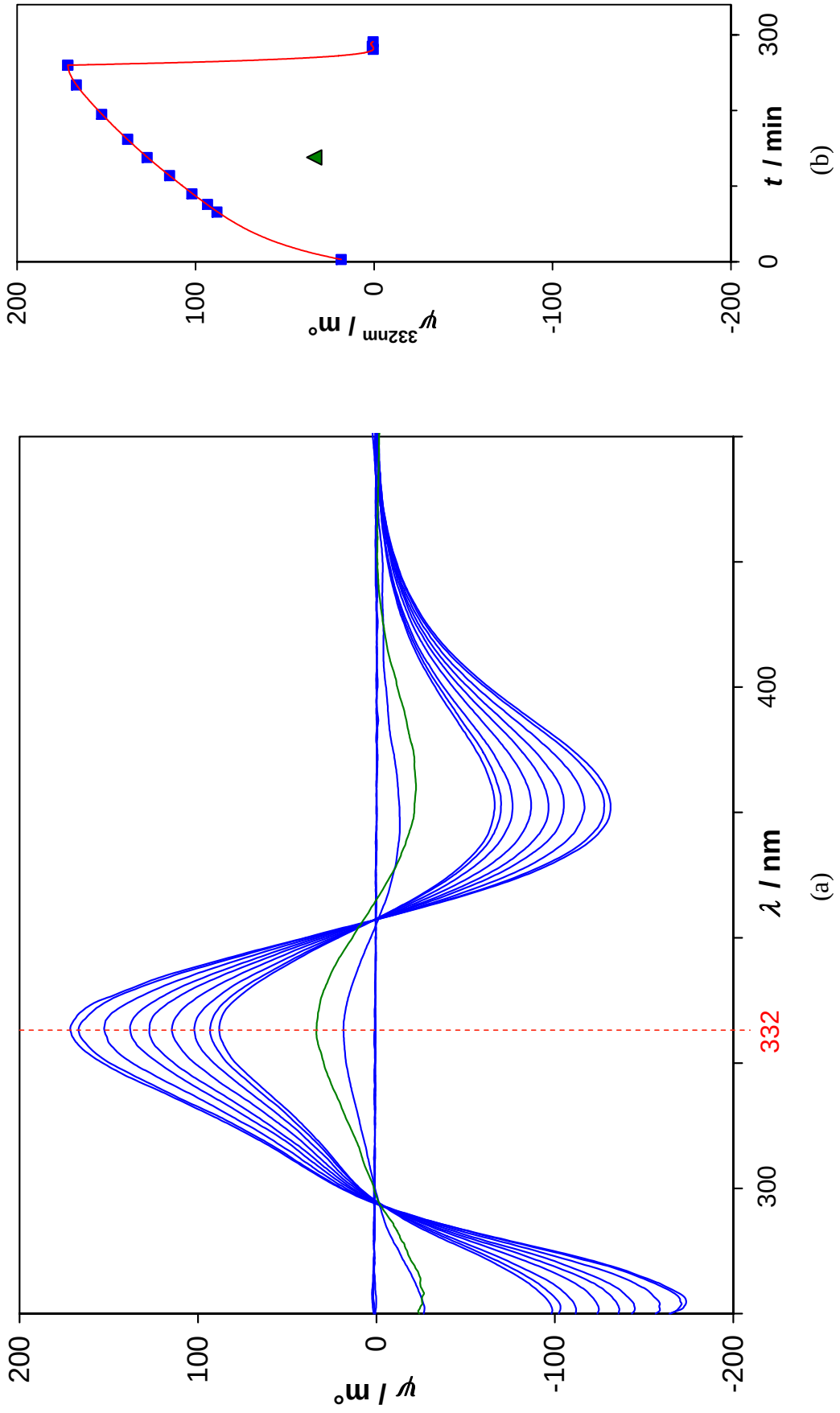

Fig. 2-1. *Evolution of the CD signal during the reaction between [Ru(CH$_3$CN)$_4$Cl$_2$]. and H$_2$(S,S)-promp at reflux in ethanol.* a) *CD spectra at different reaction stages.* b) *Time-resolved evolution of ellipticity at* λ_{max} = 332 *nm.* The green line on a) and the triangular marker on b) correspond to the CD activity after 138 h of reaction and extended exposition to sunlight at r.t.

observed signals occur in the positive mode, the compound has either been ionised twice or the ruthenium centre has been oxidised to the (+III) state. The presence of [Ru(promp)Cl] and its related species in the reaction mixture in spite of the complete loss of optical activity (see Fig. 2-1) is very curious because racemisation of a metal complex with the promp^{2-} ligand had never been observed before.

In spite of its neutral or negative charge, the ruthenium complex was irreversibly fixed on a SP Sephadex C-25 resin, probably by covalent binding.

An isolation of the compound could not yet be performed.

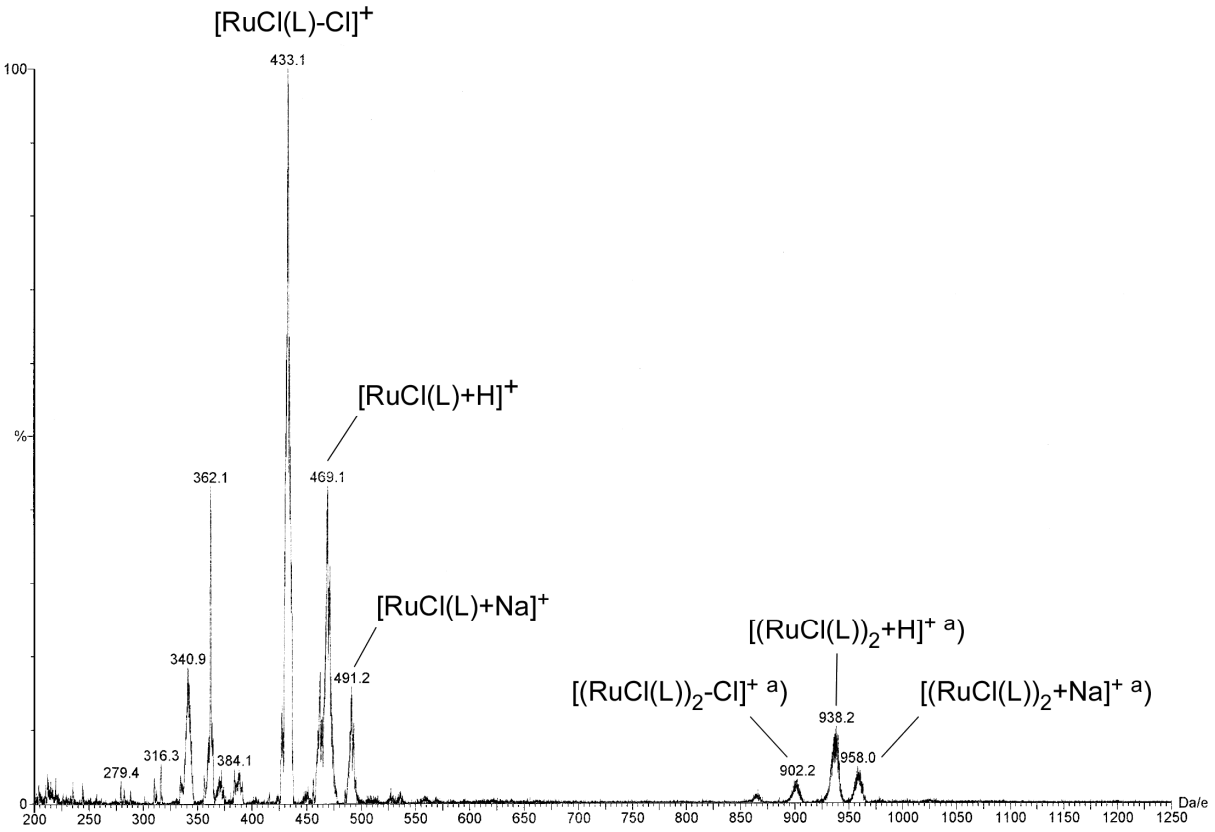

Fig.2-2. *ESI mass spectrum of the reaction mixture between [Ru(NCCH$_3$)$_4$Cl$_2$] and H$_2$(S,S)-promp (H$_2$L) after reflux in ethanolic solution.*

[a]) Due to the broad isotopic distribution within these signals and the low resolution of the mass spectrum, a tolerance of ± 1 Da·e^{-1} on the indicated maximum is admitted.

2.2 Experimental part - general

2.2.1 Reagents, gases and solvents

Commercial reagents were purchased from Acros, Geel (BE), Aldrich, Steinheim (DE), Baker, Deventer (NL), Fluka, Buchs SG (CH), JPS Chimie, St-Aubin (CH), Merck, Darmstadt (DE), Prochimie, Avenches (CH), sds, Peypin (FR), Sigma, St Louis MO (USA) and Ventron, Karlsruhe (DE) according to Table 2-1.

Table 2-1. *Origin and purity of the reagents used.*

Substance	Origin	Quality grade and purity	
D(+)-Alanine	Fluka	puriss.	≥ 99%
L(-)-Alanine	Fluka	*BioChemika*	≥ 99%
3-Aminobutyric acid	Fluka	purum	97%
Bis(hydroxymethyl)pyridine, 2,6-	JPS		not stated
	Aldrich		98%
Boric acid	Baker		≥ 99.8%
	Merck	p.a.	≥ 99.8%
Brucine, anhydrous	Acros		99%
Butylamine	Fluka	puriss. p.a.	≥ 99%
Chromium(III) potassium sulphate dodecahydrate	Fluka	puriss. p.a.	≥ 99%
Cobalt nitrate hexahydrate	Merck	pure	≥ 97%
Cobalt sulphate heptahydrate	Merck		not stated
Cobalt(II) chloride hexahydrate	Merck	p.a.	≥ 99%
trans-1,2-Diaminocyclohexane-N,N,N'N'-tetraacetic acid monohydrate (H_4cdta·H_2O)	Aldrich	ACS	99%
Hydrazine	Acros		≥ 98%
Hydrochloric acid, 1M solution	Merck	Titrisol®	
Magnesium sulphate anhydrous	Fluka	purum	≥ 99%
Mercurous nitrate dihydrate	Fluka	puriss. p.a. ACS	≥ 98%
Morpholinoethanesulfonic acid, 2- (MOPSO)	Fluka	*BioChemika*	≥ 99%
Perchloric acid 70%	Fluka	puriss. p.a. ACS	≥ 70%

Table 2-1 (continued)

Substance	Origin	Quality grade and purity
Phenylethylamine, D-(-)-	Acros	99% *e.e.* > 99%
Phenylethylamine, L-(+)-	Acros	99% *e.e.* > 99%
	Fluka	purum 94% *e.e.* > 98%
Phthalic anhydride	Acros	p.a. 99.7%
Proline, D(+)-	Fluka	puriss. ≥ 99%
	Acros	> 99%
Proline, L(-)-	Fluka	*BioChemika* ≥ 98%
Quinine, anhydrous	Acros	99%
Ruthenium(III) chloride (water soluble)	Johnson Matthey	42.75% Ru
	Fluka	purum 38 - 40% Ru
Sodium acetate trihydrate	Fluka	puriss. p.a. ACS 99.5%
Sodium hydroxide, pellets	Fluka	puriss. p.a. ACS ≥ 98%
Sodium hydroxide, 1M solution	Merck	Titrisol®
Sodium chloride	Fluka	puriss. p.a. ACS ≥ 99%
Sodium perchlorate	Fluka	puriss. p.a. ACS ≥ 99%
Thionyl chloride	Fluka	purum > 99%
Tris-(hydroxymethyl)aminomethane	Fluka	*BioChemika* ≥ 99%
Zinc < 325 mesh	Ventron	not stated

Other reagents were of technical grade and various origins. Argon (99.996%) and nitrogen (99.995%) have been supplied by Carbagas, Bern (CH) and used without further purification.

For reactions and crystallisations, solvents of technical grade were distilled before use, for extractions they were used without further purification. For spectroscopic measurements (UV/VIS, CD, NMR), solvents of analytical grade were employed. In some cases, solvents were dried before use as indicated in the corresponding procedure.

The water for the solution preparation has generally been distilled and then passed through PTFE coated sieves and fractionating layer (Instrument 'Top Dester®' sold by Merck eurolab, Dietikon, CH). For some measurements, it was outgassed, i.e. freed from dissolved O_2 by stirring under reduced pressure for 20 minutes and then kept under argon.

2.2.2 Preparative methods

Column chromatography

Flash chromatography was carried out on silica gel 30-60 µm from Baker and Silica gel 60, 4-63 µm from Fluka, Buchs (CH). Resins *Dowex-50 W X 8*, 200-400 mesh from Fluka, *SP Sephadex C-25* and *DEAE Sephadex A-25*, both from Pharmacia LKB, Uppsala (SE) were used for ion exchange chromatography.

Dialysis

Dialysis sacks made of regenerated cellulose molecularporous membrane tube *Spectra/Por*® *1*, diameter 14.6 mm, molecular weight cut-off 6000-8000 D, and standard closures from Spectrum Laboratories, Rancho Dominguez (USA) were employed.

2.2.3 Analyses

[10] and [11] have been used for the interpretation of the spectroscopic data.

Absorption spectrophotometry (UV-VIS)

The measurements have been performed on UVIKON 810 and UVIKON 930 spectrophotometers from Kontron / BioTech (manufacturer exists no more) as well as on a Cary 1E spectrophotometer from Varian, Palo Alto, (USA). The sample solutions were introduced into rectangular quartz cells from Hellma, Müllheim (DE).

Indications in the spectroscopic data collection of §2.3: **UV (*c* = amount concentration in mol·L^{-1}, solvent):** λ_{max}/nm (ε_{max}/L·mol^{-1}·cm^{-1}). If the exact concentration of the sample was unknown, this is explicitly mentioned and only the λ_{max} values are indicated.

Circular dichroism (CD)

CD spectra have been recorded on J-500 and J-710 spectropolarimeters from JASCO, Tokyo (JP). The sample solutions were introduced into cylindrical quartz cells from Hellma, Müllheim (DE).

Indications in the spectroscopic data collection: **CD (*c* = amount concentration in mol·L^{-1}, solvent):** λ_{max}/nm ($\Delta\varepsilon_{max}$/L·mol^{-1}·cm^{-1}). If the exact concentration of the sample was unknown, this is explicitly mentioned and only the λ_{max} values and the signs of the extrema (+,-) are indicated.

Cyclovoltammetry (CV)

CV curves have been recorded by a Polarecord E506 instrument coupled to a wave generator VA Scanner E612 and an AMEL 862/D plotter. A rotating platinum electrode (6.0332.000 with motor E 628) and a hanging mercury drop electrode 6.0335.000 served as working electrodes, a platinum sheet 6.02302.000 as auxiliary electrode and an Ag/AgCl electrode 6.0733.100 as reference. If not stated otherwise, all instruments came from Metrohm, Herisau (CH).

Indications in the spectroscopic data collection: CV (complex concentration, pH, ionic strength, ground electrolyte, sweeping domain, reference electrode): peak potentials *vs*. NHE, peak currents.

Elemental analysis (EA)

C, H and N microanalyses have been carried out by the University of Applied Sciences at Fribourg (CH) on an EA 1110 CHNS from Carlo Erba instruments, Milano (IT). Acetanilide was used as calibration substance. Other microanalyses have been carried out by the organic chemistry department at the Swiss Federal Institute of Technology (ETH), Zurich (CH).

Infrared spectroscopy (IR)

Solid samples were included in a KBr film and analysed by a FT-IR 1720 X spectrometer from Perkin-Elmer, Wellesley, MA (USA).

Indications in the spectroscopic data collection: **IR (sample support):** $\bar{\nu}$ /cm^{-1} *signal intensity* (shape, attribution)

Mass spectrometry (MS)

ESI spectra of compound **9** were recorded on a single quadrupole mass spectrometer from Fisons, Manchester (GB) at the University of Bern (CH). The other ESI and EI spectra were recorded on a mass spectrometer LCQ from ThermoFinnigan, San José (USA).

Indications in the spectroscopic data collection: **EI/ESI-MS:** M_r of species (relative intensity, attribution). The relative intensity is given in % towards the strongest peak of the spectrum. Only peaks with plausible assignment are indicated in the ESI mode.

Nuclear magnetic resonance (NMR)

Proton and carbon NMR spectra were recorded on spectrometers Gemini (200 MHz for ^{1}H, 50 MHz for ^{13}C) from Varian, Palo Alto, (USA) and AMX-400 (400 MHz for ^{1}H, 100 MHz for ^{13}C) from Bruker, Billerica MA (USA). The samples were measured either in deuterated chloroform (99.8% D) or in deuterium oxide (99.9% D) from Cambridge Isotope Laboratories, Andover MA (USA).

Indications in the spectroscopic data collection: **nucleus-NMR (frequency, solvent):** δ/ppm towards TMS (*multiplicity*, *J*/Hz (^{1}H only), normalised integration values (^{1}H only), atom type and number).

Melting points (M.p.)

Melting points have been determined by an uncorrected 530 apparatus from Büchi, Flawil (CH).

Optical rotation dispersion (ORD)

ORD spectra have been recorded on a J-920 spectropolarimeter from JASCO, Tokyo (JP). The sample solutions were introduced into rectangular quartz cells from Hellma, Müllheim (DE).

Indications in the spectroscopic data collection: **ORD (γ = mass concentration in g·(100 mL)$^{-1}$, solvent):** λ_{max}/nm ($[\alpha]^{r.t.}_{\lambda\,max}$ /mL·g^{-1}·dm^{-1}).

Polarimetry

Measurements were performed by a 241 polarimeter from Perkin-Elmer, Wellesley, MA (USA). In general, the sample solutions were conditioned in 10 cm cells.

Indications in the data collection:
$[\alpha]^{r.t.}_{\lambda}$ (γ = mass concentration in g·(100 mL)$^{-1}$, solvent): $[\alpha]^{r.t.}_{\lambda}$ /°·mL·g^{-1}·dm^{-1} $_{\lambda/nm}$.

Potentiometric titrations

Semi-automatic titrations were realised by a Potentiograph E536 with a 6.0210.100 glass electrode and Dosimat 655 from Metrohm, Herisau (CH).

Thin layer chromatography (TLC)

The substances have been applied on 0.2 mm silica gel 60 F_{254} plates from Merck, Darmstadt (DE) or Macherey-Nagel, Düren (DE).

Indications in the data collection : **TLC (eluent mixture):** R_f (colour, revelation).

X-ray diffraction

Intensity data were collected either using STOE AED2 four-circle diffractometer or a STOE Imaging Plate Diffraction System, both using graphite monochromated Mo Kα radiation (λ = 71.073 pm). The structures were solved by direct methods or Patterson heavy-atom technique using the programme SHELXS-97 [12]. The refinement and all further calculations were carried out using SHELXL-97 [13]. Symmetry operations were used to generate equivalent atoms. The complete service was performed by the group of Helen Stoeckli-Evans, Université de Neuchâtel (CH). Crystallographic data is indicated in the appendix (§7.1).

Particular experimental methods, such as electrolytic reduction, are explained together with the results in the corresponding paragraphs.

2.3 Experimental part - synthesis proceedings

2.3.1 2,6- bis(chloromethyl)pyridine (**4**)

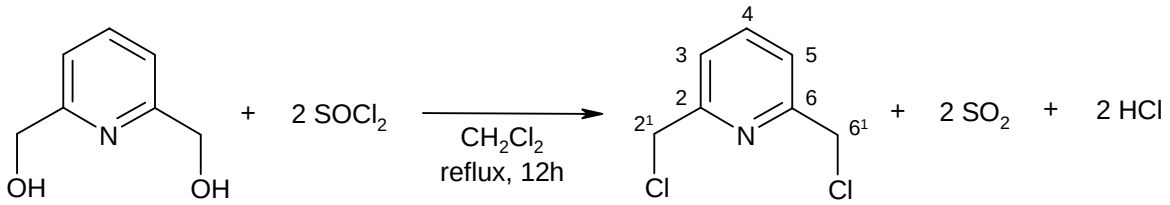

5		**4**
$C_7H_9NO_2$	$SOCl_2$	$C_7H_7Cl_2N$
139.16	118.97	176.05

According to [1]

In a 500 mL three-necked flask provided with a dropping funnel, a reflux condenser and a magnetic stirrer, 2,6-bis(hydroxymethyl)pyridine (22.5 g, 0.162 mol) were suspended in dichloromethane (200 mL) and cooled down to 4°C. Freshly distilled thionyl chloride (77.1 g, 0.65 mol, 4 eq.) was added dropwise and under vigorous stirring. The mixture was stirred at r.t. during 8 h, then at reflux during 12 h. After cooling down to r.t., the reaction mixture was poured onto ice in order to hydrolyse the excess of thionyl chloride. The two resulting phases were separated. The aqueous phase was neutralised with solid sodium carbonate. The precipitated 2,6-bis[chloromethyl]pyridine was filtered off and dried over silica gel at r.t. and reduced pressure. The brownish solid was purified by sublimation at 20 mbar and 90°C. The solvent of the organic phase was allowed to evaporate gently in a crystallising dish and the residue was purified by sublimation as indicated above.

Yield: 19.6g (69%), 7.8 g from the aqueous phase and 11.8 g from the organic phase.

^{1}H-NMR (400 MHz, $CDCl_3$): 7.77 (*t*, ^{3}J=7.8, 1 H, H-C(4)), 7.44 (*d*, ^{3}J=7.8, 2 H, H-C(3, 5)), 4.67 (*s*, 4 H, $H_2C(2^1, 6^1)$).

^{13}C-NMR (100 MHz, $CDCl_3$, DEPT): 156.8 (*s*, C(2, 6)), 138.6 (*d*, C(4)), 122.5 (*d*, C(3, 5)), 46.8 (*t*, $C(2^1, 6^1)$).

2.3.2 2,6- bis[(*R*)-3-carboxy-2-azabutyl]pyridine ((*R*,*R*)-H_2alamp, (*R*,*R*)-**1**))

2,6- bis[(*S*)-3-carboxy-2-azabutyl]pyridine ((*S*,*S*)-H_2alamp, (*S*,*S*)-**1**))

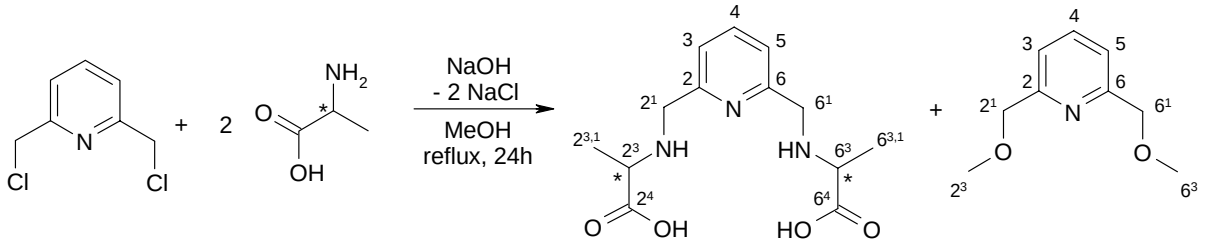

4		(*R*,*R*)- or (*S*,*S*)-**1**	**6**
$C_7H_7Cl_2N$	$C_3H_7NO_2$	$C_{13}H_{19}N_3O_4$	$C_9H_{13}NO_2$
176.05	89.09	281.31	167.21

According to [1] and [2].

In a 250 mL three-necked flask provided with a dropping funnel, a reflux condenser and a magnetic stirrer, optically pure 2-aminopropanoic acid (D- or L-alanine, 6.5 g, 0.072 mol, 2.4 eq.) were added by portions to a solution of sodium hydroxide (4.8 g, 0.12 mol, 4 eq.) in MeOH (100 mL). 2,6-bis[chloromethyl]pyridine (5.3 g, 0.03 mol) in MeOH (50 mL) and some drops of a methanolic solution of phenolphthalein were added slowly under vigorous stirring. The mixture was refluxed during 24 hours and maintained basic by addition of 3M NaOH solution, cooled to room temperature and neutralised by 16% HCl. The precipitated NaCl was removed by filtration and the filtrate evaporated to dryness at reduced pressure.

The resulting solid was redissolved in water (400 mL) and acidified to pH 3 by 2M HCl. The solution was introduced into a cation exchange column (*Dowex-50x8*, 200-400 mesh, column length 30 cm; bed volume 300 mL; form H^+). The resin was washed with water (500 mL) and the product was eluted with 0.05M NaOH. The fractions of the effluent were analysed by TLC (SiO_2, BuOH:AcOH:H_2O 12:6:5, UV^{254}/ninhydrine). The fractions containing an excess of free amino acid were evaporated to dryness; those containing only the alamp ligand were neutralised by 2M HCl and evaporated to dryness. The solid was recrystallised in a mixture of ethanol and acetone.

2,6- bis[(3*S*)-3-carboxy-2-azabutyl]pyridine ((*S*,*S*)-alamp, (*S*,*S*)-**1**))

TLC (BuOH/H_2O/AcOH 12:6:5): R_f 0.16 (UV_{254}-active).

^{1}H-NMR (400 MHz, D_2O): 7.82 (*t*, ^3J=7.8, 1 H, H-C(4)), 7.36 (*d*, ^3J=7.8, 2 H, H-C(3, 5)), 4.35 (*s*, 4 H, $H_2C(2^1, 6^1)$), 3.71 (*d*, 2 H, ^3J=7.2, $H_2C(2^3, 6^3)$), 1.48 (*q*, 6 H, ^3J=7.2, $H_3C(2^4, 6^4)$).

^{13}C-NMR (100 MHz, $CDCl_3$, DEPT): 176.1 (*s*, $C(2^4, 6^4)$), 151.3 (*s*, C(2, 6)), 139.6 (*d*, C(4)), 123.3 (*d*, C(3, 5)), 58.0 (*d*, $C(2^3, 6^3)$), 49.4 (*t*, $C(2^1, 6^1)$), 15.4 (*q*, $C(2^{3,1}, 6^{3,1})$).

2,6- bis(methoxymethyl)pyridine (**6**)

TLC (BuOH/H_2O/AcOH 12:6:5): R_f 0.06 (UV_{254}-active).

^{1}H-NMR (400 MHz, $CDCl_3$): 7.74 (*t*, ^3J=7.8, 1 H, H-C(4)), 7.35 (*d*, ^3J=7.7, 2 H, H-C(3, 5)), 4.60 (*s*, 4 H, $H_2C(2^1, 6^1)$), 3.49 (*s*, 6 H, $H_3C(2^3, 6^3)$).

^{13}C-NMR (100 MHz, $CDCl_3$, DEPT): 158.2 (*s*, C(2, 6)), 137.8 (*d*, C(4)), 120.4 (*d*, C(3, 5)), 75.7 (*t*, $C(2^1, 6^1)$), 59.2 (*q*, $C(2^3, 6^3)$).

2.3.3 2,6- bis[(3*S*)-3-carboxy-2-azabutyl]pyridine cobalt(III) complexes

These complexes were only synthesised in solution, for the purpose of generating qualitative reference CD spectra in the visible range.

2.3.3.1 Λ-Aqua 2,6- bis[(2*R*,3*S*)-3-carboxy-2-azabutyl]pyridine cobalt(III) ([Co^{III}((*S*,*S*)-alamp)H_2O]$^+$, (*S*,*S*)-**7**)

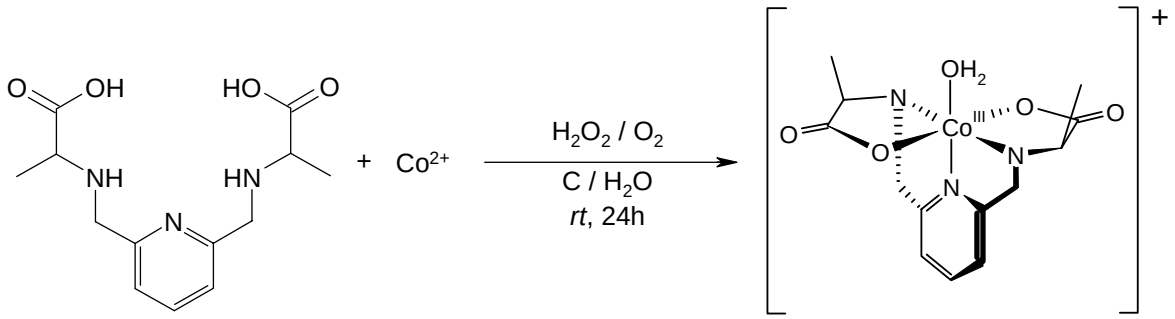

(*S*,*S*)-(+)-**3**	$CoSO_4 \cdot 7H_2O$	(*S*,*S*)-**7**
$C_{13}H_{19}N_3O_4$	$H_{14}CoO_{11}S$	$C_{13}H_{17}CoN_3O_5^+$
281.31	281.10	(354.22)

According to a modified procedure described in [14]

H_2(*S*,*S*)-alamp ((*S*,*S*)-**1**, 0.062 g, 0.22 mmol, 1.1 eq.) and cobalt(II) sulphate heptahydrate (0.057 g, 0.2 mmol) were dissolved in water (10 mL). Active charcoal (0.014 g) and 30% hydrogen peroxide solution (0.2 g) were added. The pH was adjusted and maintained at 6.5-7 by addition of several portions of 0.1M NaOH. When no more significant pH drop occurred, the reaction was allowed to complete at r.t. for one day. The active charcoal was eliminated by filtration through cotton wool.

UV (H_2O[1])): 360, 490.

CD (H_2O[1]), signs refer to the (*R*,*R*)-enantiomer**):** 361 (+), 467 (-), 540 (+).

2.3.3.2 Λ-Butylammine 2,6- bis[(2*R*,3*S*)-3-carboxy-2-azabutyl]pyridine cobalt(III) ([Co^{III}((*S*,*S*)-alamp)$C_4H_9NH_2$]$^+$, (*S*,*S*)-**8**)

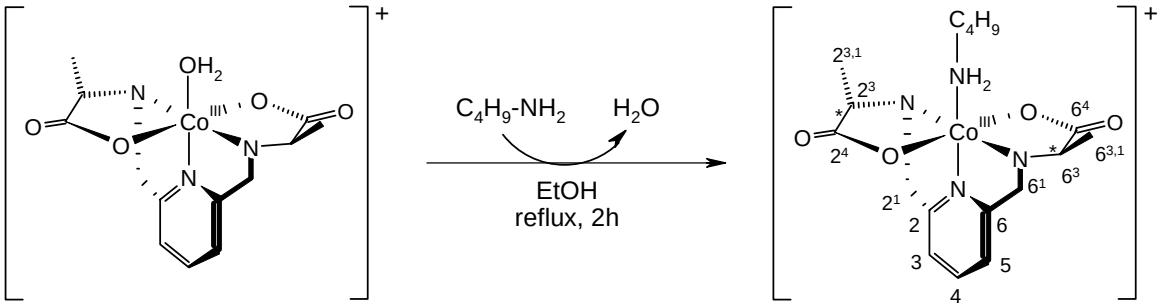

(*S*,*S*)-**7** $C_{13}H_{17}CoN_3O_5^+$ (354.22)

$C_4H_{11}N$ 73.14

(*S*,*S*)-**8** $C_{17}H_{26}CoN_4O_4^+$ (409.35)

7 (0.0336 g of crude product containing 37% **7**, $2.72 \cdot 10^{-5}$ mol as perchlorate salt) and butylamine (0.0096 g, $1.31 \cdot 10^{-5}$ mol, 4.8 eq.) in EtOH (15 mL) were heated to reflux during 15 h. The solid **7** dissolved slowly, and then the colour of the solution changed from pink to red-orange. The solvent was evaporated to the dryness. A crude orange-brownish powder

[1]) exact concentration unknown

containing less than 40% **8** (as perchlorate salt) was obtained. The CD spectrum of the product mixture had lower intensity than the aquacomplex at a similar concentration. This suggests that part of the pentadentate ligand had been replaced by butylamine. The high affinity of $[Co^{III}((S,S)\text{-alamp})H_2O]^+$ for the butylamine ligand is confirmed by the fact that a solution of the starting material in pure butylamine became orange and had no more optical activity. This indicates an irreversible formation of the hexakis(butylammine) complex.

ESI-MS (pos. mode, $M_A^+ = C_{17}H_{26}CoN_4O_4^+$, $M_B^- = ClO_4^-$**):** 509 (25, M_{AB}^+), 411 (100, M_AH^+)[1]).

CD(H_2O[2])): 363 (+), 471 (-), 548 (+), 611 (-).

2.3.4 2,6-bis[(*R*)-2-carboxypyrrolidin-1-yl)methyl]pyridine ((*R*,*R*)-H_2promp, (*R*,*R*)-**2**)
2,6-bis[(*S*)-2-carboxypyrrolidin-1-yl)methyl]pyridine ((*S*,*S*)- H_2promp, (*S*,*S*)-**2**)

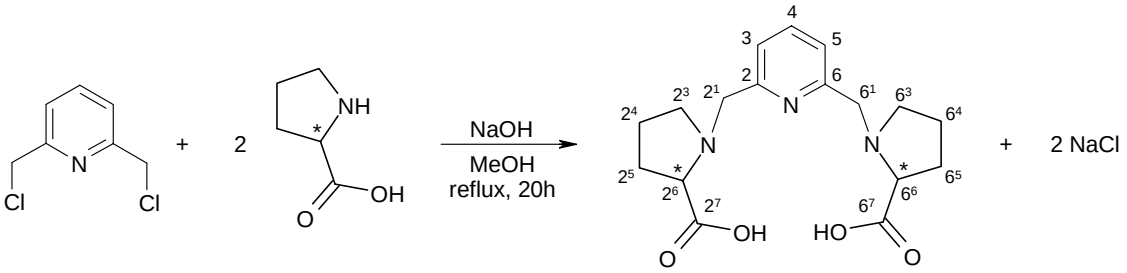

4		(*R*,*R*)- or (*S*,*S*)-**2**
$C_7H_7Cl_2N$	$C_5H_9NO_2$	$C_{17}H_{23}N_3O_4 \cdot x\ HCl$
176.05	115.13	333.38 + x·36.45

According to [1] and [3]

In a 250 mL three-necked flask provided with a dropping funnel, a reflux condenser and a magnetic stirrer, optically pure 2-pyrrolidine carboxylic acid (D- or L-proline, 6.5 g,

[1]) Due to the broad isotopic distribution and the low resolution of the mass spectrum, a tolerance of ± 1 Da·e^{-1} on the indicated maximum is admitted.

[2]) exact concentration unknown

0.072 mol, 2.4 eq.) were added by portions to a solution of sodium hydroxide (4.8 g, 0.12 mol, 4 eq.) in MeOH (100 mL). 2,6-bis[chloromethyl]pyridine (5.3 g, 0.03 mol) in methanol (50 mL) and some drops of a methanolic solution of phenolphthalein were added slowly under vigorous stirring. The mixture was refluxed during 24 hours and maintained basic by addition of 3M NaOH solution, cooled to room temperature and neutralised by 16% HCl. The precipitated NaCl was removed by filtration and the filtrate evaporated under vacuum to dryness.

The resulting solid was dissolved in water (400 mL) and acidified to pH 3 by 2M HCl. The solution was introduced into a cation exchange column (*Dowex-50x8*, 200-400 mesh, column length 30 cm; bed volume 300 mL; form H^+). The resin was washed with water (500 mL) and the product was eluted with 0.05M NaOH. The fractions of the effluent were analysed by TLC (SiO_2, BuOH:AcOH:H_2O 2:1:1, UV^{254}/ninhydrine). The fractions containing an excess of free amino acid were evaporated to dryness; those containing only the promp ligand were combined, neutralised by 2M HCl and evaporated to dryness. To form the double chlorhydrate, 12 mL of 5M HCl (0.06 mol, 2 eq. with respect to a quantitative yield) were added. The solid was crystallised from this solution by adding a mixture of acetone and ethanol.

TLC (BuOH/H_2O/AcOH 2:1:1): R_f 0.23 (UV_{254}-active).

^{1}H-NMR (400 MHz, D_2O, COSY): 7.80 (*t*, ^3J=7.8, 1 H, H-C(4)), 7.47 (*d*, ^3J=7.8, 2 H, H-C(3, 5)), 4.62 (*d*, ^2J=14.2, 2 H, H_a-C(2^1, 6^1)), 4.52 (*d*, ^2J=14.2, 2 H, H_b-C(2^1, 6^1)), 4.34 (*dd*, ^3J=6.9, 9.4, 2 H, H-C (2^6, 6^6)), 3.79-3.73 (*m*, 2 H, H_a-C(2^3, 6^3)), 3.34-3.27 (*m*, 2 H, H_b-C(2^3, 6^3)), 2.56-2.47 (*m*, 2 H, H_a-C(2^5, 6^5)), 2.20-2.10 (*m*, 4 H, H_b-C(2^5, 6^5), H_a-C(2^4, 6^4)), 2.07-1.95 (*m*, 2 H, H_b-C(2^4, 6^4)).

^{13}C-NMR (100 MHz, D_2O, DEPT, HETCOR SR): 173.9 (*s*, C(2^7, 6^7)), 152.9 (*s*, C(2, 6)), 142.4 (*d*, C(4)), 127.5 (*s*, C(3, 5)), 69.9 (*d*, C(2^6, 6^6)), 61.4 (*t*, C(2^1, 6^1)), 58.6 (*t*, C(2^3, 6^3)), 30.9 (*t*, C(2^5, 6^5)), 25.2 (*t*, C(2^4, 6^4)).

CV (10^{-3}M in 0.1M KH_2PO_4/K_2HPO_4 buffer pH 7.5, 0.000 V to -2.000 V vs Ag/AgCl):: E_{pc} = -1.27 V, -1.41; E_{pa} = -1.42 V.

In some cases, probably due to a too low pH in the reaction mixture, a mono- and bis-methoxylated by-product is also formed.

2.3.5 Chloro[2,6- bis[((*S*)-2-carboxypyrrolidin-1-yl)methyl]pyridine]ruthenic(II) acid (H[Ru^{II}((*S*,*S*)-promp)Cl], (*S*,*S*)-**9**)

2.3.5.1 Dichlorotetrakis(dimethyl sulphoxide)ruthenium(II) (**10**)

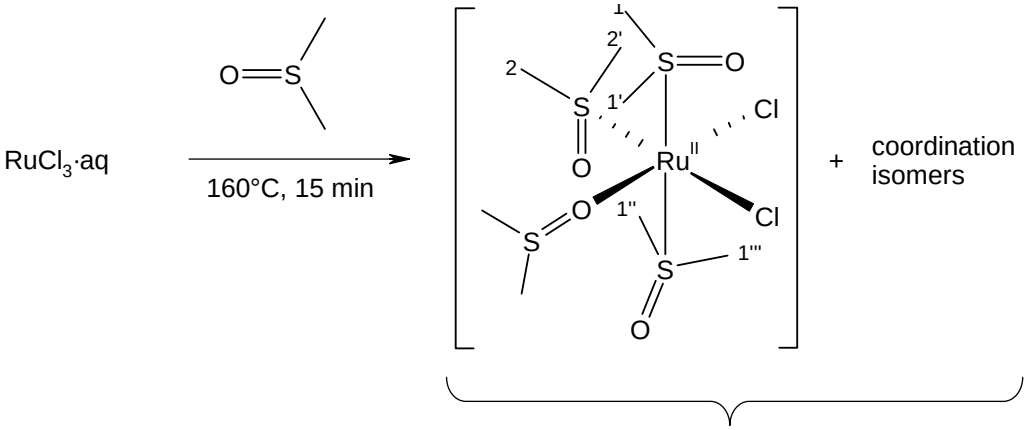

10

	C_2H_6SO	$C_8H_{24}Cl_2O_4RuS_4$
236.4[1])	78.13	484.51

According to a modified [7] procedure based on [8].

A dark brown suspension of $RuCl_3$·aq (1.0 g, 4.2 mmol) in dry distilled DMSO (20 mL) was stirred under nitrogen atmosphere at 160°C. After 10 min, the mixture cleared up to an orange solution. It was kept at 160°C for five more minutes and then concentrated to 3 mL. On cooling to r.t., a yellow precipitate formed. This was filtered off, washed with acetone and dried at reduced pressure. Yield: 1.62 g (79%), bright yellow powder.

UV (c=2.1·10^{-3}, H_2O): 310 (sh, 294), 354 (440)

IR (KBr): 3022*s* (C-H ν), 3008*m* (C-H ν), 2921*m* (C-H ν), 1422*m* (C-H δ), 1402*m* (sh, C-H δ), 1310*m* (C-H δ), 1292*w* (C-H δ), 1115*vs* (O=S--*Ru* ν), 1087*vs* (sh, O=S--*Ru* ν), 1025*vs* (sh, CH ρ), 993*vs* (sh, CH ρ), 971*s* (*d*, CH ρ), 937*vs* (sh, S=O--*Ru* ν), 718*s* (C-S ν as), 680*s* (C-S ν as), 484*s* (Ru-ligand ν), 426*vs* (CSO δ sym), 386*m* (CSO δ sym).

[1]) Empirical formula mass, based on a ruthenium content of 42.75%

^{1}H-NMR (400 MHz, $CDCl_3$): 3.51 (*s*, 2.0 H[1]), H_3C(--*S*--*Ru*)), 3.47 (*s*, 4.8 H[1]), H_3C(--*S*--*Ru*)), 3.41 (2 coal. *s*, 6.8 H [1]), H_3C(--*S*--*Ru*)), 3.30 (*s*, 4.6 H [1]), H_3C(--*S*--*Ru*)), 2.72 (*s*, 4.7 H [1]), H_3C(--*S*--*O*--*Ru*)), 2.62 (*s*, 1.0 H [1]), H_3C(uncoordinated DMSO)).

^{13}C-NMR (100 MHz, $CDCl_3$, HETCOR): 48.1 (*q*, C(--*S*--*Ru*)), 47.0 (*q*, C(--*S*--*Ru*)), 44.8 (*q*, C(--*S*--*Ru*)), 44.7 (*q*, C(--*S*--*Ru*)), 41.3 (*q*, C(uncoordinated DMSO)), 39.3 (*q*, C(--*S*--*O*--*Ru*)).

ESI-MS (pos. mode): 485 (10, M^+), 449 (11, [*M* - Cl]$^+$), 371 (33, [*M* - DMSO - Cl]$^+$), 293 (29, [*M* - 2 DMSO - Cl]$^+$), 79 (19, *DMSO*H$^+$).

2.3.5.2 Chloro[2,6-bis[((1*R*,2*S*)-2-carboxypyrrolidin-1-yl)methyl]pyridine]ruthenic(II) acid (H[Ru^{II}((*S*,*S*)-promp)Cl], (*S*,*S*)-**9**)

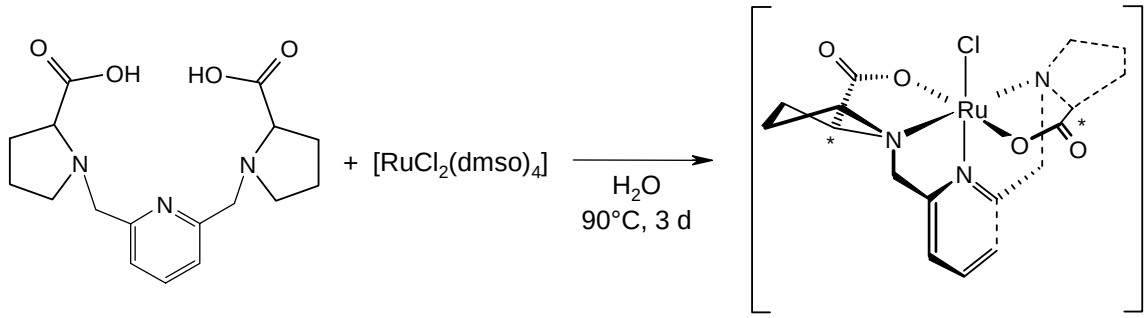

(*S*,*S*)-**2**	**10**	(*S*,*S*)-**9**
$C_{17}H_{23}N_3O_4 \cdot x\ HCl$	$C_8H_{24}Cl_2O_4RuS_4$	$C_{17}H_{21}ClN_3O_4Ru$
333.38 + x·36.45	484.41	467.89

10 (0.242 g, 0.5 mmol) in water (5 mL) and **2** (0.218 g, 0.5 mmol) in water (5 mL) were mixed and stirred at 90°C for three days. The colour of the solution changes from bright yellow to yellow-brown. The progress of the reaction is monitored by CD between 250 nm and 400 nm; an increase of the optical activity was observed. Attempts to purify the crude compound were unsuccessful.

CD(H_2O[1])): 365 (-).

[1]) with respect to the total number of hydrogen atoms in the coordinated and uncoordinated DMSO per complex moiety (24)

ESI-MS (pos. mode): 959 (15, $[2M + Na]^+$), 937 (14, $[2M + H]^+$), 491(18, $[M + Na]^+$), 469 (49, MH^+), 433.1 (100, $[M - Cl]^+$).

Alternative method

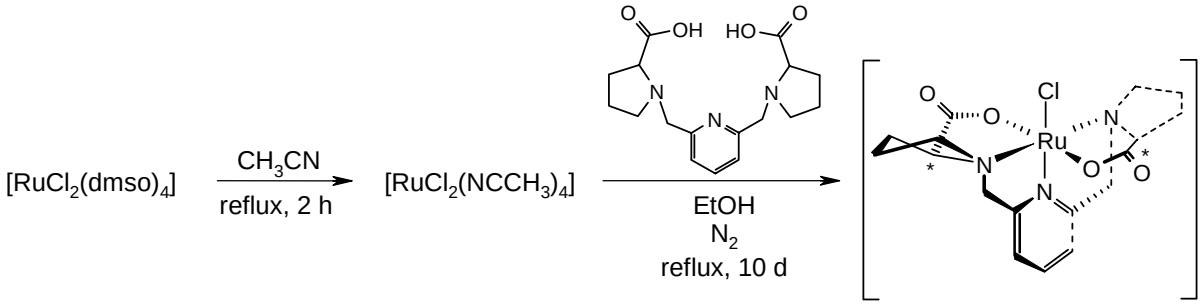

10			(*S*,*S*)-**2**	(*S*,*S*)-**9**
$C_8H_{24}Cl_2O_4RuS_4$	C_2H_3N	$C_8H_{12}Cl_2N_4Ru$	$C_{17}H_{23}N_3O_4 \cdot xHCl$	$C_{17}H_{21}ClN_3O_4Ru$
484.41	41.05	336.18	333.38 + x·36.45	467.89

According to a modified [7] procedure based on [11].

10 (0.242 g, 0.5 mmol) in acetonitrile (10 mL) were stirred at reflux under N_2 for 2 h. After cooling to r.t., Et_2O (160 mL, pre-treated with KOH and freshly distilled over Na) was added. $[Ru(NCCH_3)_4Cl_2]$ (**11**) precipitated and was filtered off under N_2. The light yellow precipitate was dried first in an N_2 stream, then under reduced pressure. In a N_2-flushed three-necked flask with separatory funnel and reflux condenser, **11** in dry EtOH (250 g) is stirred at reflux. **2** (0.218 g, 0.5 mmol) in dry EtOH (250 g) is added dropwise during 4 h. The yellow-brown solution is stirred at reflux under N_2 for 12 d. The progress of the reaction is monitored by CD between 250 nm and 400 nm. An increase of the optical activity was observed during 11 d and then it dropped nearly to zero. Upon cooling, a light brownish solid precipitated. Attempts to purify the crude compound were unsuccessful.

CD (EtOH[1])): 332 (+), 376 (-).

[1]) exact concentration unknown

ESI-MS (pos. mode): 958 (5, $[2M + Na]^+$)[1]), 938 (10, $[2M + H]^+$) [1]), 902 (10, $[2M - Cl]^+$) [1]), 491 (18, $[M + Na]^+$), 469 (43, MH^+), 433.1 (100, $[M - Cl]^+$).

2.3.6 Λ-Aqua[2,6- bis[((1*R*,2*S*)-2-carboxypyrrolidin-1-yl)methyl]pyridine]chromium(III) perchlorate($[Cr^{III}((S,S)\text{-promp})H_2O]ClO_4$, (*S*,*S*)-**12**)

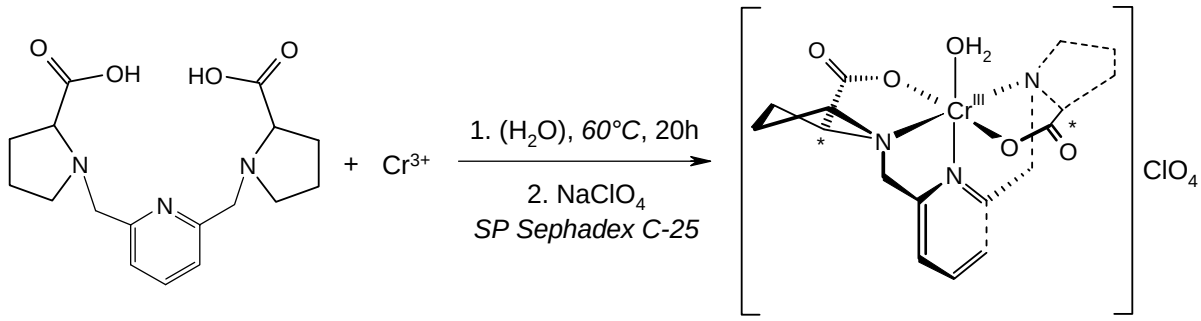

(*S*,*S*)-**2**	$KCr(SO_4)_2 \cdot 12H_2O$	(*S*,*S*)-**12**
$C_{17}H_{23}N_3O_4 \cdot xHCl$	$H_{24}CrS_2O_{20}$	$C_{17}H_{23}ClCrN_3O_9$
333.39 + x·36.45	499.40	500.83

According to a modified procedure described in [14].

H_2(S,S)-promp·2HCl (**2**, 16.2 g, 0.04 mol) and $KCr(SO_4)_2 \cdot 12H_2O$ (21.0 g, 0.042 mol, 1.05 eq.) were dissolved in water (250 mL). The solution was maintained at 60°C and pH 5 (by addition of NaOH 5M) as long as the intensity of the CD signal at 500 nm increased. The deep violet solution was concentrated nearly to dryness and part of excess chromium(III) was removed as hydroxide, precipitated by the addition of some methanol. The filtrate was diluted to 500 mL and fixed on a cation exchange column (*SP Sephadex C-25*, column length 30 cm; bed volume 700 mL; form Na^+). The resin was washed with $5 \cdot 10^{-4}$M acetic acid until the conductivity of the effluent was equal to that of the eluent. The [Cr(promp)OH] complex was eluted with 0.1M NH_3 whereas the residual Cr^{3+} remained fixed on the column. The concentrated fractions containing [Cr(promp)OH] were purified by ion exclusion chromatography

[1]) Due to the broad isotopic distribution within these signals and the low resolution of the mass spectrum, a tolerance of ± 1 Da·e^{-1} on the indicated maximum is admitted.

(*Sephadex G-10*, column length 130 cm; bed volume 2000 mL). The resulting red and blue bands, corresponding to $[Cr(promp)H_2O]^+$ and [Cr(promp)OH] were combined, acidified to pH 4 by diluted acidic and fixed again on a cation exchange column (*SP Sephadex C-25*, column length 30 cm; bed volume 300 mL; form Na^+). The resin was washed with $5\cdot10^{-4}$M acetic acid. The $[Cr(promp)\ H_2O]^+$ complex was eluted with 0.5% $NaClO_4$ acidified to pH 4 by 1% $HClO_4$. The concentrated fractions containing $[Cr(promp)H_2O]$ were neutralised and purified by ion exclusion chromatography. The salt-free fractions containing the aqua- and hydroxy-complex were concentrated and acidified to pH 4 by 1% $HClO_4$. After 7 days, dark violet plates crystallised from the solution at rt. **12** also crystallised from a hot concentrated solution in the form of needles.

UV (c=1.1·10^{-3}, 10^{-4}M HCl): 368 (110), 533 (205).

CD (c=1.1·10^{-3}, 10^{-4}M HCl): 372 (-1.51), 492 (+2.03), 638 (+0.829).

ORD (γ=0.12, 10^{-4}M HCl): 342 (+276), 396 (-933), 422 (-810), 460 (-981), 521 (+941), 579 (+44); $[\alpha]_{589}^{r.t.}$ = +45

IR (KBr): 2966*m* (sh, arC-H ν), 2941*w* (arC-H ν), 2886*m* (arC-H ν), 2030*vw* (sh), 1671*vs* (C=O ν), 1613*s* (br, sh, COO- ν as), 1483*m*, 1464*vw*, 1450*w* (sh), 1381*m* (br), 1343*m* (sh), 1312*m*, 1279*w*, 1268*vw*, 1238*vw*, 1217*w*, 1174*w*, 1110*vw*, 1094*vs*, 1056*vw*, 1023*vw*, 987*w*, 974*vw*, 959*vw*, 926*m*, 896*m*, 867*m* (sh), 832*m*, 793*m* (sh), 739*w*, 713*w*, 624*s*, 575*w*, 521*s* (sh), 488*w*, 460*s*, 434*s*.

ESI-MS (pos. mode, $M^+ = C_{17}H_{23}CrN_3O_5^+$**):** 802 (26, $2M^+$), 401 (100, M^+).

EA calc. for $C_{17}H_{23}ClCrN_3O_9$ (500.84): C 40.77, H 4.63, N 8.39, Cl 7.08; found: C 40.77, H 4.56, N 8.40, Cl 7.11.

Potentiometric titration ($c_0 = 4\cdot10^{-2}$M, 0.1M NaOH): **pK_a** =6.85, M_r = 502.9.

CV (c=10^{-3}, 0.1M KH_2PO_4/K_2HPO_4 buffer, -0.800 V to -1.420 V vs Ag/AgCl): pH 7.00: E_{pc} = -1.042 V ($i_{pc} = 1.32\cdot10^{-9}$ A), E_{pa} = -1.002 V ($i_{pa} = 1.40\cdot10^{-9}$ A); pH 8.03: E_{pc} = -1.092 V ($i_{pc} = 1.59\cdot10^{-9}$ A), E_{pa} = -1.042 V ($i_{pa} = 1.50\cdot10^{-9}$ A).

X-RAY: see §7.1.2

Λ-Hydroxy[2,6- bis[((1*R*,2*S*)-2-carboxypyrrolidin-1-yl)methyl]pyridine]chromium(III) ([Cr^{III}((*S*,*S*)-promp)OH]

UV (*c*=1.1·10^{-3}, NaOH/NaCl pH 8.2): 405 (88), 615 (150).

CD (*c*=1.1·10^{-3}, NaOH/NaCl pH 8.2): 400 (-0.61), 453 (+0.44), 538 (-0.83), 635 (-0.98).

ORD (*γ*=0.12, NaOH/NaCl pH 8.2): 317 (-373), 370 (+103), 425 (-516), 497 (+218), 574 (-1003); $[\alpha]^{r.t.}_{589}$ = -936

2.3.7 Λ-Chloro[2,6- bis[((1*R*,2*S*)-2-carboxypyrrolidin-1-yl)methyl]pyridine]chromium(III) ([Cr^{III}((*S*,*S*)-promp)Cl], (*S*,*S*)-**13**)

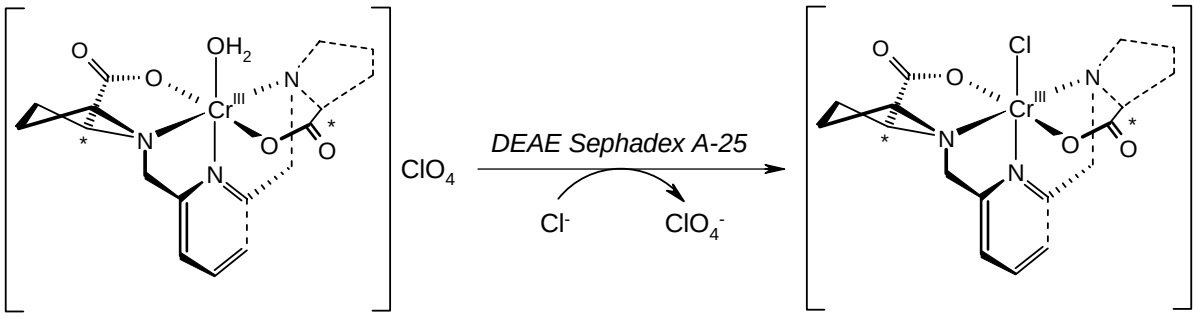

(*S*,*S*)-**12**
$C_{17}H_{23}ClCrN_3O_9$
500.83

(*S*,*S*)-**13**
$C_{17}H_{21}ClCrN_3O_4$
418.82

According to [4][15]

[Cr(promp)H_2O]ClO_4 0.025M (40 mL) was introduced into an anion exchanger column (DEAE Sephadex A-25, form Cl^-) and eluted with water. The effluent was evaporated to dryness and the solid residue left at 115°C for 24 hours. The initially dark red crystals became blue violet.

UV (*c*=2.8·10^{-3}, 10^{-4}M HCl): 381 (123), 558 (178).

CD (*c*=2.9·10^{-3}, H_2O): 385 (-0.56), 440 (-0.524), 535 (1.87), 595 (-0.253).

ORD (*γ*=0.12, H_2O): 360 (-64), 422 (-536, sh), 494 (-1238), 560 (983); $[\alpha]^{r.t.}_{589}$ = 409

EA calc. for $C_{17}H_{21}ClCrN_3O_4$ (418.82): C 48.75, H 5.05, N 10.03; found: C 48.65, H 5.02, N 9.51.

2.3.8 Optically pure 2,6- bis[4-carboxy-3-methyl-2-azabutyl]pyridine ((*R*,*R*)- and (*S*,*S*)-b3amp, (*R*,*R*)- and (*S*,*S*)-**3**)

2.3.8.1 (+/-)-3-Phthalimidobutyric acid (*rac*-**14**)

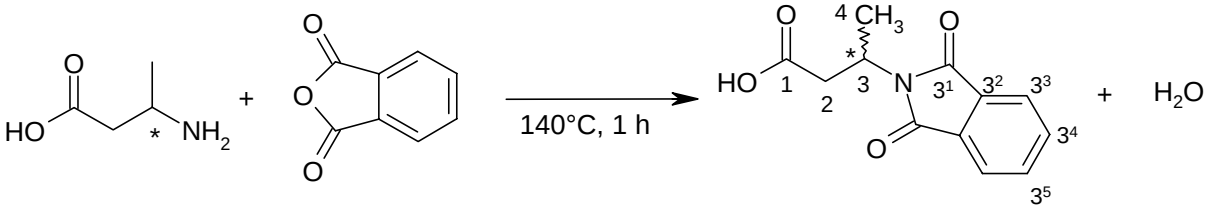

rac-**15**	**16**	*rac*-**14**
$C_4H_9NO_2$	$C_8H_4O_3$	$C_{12}H_{11}NO_4$
103.12	148.12	233.22

According to a modified procedure based on [16]

In a 500 mL two-necked flask provided with a reflux condenser and a magnetic stirrer, phthalic anhydride (**16**, 71.8 g, 0.485 mol) was introduced and covered by *rac*-3-aminobutyric acid (**15**, 50.0 g, 0.485 mol). The solid mixture was melted and stirred at 140°C for one hour. AcOEt (200 mL) was added to the hot melt through the reflux condenser under vigorous stirring. A white solid precipitated on cooling. The suspension was kept at 4°C during 12 hours, then the solid was filtered off and dried at 60°C. 85.0 g (75%) of **14** in the form of white powder were recovered. The mother liquor was heated and mixed with hexane (200 mL). On cooling, 6.2 g (6%) of more crystalline material precipitated. Both fractions were used in their raw form for further preparations. For exact characterisation, part of the solid was recrystallised in a AcOEt / hexane mixture.

TLC (AcOEt/Hexane 1:1 acidified with few AcOH): R_f 0.76 (UV_{254}-active, I_2 vapour : white on brownish background).

M.p. 120°C.

IR (KBr): 2937*w* (C-H ν), 1769*m* (C=O ν phthalimide), 1703*vs* (sh), 1466*w*, 1431*w*, 1397*s*, 1375*s*, 1306*m*, 1229*m*, 1190*vw*, 1142*w*, 1078*w*, 1026*w*, 901*vw*, 874*m*, 716*s*, 685*w*, 605*vw*, 534*w*.

^{1}H-NMR (400 MHz, $CDCl_3$): 7.83 (*dd*, ^{3}J=5.5, ^{4}J=3.0, 2 H, H-C(3^3, $3^{3'}$)), 7.71 (*dd*, ^{3}J=5.4, ^{4}J=3.1, 2 H, H-C(3^4, $3^{4'}$)), 4.84-4.75 (*m*, 1 H, H-C(3)), 3.22 (*dd*, ^{2}J=16.6, ^{3}J=8.6, 1 H, H_a-C(2)), 2.87 (*dd*, ^{2}J=16.6, ^{3}J=6.2, 1 H, H_b-C(2)), 1.50 (*d*, ^{3}J=7.0, 3 H, H_3C(4)).

^{13}C-NMR (100 MHz, $CDCl_3$, DEPT): 177.0 (*s*, C(1)), 168.5 (*s*, C(3^1, $3^{1'}$)), 134.45 (*d*, C(3^4, $3^{4'}$)), 132.2 (*s*, C(3^2, $3^{2'}$)), 123.7 (*d*, C(3^3, $3^{3'}$)), 43.6 (*d*, C(3)), 38.1 (*t*, C(2)), 19.2 (*q*, C(4)).

ESI-MS (pos. mode): 256 (100, $[M + Na]^+$).

2.3.8.2 (-)-(3*R*)-Phthalimidobutyric acid (1*R*)-phenylethylammonium salt ((*R*,*R*)-**17**)
(+)-(3*S*)-Phthalimidobutyric acid (1*S*)-phenylethylammonium salt ((*S*,*S*)-**17**)

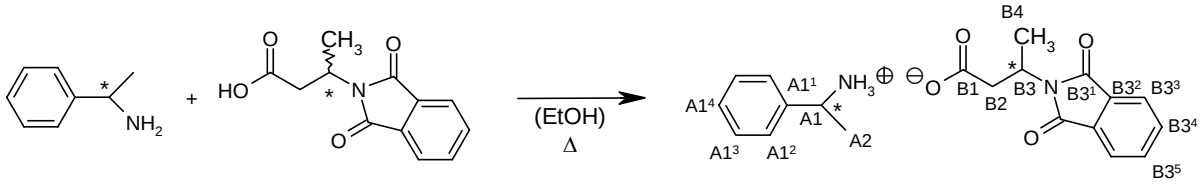

(*R*)-(+)- or (*S*)-(-)-18	*rac*-**14**	(*R*,*R*)-(-)- or (*S*,*S*)-(+)-**17**
$C_8H_{11}N$	$C_{12}H_{11}NO_4$	$C_{20}H_{22}N_2O_4$
121.18	233.22	354.40

Analogous procedure to [5]

In the given conditions, (3*R*)-(-)-phthalimidobutyrate ((*R*)-**14**) precipitates preferentially with (+)-(1*R*)-phenylethylammonium and ((*S*)-**14**) with the (-)-(1*S*) enantiomer.

A solution of **14** (14.0 g, 60.1 mmol) in EtOH (35 mL) was cooled to 0°C. (*R*)-(+)-1-phenylethylamine (**18**, 7.28 g (60.1 mmol) are added. The resulting suspension was heated until a homogeneous solution was obtained. It was left at room temperature during 12 h, then at 4°C during 24 h. The formed precipitate was filtered off, washed with Et_2O and dried over silica gel at reduced pressure during 12 h. 4.81 g (45%) of enriched (*R*,*R*)-(-)-**17** were obtained. Recrystallisation from EtOH yielded 1.65 g (16%) of more enriched (*R*,*R*)-(-)-**17**.

The mother liquor of the first crystallisation was concentrated and resulted in a viscous matter. After some days, white pellets crystallised. They were removed, washed with cold EtOH and recrystallised from hot EtOH.

The (*S*,*S*)-(+) enantiomer of **17** was isolated by adding a stoichiometric amount of (*S*)-(-)-**18** to the mother liquor of the first crystallisation.

(If not stated otherwise, the indicated physical data refers to the compound after the first crystallisation.)

M.p. 122°C.

UV (c=2.8·10^{-3}, H_2O): 299 (511)

IR (KBr): 2934*m* (C-H ν), 2667*m*, 2545*m* (N-H st.), 1775*m* (C=O ν phthalimide), 1747*m*, 1706*vs* (C=O ν carboxylate), 1618*m*, 1557*s*, 1530*s*, 1468*m*, 1458*m*, 1406*s* (sh), 1374*s*, 1366*s*, 1326*m*, 1232*w*, 1188*vw*, 1172*vw*, 1160*vw*, 1141*vw*, 1093*w*, 1074*w*, 1027*w*, 923*vw*, 906*w*, 873*m*, 798*vw*, 778*m*, 723*s*, 712*m*, 592*vw*, 549*w*, 532*m*, 501*w*, 489*w*, 438*vw*, 412*vw* (sh).

^{1}H-NMR (400 MHz, D_2O, COSY): 7.60 (*dd* coal. with 7.57 *dd* to *s* at 7.59, ^3J=3.3, ^4J=4.0, 2 H, H-C(B3^3, B3$^{3'}$)), 7.57 (*dd* coal. with 7.60 *dd* to *s* at 7.59, ^3J=3.3, ^4J=4.0, 2 H, H-C(3^4, 3$^{4'}$)), 7.34-7.26 (*m*, 5 H, H-C(A1^2, A1^3, A1^4, A1$^{2'}$, A1$^{3'}$)), 4.55-4.49 (*m*, 1 H, H-C(B3)), 4.38 (*q*, ^3J=6.9, 1 H, H-C(A1)), 2.68 (*dd*, ^2J=14.7, ^3J=8.5, 1 H, H_a-C(B2)), 2.53 (*dd*, ^2J=14.7, ^3J=7.1, 1 H, H_b-C(B2)), 1.50 (*d*, ^3J=6.9, 3 H, H_3C(A2)), 1.29 (*d*, ^3J=7.0, 3 H, H_3C(B4)).

^{13}C-NMR (100 MHz, D_2O, DEPT): 179.6 (*s*, C(B1)), 170.6 (*s*, C(B3^1, B3$^{1'}$)), 138.0 (*s*, C(A1^1)), 134.5 (*d*, arom. C), 132.2 (*s*, C(B3^2, B3$^{2'}$)), 129.6 (*d*, arom. C), 129.5 (*d*, arom. C), 126.8 (*d*, arom. C), 123.4 (*d*, arom. C), 51.3 (*d*, C(A1)), 45.6 (*d*, C(B3)), 41.9 (*t*, C(B2)), 19.6 (*q*, C(B4)), 18.0 (*q*, C(A2)).

ESI-MS (pos. mode, M_A^+ = $C_8H_{12}N^+$, M_B^- = $C_{12}H_{10}NO_4^-$**):** 256 (45, [M_BH + Na]$^+$, 122 (100, M_A^+). **ESI-MS (neg. mode**, M_B^- = $C_{12}H_{11}NO_4^-$**):** 232 (100, M_B^-).

As the enantiomeric enrichment per crystallisation step is relatively weak, further separation of both enantiomers has been accomplished by using quinine, respectively brucine instead of phenylethylamine as precipitation reagent (see §2.3.8.3 to §2.3.8.6)

2.3.8.3 (-)-(3*S*)-Phthalimidobutyric acid (-)-quininium salt ((A9*R*,B3*S*)-(-)-**19**)

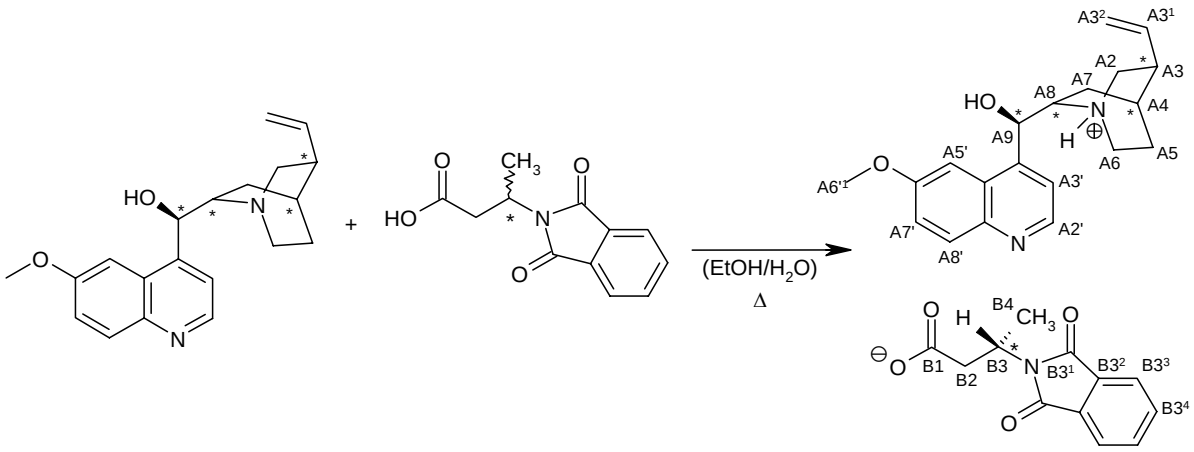

20	*rac*-**14**	(A9*R*,B3*S*)-(-)-**19**
$C_{20}H_{24}N_2O_2$	$C_{12}H_{11}NO_4$	$C_{32}H_{35}N_3O_6$
324.42	233.22	557.64

Procedure based on [4] and [5]

An equimolar mixture of both compounds was dissolved in ethanol. Water was added until the solution became turbid then the latter was heated until it became clear again. After a few days, white to slightly brownish flakes containing mainly (A9*R*,B3*S*)-(-)-**19** precipitated whereas the mother liquor contained mainly the (*R*)-(-)-phthalimidobutyrate anion.

The precipitation could be strongly accelerated by adding existing crystals of **19**: Enriched (*S*)-(+)-**14** (66 g, 0.283 mol) and optical pure quinine (**20**, 91.9 g, 0.283 mol) were suspended in EtOH (400 mL) and stirred at 30°C until a clear solution resulted. Water at 30°C (400 mL) was added slowly while stirring. Some crystals of optically enriched (A9*R*,B3*S*)-(-)-**19** were added to the lukewarm solution. On cooling, white flakes precipitated. After cooling at 4°C overnight, the solid was filtered off and, in order to determine its specific rotation, a small sample was dried at 30°C and under reduced pressure until its mass remained constant. The remainder of the solid was taken up in ethanol (300 mL) and stirred at 30°C until a clear solution resulted. Water at 30°C (300 mL) was added slowly while stirring. Some crystals of optically enriched (A9*R*,B3*S*)-(-)-**19** were added to the lukewarm solution. The recrystallisation was repeated until the specific rotation remained constant (in general one recrystallisation was sufficient). The solid was filtered off and dried at 50°C for 15 hours. Yield: 74.2 g (47%) of white crystals.

The mother liquor of the first crystallisation, containing optically enriched (*R*)-(-)-phthalimidobutyrate and those of the recrystallisations were concentrated separately to dryness. The resulting yellow viscous matter was separately decomposed according to §2.3.8.4. The recrystallised solid, containing highly enriched (+)-phthalimidobutyrate, was also decomposed according to §2.3.8.4.

$[\alpha]_{\lambda}^{r.t.}$, UV and CD were measured with the diasteroisomeric salt prepared from highly enriched (+)-**14**, the other data was collected with diasteroisomeric salt prepared from slightly enriched (+)-**14**.

$[\alpha]_{\lambda}^{r.t.}$ (γ=0.33, EtOH): - 581_{365}, -230_{436}, -113_{546}, -96_{578}.

UV (EtOH[1])): 281, 289, 320, 333.

CD (c=10^{-4}M, EtOH): 334 (-24).

IR (KBr): 2974*w* (C-H ν), 2940*w* (C-H ν), 1773*w* (C=O ν phthalimide), 1710*vs* (sh, C=O ν phthalimide), 1621*m* (sh, C=O ν carboxylate), 1591*m* (C=C ν, 1554*m* (br., -N^+H δ), 1510*m* (br., -N^+H δ), 1471*w*, 1455*w*, 1430*w*, 1395*s*, 1366*s*, 1331*s* (sh), 1241*m*, 1227*m*, 1187*vw*, 1173*vw*, 1128*w* (sh.), 1095*w*, 1080*w*, 1033*m*, 1008*vw*, 985*vw*, 932*w*, 917*vw*, 876*w*, 859*w*, 830*w*, 806*vw*, 721*s* (sh.), 700*vw* (sh.), 664*vw*, 645*w*, 622*vw*, 532*w*.

^{1}H-NMR (400 MHz, $CDCl_3$, COSY): 8.66 (*d*, ^3J=4.5, 1 H, H-C(A2')), 7.80 (*d*, ^3J=9.2, 1 H, H-C(A2')), 7.73 (*dd*, ^3J=5.4, ^4J=3.1, 1.5 H, 75% of H-C($B3^3$, $B3^{3'}$)), 7.61 (*dd*, ^3J=8.2, ^4J=2.7, 75% of H-C($B3^4$, $B3^{4'}$)), 7.61 (*d*, ^3J=5.4, 1 H, H-C(A3')), 7.46 (*dd*, ^3J=5.4, ^4J=3.0, 0.5 H, 25% of H-C($B3^3$, $B3^{3'}$)), 7.30 (*dd*, ^3J=5.5, ^4J=3.0, 0.6 H, 25% of H-C($B3^4$, $B3^{4'}$)), 7.12 (*dd*, ^3J=9.2, ^4J=2.6, 1 H, H-C(A7')), 6.87 (*d*, ^3J=6.9, 1 H, H-C(A5')), 7.90-6.20[2]) (*s*, 1 H, NH^+), 5.56-5.47 (*m*, 1 H, H-C($A3^1$)), 5.00-4.94 (*m*, H_{trans}-C($A3^2$)) overlapped with 4.96 (*dd*, ^2J=1.0, ^3J=2.6, H_{cis}-C($A3^2$)), totally 2 H, 4.88-4.81 (*m*, 1 H, H-C(B3)), 4.27-4.22 (*m*, 1 H, H-C(A8)), 3.31 (*dd*, ^2J=13.5, ^3J=10.6, H_a-C(A2)), 3.26-3.21 (*m*, 1 H, H_a-C(A6)), 3.06 (*dd*, ^2J=14.8, ^3J=9.7,

[1]) exact concentration unknown

[2]) very broad singlet, overlapped with the eight preceding signals.

0.25 H, 25% of H_a-C(B2)), 3.02-2.92 (*m*, H_a-C(B2), H_b-C(A2), HC(A4, A9)) overlapped with 2.94 (*dd*, ^2J=15.0, ^3J=8.4, 75% of H_a-C(B2)), totally 3 H^{14}), 2.76 (*dd*, ^2J=15.0, ^3J=6.6, 0.75 H, 75% of H_b-C(B2)), 2.66 (*dd*, ^2J=14.8, ^3J=5.4, 0.25 H, H_b-C(B2)), 2.61-2.52 (*m*, 1 H, HC(A3)), 2.18-2.10 (*m*, 1 H, H_a-C(A7)), 2.04-1.99 (*m*, 2 H, H_a-C(A5), H_b-C(A6)), 1.77-1.73 (*m*, 1 H, H_b-C(A7)), 1.53 (*d*, ^3J=6.9, 3 H, H_3C(B4)), 1.22-1.15 (*m*, 1 H, H_b-C(A5)).

^{13}C-NMR (100 MHz, $CDCl_3$, DEPT, HETCOR SR): 176.9 (*s*, C(B1)), 168.8 (*s*, C($A11^1$, $B3^1$, $B3^{1'}$)), 150.1 (*s*, C(A22)), 147.0 (*s*, C(A20)), 138.0 (*s*, C($A1^1$)), 134.5 (*d*, arom. C), 132.2 (*s*, C($B3^2$, $B3^{2'}$)), 129.6 (*d*, arom. C), 129.5 (*d*, arom. C), 126.8 (*d*, arom. C), 123.4 (*d*, arom. C), 51.3 (*d*, C(A1)), 45.6 (*d*, C(B3)), 41.9 (*t*, C(B2)), 19.6 (*q*, C(B4)), 18.0 (*q*, C(A2)).

ESI-MS (pos. mode, M_A^+ = $C_{20}H_{25}N_2O_2^+$**):** 325 (100, M_A^+). **ESI-MS (neg. mode**, M_B^- = $C_{12}H_{10}NO_4^-$**):** 556 (92, $[M_{AB} - H^+]^-$), 232.0 (100, M_B^-), 146 (34, $C_8H_4NO_2^-$).

2.3.8.4 Optically enriched 3-phthalimidobutyric acid ((*S*)-(+)-or (*R*)-(-)-**14**)

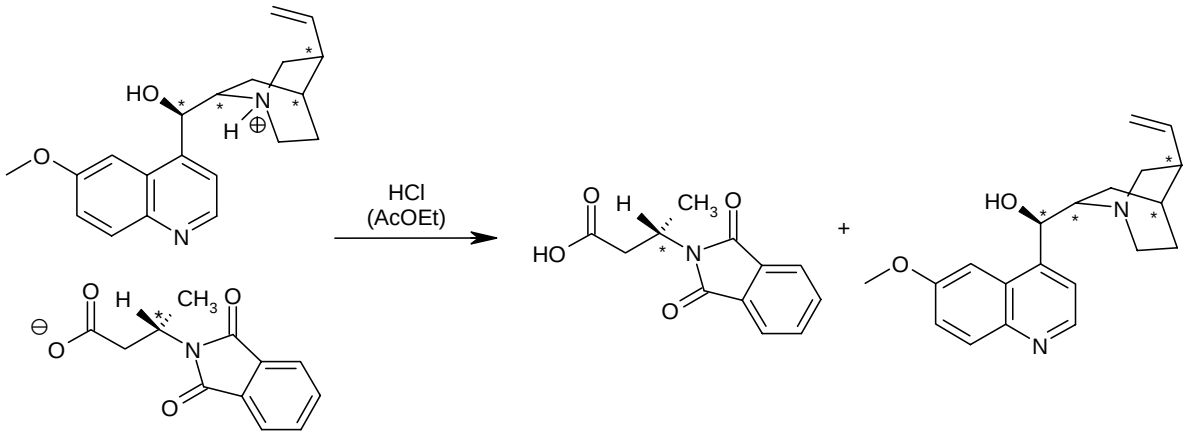

"(-,+)- or (-,-)-**19**"	(*S*)-(+)- or (*R*)-(-)-**14**	(-)-**20**
$C_{32}H_{35}N_3O_6$	$C_{12}H_{11}NO_4$	$C_{20}H_{24}N_2O_2$
557.65	233.22	324.42

According to a modified [4] procedure based on [5]

Optically enriched crystalline (-,+)-**19** (81.6 g, 0.146 mol), AcOEt (300 mL) and 2M HCl (200 mL) were intensely mixed. The aqueous phase was extracted three times with AcOEt (250 mL) and conserved for the quinine recovery (see below). All organic phases were unified, concentrated to 300 mL and washed three times with 1M HCl (200 mL). The solvent was removed and the residue dried at 80°C and reduced pressure until the gas evolution ceased.

35.3 g ("103%") of brownish viscous oil were obtained. It was dissolved in AcOEt (100 mL) and heated to boiling. Hexane (200 mL) and some crushed crystals of *rac*-**14** were added. On cooling, a white crystalline precipitate formed. Isolation, washing with hexane and drying at reduced pressure yielded 8.6 g (25%) of very slightly enriched (*S*)-(+)-**14** (3% *e.e.*[1])). The mother liquor was cooled to 20°C and yielded 11.2 g (33%) of highly enriched (*S*)-(+)-**14** (95% *e.e.*). By gradual increase of the hexane concentration in the mother liquor, other fractions of enriched **14** precipitated: 4.7 g (14%) with 94% *e.e.*[10]) and 3.0 g (9%) with 89% *e.e.*[10]). The remainder of the mother liquor was evaporated to dryness and yielded 4.7 g (14%) of a light brown oil, containing (+)-**14** with 87% *e.e.*[10]). The fractions whose *e.e.* were higher than 85% were combined and purified a second time according to §2.3.8.3 and §2.3.8.4. Finally, 13.1 g (39%) of white crystalline (*S*)-(+)-**14** with 99% *e.e.*) were obtained.

The treatment of viscous (-,-)-**19** (0.0726 mol) was performed in the same way and yielded 1.8 g (11 %) of crystalline (*R*)-(-)-**14** with 12% *e.e.* and 12.5 g (74%) of viscous oil containing (*R*)-(-)-**14** with 75% *e.e.*). The e.e. value of this compound was increased by the method described in § 2.3.8.5.

The analysis data was collected from the most highly enriched fractions.

Quinine recovery

The combined HCl-containing aqueous phases were heated to 40°C. 2M NaOH was added under vigorous stirring until a very slight but persisting precipitate formed (the pH was at about 6). On cooling to 4°C, more white quinine precipitated. It was filtered off, washed with water and dried at 40°C under reduced pressure. The mother liquor was strongly alkalinised and allowed to cool. After filtering, the solid residue was washed with water and dissolved in 50 mL 1M HCl. The solution was cooled to 4°C. NaOH 2M was added under vigorous stirring until strong alkalinity. The precipitated light brownish quinine of lower melting point was filtered off, washed with water and dried at 40°C under reduced pressure. It was used to precipitate **19**

[1]) All e.e. were calculated with respect to a theoretical $[\alpha]_{436}$ value of +/- 48.5°·dm^{-1}. (a value of -48.5°·dm^{-1} was found for the most enriched fraction of the corresponding (-)- (*R*)-**14** obtained according to § 2.3.8.6).

from racemic phthalimidobutyric acid whereas white quinine was used to precipitate **19** from enriched phthalimidobutyric acid.

(*S*)-(+)-3-phthalimidobutyric acid ((*S*)-(+)-14)

$[\alpha]_{\lambda}^{r.t.}$ (γ=1.1, H_2O): $+114_{365}$, $+47.8_{436}$, $+23.6_{546}$, $+20.3_{578}$.

2.3.8.5 (3*R*)-(-)-Phthalimidobutyric acid brucinium salt (A2*R*,A3*S*,A15*S*)-(-)-**21**)

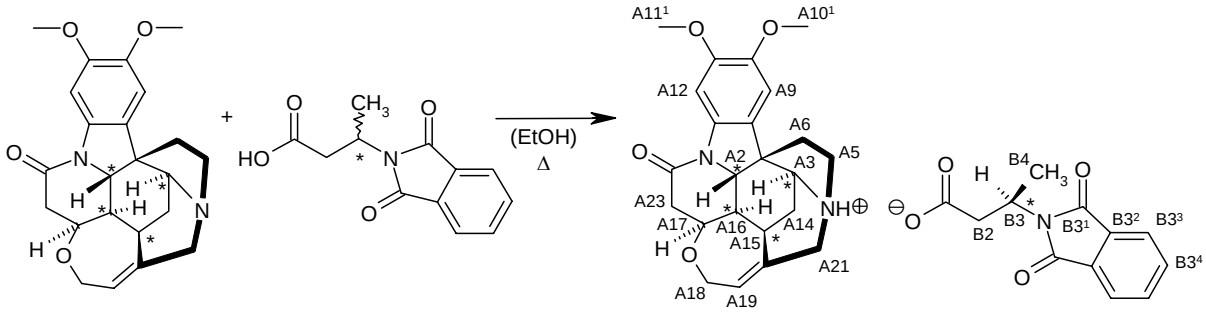

(+)-**22**	*rac*-**14**	(A2*R*,A3*S*,A15*S*)-(-)-**21**
$C_{23}H_{26}N_2O_4$	$C_{12}H_{11}NO_4$	$C_{35}H_{37}N_3O_8$
394.47	233.22	627.70

Synthesis performed by K. Bernauer according to a modified [4] procedure based on [5]

Brucine (4.66 g, 0.01 mol) was dissolved in hot ethanol (25 mL) and added to a stoichiometric amount of 3-phthalimidobutyric acid in ethanol (10 mL). The crystallisation was initiated by some crystals of enriched (A2*R*, A3*S*, A15*S*)-(-)-**21**, the solution cooled to r.t. and then was left at 4°C overnight. The solid was filtered off and washed with cold ethanol. Yield: 3.58 g (58%). After determination of the specific rotation, the salt was recrystallised in hot ethanol (about 10 mL for 2 g) until the specific rotation was constant. Yield: 1.95 g (31%), yellowish powder.

M.p., $[\alpha]_{\lambda}^{r.t.}$, UV and CD were measured with the diastereoisomeric salt prepared from highly enriched (+)-**14**, the other data was collected with diastereoisomeric salt prepared from slightly enriched (+)-**14**.

$[\alpha]_{\lambda}^{r.t.}$ (γ=0.44, EtOH): -240_{365}, -116_{436}, -56.7_{546}, -47.5_{578}.

IR (KBr): 3055*w*, 2975*vw*, 2961*vw*, 2940*w*, 2904*w*, 2867*w*, 2848*w*, 1770*m*, 1704*vs* (C=O ν), 1658*vs* (sh, C=O ν), 1503*vs*, 1452*s*, 1421*w*, 1412*w*, 1375*m*, 1351*w*, 1335*w*, 1311*w*, 1297*w*, 1288*m* (sh), 1248*vw* (doublet), 1221*m*, 1200*m* (sh), 1139*vw*, 1116*s* (sh), 1083*m*, 1057*w*, 1047*vw*, 1028*m*, 1012*m*, 990*w*, 967*w*, 951*w* (sh), 917*m* (sh), 880*m*, 863*vw*, 850*w*, 821*vw* (sh), 790*w* (sh), 772*m*, 753*w*, 721*s* (sh), 683*w* (sh), 649*w*, 628*vw*, 609*m*, 594*w*, 549*m*, 532*w*, 517*w*, 486*vw*, 469*w*, 441*w*, 427*w*, 403*w*.

^{1}H-NMR (400 MHz, $CDCl_3$, COSY, D_2O exchange): 7.79 (*s*, 1 H, H-C(A9)), 7.78 (*dd*, ^{3}J=5.7, ^{4}J=2.6, 2 H, H-C(B3^{3}, B3$^{3'}$)), 7.66 (*dd*, ^{3}J=5.4, ^{4}J=3.1, H-C(B3^{4}, B3$^{4'}$)), 6.90 (*s*, 1 H, H-C(A12)), 6.75-6.15 (br. *s*, 1 H, NH^{+}), 6.10 (*t*, ^{3}J=6.4, 1 H, H-C(A19)), 4.88-4.82 (*m*, 1 H, H-C(B3)), 4.30 (*dt*, ^{3}J=8.5, 3.2, 1 H, H-C(A17)), 4.18 (*dd*, ^{2}J=14.0, ^{3}J=7.0, 1 H, H_a-C(A18)), 4.17-4.12 (*m*, 1 H, H-C(A3)), 4.06 (*dd*, ^{2}J=13.6, ^{3}J=5.7, 1 H, H_b-C(A18)), 3.91 (*s*, 3 H, H_3C(A10^{1} or A11^{1})), 3.90-3.84 (*m*, H-C(A2)) overlapped with 3.90 (*s*, 3 H, H_3C(A10^{1} or A11^{1})) and 3.71 (*dd*, ^{2}J=15.0, ^{3}J=4.6, H_a-C(A21)), totally 5 H; 3.44 (*dd*, ^{2}J=11.0, ^{3}J=7.4, 1 H, H_a-C(A5)), 3.22-3.17 (*m*, -C(A2)), 3.12 (*dd*, ^{2}J=17.6, ^{3}J=8.5, 1 H, H_a-C(A23)), 3.03 (*dd*, ^{2}J=14.9, ^{3}J=9.1, 1 H, H_a-C(B2)), 2.93-2.85 (*m*, H_b-C(A5, A21)), 2.73 (*dd*, ^{2}J=14.9, ^{3}J=5.9, 1 H, H_b-C(B2)), 2.65 (*dd*, ^{2}J=17.5, ^{3}J=3.2, 1 H, H_b-C(A23)), 1.95 (*dd*, ^{2}J=13.0, ^{3}J=7.5, 1 H, H_a-C(A6)), 1.86 (*dd*, ^{2}J=13.1, ^{3}J=6.2, 1 H, H_b-C(A6)), 2.32 (*dt*, ^{3}J=14.8, 4.3, 1 H, H_a-C(A14)), 1.55 (*d*, ^{3}J=7.0, 3 H, H_3C(B4)), 1.48 (*d*, ^{2}J=14.9, 1 H, H_b-C(A14)), 1.31 (*dt*, ^{3}J=10.5, 3.1, 1 H, H_a-C(A16)).

^{13}C-NMR (100 MHz, $CDCl_3$, DEPT, HETCOR SR): 176.9 (*s*, C(B1)), 169.1 (*s*, C(B3^{1} or B3$^{1'}$)), 168.8 (*s*, C(B3^{1} or B3$^{1'}$)), 150.1 (*s*, C(A22))[1]), 147.0 (*s*, C(A20)[1])), 137.0 (*s*, C(A8)[1])), 136.0 (*s*, C(A7, A11)[1])), 134.1 (*d*, C(B3^{4}, B3$^{4'}$)), 132.6 (*s*, C(B3^{2}, B3$^{2'}$)), 132.1 (*d*, C(A19)), 123.3 (*d*, C(B3^{3}, B3$^{3'}$)), 121.6 (*s*, C(A10)), 105.9 (*d*, C(A12)), 101.2 (*d*, C(A9)), 78.0 (*d*, C(A17)), 64.7 (*t*, C(A18)), 59.5 (*d*, C(A3)), 57.0 (*q*, C(A10^{1} or A11^{1})) and 56.6 (*q*, C(A10^{1} or A11^{1})), 52.5 (*s*, C(A4)), 51.9 (*t*, C(A21)), 49.7 (*t*, C(A5)), 48.1 (*d*, C(A16)), 45.3 (*d*, C(A12)), 42.6 (*t*, C(A23)), 41.7 (*t*, C(A6)), 40.8 (*t*, C(B2)), 31.4 (*d*, C(A15)), 26.3 (*t*, C(A14)), 19.3 (*q*, C(B4)).

[1]) Uncertain assignment.

ESI-MS (pos. mode, M_A^+ = $C_{23}H_{27}N_2O_4^+$**):** 395 (100, M_A^+). **ESI-MS (neg. mode**, M_B^- = $C_{12}H_{11}NO_4^-$**):** 232 (100, M_B^-).

2.3.8.6 (*R*)-(-)-3-Phthalimidobutyric acid ((-)-**14**)

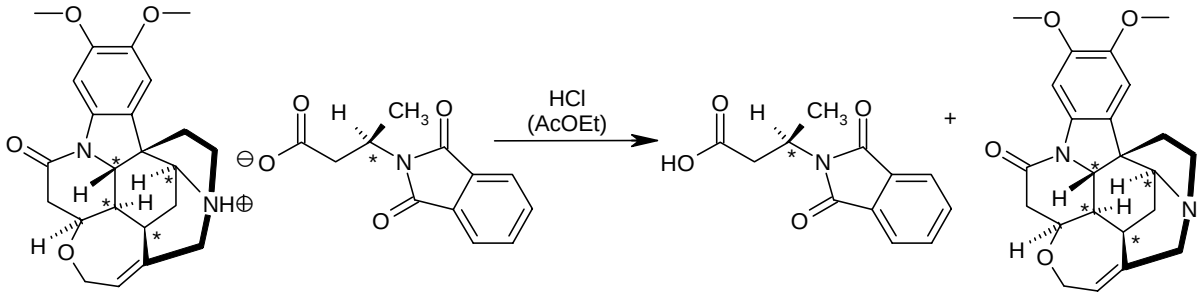

(A2*R*, A3*S*, A15*S*)-(-)-**21**	(*R*)-(-)-**14**	**22**
$C_{35}H_{37}N_3O_8$	$C_{12}H_{11}NO_4$	$C_{23}H_{26}N_2O_4$
627.70	233.22	394.46

Synthesis performed by K. Bernauer according to a modified [4] procedure based on [5]

A solution of A2*R*, A3*S*, A15*S*)-(-)-**21** (4.0 g, 6.4 mmol) and NaCl (2 g) in water (500 mL) was acidified to pH 2 by 2M HCl and extracted three times with AcOEt (50 mL). All organic phases were combined and washed two times with 0.2M HCl (40 mL) and two times with water (50 mL). The solution was concentrated to dryness.

Yield: 1.43 g (96%), colourless crystalline solid.

M.p., $[\alpha]_\lambda^{r.t.}$, UV and CD were measured with the most highly enriched (+)-**14**, the other data was collected with diastereoisomeric salt prepared from slightly enriched (+)-**14**.

$[\alpha]_\lambda^{r.t.}$ (γ=0.14, H_2O): -118_{365}, -48.5_{436}, -16.9_{546}, -15.4_{578}.

2.3.8.7 Optically enriched 3-aminobutyric acid ((*S*)-(+)-or (*R*)-(-)-**15**)

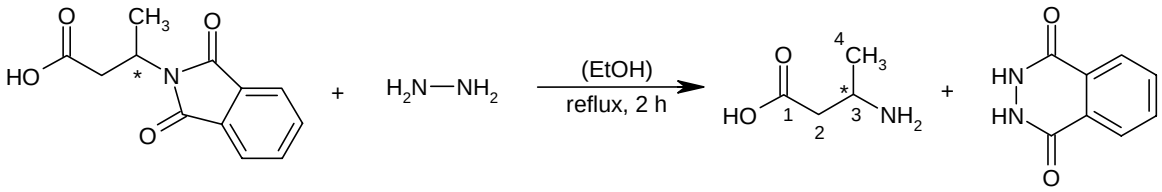

(*R*)-(-)- or (*S*)-(+)-**14**	$(H_2N)_2 \cdot H_2O$	(*R*)-(-)- or (*S*)-(+)-**15**	
$C_{12}H_{11}NO_4$	H_6N_2O	$C_4H_9NO_2$	$C_8H_6N_2O_2$
233.22	50.06	103.12	162.15

According to [5]

In a 1 L three-necked flask provided with a dropping funnel, a reflux condenser and a magnetic stirrer, **14** (13.12 g, 0.0563 mol) in EtOH (400 mL) was heated to the boil. Hydrazine hydrate (3.70 g, 0.0731 mol, 1.3 eq.) in EtOH (50 mL) was added slowly. After refluxing the solution during 2 h, white phthaloyl hydrazide precipitated. The suspension was allowed to cool to r.t. H_2O (200 mL) was added and the pH was adjusted to 5 by conc. AcOH. The solid was removed by filtration and the filtrate was concentrated to 10 mL. The formed white precipitate was filtered off and the filtrate evaporated to dryness. The resulting amorphous solid was recrystallised in a EtOH / H_2O mixture.

(*S*)-(+)-3-aminobutyric acid ((*S*)-(+)-**15**)

TLC (BuOH/AcOH/H_2O 12:6:5): R_f 0.50 (UV_{254}-active, ninhydrine: red).

$[\alpha]_\lambda^{r.t.}$ (γ=1.004, H_2O): $+115_{365}$, $+73.0_{436}$, $+42.7_{546}$, $+37.5_{578}$, $+36.1_{589}$.

IR (KBr): 3045*s* (sh), 2979*w*, 2948*w*, 2886*vw*, 2818*vw*, 2770*vw* (sh), 2623*vw* (sh), 2516*w*, 2177*m* (sh, N-H st.), 1641*s* (sh, C=O ν), 1579*vs* (sh, C=O ν), 1515*vw*, 1441*m*, 1413*vs*, 1389*vw*, 1376*vw*, 1353*w*, 1287*m*, 1267*m*, 1212*m*, 1142*m*, 1122*w*, 1020*m*, 1006*vw*, 973vw, 937m, 914*m*, 841*w*, 750*s* (sh), 650*s*, 541*w*, 475*m*, 448*vw*, 425*m*.

^{1}H-NMR (400 MHz, $CDCl_3$): 3.48 (*sext.*, ^3J=6.6, 1 H, H-C(3)), 2.35-2.37 (*m*, 2 H, $H_2C(2)$), 1.18 (*d*, ^3J=6.7, 3 H, $H_3C(4)$).

^{13}C-NMR (100 MHz, $CDCl_3$, DEPT): 178.4 (*s*, C(1)), 45.7 (*d*, C(3)), 41.0 (*t*, C(2)), 18.0 (*q*, C(4)).

2.3.9 2,6-bis[(*R*)-3-carboxymethyl-2-azabutyl]pyridine ((*R*,*R*)-b3amp, (*R*,*R*)-**3**))
2,6-bis[(*S*)-3-carboxymethyl-2-azabutyl]pyridine ((*S*,*S*)-b3amp, (*S*,*S*)-**3**))

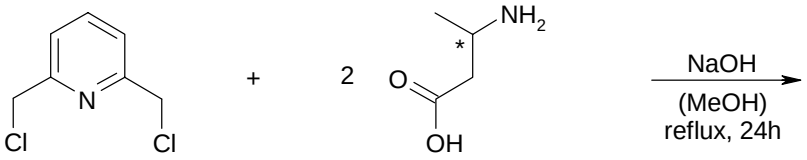

4 (*R*)-(-)- or (*S*)-(+)-**15**

$C_7H_7Cl_2N$ $C_4H_9NO_2$ HNaO

176.04 103.12 40.00

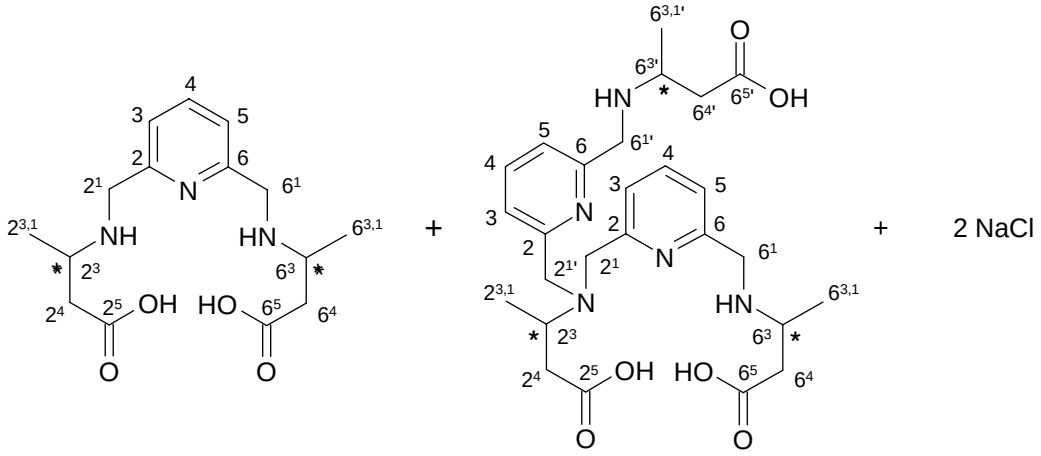

(*R*,*R*)-(-)- or (*S*,*S*)-(+)-**3** (*R*)-(-)- or (*S*)-(+)-**23**

$C_{15}H_{23}N_3O_4$ $C_{26}H_{37}N_5O_6$

309.36 515.60

According to a modified procedure based on [1] and [4]

In a 100 mL three-necked flask provided with a dropping funnel, a reflux condenser and a magnetic stirrer, (*S*)-(+)-**15** (3.09 g, 0.06 mol, 4 eq.) were added by portions to a solution of sodium hydroxide (3.0 g, 0.075 mol, 5 eq.) in methanol (50 mL). 2,6-bis[chloromethyl]pyridine (2.6 g, 0.015 mol) in methanol (30 mL) and some drops of a methanolic solution of phenolphthalein were added slowly under vigorous stirring. The mixture was refluxed during 24 hours and maintained basic by addition of 3M NaOH solution; then it was cooled to room temperature and neutralised by 16% HCl. The precipitated NaCl was removed by filtration and the filtrate evaporated under vacuum to dryness.

The resulting solid was dissolved in water (300 mL), acidified to pH 3 by 2M HCl. The solution was introduced into a cation exchange column (*Dowex-50x8*, 200-400 mesh, column length 17 cm; bed volume 30 mL; form H^+). The resin was washed with water (200 mL) and the product eluted with 0.05M NaOH. The effluent was fractionated and the fractions were analysed by TLC (SiO_2, BuOH:AcOH:H_2O 12:6:5, UV^{254}/ninhydrin). The fractions containing an excess of free amino acid were evaporated to dryness; those containing the b3amp isomers were unified, evaporated to dryness and purified by flash chromatography (50g *SiO_2*, 30-60 µm, column length 8 cm; bed volume 100 mL) with BuOH:AcOH:H_2O 12:6:5 as mobile phase. The fractions containing only **3** (and traces of **23**) were united, evaporated to dryness and then redissolved in water. In order to remove the remaining acetic acid, the solution was introduced in a cation exchange column (*Dowex-50x8*, 200-400 mesh, column length 15 cm; bed volume 12 mL; form H^+). The resin was washed with water (200 mL) and the product was eluted with 0.05M NaOH. The fractions containing **3** were evaporated to dryness. Yield: 0.92 g (40%) of **14** as brownish film.

2,6- bis[4-carboxy-3-(S)-methyl-2-azabutyl]pyridine ((*S*,*S*)-b3amp, (*S*,*S*)-3))

TLC (BuOH/AcOH/H_2O 12:6:5): R_f 0.18 (UV_{254}-active, ninhydrine: sl. yellow).

IR (KBr): 3200*m* (C-H ν), 3159*w* (C-H ν), 3051*m*, 2989*vw*, 2946*m*, 2911*vw*, 2848*vw* (br), 2734vw (sh), 2693*w*, 2658*w* (doublet), 2587*w* (sh), 2469*m*, 2422*w*, 1725*vw* (C=O ν), 1718*vs* (C=O ν), 1675*vs* (sh, C=O ν), 1598*m* (sh), 1589*vw*, 1580*vw*, 1449*vs* (sh), 1425*w*, 1407*vs*, 1388*m*, 1348*vw*, 1330*vw*, 1309*s* (sh), 1267*m*, 1225*m* (sh), 1194*vs*, 1182*vw*, 1154*m*, 1127*vw*, 1093*w*, 1082*m*, 1034*w*, 1019*w* (sh), 999*s*, 967*vw*, 954*w*, 945*w*, 900*vw*, 883*m*, 865*w*, 844*w*, 817*m*, 746*w*, 737*w*, 670*m* (sh), 600*w* (sh), 556*w*, 520*vw*, 490*w*, 473*m*, 428*m*, 406*m*.

^{1}H-NMR (400 MHz, $CDCl_3$): 7.70 (*t*, ^3J=7.6, 1 H, H-C(4)), 7.23 (*d*, ^3J=7.6, 2 H, H-C(3, 5)), 3.98 (*d*, ^2J=14.3, 2 H, H_a-C(2^1, 6^1)), 3.93 (*d*, ^2J=14.3, 2 H, H_b-C(2^1, 6^1)), 3.13-3.20 (*m*, 2 H, H-C(2^3, 6^3)), 2.40 (*dd*, ^2J=14.9, ^3J=6.2, 2 H, H_a-C(2^4, 6^4)), 2.18 (*dd*, ^2J=14.9, 2 H, H_b-C(2^4, 6^4)), 1.09 (*d*, ^3J=6.2, 6 H, H_3C($2^{3,1}$, $6^{3,1}$)).

^{13}C-NMR (100 MHz, $CDCl_3$, DEPT): 180.1 (*s*, C(2^5, 6^5)), 155.5 (*s*, C(2, 6)), 139.1 (*d*, C(4)), 122.5 (*s*, C(3, 5)), 51.3 (*d*, C(2^3, 6^3)), 49.8 (*t*, C(2^1, 6^1)), 42.7 (*t*, C(2^4, 6^4)), 18.1 (*q*, C($2^{3,1}$, $6^{3,1}$)).

ESI-MS (positive mode): 332 (9, $[M + Na]^+$), 310 (100, MH^+), 292[1]) (7, $[MH - H_2O]^+$), 250[1]) (100, $[MH - C_2H_2O - H_2O]^+$).

2-((3*S*)-N-(2'-(6'-((3"*S*)-3"-carboxymethyl-2"-azabutyl)pyridyl)methyl)-3-carboxymethyl-2-azabutyl)-6-((3*S*)-3-carboxymethyl-2-azabutyl)pyridine ((*S*,*S*,*S*)-23))

TLC (BuOH/AcOH/H2O 12:6:5): R_f 0.04 (UV_{254}-active, ninhydrine: sl. yellow).

^{1}H-NMR (400 MHz, $CDCl_3$): 7.46 (*t*, ^3J=7.7, 2 H, H-C(4, 4')), 7.17 (*d*, ^3J=7.9, 2 H, H-C(3, 3')), 6.98 (*d*, ^3J=7.6, 2 H, H-C(5, 5')), 3.66 (*s*, 4 H, $H_2C(2^1, 2^{1\prime})$), 3.57 (*s*, 4 H, $H_2C(6^1, 6^{1\prime})$), 3.31-3.23 (*m*, 1 H, H-C(2^3)), 2.93-2.87 (*m*, 2 H, H-C(6^3, $6^{3\prime}$)), 2.53 (*dd*, ^2J=13.3, ^3J=5.9, 1 H, H_a-C(2^4)), 2.37 (*dd*, ^2J=14.0, ^3J=5.5, 2 H, H_a-C(6^4, $6^{4\prime}$)), 2.13 (*dd*, ^2J=13.4, ^3J=8.5, 1 H, H_b-C(2^4)), 1.99 (*dd*, ^2J=13.9, ^3J=8.3, 2 H, H_b-C(6^4, $6^{4\prime}$)), 1.07 (*d*, ^3J=6.3, 3 H, $H_3C(2^{3,1})$), 0.97 (*d*, ^3J=6.1, 6 H, $H_3C(6^{3,1}, 6^{3,1\prime})$).

^{13}C-NMR (100 MHz, $CDCl_3$, DEPT, HETCOR SR): 182.0 (*s*, C(2^5)), 181.3 (*s*, C(6^5, $6^{5\prime}$)), 159.6 (*s*, C(2, 2')), 157.3 (*s*, C(6, 6')), 138.2 (*d*, C(4, 4')), 123.2 (*d*, C(3, 3')), 121.3 (*d*, C(5, 5')), 56.8 (*t*, C(2^1, $2^{1\prime}$, 2^3)), 51.1 (*t*, C(6^1, $6^{1\prime}$)), 50.7 (*t*, C(6^3, $6^{3\prime}$)), 44.8 (*t*, C(6^4, $6^{4\prime}$)), 41.8 (*t*, C(2^4)), 19.3 (*q*, C($6^{3,1}$, $6^{3,1\prime}$)), 19.3 (*q*, C($2^{3,1}$)).

[1]) Peak on the subspectrum of parent ion 310.

2.3.10 Aqua[2,6-bis[(3*S*)-3-carboxymethyl-2-azabutyl]pyridine]cobalt(III) perchlorate ((*S*,*S*)-[Co(b3amp)H_2O]ClO_4, (*S*,*S*)-**24**)

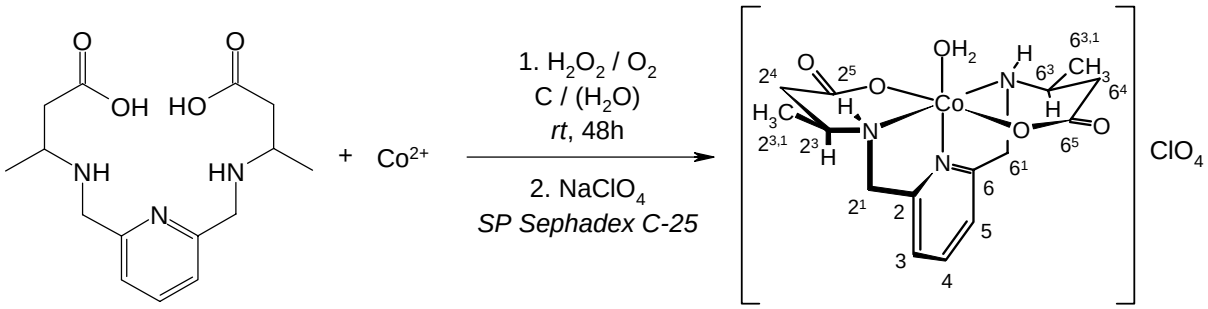

(*S*,*S*)-(+)-**3**	$CoSO_4 \cdot 7H_2O$	(*S*,*S*)-**24**, isomers **A1-1**, **A2-1**, **B1-1**
$C_{15}H_{23}N_3O_4$	$H_{14}CoSO_{11}$	$C_{15}H_{23}ClCoN_3O_9$
309.36	281.10	483.74

According to a modified procedure described in [14] and [4].

H_2(*S*,*S*)-(+)-b3amp ((*S*,*S*)-**3**, 0.309 g, 1.0 mmol) and cobalt(II) sulphate heptahydrate (0.337 g, 1.2 mmol) were dissolved in water (50 mL). Active charcoal (0.1 g) and 30% hydrogen peroxide solution (2 mL) were added. The pH was adjusted and maintained at 6.5-7 by addition of several portions of 0.5M NaOH. When no more significant pH drop occurred, the reaction was allowed to complete at 40°C for one day. The active charcoal was eliminated by filtration through cotton wool and the pH of the filtrate was adjusted to 3.5 by 1% perchloric acid in order to prevent a fast isomerisation.

The solution was introduced in a cation exchange column (*SP Sephadex C-25*, column length 120 cm; bed volume 1100 mL; form Na^+) whose pH had been previously adjusted to pH 3.5 by diluted $HClO_4$. The column is washed with diluted $HClO_4$ at pH 3.5 (200 mL) to eliminate a red-brown neutral fraction.

The resin was washed with 200 mL of water to eliminate the neutral fractions. The [Co(b3amp)H_2O]$^+$ isomers were eluted with 1% $NaClO_4$ whereas the excess of free Co^{2+} remained fixed on the column. The first two fractions contain the red isomers A1-1 and A1-2 (see chapter 5), the third one the brown isomer B1-1. From the concentrated effluent fractions $NaClO_4$ was eliminated by ion exclusion chromatography (*Sephadex G-10*, column length 130 cm; bed volume 2000 mL) with diluted $HClO_4$ at pH 3.5. The salt-free solutions were concentrated until precipitation of red crystals.

Cobalt complexes with ligands synthesised from racemic 3-aminobutyric acid

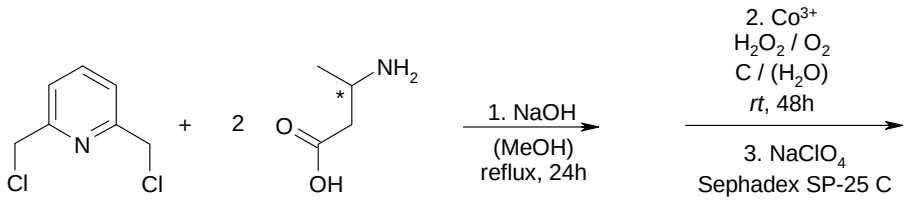

4	*rac*-**15**	$Co(NO_3)_2{\cdot}6H_2O$
$C_7H_7Cl_2N$	$C_4H_9NO_2$	$H_{12}CoN_2O_{12}$
176.04	103.12	291.03

Cobalt complexes were prepared as indicated in §2.3.9 and 2.3.10, using the crude mixture of ligands obtained from racemic 3-aminobutyric acid. Several reaction products formed. The following have been isolated as perchlorate salts and identified by X-ray crystallography:

rac-aqua[2,6-bis(4-carboxy-3-methyl-2-azabutyl)pyridine]cobalt(III) perchlorate (*rac*-$[Co^{III}(b3amp)H_2O]ClO_4$, *rac*-**24**) isolated from racemic mixture

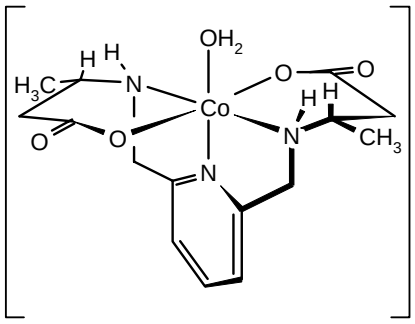

$[C_{15}H_{23}CoN_3O_5]ClO_4$

$C_{15}H_{23}ClCoN_3O_9$

M_r = 483.74

IR (KBr): 3248*m* (C-H ν), 3082*vw*, 2969*vw*, 2916*w*, 2875*vw*, 2009*vw*, 1652*vs* (C=O ν), 1610*m*, 1589*vw*, 1548*m* (br), 1533*m*, 1485*vw*, 1467*vw*, 1431*w*, 1409*s*, 1388*w*, 1360*m*, 1336*s*, 1290*w*, 1256*w* (sh), 1210*m*, 1173*m*, 1158*vw*, 1100*vs*, 1081*vw*, 973*vw* (doublet), 954*w* (sh), 931*vw* (sh), 826*m*, 780*w*, 753*vw*, 692*w* (sh), 663*vw*, 632*vw*, 623*s*, 592*vw*, 534*vw*, 511*vw*, 486*m* (doublet), 434*m* (sh).

ESI-MS (pos. mode): 384 (1, M^+), 366 (100, $[M_A - H_2O]^+$).

X-RAY of *Δ*-Aqua[2,6-bis[(2*S*,3*S*)-3-carboxymethyl-2-azabutyl]pyridine]cobalt(III) perchlorate (($C_SC_SN_SN_S$)-[*Co^{III}((S,S)-b3amp)H_2O]ClO_4, **A1-1**): see §7.1.3

2-((2*R*,3*R*)-*N*-(2'-(6'-(2''-azabutyl)pyridyl)methyl)-3-carboxymethyl-2-azabutyl)-6-((3*R*)-3-carboxymethyl-2-azabutyl)pyridine cobalt(III) perchlorate (**25**) isolated from racemic mixture

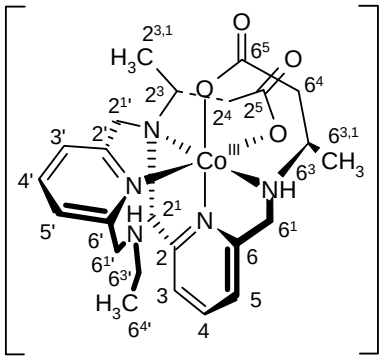

$ClO_4 \cdot 1.5\ H_2O$

$[C_{24}H_{32}CoN_5O_4]ClO_4 \cdot 1.5H_2O$

$C_{24}H_{35}ClCoN_5O_{9.5}$

M_r = 639.95

^{1}H-NMR (400 MHz, D_2O, COSY): 8.09-7.95 (*m*, 2 H, H-C(4, 4')), 7.58-7.52 (*m*, 4 H, H-C(3, 5, 3', 5')), 5.04 (*d*, ^2J=17.2, 1 H, H_a-C(2^1))[1]), 5.00 (*d*, ^2J=14.4, 1 H, H_a-C($6^{1'}$))[13]), 4.88-4.76 (*m*, 3 H[2]), $H_2C(2^{1'}, 6^1)$)[13]), 4.46 (*d*, ^2J=16.7, 1 H, H_b-C($6^{1'}$))[13]), 4.41 (*d*, ^2J=17.0, 1 H, H_b-C(2^1))[13]), 3.89-3.80 (*m*, 1 H, HC(2^3))[13]), 3.79-3.70 (*m*, 1 H, HC(6^3))[13]), 3.17-3.12 (*m*, 1 H, H_a-C($6^{3'}$))[13]), 3.12-3.07 (*m*, 1 H, H_b-C($6^{3'}$)), 2.49 (*dd*, *J*=6.9, 2.1, 1 H), 2.45 (*dd*, *J*=6.8, 2.1, 1 H), 2.34-2.02 (*m*, 5 H[14]), $H_2C(2^4, 6^4)$)[13]), 1.50 (*d*, ^3J=6.6, 3 H, $H_3C(2^{3,1}$ or $6^{3,1})$), 1.49 (*d*, ^3J=5.7, 3 H, $H_3C(2^{3,1}$ or $6^{3,1})$), 1.43 (*dd*, ^2J=8.5, ^3J=6.7, 5 H[14]), $H_3C(6^{4'})$).

X-RAY: see §7.1.4; H on N(6^2) is not represented on the X-ray structure but is required to meet electroneutrality.

[1]) Uncertain assignment.

[2]) Measured integral value does not correspond to assigned proton(s).

(2*S*,3*R*,11*R*)-3,11,17,18-tetraaza-3,11-bis[(*R*)-1-methylcarboxyethyl]-2-methyltricyclo [11.3.1.1^{5,9}]octadeca-5,7,9(18),13(17),14,16-hexaene cobalt(III) perchlorate hydrate (**26**)[1])

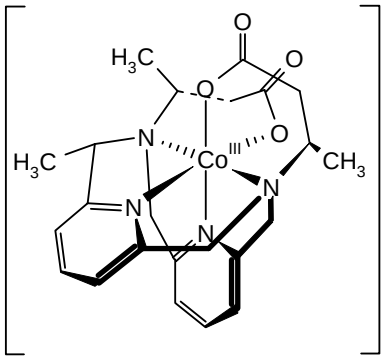

$ClO_4 \cdot H_2O \cdot NaClO_4$

$[C_{23}H_{28}CoN_4O_4]ClO_4 \cdot H_2O \cdot NaClO_4$

$C_{23}H_{30}Cl_2CoN_4NaO_{13}$

M_r = 723.33

This compound was obtained when the cobalt salt was added directly to the crude reaction mixture in the ligand synthesis. For the ligand synthesis, only three instead of 4 eq. of amino acid (*rac*-**15**) were engaged.

X-RAY: see §7.1.5

2.4 References

[1] L. Verardo, Ph.D. Thesis, Université de Neuchâtel, 1996.

[2] K. Bernauer, P. Pousaz, J. Porret, A. Jeanguenat, *Helv. Chim. Acta* **1988**, *71*, 1339.

[3] K. Bernauer, H. Stoeckli-Evans, D. Hugi-Cleary, H.J. Hilgers, H. Abd-el-Khalek, J. Porret, J.J. Sauvain, *Helv. Chim. Acta* **1992**, *75*, 2327.

[4] K. Bernauer (Faculty of Natural Sciences, University of Neuchâtel), personal communication

[5] a) B. Ringdahl, J.C. Craig, *Acta Chem. Scand.* **1980**, *B34*, 731; b) P. Newman, 'Optical Resolution Procedures for Chemical Compounds', Optical Resolution Information Center, New York, 1981.

[1]) For the naming of the bicyclic ligand in this complex, cf. §7.3 in the appendix.

[6] a) E.E. Mercer, R.R. Buckley, *Inorg. Chem.* **1965**, *4*, 1693-1695; b) A.A. Diamantis, J.W. Dubrawski, *Inorg. Chem.* **1981**, *20*, 1142-1150.

[7] H.R. Mürner, Ph.D. Thesis, Universität Freiburg (Schweiz), 1996.

[8] P. Hayoz, A. von Zelewsky, H. Stoeckli-Evans, *J. Am. Chem. Soc.* **1993**, 5111.

[9] K. Hansongnern, N. Leesakul, P. Amornpitoksuk, P. Chooto, Conference presented at the 24th Congress on Science and Technology of Thailand, Bangkok, 19-21.10.1998.

[10] E. Pretsch, T. Clerc, J. Seibl, W. Simon, 'Tabellen zur Strukturaufklärung organischer Verbindungen mit spektroskopischen Methoden', Springer, Heidelberg, 1990.

[11] I.P. Evans, A. Spencer, G. Wilkinson, *J. Chem. Soc., Dalton Trans.* **1973**, 204.

[12] G.M. Sheldrick, SHELXS97, Program for Crystal Structure Determination, Universität Göttingen, Göttingen, Germany, 1990; G.M. Sheldrick, *Acta Crystallogr*. **1990**, *A46*, 467; G.M. Sheldrick, SHELXL97.

[13] G.M. Sheldrick, SHELXL97, Program for the Refinement of Crystal Structures, Universität Göttingen, Göttingen, Germany, 1999.

[14] K. Bernauer, P. Pousaz, *Helv. Chim. Acta* **1984**, *67*, 796.

[15] L.A. Leuthold, Travail avancé en chimie inorganique, Université de Neuchâtel, 1998.

[16] M. Erne, F. Ramirez, A. Burger, *Chem. Ber*. **1951**, *16*, 143.

CHAPTER 3:
REDUCTION OF CYTOCHROME *C* BY OPTICALLY ACTIVE COBALT(II) COMPLEXES

3.1 Reduction of metalloproteins involving transition metal complexes

3.1.1 Transition metal complexes as probes for electron transfer with metalloproteins

Electron-transfer mediated coupling of transition metal complexes to the surface of a protein is an effective means to distinguish between inner- and outer-sphere mechanisms (see §3.2.3). The isolation of the complex can be isolated either by ion exclusion column chromatography or by dialysis [1].

3.1.2 Use of chiral complexes

Several metal complexes with the ligands presented in chapter 1 were used to investigate the electron-transfer from and to metalloproteins. In such a way, the reduction of spinach plastocyanin by the two enantiomers of [Fe^{II}(alamp)] allowed the first clear demonstration of a stereoselective electron transfer involving metalloproteins [2] and the investigation of genetically modified plastocyanins showed that the stereoselectivity was due to the side chain of the Leu 12 residue [3a].

The analysis of the CD spectra of the complete reduction / oxidation cycle revealed that the inner-sphere electron transfer occurred by the coordinated imidazole unit of His 87 in plastocyanin, whereas in the same reaction with azurin the uncoordinated His 83, some 20 Å distant from the copper centre, was involved [4]. The use of chiral electron-transfer agents has also been applied to other metalloproteins like superoxide dismutase [5], plant ferredoxin [6] and cytochrome *c* [7][8][9]. Nevertheless, for cytochrome *c* chiral interactions using cobalt(II) complexes as reducing agents have not been demonstrated so far. Considering the additional information obtained by the use of these compounds in the reduction of the blue copper pro-

teins plastocyanin and azurin [3], we applied the same technique to cytochrome *c* which contains the redox active centre in a porphyrin system.

3.2 Horse heart cytochrome *c* as electron acceptor

3.2.1 Biological and physico-chemical properties of horse heart cytochrome *c*

Horse heart cytochrome *c* is one of the most thoroughly studied metalloproteins [10][11]. This mitochondrial protein built of 104 amino acids occupies a key position in the enzyme-catalysed electron transport between ubiquinone (coenzyme Q_{10}) and O_2 in the respiratory chain. Cytochrome c_1 (a part of cytochrome *c* reductase) and cytochrome *c* oxidase are its immediate redox partners. It belongs to the class I cytochromes *c* that contain one haem group as redox-active centre whose iron ion is either at the oxidation state +II (ferrocytochrome *c*) or +III (ferricytochrome *c*). The haem is covalently bound to the protein by the side-chains of Cys 14 and Cys 17. The apical coordination positions of the iron are occupied by the sulphur atom of Met 80 and the imino nitrogen, N(3), in the imidazole group of His 18. As shown on Fig. 3-1, the polypeptide chain of 104 amino acids enfolds almost completely the haem, leaving only a small area accessible, the so called *exposed haem edge*. Structure differences between the peptide chains in ferro- and ferricytochrome *c* crystals of various sources are barely larger than the resolution limits of the X-ray structure and not yet unambiguously confirmed [11b]. The volume increase during oxidation amounts only to 5 $cm^3 \cdot mol^{-1}$ [12].

Nevertheless, other physico-chemical properties are very different at both oxidation states: Oxidation from ferro- to ferricytochrome *c* is accompanied by a volume increase of 5 $cm^3 \cdot mol^{-1}$ [13]. Ferricytochrome is less stable than ferrocytochrome towards extremes of temperature and pH, towards alcohol, some proteases, side chain modification and proton exchange. The chloride binding and the acidity of some surface groups are stronger in the oxidised protein so that the neat charge of the latter is remarkably higher (+7.1 vs. +6.6 at pH 7.15 [14]). Furthermore, the crystal forms of both oxidation states are not the same.

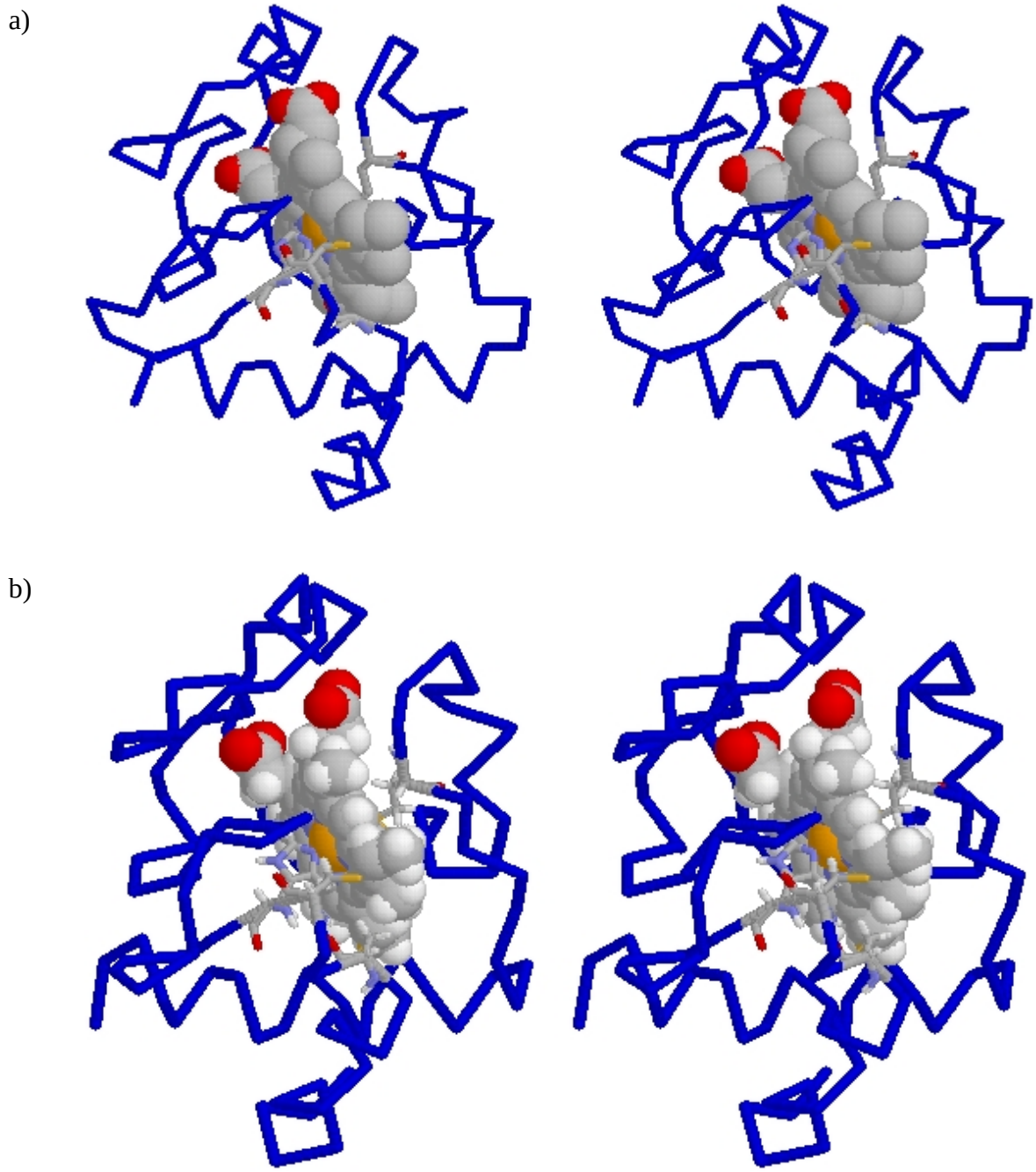

Fig. 3-1. *Stereo views of horse heart ferricytochrome* c *seen from the exposed haem edge.* Haem and haem binding sites Cys 14, Cys 17, His 18 and Met 80(sticks) represented in CPK colours (see fig. 6-1).

a) *High-resolution (190 pm) X-ray structure [15].*

b) *Minimum average structure in 0.1M phosphate buffer at pH 7.0 structure based on NOE-NMR analysis [16].*

The exposed haem edge is located on the upper right edges of the illustrations. Images generated by [17].

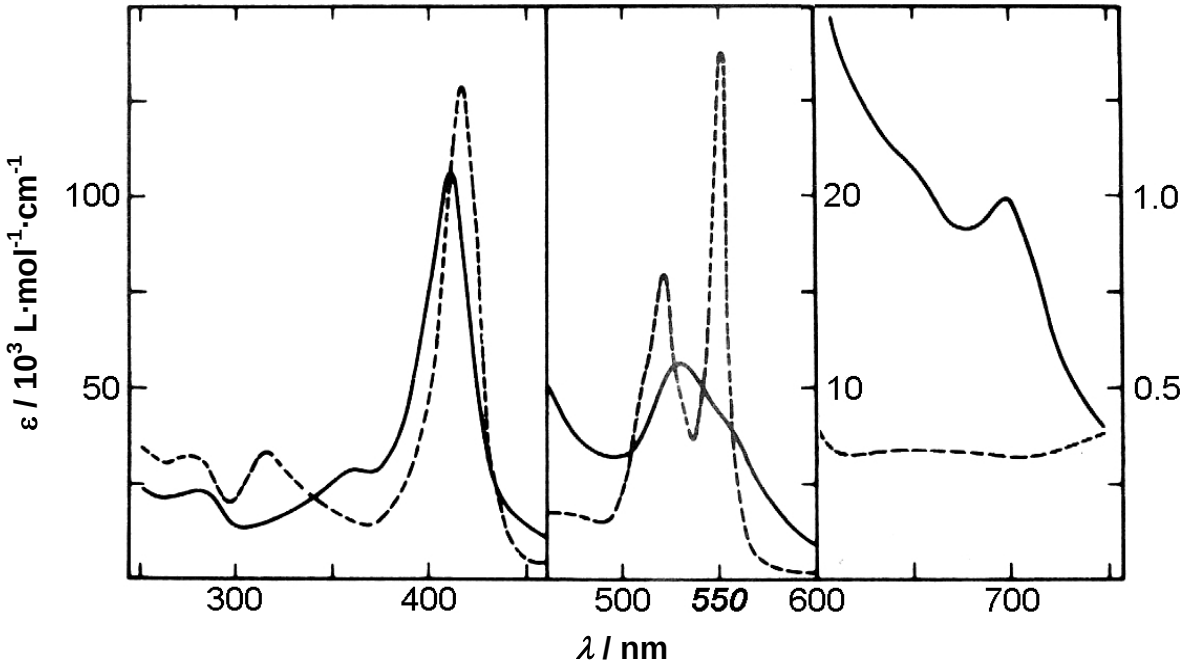

Fig. 3-2. *Normalised UV-VIS absorption spectra of horse heart cytochrome* c *at pH 7.*
Modified reprint from [11a] (p. 908), with kind permission from Elsevier.
(——) ferricytochrome *c*; (-----) ferrocytochrome *c*.

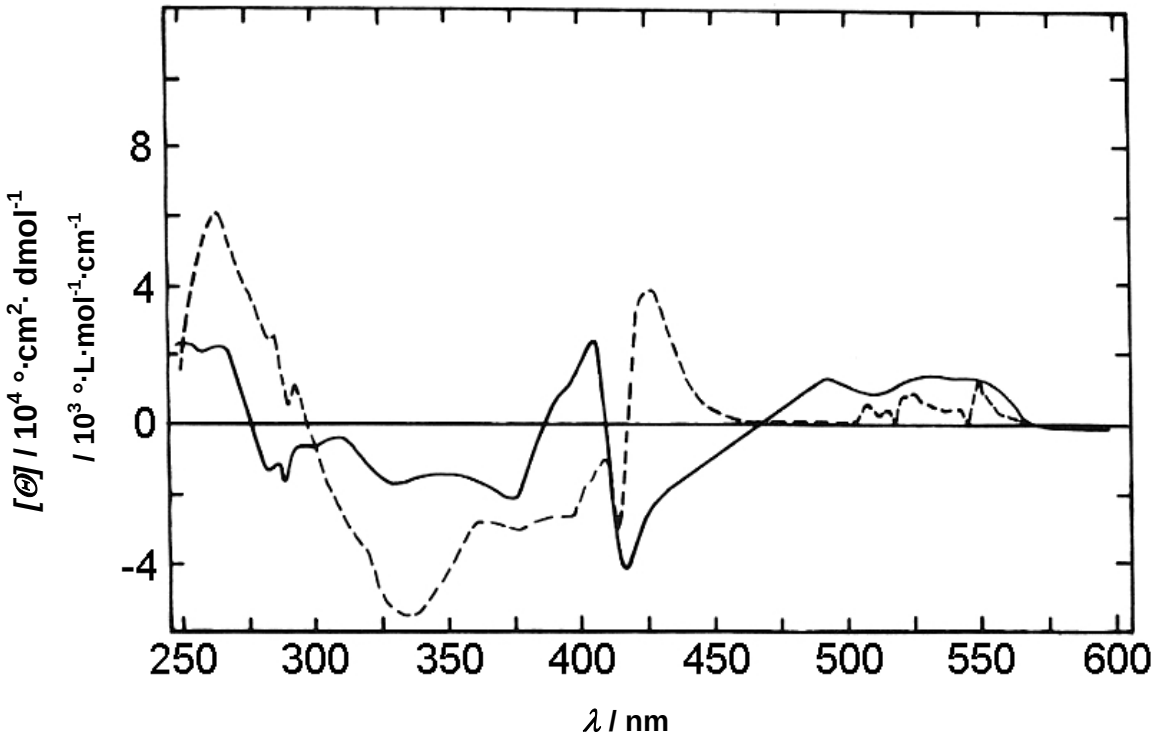

Fig. 3-3. *Normalised circular dichroism spectra of horse heart cytochrome* c *(pH is not stated).*
Modified reprint from [11a] (p. 930), with kind permission from Elsevier.
(——) ferricytochrome *c*; (-----) ferrocytochrome *c*.

In this work, we focus primarily on the optical and chiroptical differences: A sharp absorption band at 550 nm is present in the UV-VIS spectrum of ferrocytochrome *c* (Fig. 3-2) only and has so been used to establish the kinetic trace of protein reduction (see §3.3.2). The four isosbestic points between 500 and 570 nm allowed approximate verification of the total protein concentration. The differences in the CD spectra (Fig. 3-3) served to identify the oxidation state of cytochrome *c* and to estimate the ratio between both forms after the fixation of a metal complex and dialysis (see §3.4.3).

The acid-base behaviour of ferrocytochrome *c* is quite complex; several widespread apparent pK_a values and their assignments are reported in literature [18]. In moderately basic solution, the so-called alkaline form of ferricytochrome *c* is formed: After deprotonation, the side chain amino group of Lys 79, whose nitrogen atom is located at a distance of only 113 pm from the iron(III) (see Fig. 3-4), replaces Met 80 as ligand on the metal centre [19]. The pK_a of 11 and the alkaline isomerisation constant of 120 at 25°C yield an apparent pK_a value of 9.0.

The midpoint reduction potential of horse heart cytochrome *c* is 0.260 mV at pH 7 and 25°C. Temperature dependence is very strong and influenced by the medium. When chloride ions and phosphate buffer are present, the slope of the $E = f(T)$ plot increases sharply by a factor of 6.5 between 40 and 45°C [20], whereas it is constant in the presence of other halides. It is unknown if this variation is similar in our case where chloride ions are used in addition to Tris buffer. The reduction potential is stable between pH 5.0 and 8.0, then it drops from 270 mV to 120 mV between pH 8.0 and 10.0. As the conformational change in deprotonated ferricytochrome *c* described above affects directly the coordination sphere of the iron *Davis et al*. [19] suggest that this may be the origin of the potential drop. Cyclovoltammetric measurements performed by Sauvain [2b] and Hilgers [21] show that the complexes $[Co^{II}(promp)H_2O]$ and $[Co^{II}(alamp)H_2O]$ are able to reduce the metalloprotein between pH 4 and 10.

3.2.2 Determination of potential electron transfer sites

The following discussion is based on the solution structure of ferricytochrome *c*, as represented on Fig. 3-1a and Fig. 3-4 with the exposed haem edge at the so called "front" surface of the protein. The asymmetric distribution of the neat positive charge of +7 to +9 at pH 7 could favour a reaction at the exposed haem edge only if the redox partner is negatively

charged [14][22]. The significant transfer sites in horse heart cytochrome *c* for most of the physiological partners as well as for low molecular weight metal complexes that have been investigated until now are located on the front surface [23]. For the binding of the latter in the precursor complex, NMR and kinetic measurements have revealed mainly three reactive areas [20][24] that are represented on Fig. 3-4: Sites I and III have a marked activity for anionic reagents, I is the preferential site for the physiological partners. The positive end of the molecular dipole moment vector crosses the protein surface on the front side. The high value of 308 D in the reduced form and 325 D in the oxidised form is mainly due to the 19 lysine residues most of which are clustered around the exposed haem edge [11b]. Their side chain ammonium groups have pK_a values around 10 so that they react preferentially with neutral and negatively charged species at physiological *pH*. It was shown that Lys 13 and Lys 72 can be involved in both oxidation and reduction: When these residues are substituted by the carrier of a negative charge – a modification that does not generate a noticeable change either in the native structure or in the redox potential of the protein – the rate constants increase significantly in reactions with positively charged cobalt and iron complexes and decrease in reactions with negatively charged iron complexes.

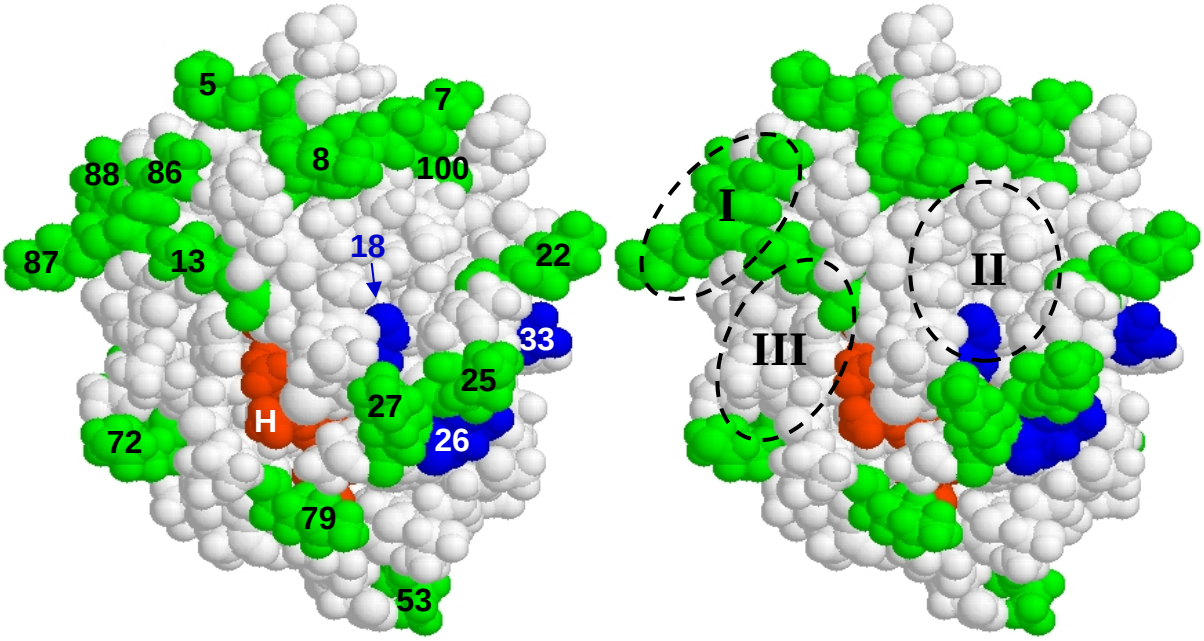

Fig. 3-4. *Stereo view of horse heart ferricytochrome* c *[16] seen from the exposed haem edge with histidine (blue) and lysine positions (green) highlighted.* Lys 39, 55, 60, 72 and 99 are not visible on this protein face. The haem group (H) is represented in red. Specific regions containing redox partner binding sites according to [11b] and [24] are surrounded by dotted lines (right). Region I extends also to the "backside" of this protein view. For further experimental details, see Fig. 3-1. Images generated by [17].

On the other hand, positively charged complexes tend to interact, unproductively, at a much greater frequency with the back surface of the protein than with the positively charged front surface where part of the collisions lead to an electron transfer. These observations show that the effective charge at the transfer site has a major influence on the reaction rate than the global charge of the protein.

The imino nitrogen in the imidazole side chain of histidine can also play the role of a possible bridging group in the electron transfer-pathway as has been observed for several histidines of azurin [25]. Horse heart cytochrome *c* contains three histidine residues at positions 18, 26 and 33 whose imino nitrogens are located at distances of 199, 1215, and 1507 pm from the iron centre. Isied et al. [26][27] have permanently bound pentammineruthenium(II) to His 33 and investigated the intramolecular electron transfer to the iron(III) of the haem. The reported pK_a values for the iminium nitrogens in His 18, His 26 and His 33 are 0.4-5.0 (iron coordination!), <3.2, and 6.4-6.9, depending on the method of determination [18], thus these histidines are mainly neutral at physiological pH and can react even with positively charged reagents. As it was seen with plastocyanin and azurin, all three histidines, including His 18 that ensures the link of the protein to the metal centre of the haem, may be accessible for electron-transfer mediated binding of the reagent.

A stable complex between pentaammineruthenium(III) and the His 33 group of horse heart ferrocytochrome *c* was prepared by reductive fixation of $[Ru^{II}(NH_3)_5H_2O]^{2+}$ on ferricytochrome *c* [1]. HPLC of the trypsine hydrolysate identified His 33 as binding site of ruthenium(III). UV-VIS, CD and NMR measurements of the complex confirmed this result and showed that no significant conformation change takes place in the haem region during the coupling. CV analysis revealed the same reduction potential for the haem in the ruthenium-modified protein as for the native one. Nevertheless, the reduction potential of Ru^{III} is some 40 mV higher in the protein complex than in the analogous model compound $[Ru^{III}(NH_3)_5His]^{3+}$. The rate of the ruthenium(III) modified ferricytochrome *c* reduction by $CO_2^{\cdot-}$ radicals is not affected by proton concentration between pH 5 and 9 but increases exponentially between pH 5 and pH 2. This behaviour has been corroborated by the reduction kinetics carried out with other cobalt(III) and ruthenium(III) complexes [24]. Interestingly, there is a significant decrease of the reaction rate between 7 and 5 when ferrocytochrome *c* is *oxidised* by cationic cobalt(III) complexes, even while using the same ligands as in the reduction. This effect is not observed when His 33 is absent (for instance in tuna cytochrome *c*) or

substituted on the imino group of the imidazole. So, protonation of His 33 can be considered as essential in cyt *c* oxidation but seems to have no weight in reduction. As the pK_a of this residue is little influenced by the oxidation state and, on the other hand, the redox potential does not depend on the protonation of this residue, the observed tendency must be a local effect such as the accessibility for a redox partner or the site selection for electron transfer that are conditioned by slight conformation changes.

Other authors [7] imagine that the inorganic redox partner has to enter into the apolar crevice containing the exposed haem edge. They explain the effects of temperature, pH and polarity on the reaction rate and the stereoselectivity by the opening of the crevice and the apolar interactions of the redox partner with the residues in the crevice.

3.2.3 Kinetic and mechanistic aspects

Roughly speaking, the reaction between two redox partners A(red) and B(ox) can be subdivided into three steps [28]:

a) formation of a precursor complex

$$\text{A(ox)} + \text{B(red)} \overset{K_{AB}}{\rightleftharpoons} \text{A(ox)B(red)}$$

b) electron-transfer reaction, i.e. formation of a successor complex

$$\text{A(ox)B(red)} \xrightarrow{k_{et}} \text{A(red)B(ox)}$$

c) dissociation of the successor complex (does not always take place)

$$\text{A(red)B(ox)} \overset{K_{diss}}{\rightleftharpoons} \text{A(red)} + \text{B(ox)}$$

The last step, if it takes place, is in general very fast and strongly product favoured (high k_{diss} and K_{diss} values); it can therefore be neglected in the kinetic discussion.

If the overall concentrations $c_A << c_B$ (in our case, the protein is always the limiting reagent), the rate law of the reduction is:

$$v = -\frac{dc_{A(ox)}}{dt} = +\frac{dc_{A(red)}}{dt} = \frac{k_{et}K_{AB}c_{B(red)}}{1+K_{AB}c_{B(red)}}c_{A(ox)}$$ (demonstration see appendix, §7.6.2)

Pseudo first order kinetics with an apparent rate constant $k_{obs} = \frac{k_{et}K_{AB}\cdot c_{B(red)}}{1+K_{AB}c_{B(red)}}$ are verified. They are comparable to the enzyme kinetics based on the Michaelis-Menten model.

Three cases can be considered:

a) Lower limiting case: $K_{AB}c_B << 1$

$$-\frac{dc_{A(ox)}}{dt} = K_{AB}k_{et}c_{B(red)}c_{A(ox)}$$

Linear domain: The apparent rate constant $k_{obs} = K_{AB}k_{et}c_{B(red)}$ is proportional to the concentration of the B, as in a classical second order kinetics.

b) Intermediate case: $K_{AB}c_B \approx 1$

Nonlinear domain: k_{obs} is no longer proportional to the concentration of B because the ion-pair formation is so effective that the precursor complex is formed faster than it is consumed.

c) Upper limiting case: $K_{AB}c_B >> 1$

$$-\frac{dc_{A(ox)}}{dt} = k_{et}c_{A(ox)}$$

Rate saturation: k_{obs} is constant and equal to k_{et}.

Van Eldik and al. [12] have reported the only case where a rate saturation has been observed in an electron transfer between cytochrome c and a cobalt complex at higher complex concentrations: A racemic mixture of the anionic chiral reagent $[Co^{III}(ox)_3]^{3-}$ has been used to oxidise ferrocytochrome *c*. Rate saturation occurs at 25°C, a pH of 7.2 and an ionic strength of 0.1 (Tris-$LiNO_3$) when the $[Co^{III}L]$/[cyt *c*-Fe^{II}] ratio exceeds 100. From the limiting k_{obs} value, the activation parameters can be calculated separately for the precursor formation and the electron transfer. Interestingly, at an ionic strength of 0.5 (phosphate), no rate saturation has been observed for the same reaction system [29]; this illustrates that ion-pair association is favoured by a low ionic strength.

As long as k_{obs} varies in a linear manner with the excess reactant concentration, it is generally admitted that the global activation parameters and especially the entropy, describe mainly the precursor complex formation.

In an *outer-sphere* mechanism, the contact of both reaction partners is produced by electrostatic or weak intermolecular interaction with small orbital overlap. The coordination or van-der-Waals spheres of both reagents remain intact. The Franck-Condon principle claims that the time of the electron transfer (step b) is significantly shorter (10^{-15} s) than the time that is necessary to operate changes in the nuclei position or the electron shell of the donor and acceptor atoms: Consequently, the positional changes have to take place before the electron transfer: The M-L bond lengths of both metal centres must reach an equilibrium value between the oxidised and the reduced state. If there is also a change of the electron spin state, the latter occurs either before or after the electron transfer step. In exothermic reactions, the negative reaction enthalpy provides the necessary energy for these changes so that the reaction rates are rather elevated whereas they are very low in entropy driven reactions.

The electron transfer rate constants in outer-sphere redox reactions between two different species, 1 and 2, can be simply predicted according to the Marcus cross-relation [30]:

$$k_{12} = \sqrt{k_{11} k_{22} K_{12}}$$

k_{11}, k_{22} = self-exchange constants of each redox partner

K_{12} = equilibrium constant of the overall reaction

Inconsistency of kinetic data with this equation are generally interpreted as an especially strong electrostatic interaction between electron donor and acceptor, a particular behaviour in the reagent collision[1]) or as an indication for an *inner-sphere* mechanism. Though the Marcus model has been developed for metal complexes of moderate size, it has been widely used to analyse electron-transfer reactions between cyt *c* and cobalt complexes [12][20][23][29][31][32].

In a reaction following an *inner-sphere* mechanism, there is interpenetration of the coordination spheres in the donor and acceptor species and the formation of a covalent bond. In the

[1]) In this case, a correcting factor $\sqrt{f_{12}}$ is introduced into the right term of the Marcus cross relation.

case of metal complexes, this bond is established by the coordination of a so-called *bridging-ligand* provided in most cases by the electron acceptor. If the bridge remains after the electron transfer it can be detected by spectroscopic means and yields a confirmation of an inner sphere mechanism. Nevertheless, even if no bridging ligand is identified, the reaction may evolve through an inner sphere mechanism. Indeed, in some cases, the bridging bond is dissociated at the same place where it had been formed before.

The kind of mechanism followed by electron-transfer reactions with proteins as well as the site of interaction depends not only on the redox partners but also on the reaction conditions such as pH (protonation / deprotonation of potential binding groups) and temperature (conformation changes within the protein).

3.2.4 Stereoselectivity in cytochrome *c* oxidation and reduction

In 1984, Toma and Murakami have published [32] the first attempt to reduce ferricytochrome *c* separately by two enantiomers, those of a [Co^{II}sepulchrate], but they did not detect any stereoselectivity. In 1990, Lappin and al. [33] have analysed the ferrocytochrome *c* - $[Co^{III}(C_2O_4)_3]^{3-}$ system by circular dichroism. As van Eldik, they observed that the reaction rate is almost independent of proton concentration between pH 4.5 and 7.5. Moreover, below pH 4.5, it decreases very slightly with increasing pH, then it undergoes a more marked decrease above pH 8. In a second experience, a solution of ferricytochrome *c* was dialysed against racemic $[Co^{III}(ox)_3]^{3-}$ in order to examine the enantioselectivity in the complex-protein binding equilibrium. CD measurements revealed an excess of the Δ enantiomer in the bulk solution so indicating a preferential binding of the Λ isomer with a $K\Lambda/K\Delta$ ratio of 1.04. To confirm this preference, the bound complex was released by dialysis of the modified protein against buffer solution. As expected, the bulk solution contained an excess of the Λ enantiomer. The reversibility of the binding suggests an ion pair association, binding type that may also be implied in the outer-sphere mechanism of the electron transfer. Finally, the reduced protein was mixed with an excess of racemic $[Co^{III}(C_2O_4)_3]^{3-}$ at different pH values between 4.2 and 9.6. After removing the protein on a *Sephadex* column, the stereoselectivity $k\Lambda/k\Delta$ of the reaction can be calculated from the CD signal of the remaining solution. Its value is little affected by the pH change and averages 1.19 at 23°C and 0.1 $mol \cdot L^{-1}$ ionic strength. NMR in-

vestigations of the binding of the paramagnetic analogue $[Cr^{III}(C_2O_4)_3]^{3-}$ suggest a preferential fixation near the exposed haem edge but no suggestions about the exact residue are advanced.

Sakaki et al. [7] have determined the stereoselectivities in the electron transfer between ferrocytochrome *c* and two chiral cobalt(III) complexes in form of racemate. Significant differences in CD spectra were measured in the solution after the reaction. The stereoselectivity in this case increases upon lowering the pH. According to the authors, ferrocytochrome *c* should be more flexible at pH 4, given that the intramolecular hydrogen bonding in the protein is weaker due to the protonation of some residues. This would cause a larger opening of the apolar crevice, a deeper penetration of the oxidant and a higher number of steric interactions between both redox partners. To date, no experimental proof has been presented for this hypothesis.

A disadvantage of this system is that true equilibrium conditions cannot be established because $[Co^{III}(ox)_3]^{3-}$ racemises within a few hours in solution. Simultaneously, there seems to be some photochemical decomposition [12]. So, we have chosen to use the same investigation methods on ferricytochrome *c* reduction with the complexes $[Co^{II}(alamp)H_2O]$ and $[Co^{II}(promp)H_2O]$ (see chapter 1), given that they can be obtained in optically pure form and undergo no racemisation at all. Furthermore, the desolvation of a complex, that is preceding electron transfer, is facilitated if the complex is neutral. If the binding takes place near the exposed haem edge, a deeper penetration into the hydrophobic pocket, towards the metal centre in the protein is facilitated.

3.3 Analysis of the experimental data

3.3.1 Kinetic data collection

Ferricytochrome *c* $3 \cdot 10^{-5}$ M is reduced by a 30- to 500-fold excess of $[Co^{II}L(H_2O)]$ where L = (*R*,*R*)-alamp^{2-}, (*S*,*S*)-alamp^{2-}, (*R*,*R*)-promp^{2-} and (*S*,*S*)-promp^{2-} (cf. §1.2 for the ligand structures) in buffered aqueous solutions. The complex is formed by a mixing of cobalt(II) solutions with a small ligand excess. A large excess of anionic ligand - present at pH values higher than 8 - can have a decelerating effect on the rate of reaction, especially with anionic redox partners [12], probably because of an interfering ion-pair association with the positively

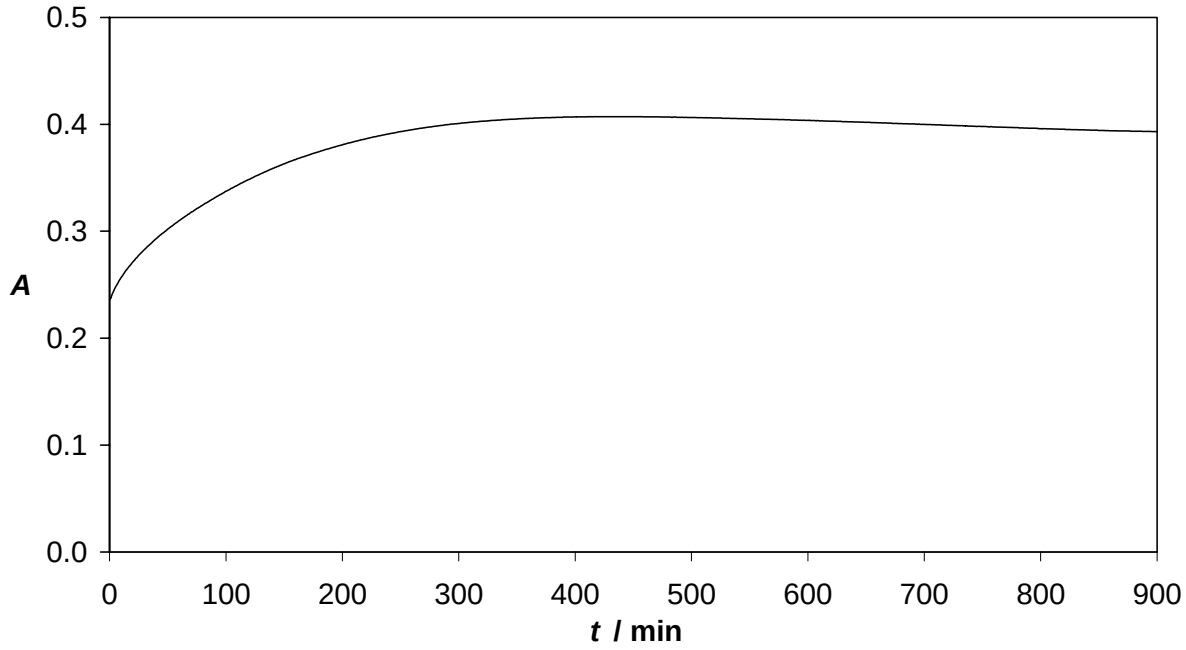

Fig. 3-5. *Time-resolved variation of absorbance at 550 nm during the reduction of $3.5 \cdot 10^{-5}$ M horse heart ferricytochrome* c *by $2.0 \cdot 10^{-3}$ M Λ-[Co((S,S)-promp)H_2O] at pH 4.5 and 20°C.* Optical path length: 1 cm.

charged sites of the protein. Absorption as a function of time has been measured at the local absorption maximum at 550 nm (Fig. 3-2). Nevertheless, in some cases, a lowering of the absorption at this wavelength was observed after a certain time (see Fig. 3-5), an irreproducible phenomenon due either to re-oxidation by oxygen traces or to partial decomposition of the protein. A similar behaviour at a ms timescale has been described in literature [34] for the reduction by $[Fe^{II}(CN)_6]^{4-}$ in alkaline medium and assigned to the equilibrium with an isomer of the deprotonated protein that cannot be reduced in the given conditions (see also §3.2.1). To better control the influence of this side-effect, absorption spectra of the reactions were scanned between 500 and 570 nm. Fig. 3-6 reveals four *apparent* isosbestic points in this wavelength range, i.e. at λ = 504 nm, 526 nm, 541 nm and 556 nm. A priori, one should not expect any isosbestic point in a four-compound system. However, in the considered wavelength range, the extinction coefficients (ε) of the cobalt(II) complexes are very weak. Even if its concentration is rather high, the concentration change during the reaction should not exceed 4% of the initial cobalt(II) concentration.

As for the cobalt(III) complex formed during the cytochrome *c* reduction, the ε value of the most absorbing complex, $[Co^{III}(promp)H_2O]^+$, represents 4.4% of the ε of ferrocytochrome *c* at 504 nm, 2.4% at 541 nm and 0.8% at 550 nm. These percentages ideally indicate the maximum contribution of the cobalt(III) complexes to the global absorption of our redox

system; they are very weak in the beginning of the reaction and increase with the conversion ratio, as it is illustrated by the decreasing resolution of the apparent isosbestic points on Fig. 3-6 at longer reaction times. This absorption increase has been neglected in the processing of our spectroscopic data.

3.3.2 Kinetic data processing

Background absorption is quite difficult to evaluate because it is not reproducible, neither between two analogous samples nor with respect to time. Indeed, if the absorption change due to the $[Co^{II}L(H_2O)]$ consumption is very weak, traces of oxygen produce the corresponding cobalt(III) complex at longer term: This can be seen on Fig. 3-6 for the reduction with $[Co^{II}(promp)H_2O]$ where the resolution of the apparent isosbestic points decreases at longer reaction times, especially at 504 nm, the absorption maximum of $[Co^{III}(promp)H_2O]^+$. In the case of alamp complexes, the deep yellow oxygen adducts $[Co^{II}alamp(O_2)]$ are formed instantly. Both oxidation products have sensibly higher ε values in the considered spectral range. In order to obtain at least a statistical approximation, several blank samples containing all components except cytochrome *c* have been measured in the same wavelength range as a function of time. A mean absorption contribution was thus determined for each $[Co^{II}(alamp)H_2O]$ concentration. Due to the oxygen traces, these absorption contributions seem to vary randomly with the complex concentration so that their mean value has been used as correction term for all kinetic measurements, independently of the actual complex concentration. For $[Co^{II}(promp)H_2O]$, the mean absorption of a $2 \cdot 10^{-3}$ M solution has been used as correction term for all kinetic measurements. The indicated reaction time represents the effective time from mixing and refers to the moment at which the wavelength scan (100 nm·min^{-1}) reaches 550 nm. In addition to the influence of $[Co^{III}L(H_2O)]^+$ absorption discussed above, some spectra presented important baseline shifts. The absorbances of each series were raised or lowered by the same value on the whole wavelength range in order to have an identical absorbance at 541 nm, one of the apparent isosbestic points of oxidised and reduced cytochrome *c* (Fig. 3-6). The corrected absorbances at 550 nm (or the neighbouring λ_{max} value) were plotted against time and yield a parabolic curve segment.

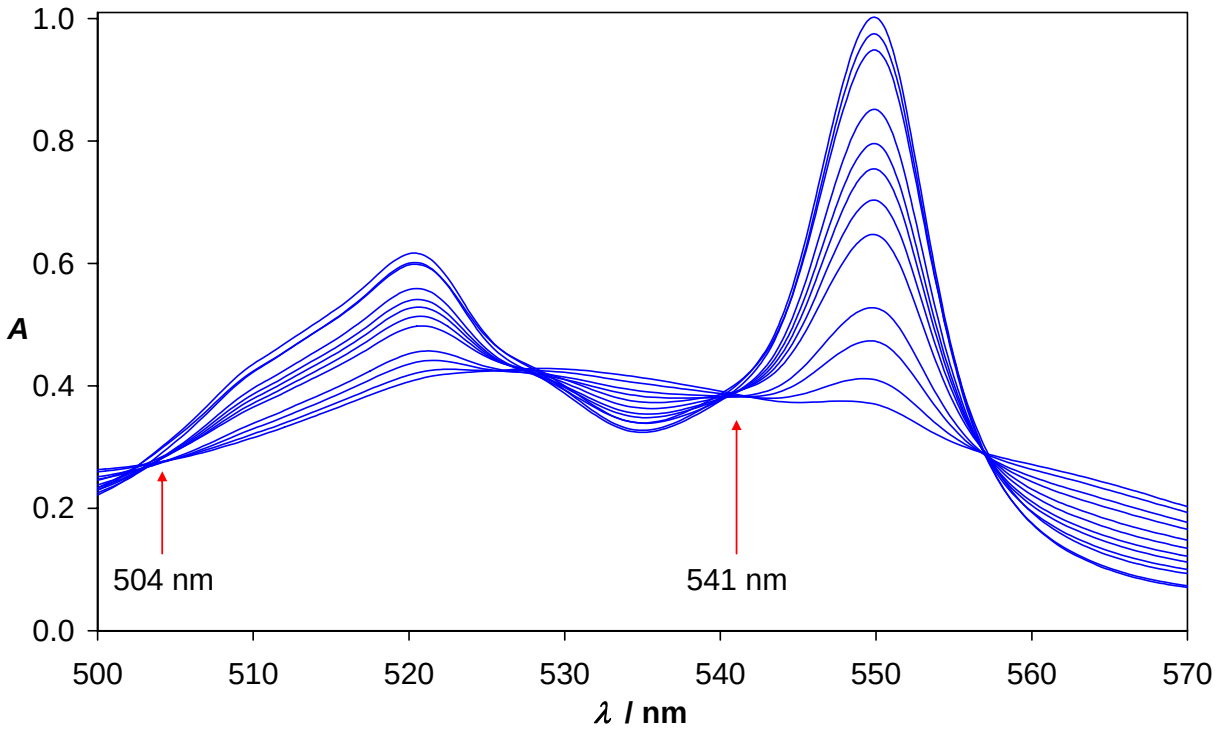

(a)

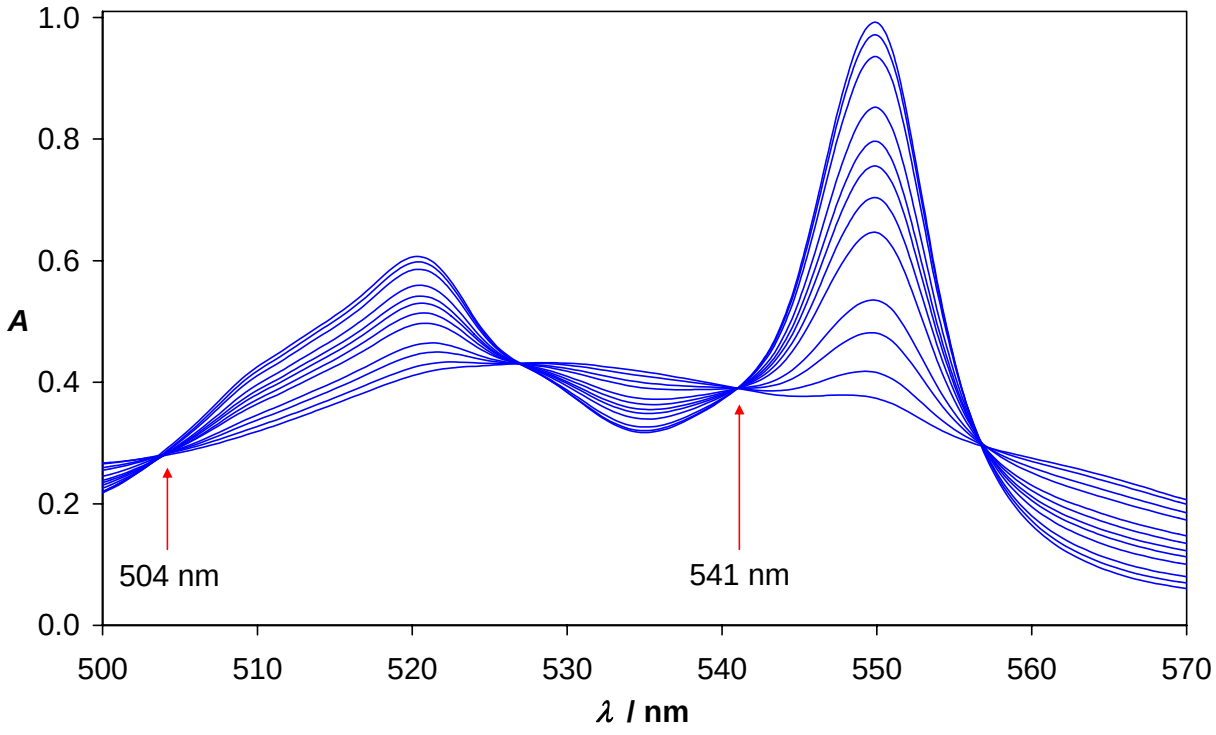

(b)

Fig. 3-6. *Absorption spectra between 500 nm and 570 nm during the reduction of $3.1 \cdot 10^{-5}$ M horse heart ferricyto-chrome* c *by $2.0 \cdot 10^{-3}$ M [Co((S,S)-promp)H_2O] at pH ≈ 7.5 and 45°C.* Optical path length: 1 cm. Spectra recorded 1, 3, 7, 12, 21, 30, 40, 53, 70 , 90, 240 and 480 min after mixing.

a) *Original spectra and* b) *corrected spectra.*

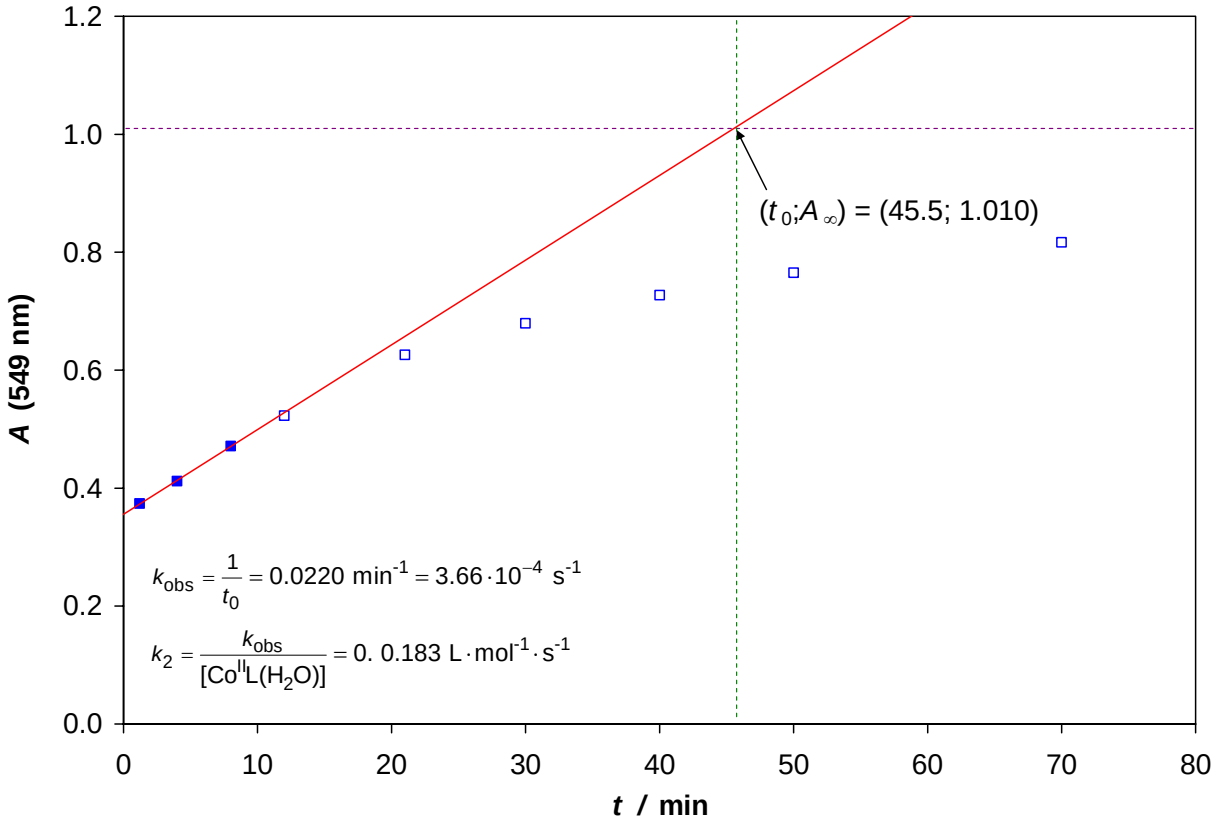

Fig. 3-7. *Time-resolved changes in absorbance at 549 nm for the data of* Fig. 3-6

■ Data taken into account for tangent construction, □ other data, ---- asymptote in A_∞

Since there is superimposition of at least two consecutive reactions, the rate constant of the first reaction was determined by the initial rate method (see appendix, §7.6.1): The asymptote of the $A^{550} = f(t)$ should cross the ordinate at A_∞, a value that cannot be determined by direct measurement since A^{550} diminishes after a certain time. Nevertheless, the mean absorbances at four isosbestic points and the corresponding ε values from Fig. 3-2 were used to estimate the cytochrome *c* concentrations and thus A_∞ at 550 nm. The tangent to the curve at $t = 0$ is constructed by linear regression of at least two experimental data sets. The pseudo-first order constant k_{obs} and the second order constant k_2 were derived from the abscissa of the curve tangent at the mean A_∞ value.

3.3.3 Error calculation

The experimental errors σ on the independent variables *u*, *v*, etc. are propagated on a variable *f* which is function of *u*, *v*, etc. according to the Gauss' law of error propagation:

$$\sigma(f) = \sqrt{\left[\frac{\partial f}{\partial u}\cdot\sigma(u)\right]^2 + \left[\frac{\partial f}{\partial v}\cdot\sigma(v)\right]^2 + \ldots}$$

In our case, the error propagation on the activation parameters cannot be calculated in an entirely analytical way because the v_0 determination is based on a personal interpretation of the kinetic trace. Instead, an individual error was estimated for the y values of each Arrhenius and Eyring plots, i.e. $\ln(k_2)$ and $\ln(k_2 \cdot T^{-1})$. The errors on the slopes, $\sigma(a)$, and ordinate intercepts, $\sigma(y_0)$, of the Arrhenius and Eyring plots were calculated according to Bevington [35]:

$$\sigma(a) = \sqrt{\frac{1}{\Delta}\cdot\sum_{i=1}^{N}\frac{1}{\sigma(y)^2}}$$

$$\sigma(y0) = \sqrt{\frac{1}{\Delta}\cdot\sum_{i=1}^{N}\frac{x_i^{\,2}}{\sigma(y)^2}}$$

where x_i = single T^{-1} value

$$\Delta = \sum_{i=1}^{N}\frac{1}{\sigma(y)^2}\cdot\sum_{i=1}^{N}\frac{x_i^{\,2}}{\sigma(y)^2} - \left(\sum_{i=1}^{N}\frac{x_i}{\sigma(y)^2}\right)^2$$

$\sigma(\hat{y})$, the error on the predicted $\ln(k_2)$ values at 25°C (that has been propagated on the stereoselectivity), has been determined only on the base of the point scattering around the regression line and is independent upon $\sigma(y)$:

$$\sigma(\hat{y}) = \frac{1}{\sqrt{N\cdot(N-2)}}\cdot\sqrt{N\cdot\sum_{i=1}^{N}y_i^{\,2} - \left(\sum_{i=1}^{N}y_i\right)^2 \cdot \frac{\left[N\cdot\sum_{i=1}^{N}x_i\cdot y_i - \left(\sum_{i=1}^{N}y_i\right)\cdot\left(\sum_{i=1}^{N}y_i\right)\right]^2}{N\cdot\sum_{i=1}^{N}x_i^{\,2} - \left(\sum_{i=1}^{N}x_i\right)^2}}$$

where y_i = single $\ln(k_2)$ value.

3.3.4 Dialysis data processing

Electron-transfer mediated coupling was investigated as follows: During the fixation assays, two of three identical samples of cytochrome *c* were allowed to react separately with the enantiomers of the cobalt(II) complex under study. After dialysis against large volumes of buffer solution at the pH of the reaction mixture, both samples were diluted to identical concentrations and their CD spectra were recorded.

As shown in Fig. 3-8, half of the difference between the CD spectra of a cytochrome *c* sample reduced by the (*R*,*R*) complex and the one of the cytochrome *c* samples reduced by the corresponding (*S*,*S*) enantiomer yields the contribution of the eventually fixed cobalt(III) complex to the global protein spectrum. The signs of the CD signals correspond - independently of a possible stereoselectivity - to those of [Co^{III}((*R*,*R*)-L)cytochrome *c*] but their intensities to the

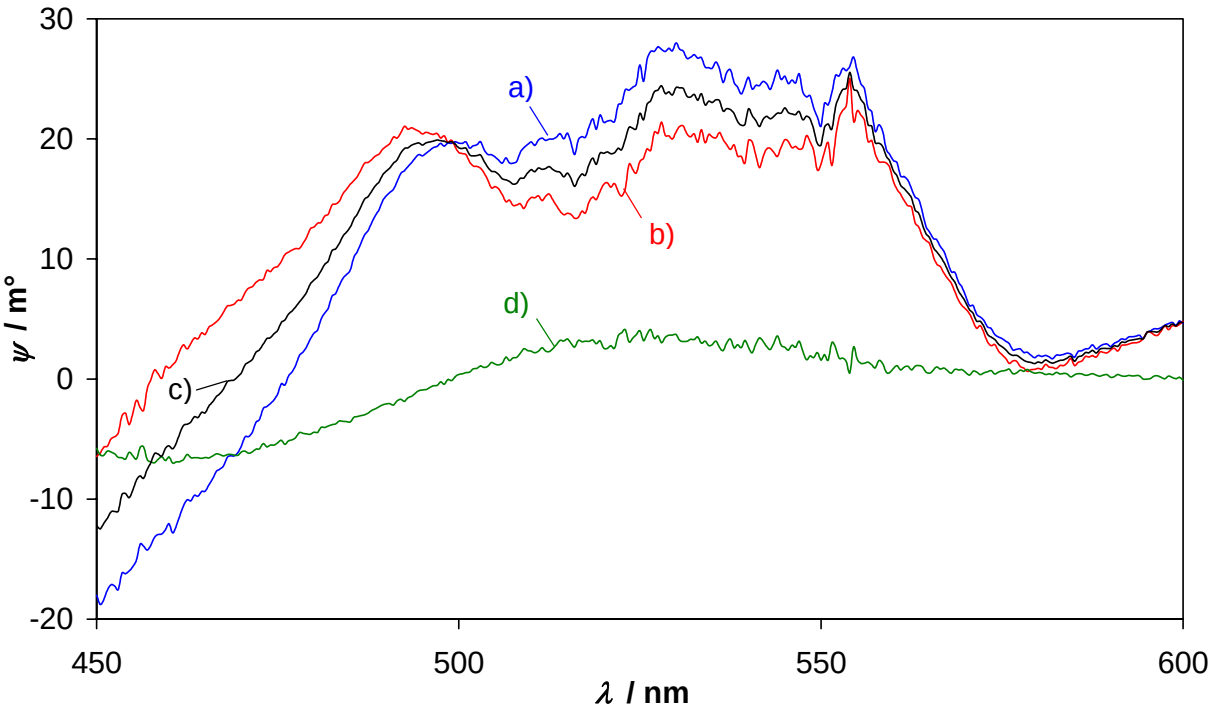

Fig. 3-8. *Reductive fixation assay of [Co^{II}(alamp)H_2O] on horse heart ferricytochrome* c. *CD spectra after dialysis against buffer solution (without ascorbic acid).*

pH = 7.59 / 7.70 (μ = 0.1, Tris/HCl); Θ = 35°C during 215 / 174 min, Θ = r.t. during 25 h (dialysis)

[cytochrome c] = $3.7 \cdot 10^{-5}$ mol·L^{-1} (by weight), optical path length: l = 5.00 cm.

a) *Δ-[Co^{II}((*R,R*)-alamp)H_2O]* (——), b) *Λ-[Co^{II}((*S,S*)-alamp)H_2O]* (——), c) *Mean contribution of the cytochrome* c *to spectra* a) *and* b)*:* (c) = 0.5·[(a)+(b)] (——), d) *Mean contribution of the fixed [Co^{III}alamp]$^+$ to spectra* a) *and* b): (d) = 0.5·[(a)-(b)] (——)

weighed average contributions (in absolute values) of both enantiomers. These interpretations are only applicable if the fixations of both cobalt(II) complexes produce no modifications in the protein conformation or only modifications that generate identical changes on the CD spectra of the protein.

3.4 Results and discussion

3.4.1 Influence of temperature on reaction rates

The evolution of the absorbance (Fig. 3-5) shows a typical biphasic behaviour which has also been observed for various other reducing agents [9]. It has been interpreted as equilibrium of (at least) two protein conformers that are reduced at different rates and whose interconversion is slower than the reduction.

Activation parameters E_a and A (frequency factor) were determined by a $\ln(k_2) = f(T^{-1})$ plot according to the Arrhenius equation (Fig. 3-9):

$$\ln\left(k_2\right) = \ln(A) - \frac{E_a}{R} \cdot \frac{1}{T}$$

The activation enthalpy and entropy, $\Delta^{\#}H$ and $\Delta^{\#}S$, were deduced from a $\ln(k_2 \cdot T^{-1}) = f(T^{-1})$ plot (Fig. 3-10) according to the Eyring equation:

$$\ln\left(\frac{k_2}{T}\right) = -\frac{\Delta^{\#}H}{R} \cdot \frac{1}{T} + \frac{\Delta^{\#}S}{R} + \ln\frac{k_B}{h}$$

The numerical values of the regression line parameters listed in Table 3-1 were calculated by the least squares method.

The difference in the Gibbs free activation energy is not calculated from the corresponding activation enthalpy and activation entropy values, but directly from the ratio of the rate constants, in order to decrease the experimental error on this variable:

$$\Delta_{\Delta\text{-}\Lambda}\Delta^{\#}G = -R \cdot T \cdot \ln\frac{k_\Delta}{k_\Lambda}$$

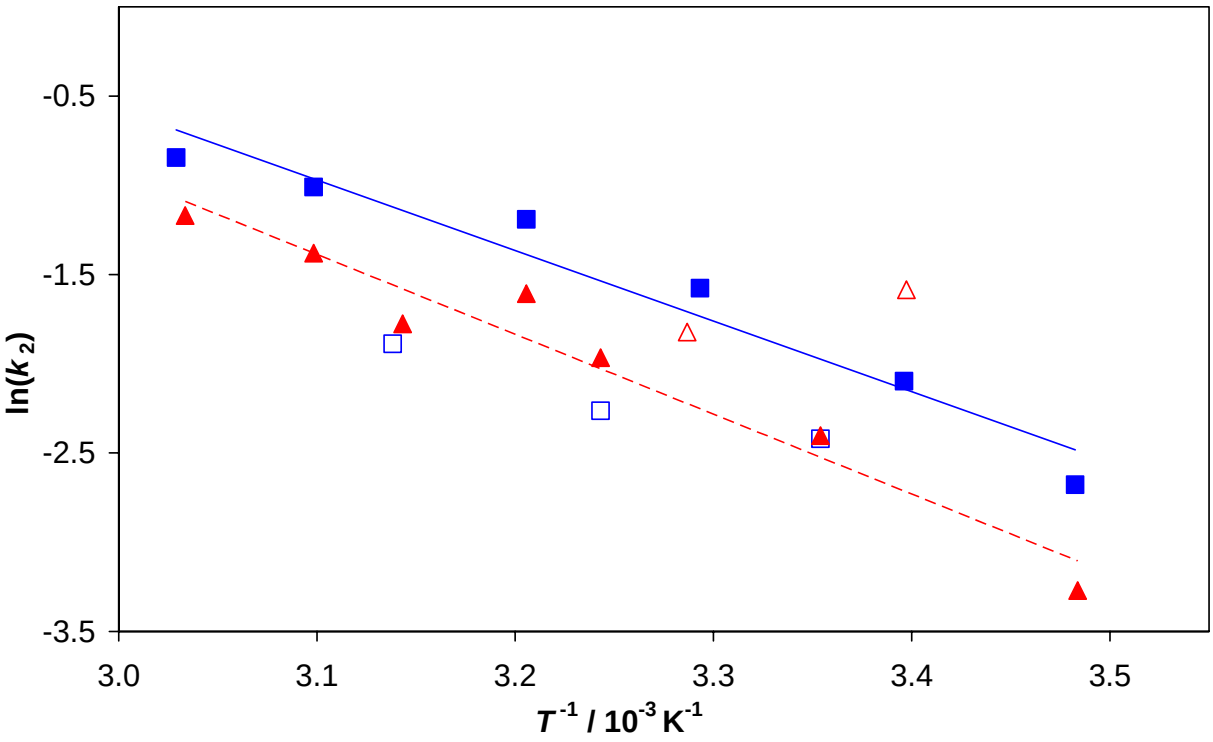

(a)

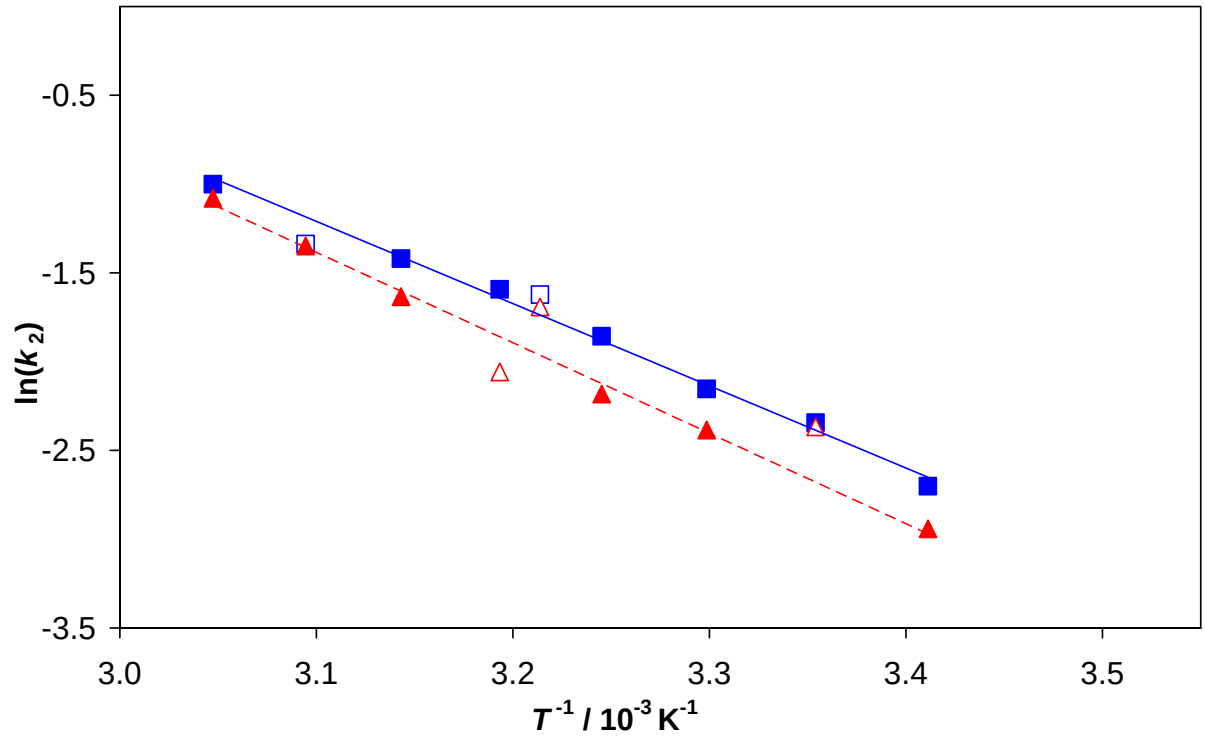

(b)

Fig. 3-9. *Arrhenius plot for the reduction of horse heart ferricytochrome* c *by* a) *[Co(alamp)H_2O] and* b) *[Co(promp)H_2O] at pH ≈ 7.5.* (—■—) Δ-(*R*,*R*) enantiomer, (---▲---) Λ-(*S*,*S*) enantiomer. Points with hollow markers (□,△) have not been taken into account for the calculation of the activation parameters.

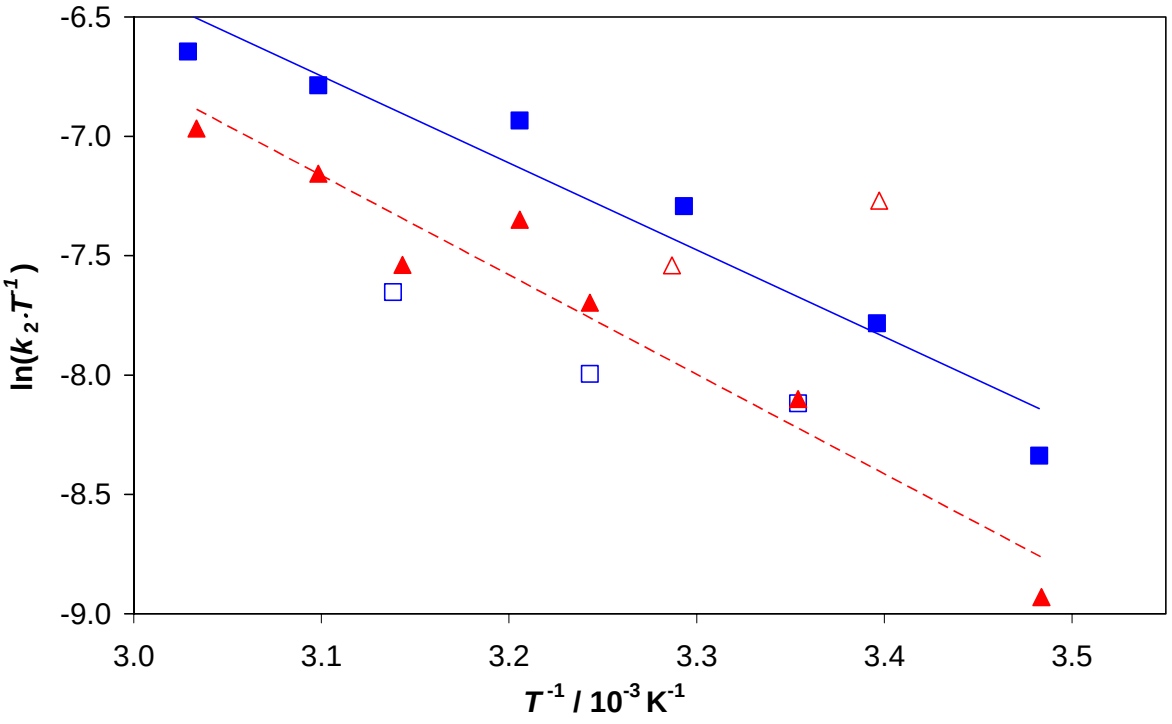

(a)

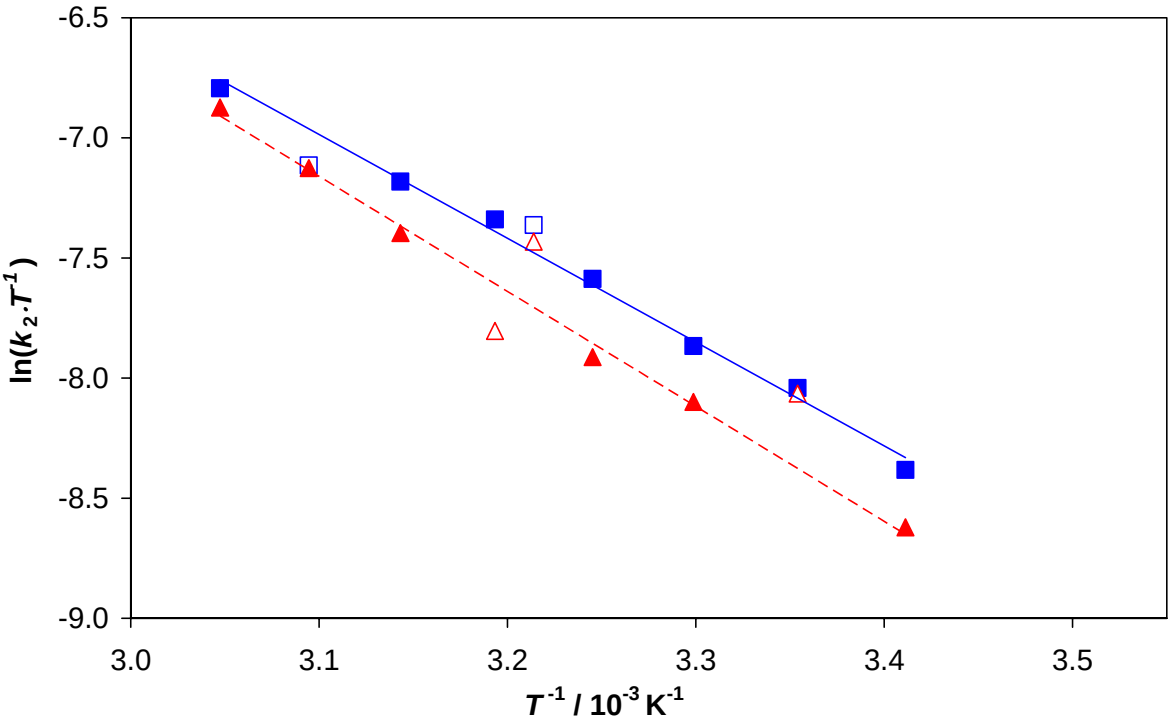

(b)

Fig. 3-10. *Eyring plot for the reduction of horse heart ferricytochrome* c *by* a) *[Co(alamp)H_2O] and* b) *[Co(promp)H_2O] at pH ≈ 7.5.* (—■—) Δ-(*R*,*R*) enantiomer, (---▲---) Λ-(*S*,*S*) enantiomer. Points with hollow markers (□,△) have not been taken into account for the calculation of the activation parameters.

As seen from Fig. 3-9 and Fig. 3-10, the experimental errors of our measurements are quite important, especially for the extrapolated values A and $\Delta^{\#}S$. This is particularly true for kinetics with $[Co^{II}(alamp)H_2O]$ where the formation of oxygen adducts influences the absorption measurements. Nevertheless, some general tendencies can be detected on Table 3-1. As expected, the error on the collision factor A is important, even bigger than the value itself[1]).

Table 3-1: *Standard Second Order Rate Constants (*$k = k_2$*) and Activation Parameters for the Reduction of Cytochrome* c *by Both Enantiomers of* $[Co^{II}(alamp)H_2O]$ *and* $[Co^{II}(promp)H_2O]$ *at pH ≈ 7.5 (Tris/HCl) and* $\mu = 0.1$.

Reducing agent	$[Co^{II}(alamp)H_2O]$		$[Co^{II}(promp)H_2O]$	
Enantiomer	Δ-(*R*,*R*)	Λ-(*S*,*S*)	Δ-(*R*,*R*)	Λ-(*S*,*S*)
k [a]) [b]) / L·mol^{-1}·s^{-1}	0.139±0.023	0.080±0.014	0.092±0.004	0.069±0.003
k_Δ / k_Λ [a]) [b])	1.73±0.59		1.34±0.11	
σ[ln (k)] [c])	0.2	0.2	0.05	0.05
E_a / kJ·mol^{-1}	32.8±4.3	38.6±4.4	38.5±1.4	42.4±1.4
A / L·mol^{-1}·s^{-1}	(7.9±13.2)·10^4	(4.7±8.0)·10^5	(5.1±2.7)·10^5	(1.8±1.0)·10^6
σ[ln (k·T^{-1})] [c])	0.2	0.2	0.05	0.05
$\Delta^{\#}H$ / kJ·mol^{-1}	30.3±4.3	34.7±4.4	35.9±1.4	39.8±1.4
$\Delta^{\#}S$ / J·mol^{-1}·K^{-1}	-160±14	-150±14	-144±4	-134±4
$\Delta_{\Delta-\Lambda}\Delta^{\#}H$ / kJ·mol^{-1}	-4.3±8.7		-3.9±2.8	
$\Delta_{\Delta-\Lambda}\Delta^{\#}S$ / J·mol^{-1}·K^{-1}	-10±28		-10±8	
$\Delta_{\Delta-\Lambda}\Delta^{\#}G$ [a]) / kJ·mol^{-1}	-1.36±0.84		-0.73±0.20	

[a]) At 25°C. [b]) Calculated by interpolation.

[c]) Values estimated visually from the Arrhenius or Eyring plot

[1]) A negative collision factor is excluded for the considered data sets.

Apart from that, *A* is 6 to 7 orders of magnitude lower than in bimolecular reactions between small molecules with zero charge product. This behaviour, equally underlined by the strongly negative activation entropy is typical for the reactions with macromolecules, their very large surface allowing only a small part of the collisions to be efficient.

Subdivision of the Gibbs free energy of a global electron transfer into enthalpy and entropy contributions is a delicate enterprise for measurements covering only a small range of temperature. Because of the consecutive nature (i.e. precursor formation and electron transfer) of the reaction, it may be more significant to consider the activation step separately from the proper electron transfer process by the means of the Eyring model. Activation enthalpy is used for the desolvation of the transfer site of cytochrome *c*, the endothermic structural changes in the donor and acceptor atoms according to the Franck-Condon principle and - in the case of inner sphere reactions - the water removal from the sixth coordination position of the cobalt(II) complex. Besides, an endergonic conformation change of the protein may also be necessary in some cases to open the access to the transfer site. Finally, the change from high spin $[Co^{II}L]$ to low spin $[Co^{III}L]$ may also raise the activation enthalpy if the change of the spin change takes place before the electron transfer. The differences in activation entropy can be due to several factors whose respective influence is difficult to evaluate, for example: number and accessibility of the active sites, probability of efficient contacts in the active sites and the number of water molecules released during the desolvation process, etc.

Fig. 3-9 and Fig. 3-10 show that both cobalt(II) complexes exhibit relatively low stereoselectivity in cytochrome *c* reduction. If there is little doubt of some stereoselective effect, a quantitative evaluation of the effect is not possible in the reductions with $[Co^{II}(alamp)H_2O]$, due to the high experimental error. Furthermore, permanent fixation has been observed during the electron transfer only for $[Co^{II}(alamp)H_2O]$ but not for $[Co^{II}(promp)H_2O]$. Probably the reaction takes place by an outer-sphere mechanism in the latter case so that the complex is released after the electron transfer. Similar behaviour is observed in the reduction of plastocyanin by these two complexes [3], whereas in the reduction of azurin [4] fixation takes also place for $[Co^{II}(promp)H_2O]$, although to a lower extent than for $[Co^{II}(alamp)H_2O]$. The supposed reaction surface of $[Co^{II}(promp)H_2O]$ is larger and flatter than in the corresponding $[Co^{II}(alamp)H_2O]$ complex (see Fig. 3-11) which means that it probably penetrates less into the solvation sphere of the protein. As a consequence, the chiral recognition by the protein surface is minor which could explain that stereoselectivity seems to be lower.

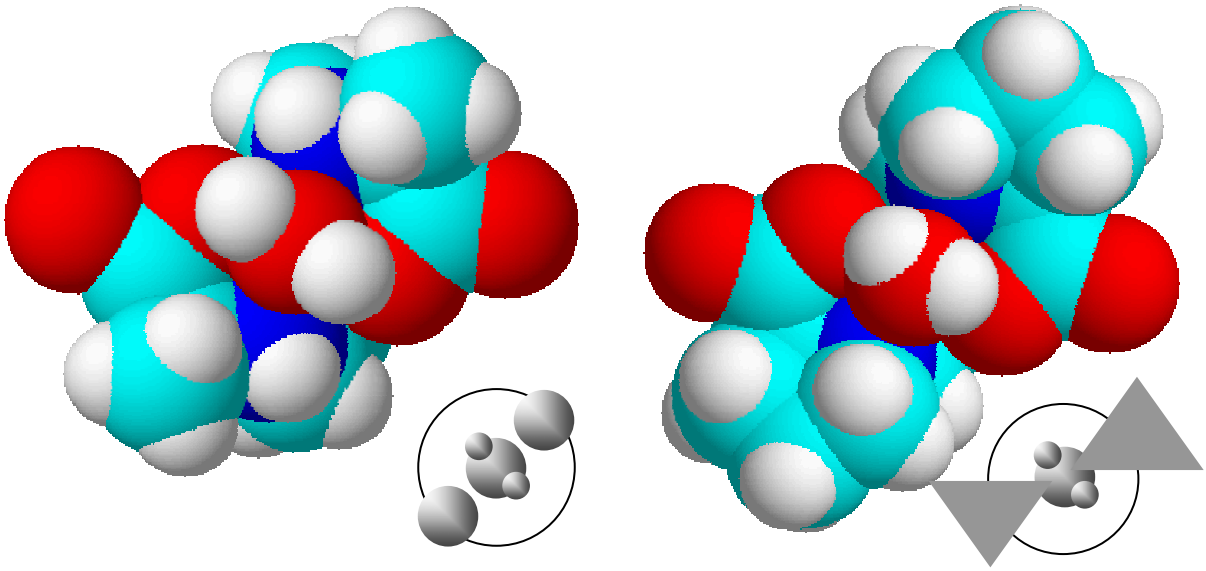

(a) (b)

Fig. 3-11. *View on the faces containing the aqua ligands of [Co^{II}(S,S)-alamp(H$_2$O)] and [Co^{II}(S,S)-promp(H$_2$O)]*. Space filling models based on the X-ray structure of corresponding cobalt(III) complexes. Images generated by [17b]

As exposed on Fig. 3-12, the stereoselectivity in the reduction of ferricytochrome *c* by [Co^{II}(promp)H$_2$O] is strongly temperature dependent and undergoes an inversion between 20 and 40°C, the inversion temperature θ_i being approximately 28°C. A similar inversion phenomenon at nearly the same temperature has also been observed when ferricytochrome *c* is reduced by the iron complexes [Fe^{II}(alamp)H$_2$O] ($\theta_i \approx$ 25°C) and [Fe^{II}(promp)H$_2$O] ($\theta_i \approx$ 30°C) [9]. Whereas a linear dependence between the logarithm of the stereoselectivity and the reciprocal temperature is observed for the reduction by [Co^{II}(promp)H$_2$O] at lower temperatures, this is no longer observed at temperatures higher than 40°C. A nonlinear behaviour has also been observed in the kinetics of ferricytochrome *c* reduction by iron(II) complexes, especially for reactions in water-alcohol mixtures [9b]. We tentatively attribute this phenomenon to a change in the configuration of the protein. Arrhenius-like plots of the relation between stereoselectivities and temperature in the reduction by [Co^{II}(alamp)H$_2$O] at pH 7.5 and 8.9 do not exhibit a clear tendency, probably because of the high experimental error.

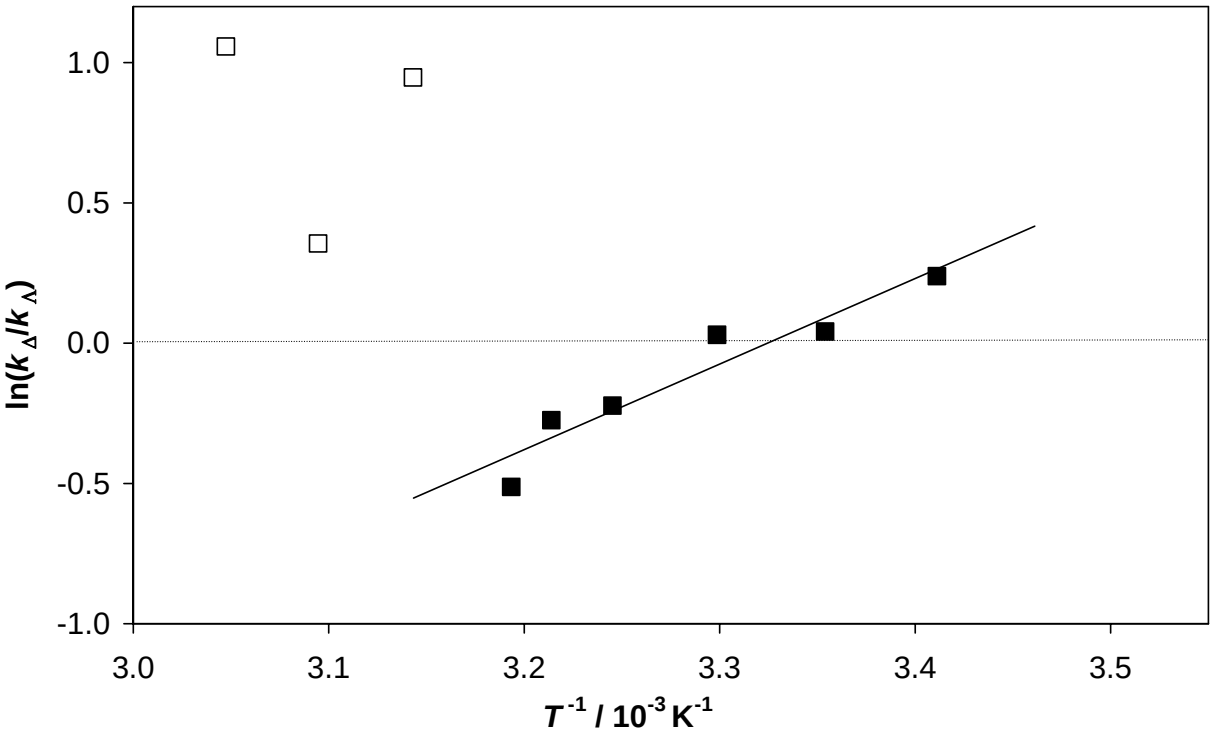

Fig. 3-12. *Variation of the logarithm of the stereoselectivity in ferricytochrome* c *reduction by [Co^{II}(promp)H_2O] at pH 7.5 with the reciprocal temperature.* Points with hollow markers (□) have not been taken into account for the trendline.

The rate constants measured for cobalt(II) complexes are three to four orders of magnitude lower than those found by Jauslin [9] for [Fe^{II}(alamp)H_2O] and [Fe^{II}(promp)H_2O] as electron donors in ferricytochrome *c* reduction under comparable reaction conditions (cf. Table 3-2). The reactions involving iron(II) complexes exhibit a 50 to 60 J·mol^{-1}·K^{-1} less negative activation entropy than for the corresponding cobalt(II) complexes. In spite of very similar sizes and geometries, the iron(II) and cobalt(II) complexes with the *alamp* ligand reveal different stereoselectivity: Whereas activation enthalpy is higher for the *Δ* enantiomer [Fe^{II}(alamp)H_2O][1]), the opposite is true for [Co^{II}(alamp)H_2O]. These differences make it plausible that the [Fe^{II}(alamp)H_2O] complexes do not interact at the same sites of the protein than the corresponding cobalt(II) species. Gray and al. [36] advance this interpretation to explain very different activation parameters in the reduction of cyt *c* by an iron(II) complex and in the oxidation by a cobalt(III) complex, both containing the same, achiral, 2,6-dicarboxylpyridine ligand. This hypothesis seems also be supported by the observation that the dif-

[1]) 36.3 kJ·mol^{-1} for the Δ enantiomer and 28.8 kJ·mol^{-1} for the Λ enantiomer [9].

ference in reaction rates between Co^{II} and Fe^{II} is essentially due to the different activation entropies. Contrary to this, analogous measurements with another metalloprotein - plastocyanin - show rate differences of more than four orders of magnitude, due to smaller differences in activation entropy than for cytochrome *c* but equally to large differences of activation enthalpy (cf. Table 3-2). On might therefore discuss a possible influence of spin state change in the Co^{II} complexes, which may be important for plastocyanin but not for cytochrome *c*.

The kinetics represented on Fig. 3-13 do not exhibit any rate saturation on the studied concentration range so that a detailed microscopic interpretation would be speculative.

Table 3-2: *Standard second order rate constants* ($k = k_2$) *and Eyring activation parameters for the reduction of plastocyanin and cytochrome* c *by both enantiomers of* $[Fe^{II}(promp)H_2O]$ *and* $[Co^{II}(promp)H_2O]$

Protein		Plastocyanin		Cytochrome c	
Metal centre		Fe^{II} [a])	Co^{II} [b])	Fe^{II} [c])	Co^{II} [d])
Reference		[2b]	[3b]	[9a]	this work
Δ-(*R*,*R*)	k [e]) / L·mol^{-1}·s^{-1}	(1.2±0.1)·10^4	1.14±0.03	458±7	0.092±0.004 [f])
	$\Delta^{\#}H$ / kJ·mol^{-1}	29.1±1.2	39.4±0.7	31.4±0.7	35.9±1.4
	$\Delta^{\#}S$ / J·mol^{-1}·K^{-1}	-68±6	-111±2	-89±2	-144±4
Λ-(*S*,*S*)	k [e]) / L·mol^{-1}·s^{-1}	(1.7±0.2)·10^4	1.38±0.06	415±7	0.069±0.003 [f])
	$\Delta^{\#}H$ / kJ·mol^{-1}	26.1±1.0	39.7±1.3	36.1±0.5	39.8±1.4
	$\Delta^{\#}S$ / J·mol^{-1}·K^{-1}	-75±6	-107±4	-74±2	-134±4
k_Δ / k_Λ [e])		0.74±0.15	0.83±0.07	1.10±0.04	1.34±0.11 [e])
$\Delta_{\Delta\text{-}\Lambda}\Delta^{\#}H$ / kJ·mol^{-1}		+3.0±2.2	-0.3±2.0	-4.7±1.2	-3.9±2.8
$\Delta_{\Delta\text{-}\Lambda}\Delta^{\#}S$ / J·mol^{-1}·K^{-1}		+7±12	+4±6	-15±4	-10±8
$\Delta_{\Delta\text{-}\Lambda}\Delta^{\#}G$ [e]) / kJ·mol^{-1}		+0.75±0.50	+0.46±0.21	-0.236±0.090	-0.73±0.20

[a]) Phosphate buffer, pH = 7.0, μ = 0.1.
[b]) Phosphate buffer, pH 7.0, μ = 0.12.
[c]) Tris / HCl buffer, pH = 7.5, μ = 0.1.
[d]) Tris / HCl buffer, pH = 7.5, μ = 0.1.
[e]) At 25°C.
[f]) Calculated by interpolation.

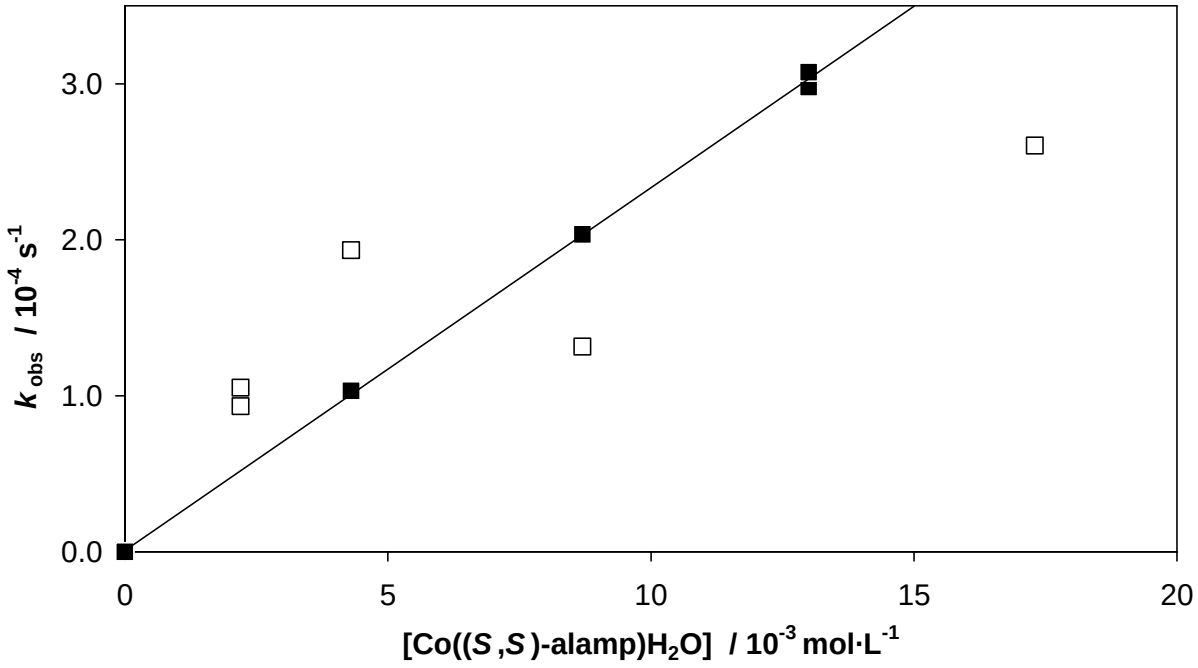

(a)

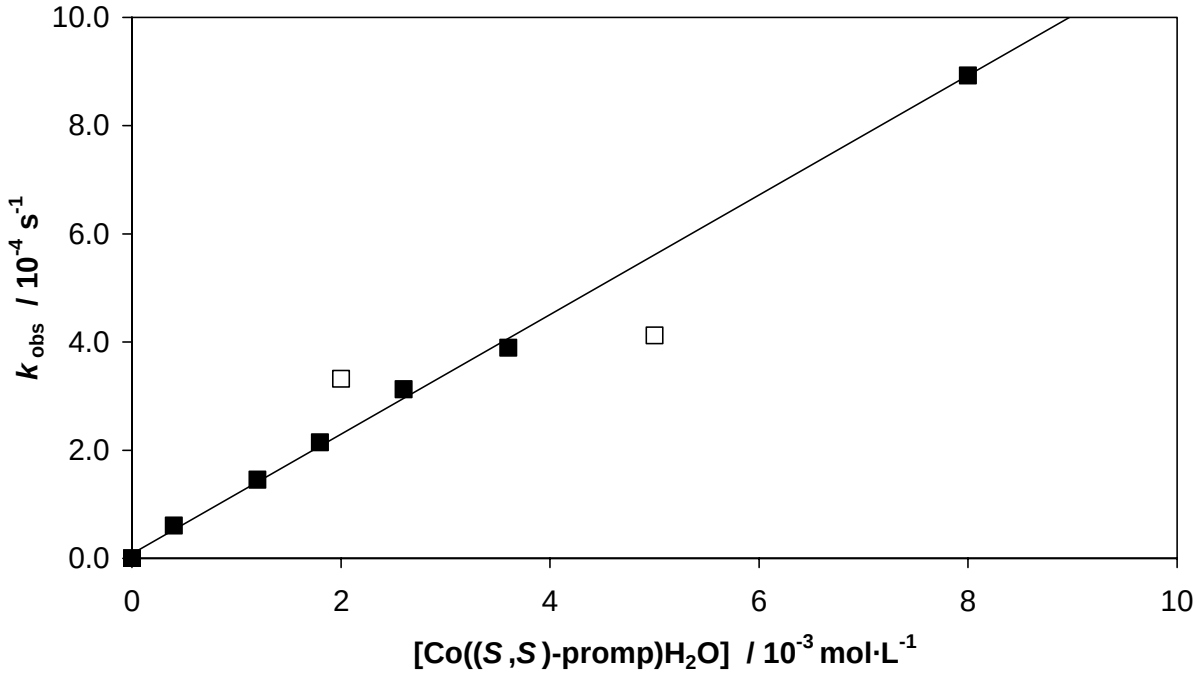

(b)

Fig. 3-13. *Concentration dependence of the observed rate constants for the reduction of oxidised horse heart cytochrome* c. a) *[Co^{II}(S,S)-(alamp)H_2O] at pH 8.9 and 23°C.* $k_2(S,S)$ = (2.33±0.18)·10^{-2} L·mol^{-1}·s^{-1} (23°C, pH 8.9). Estimated error on k_{obs}: $\sigma(k_{obs})$ = 2·10^{-5} s^{-1}. b) *[Co^{II}(S,S)-(promp)H_2O] at pH ≈ 7.4 and 38°C.* b) $k_2(S,S)$ = 0.111±0.003 L·mol^{-1}·s^{-1} (38°C, pH 7.5). Estimated error on k_{obs}: $\sigma(k_{obs})$ = 2·10^{-5} s^{-1}.
Points with hollow markers (□) have not been taken into account for the calculation of the second order constant. Note the different scales on (a) and (b).

3.4.2 Influence of pH on reaction rates

The kinetics of the electron transfer between $[Co^{II}(alamp)H_2O]$ complexes and cytochrome *c* have also been studied at pH 8.9 in the same buffer system. At this pH, the protein has a lower positive charge whereas the cobalt complexes are essentially neutral. The alkaline form of the protein, the reduction potential of which is less positive, is present at 44%. At the same time, the reduction potential of the cobalt complexes used decreases also when pH increases [21b].

Table 3-3 shows that the differences in activation parameters between enantiomers are considerably more pronounced than at pH 7.5. Besides, $\Delta_{\Delta\text{-}\Lambda}\Delta^{\#}H$ and $\Delta_{\Delta\text{-}\Lambda}\Delta^{\#}S$ are inversed.

Table 3-3: *Standard second order rate constants ($k = k_2$) and activation parameters for the reduction of cytochrome* c *by both enantiomers of $[Co^{II}(alamp)H_2O]$ at pH 8.9 (Tris/HCl) and $\mu = 0.1$.* Temperature range from 13 to 54°C

Reducing agent	Δ-(*R*,*R*)-$[Co^{II}(alamp)H_2O]$	Λ-(*S*,*S*)-$[Co^{II}(alamp)H_2O]$
k [a] [b] / $L\cdot mol^{-1}\cdot s^{-1}$	0.069±0.016	0.067±0.017
k_Δ / k_Λ [a] [b]	1.03±0.50	
$\sigma[\ln(k)]$ [c]	0.3	0.3
E_a / $kJ\cdot mol^{-1}$	45.3±6.3	30.3±5.7
A / $L\cdot mol^{-1}\cdot s^{-1}$	$(5.8\pm14.1)\cdot10^6$	$(1.4\pm3.0)\cdot10^4$
$\sigma[\ln(k\cdot T^{-1})]$ [c]	0.3	0.3
$\Delta^{\#}H$ / $kJ\cdot mol^{-1}$	42.7±6.3	27.8±5.7
$\Delta^{\#}S$ / $J\cdot mol^{-1}\cdot K^{-1}$	-124±20	-174±18
$\Delta_{\Delta\text{-}\Lambda}\Delta^{\#}H$ / $kJ\cdot mol^{-1}$	14.9±12.0	
$\Delta_{\Delta\text{-}\Lambda}\Delta^{\#}S$ / $J\cdot mol^{-1}\cdot K^{-1}$	50±38	

[a]) At 25°C. [b]) Calculated by interpolation.

[c]) Values estimated visually according to the Arrhenius or Eyring plot

3.4.3 Electron-transfer mediated binding of the reactant

The analysis of the reaction products by CD spectroscopy as described in §3.3.4 not only indicates whether there is fixation of the reacted complex or not, but also gives some information about the possible docking site.

In order to identify the chemical nature of the group bridging the protein to the Co^{III} centre, CD spectra of the following compounds have been recorded: Δ-$[Co^{III}((R,R)\text{-alamp})H_2O]^+$, Δ-$[Co^{III}((R,R)\text{-alamp})(Bu\text{-}NH_2)]^+$, and Δ-$[Co^{III}((R,R)\text{-alamp})(im)]^+$. Fig. 3-14 compares these spectra (curves b-d) with the difference spectrum of the solution obtained from the reaction between cytochrome *c* and Δ-$[Co^{III}((R,R)\text{-alamp})H_2O]^+$ (curve a[1])). It clearly shows that only the spectrum of Δ-$[Co^{III}((R,R)\text{-alamp})(im)]^+$ corresponds to the spectrum of the protein-bound reactant. The spectra of both Δ-$[Co^{III}((R,R)\text{-alamp})H_2O]^+$ and Δ-$[Co^{III}((R,R)\text{-alamp})(Bu\text{-}NH_2)]^+$ show absorption maxima at different wavelengths and the wavelength at which the CD activity is equal to zero is different too. The difference to the aqua-complex indicates that the extra CD activity of the reaction product cannot be due to an incomplete dialysis of the reacting Co^{II} complex, present in large excess and oxidised during dialysis. The difference compared to $[Co^{III}(alamp)(Bu\text{-}NH_2)]^+$, on the other hand, excludes binding to one of the solvent exposed lysine side chains of the protein. The possibility of the binding of the Co^{III} complex to the protein in a reaction consecutive to electron transfer has been tested in later experiences [37]: Cytochrome *c* was reduced by ascorbic acid under identical reaction conditions in the presence of a large excess of $[Co^{III}(alamp)H_2O]^+$, ascorbic acid being inactive against the Co^{III} complex. Some binding to the protein has been observed only at temperatures higher than 45°C, at lower temperatures the CD spectra of the reduced cytochrome *c* were identical in the presence and absence of the Co^{III} complex. Therefore, the most reliable hypothesis is electron-transfer mediated binding of $[Co^{II}(alamp)H_2O]$ to one of the histidine residues of the protein.

Since the molar dichroic absorption of *Δ*-$[Co^{III}((R,R)\text{-alamp})(im)]^+$ is known [38], the corresponding relative amount of protein-bound complex can be calculated, assuming the same CD as for the free imidazole complex. The spectra represented in Fig. 3-14 show that the calcu-

[1]) This curve is the same as curve d on Fig. 3-8. For the exact meaning of this curve, refer to §3.3.4.

lated contribution of $[Co^{III}((R,R)\text{-alamp})(\text{cyt } c)]^+$ becomes almost superimposable to the CD-spectrum of $[Co^{III}((R,R)\text{-alamp})(\text{im})]^+$ at a concentration corresponding to 28% of the initial cytochrome *c* concentration (curve e). Additional measurements allowed to distinguish the binding rates for both enantiomers and to reveal a stereoselectivity in site selection: At 15°C, separate reductions showed that 43% of the cytochrome *c* has bound the *R,R*- and 15% the (*S,S)* enantiomer [37]. The stereoselectivity observed for the overall reaction is the result of both the inner and outer-sphere part. The stereoselectivities can therefore be estimated to 5.1 for the inner- and 1.4 for the outer-sphere part (cf. appendix, §7.6.3 for the calculation method). Interestingly, the spectra of the product obtained by the reduction with the two enantiomeric cobalt complexes are not symmetrically located on either side of the spectrum of the sample reduced by ascorbic acid. Fig. 3-15 compares the spectrum of (partially) modified cytochrome *c* without the contribution of the bound Co^{III} complex (a), with the blank sample

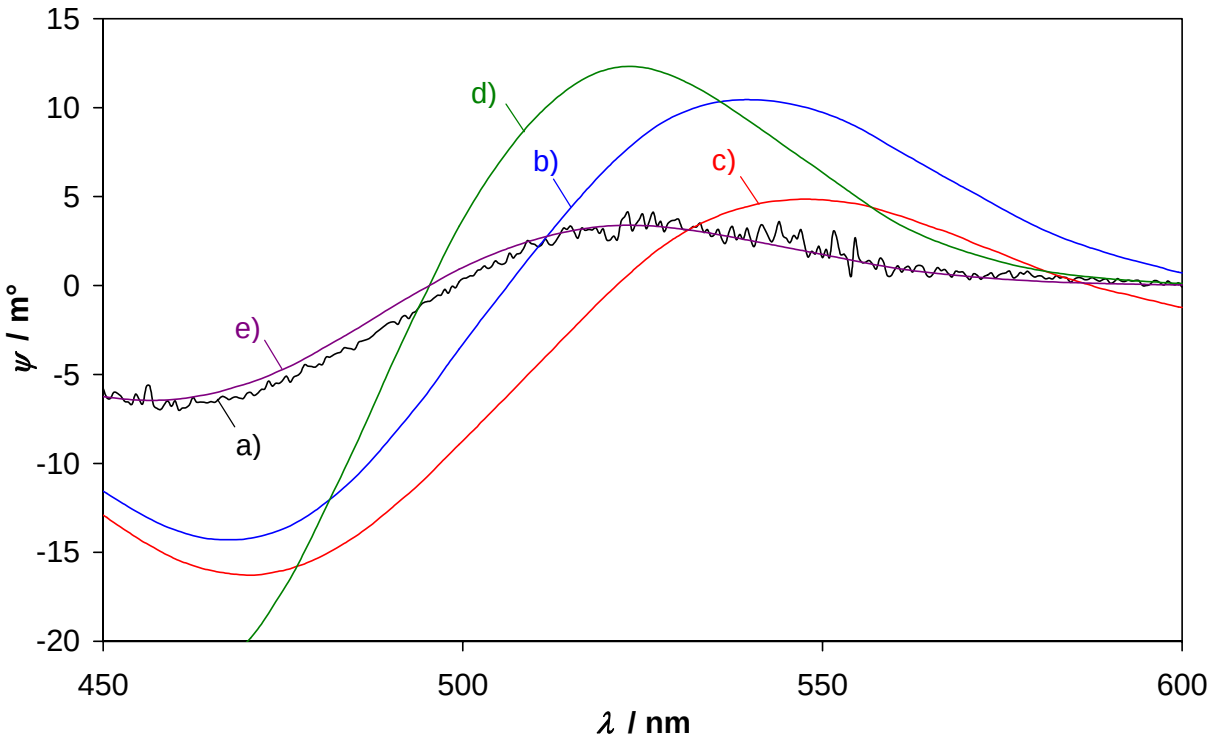

Fig. 3-14. *CD spectra recorded after the reductive fixation assay of $[Co^{II}(alamp)H_2O]$ on oxidised horse heart cytochrome* c. For further experimental details, see legend of Fig. 3-8.

a) *Mean contribution of the fixed $[Co^{III}alamp]^+$ to CD spectra after dialysis* (——). CD spectra of free metal complexes at $3.6\cdot10^{-5}$ mol·L^{-1} for comparison: b) *Δ-$[Co^{III}$((*R,R*)-alamp)$H_2O]^+$* (——),

c) *Δ-$[Co^{III}$((*R,R*)-alamp)(Bu-NH_2)$]^+$* (——), d) *Δ-$[Co^{III}$((*R,R*)-alamp)(im)$]^+$* (——),

e) *Δ-$[Co^{III}$((*R,R*)-alamp)(im)$]^+$ at $0.28\cdot3.6\cdot10^{-5}$ mol·L^{-1}* (——)

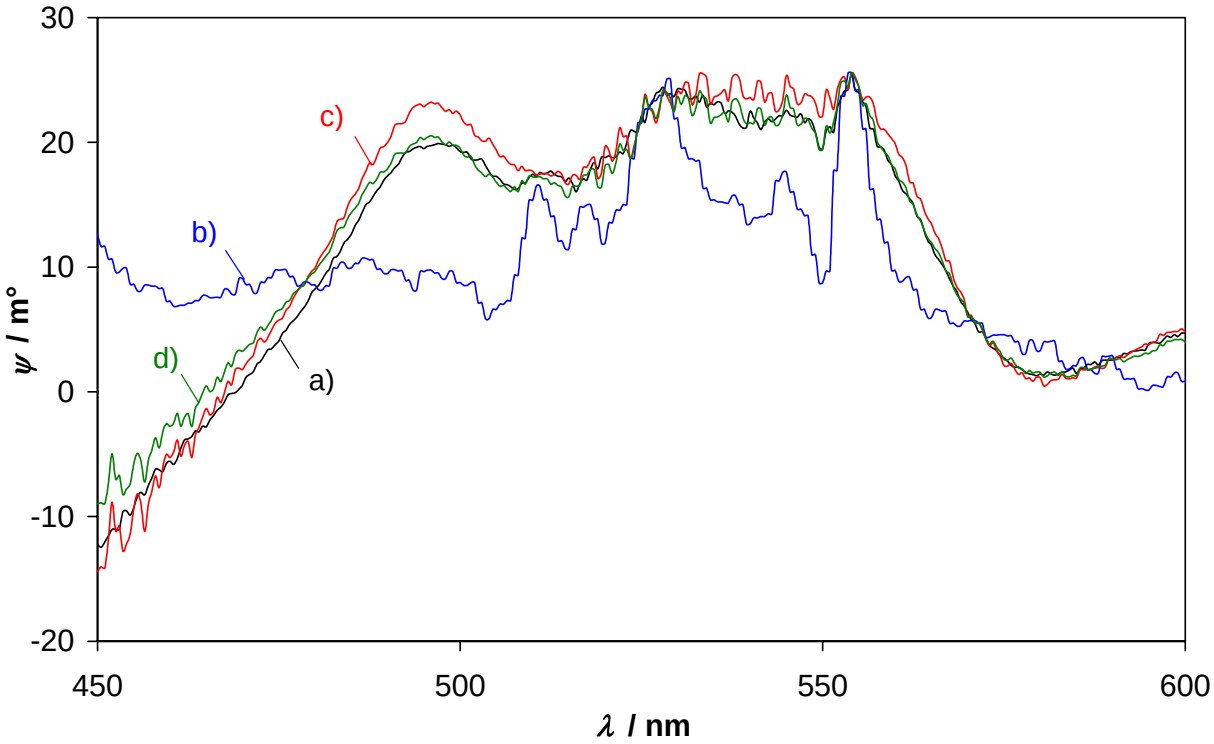

Fig. 3-15. *CD spectra recorded after the reductive fixation assay of [Co^{II}(alamp)H_2O] on oxidised horse heart cytochrome* c.

a) *Mean contribution of cytochrome* c *(haem and apoprotein) to spectra after dialysis, as on Fig. 3-8c* (——), b) *ferrocytochrome* c *obtained by the reduction of ferricytochrome c with ascorbic acid* (——), c) *ferricytochrome* c *that has undergone the same treatment as the samples that have reacted with the cobalt complex* (——), d) *calculated spectrum based on (b) and (c): mixture containing 80% of ferricytochrome* c *and 20% of ferrocytochrome* c (——).

Spectra b) and c) have been adjusted in order to present the same ellipticity as a) at 554 nm (isodichroic point). For further experimental details, see Fig. 3-8.

of ferricytochrome *c* that has undergone the same treatment than the sample (c) and ferrocytochrome *c* obtained by reduction of ferricytochrome *c* with ascorbic acid (b). When looking closer, it becomes obvious that (a) is an intermediate between (b) and (c) and that the difference between (a) and (c) is due to an almost complete re-oxidation of the protein and not to chiral induction. This assertion is confirmed by the similarity of curve (a) to curve (d), a calculated spectrum for a cytochrome c sample that contains 80% of the oxidised form.

A priori, two explanations are possible:

a) Cytochrome *c* quantitatively fixes the cobalt(III) complex, is then oxidised by air during dialysis and ejects the cobalt(III) complex. In our case, this does not seem to be the main pathway because the amount of fixed cobalt is significantly higher than the amount of re-

duced protein which suggests that the metal complex remains fixed on cytochrome *c* even when the latter is oxidised.

b) All of the protein has been reduced initially but only 30% of the cobalt(III) complex is fixed. As observed in similar cases [3a][37], one can imagine competition between reductions at different sites and partially by an outer-sphere mechanism. Reoxidation of ferrocytochrome *c* and [Co^{III}(alamp)(cyt *c*)] ($E°$ = 0.270 mV) then probably occurs by air during the dialysis that takes place during 24 h.

In additional measurements [37], the binding assays were repeated and this time the reaction products were dialysed against ascorbic acid to prevent reoxidation of the protein after the electron transfer by air oxygen. Between 500 and 540 nm, the spectra of the product obtained after the reduction with the two enantiomeric cobalt complexes were not symmetrically located on either side of the spectrum of the sample reduced by ascorbic acid. This modification of the CD spectrum of the protein is weak but nevertheless it indicates steric interactions between the protein and the chiral framework of the ligand. The fact that there is only a weak induced CD signal of the haem chromophore and no induced CD at all for the cobalt suggests that the fixation has not involved directly the coordination sphere of the iron centre. Consequently, His 18 can be disregarded as binding site in the studied system. On the other hand, His 26 and His 33 are both located on the protein surface and solvent exposed. The imino nitrogen of their imidazole groups can easily substitute the aqua ligand of labile [Co(alamp)H_2O] devoid of detectable conformation change in the protein. The long distances of 1215 and 1507 pm explain the lack of direct chiral interactions between the cobalt(III) and the haem chromophores. His 26 has a pK_a below 3.2 whereas His 33 has a pK_a value of 6.4 [18]. Fixation measurements at pH 5 can provide additional information: If the electron transfer takes place on His 33, the binding would be notably lower at pH 5 than at pH 7.5. This would contrast with the results of the reduction kinetics performed with other cobalt(II) complexes [24]. If no alternative binding sites with comparable $\Delta^{\#}G$ values are accessible on the protein, the rate constant should equally decrease notably. The observed enhancement of steric recognition in basic medium can be explored by fixation assays at various pH. Finally, a clear attribution of the binding site(s) would be possible only by either the chemical analysis of protein fragments or by the reaction with the protein modified at one or the other site.

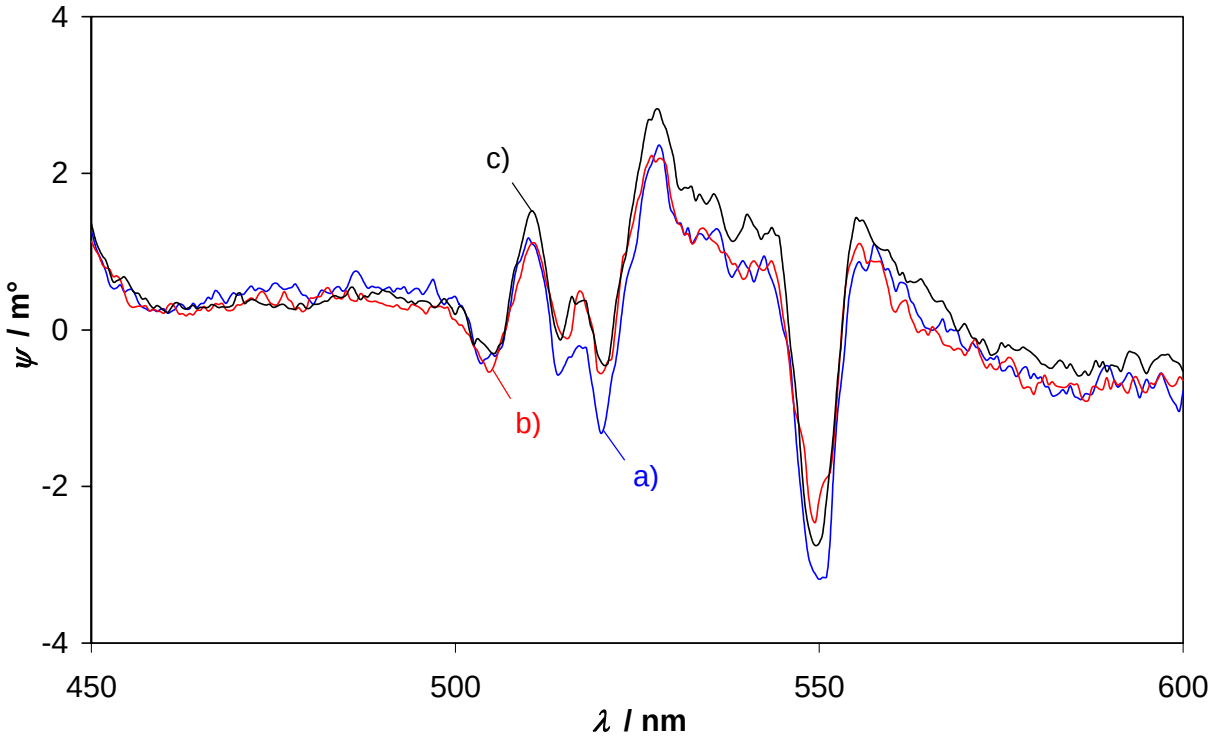

Fig. 3-16. *CD spectra recorded after the reductive fixation assay of [Co^{II}(alamp)H$_2$O] on oxidised horse heart cytochrome* c. pH = 7.59 / 7.70 (μ = 0.1, Tris/HCl); Θ = 15°C during 215 / 174 min, Θ = r.t. during 25 h (dialysis); [cytochrome *c*] = 3.7·10^{-5} mol·L^{-1} (by weight), optical path length: *l* = 5.00 cm. Data from [37].
a) *Contribution of the cytochrome* c *to the spectrum of the reaction mixture after reduction by [Co^{II}((*R,R*)-alamp)H$_2$O] and dialysis* (——), b) *Contribution of the cytochrome* c *to the spectrum of the reaction mixture after reduction by [Co^{II}((*S,S*)-alamp)H$_2$O] and dialysis* (——), c) *ferrocytochrome* c *obtained by reduction of ferricytochrome c with ascorbic acid* (——).
Spectra b) and c) have been adjusted in order to present the same ellipticity as a) at 554 nm (isodichroic point).

3.5 Experimental part

3.5.1 General

Reagents, solvents, material and instruments for preparative and analytical material have been used as indicated in §2.2.

3.5.1.1 Buffer solutions

See §2.1.2. pH 9 buffer with ionic force μ = 0.2 has been prepared from 1.0M hydrochloric acid, solid Tris and NaCl (0.15M). Although the solution is at the upper limit of the Tris buffer domain, no significant pH shift has been observed during the reaction.

3.5.1.2 Sample handling

All samples were freed from dissolved O_2 by gently bubbling Ar for at least 15 min and handled in an inert atmosphere. Small volumes were measured with micropipettes or weighed.

3.5.2 Cyt *c* reduction with optically active cobalt(II) complexes

3.5.2.1 Measurements

H_2L' = H_2(*R*,*R*)- or H_2(*S*,*S*)-promp·*x*HCl (M_r = 333.39 + *x*·36.45), H_2(*R*,*R*)- or H_2(*S*,*S*)-alamp (M_r = 281.36). Co^{II} complexes in μ = 0.1 buffer were prepared from solutions of $CoSO_4 \cdot 7H_2O$, of neutralised H_2L in 1.25-fold excess and the corresponding buffer. Freshly defrosted cytochrome *c* (M_r = 13'000) was dissolved at a concentration of $7.30 \cdot 10^{-5}$M in the corresponding μ = 0.1 buffer. The compartments of a 2x0.475 cm tandem cell were respectively filled with 0.5 mL complex and protein solution and thermostated at the desired temperature. Absorption spectra between 500 and 570 nm (scan speed: 100 nm·min^{-1}) towards μ = 0.1 buffer were recorded before mixing and at regular intervals after mixing. The *in situ* concentrations of Co^{II} complex were $2.00 \cdot 10^{-3}$M for the activation parameter determination and varied from $2.00 \cdot 10^{-3}$M to $20.0 \cdot 10^{-3}$M for the second order constant determination.

For each complex type and concentration, the absorption of a blank sample containing all components except cytochrome *c* is measured as a function of time. This sample yields the mean contribution of the $[Co^{II}L(H_2O)]$ complex to the total absorption of the sample.

The effective ligand concentrations were checked by a spectropolarimetric titration with a copper(II) solution at pH 5 in 0.1M acetate buffer. The molar dichroic absorption of the formed dark blue complex is $\Delta\varepsilon$ = 0.465 L·mol^{-1}·cm^{-1} at 560 nm.

3.5.3 Fixations

3.5.3.1 Measurements

Co^{II} complex at a concentration of 0.05M in μ = 0.1 buffer was prepared from solutions of $CoSO_4 \cdot 7H_2O$, neutralised H_2L in 1.5-fold excess and the corresponding buffer. Freshly defrosted cytochrome *c* (M_r = 13'000) was dissolved at a concentration of $3.65 \cdot 10^{-4}$M in μ = 0.1 buffer. Complex (0.5 mL) and protein solutions (0.5 mL) were mixed and confined in sealed test tubes under argon. Simultaneously, three samples containing the (*R*,*R*) or the (*S*,*S*) enantiomer of the Co^{II} complex (both in 55-fold excess vs. the protein) or ascorbic acid (in 500-fold excess) as reducing agent were prepared. The samples were kept at 35°C until no more increase of the absorption at 550 nm was observed for an aliquot sample containing the Co^{II} complex. Each solution was dialysed separately during 20 h in 1.5 L of μ = 0.01 buffer solution. All buffer solutions were replaced after 10 h. The samples were drawn out of the dialysis bags, diluted to 1.2 g and their CD spectra between 300 nm and 700 nm (scan speed: 20 nm·min^{-1}) were recorded towards μ = 0.1 buffer.

3.6 References

[1] K.M. Yocom, J.B. Shelton, J.R. Shelton, W.A. Schroeder, G.W. Worosila, S.S. Isied, E. Bordignon, H.B. Gray, *Proc. Natl. Acad. Sci. USA* **1982**, *79*, 7052.

[2] a) K. Bernauer, J.J. Sauvain, *J. Chem. Soc., Chem Commun.* **1988**, *353*; b) J.J. Sauvain, Ph.D. Thesis, Université de Neuchâtel, 1990.

[3] a) K. Bernauer, P. Schürmann, C. Nusbaumer, L. Verardo, S. Ghizdavu, *Pure Appl. Chem.* **1998**, *70*, 985; b) L. Verardo, Ph.D. Thesis, Université de Neuchâtel, 1996.

[4] K. Bernauer, S. Ghizdavu, L. Verardo, *Coord. Chem. Rev.* **1999**, *190-192*, 357.

[5] J.R. Pladziewicz, S.O. Gullerud, M.A. Accola, *Inorg. Chim. Acta* **1994**, *225*, 151.

[6] K. Bernauer, M. Monzione, P. Schürmann, V. Viette, *Helv. Chim. Acta* **1990**, *73*, 346.

[7] a) S. Sakaki, Y. Nishijima, H. Koga, K. Ohkubo, *Inorg. Chem.* **1989**, *28*, 4061 and references therein; b) S. Sakaki, Y. Nishijima, H. Koga, K. Ohkubo, *J. Chem. Soc. Dalton Trans*, **1991**, 1143.

[8] J.T. Ficke, J.R. Pladziewicz, E.C. Sheu, A.G. Lappin, *Inorg. Chem.* **1991**, *30*, 4282.

[9] a) K. Bernauer, P. Jauslin, *Chimia* **1993**, *47*, 218 and references therein; b) P. Jauslin, Ph.D. Thesis, Université de Neuchâtel, 1994.

[10] G.W. Pettigrew, G.R. Moore, 'Cytochromes c, Biological Aspects', Springer, Berlin, 1987 and references therein.

[11] a) H.A. Harbury and R.H.L. Marks, in 'Inorganic Biochemistry', Ed. G.L. Eichhorn, Elsevier, Amsterdam, 1973, Vol. 2, pp 902 and references therein; b) G.R. Moore, G.W. Pettigrew, 'Cytochromes c, Evolutionary, Structural and Physicochemical Aspects', Springer, Berlin, 1990 and references therein.

[12] J. Macyk, R. van Eldik, *J. Chem. Soc., Dalton Trans.* **2001**, *2288* and references therein.

[13] J. Sun, J.F. Wishart, R. von Eldik, D. Shalders, T.W. Swaddle, *J. Am. Chem. Soc.* **1995**, *117*, 2600.

[14] D. Eden, J.B. Matthew, J.J. Rosa, F.M. Richards, *Proc. Natl. Acad. Sci. USA* **1982**, *79*, 815.

[15] G.W. Bushnell, G.V. Louie, G. D. Brayer, *J. Mol. Biol.* **1990**, 585. Data file from www.pdb.org.

[16] L. Banci, I. Bestini, H.B. Gray, C. Luchinat, T. Reddig, A. Rosato, P. Turano, *Biochemistry* **1997**, *36*, 9867. Data file from www.pdb.org.

[17] a) Eric Martz, 'Protein Explorer', version 1.982, Program for the visualisation of .pdb data files, University of Massachusetts, Amherst, United States of America, 2002; b) 'MDL® Chime', version 2.6 SP6, Browser plug-in for the three-dimensional visualisation of chemical structures, Elsevier MDL, San Ramon, United States of America, 2004.

[18] R.W. Shaw, C.R. Hartzell, *Biochemistry* **1976**, *15*, 1909 and references therein.

[19] L.A. Davis, A. Schneiter, G.P. Hess, *J. Biol. Chem.* **1974**, *249*, 2624.

[20] G.R. Moore, C.G.S. Eley, G. Williams, in 'Advances in Inorganic and Bioinorganic Mechanisms', Ed. A.G. Sykes, Academic Press, London, 1984, Vol.3, p. 1-96.

[21] a) H.J. Hilgers, K. Bernauer, *Inorg. Chim. Acta* **1998**, 275-276, 9; b) H.J. Hilgers, Ph.D. Thesis, Université de Neuchâtel, 1995.

[22] a) W.H. Koppenol, C.A. Vroonland, R. Braams, *Biochim. Biophys. Acta* **1978**, *503*, 499; b) W.H. Koppenol, S. Ferguson-Miller, N. Osheroff, S.H. Speck, E. Margoliash in 'Oxidases and Related Redox Systems', Ed. T.E. King, M. Morrison, Pergamon, New York, 1982.

[23] a) J. Butler, D.M. Davies, A.G. Sykes, W.H. Koppenol, N. Osheroff, E. Margoliash, *J. Am. Chem. Soc.* **1981**, *103*, 469; b) J.Butler, S.K. Chapman, D.M. Davies, A.G. Sykes, S.H. Speck, N. Osheroff, E. Margoliash, *J. Biol. Chem.* **1983**, *258*, 6400 and references therein.

[24] P.L. Drake, R.T. Hartshorn, J. Mc Ginnis, A.G. Sykes, *Inorg. Chem.* **1989**, *28*, 1361.

[25] R. Langen, I. Chang, J. P. Germanas, J. H. Richards, J. R. Winkler, H. B. Gray, *Science* **1995**, *268*, 1733.

[26] S.S. Isied, C. Kuehn, G. Worosila, *J. Am. Chem. Soc.* **1981**, *106*, 1722.

[27] R. Bechtold, M.B. Gardineer, A. Kazmi, B. van Hemelryck, S. Isied, *J. Phys. Chem.* **1986**, *90*, 3800.

[28] M.L. Tobe, 'Reaktionsmechanismen der Anorganischen Chemie', Verlag Chemie, Weinheim, 1972.

[29] R.A. Holwerda, D.B. Knaff, H.B. Gray, J.D. Clemmer, R. Crowley, J.M. Smith, A.G. Mauk, *J. Am. Chem. Soc.* **1980**, *102*, 1142.

[30] N. Sutin, *J. Phys. Chem.* **1986**, *90*, 3465.

[31] G.D. Armstrong, J.D. Sinclair-Day, A.G. Sykes, *J. Phys. Chem.* **1986**, *90*, 3805.

[32] H.E. Toma, R.A. Murakami, *Inorg. Chim. Acta* **1984**, *93*, L33.

[33] R.A. Marusak, T.P. Shields, A.G. Lappin, in 'ACS Advances in Chemistry', Ed. M.K. Johnson, R.B. King, D.M. Kurtz, C. Kutal, M.L. Norton, R.A. Scott, ACS Publications, Washington D.C., 1990, Vol. 226, p.237-252.

[34] K.G. Brandt, P.C. Parks, G.H. Czerlinski, G.P. Hess, *J. Biol. Chem.* **1966**, *241*, 4180.

[35] J. Weber, 'Memo sur le calcul d'erreur (Travaux pratiques de physique)', Université de Neuchâtel, 1994. P.R. Bevington, D.K. Robinson, 'Data Reduction and Error Analysis for the Physical Sciences', McGraw-Hill, New York, 1992.

[36] A.G. Mauk, C.L. Coyle, E. Bordignon, H.B. Gray, *J. Am. Chem. Soc.* **1979**, *101*, 5054.

[37] U. Scholten, A. Castillejo Merchán, K. Bernauer, *J. Roy. Soc. Interface* **2005**, *2*, 109.

[38] A. Thiam, Ph.D. Thesis, Université de Neuchâtel, 1996.

CHAPTER 4:
CYTOCHROME *C* REDUCTION
CATALYSED BY AN OPTICALLY ACTIVE CHROMIUM(II) COMPLEX

4.1 Use of chromium(II) complexes in electron transfer with metalloproteins

Compared to $[Co^{III}(H_2O)_6]^{3+}$, the aqua-ion of chromium(III) has a much lower normal reduction potential: -0.407 V [1]. The considerable difference of the ionic radii in the +III and +II oxidation states (63 and 89 pm [1]) allow fine tuning of the redox potential by the choice of a ligand system with the appropriate coordination cage dimensions such that the chromium(II) complex becomes accessible as electron donor for several low-potential metalloproteins such as ferredoxin [2]. In general, aqueous solutions of chromium(II) can be prepared by oxidation of metallic chromium by acids (e.g. HCl, H_2SO_4 or $HClO_4$) under rigorously oxygen free conditions [3]. The aquacomplex of chromium(II) is sensitive not only towards air oxygen; it can even be oxidized (slowly) by water itself [4]. Nevertheless, it has been used successfully for the reduction, modification and affinity labelling of various metalloproteins such as azurin, stellacyanin [5] and plastocyanin [6].

The aqua-ion of chromium(II) was one of the first inorganic compounds employed for reducing cytochrome *c*. Kowalsky [7] used Cr^{2+} as perchlorate and observed a binding rate of approximately 50% vs. cytochrome *c* at pH 4.8 and 7; the rate rose nearly to 100% when phosphate was present. In this case, phosphate was also bound in a 1:1 ratio to cytochrome *c* and the modified protein exhibited still some activity towards biological redox-partners, such as cytochrome oxidase. The chromium-modified cytochrome *c* could be re-oxidized by ferricyanide and again reduced by dithionite with little loss. However, a reduction of the re-oxidized Cr-modified protein by Cr^{2+} ions occurred only partially. The thioether linkage at Cys 17 was suggested as ligand for the chromium but this could not be proven. Others think that the metal is most likely bound to Tyr 67 and Asp 52 [8]. This assumption is in disagreement with measurements of the paramagnetic effects of the attached Cr^{III} moiety on the ^1H nuclear relaxation rates [9]. These located this metal at a distance of 1.4 nm from the heme, which points near the His 26 group, an amino-acid that has already been considered as ligand for other metals (see chapter 3). Kinetic studies revealed that the chromous ion reduced cytochrome *c* with

clearly positive activation entropy whereas the latter was negative in the reduction of *Rhus* laccase or spinach plastocyanin [10]. Catalytic effect of anions, such as I^-, N_3^- and SCN^- have been reported [11]. In presence of chloride, the maximum reduction rate is observed at pH 3.7.

Nevertheless, the reduction with an optically active chromium(II) complex has not been mentioned thus far. The ligand system presented in chapter 1 constitutes an interesting solution: Indeed, the chromium(II) complexes with these ligands should be enantiomerically pure and labile towards ligand exchange; furthermore, they should exhibit a negative reduction potential, even noticeably lower than the aqua ion because of the very constricting nature of the three-dimensional ligand framework. Finally their optical activity may allow determination of the group(s) of the protein coordinated on the chromium centre by circular dichroism. As direct synthesis from $CrCl_2$ and the ligand in aqueous solution under air-free conditions did not succeed, we prepared the $[Cr^{III}((S,S)\text{-promp})H_2O]^+$ complex and tried its reduction by electrolytic and chemical means.

4.2 Properties of $[Cr^{III}((S,S)\text{-promp})H_2O]^+$ and its derivatives

4.2.1 Crystal structure

$[Cr^{III}((S,S)\text{-promp})H_2O]^+$ crystallizes as perchlorate salt in the form of needles or plates, depending on the perchloric acid concentration of the solution. The X ray structure (Fig. 4-1a) reveals, as expected, a Λ configuration of the aminocarboxylate rings for the (*S*,*S*) enantiomer. As already observed in the corresponding cobalt(III) complex [12], the pyrrolidine rings are disordered and allow two possible positions for atoms C(8) (occupancy 0.657/0.343) and C(14) (occupancy 0.491/0.509). As shown by the comparison on Table 4-1, coordination bond lengths are slightly longer for the chromium(III) complex then for the cobalt(III) complex; indeed periodic trends predict a bigger ionic radius for Cr^{3+}. This difference is equally underlined by the more important distortion of the plane containing the metallic centre and the aminocarboxylate donor atoms N(2), N(3), O(1) and O(3): In opposition to the O-M(1)-N(1) angles, the N-M(1)-N(1) angles are considerably smaller than 90° because the five-membered chelate rings containing these atoms are rigid due to the aromatic C-N bonds and cannot compensate the strain imposed by the coordination centre.

Within one crystal layer, the pyridine rings adopt a coplanar arrangement (cf. Fig. 4-1b); they are tilted towards the crystal axis and in a staggered position relative to the pyridine planes of the adjacent layer. Each carbonyl oxygen atom, O2 and O4, is linked to the water ligand of two neighbouring cations by hydrogen bonding, forming a supramolecular helical polymer. A disordered water molecule was located in a 1:4 ratio with respect to the ion pairs [13c].

Table 4-1. *Comparison of found bond lengths and angles involving the coordination centre in Λ-[M^{III}((*S,S*)-promp)H_2O]ClO_4*..Uncertainties on the last digits are indicated in parentheses. Data for the cobalt(III) complex from [12]. Atom numbering according to Fig. 4-1a. W = coordinated water molecule.

Bond	M = Co	M = Cr	Bond	M = Co	M = Cr
	d / pm	*d* / pm		*d* / pm	*d* / pm
M(1)-O(1)	187.1(3)	192.9(2)	M(1)-O(1W)	196.1(3)	200.6(2)
M(1)-O(3)	188.5(3)	194.6(2)	M(1)-N(3)	187.1(3)	209.5(2)
M(1)-N(1)	184.6(3)	198.6(2)	M(1)-N(2)	187.1(3)	209.7(2)
N(1)-M(1)-N(2)	82.2(1)	79.3(1)	N(2)-M(1)-O(3)	93.6(1)	96.5(1)
N(1)-M(1)-N(3)	82.6(1)	78.7(1)	N(3)-M(1)-O(1)	92.5(1)	96.8(1)
N(1)-M(1)-O(1)	90.4(1)	90.0(1)	N(3)-M(1)-O(1W)	96.1(1)	100.2(1)
N(1)-M(1)-O(1W)	177.6(1)	177.2(1)	N(3)-M(1)-O(3)	87.2(1)	83.6(1)
N(1)-M(1)-O(3)	94.3(1)	94.6(1)	O(1)-M(1)-O(1W)	87.7(1)	87.5(1)
N(2)-M(1)-N(3)	164.8(1)	157.9(1)	O(1)-M(1)-O(3)	175.2(1)	175.4(1)
N(2)-M(1)-O(1)	87.9(1)	84.8(1)	O(3)-M(1)-O(1W)	87.6(1)	87.9(1)
N(2)-M(1)-O(1W)	99.1(1)	101.8(1)			

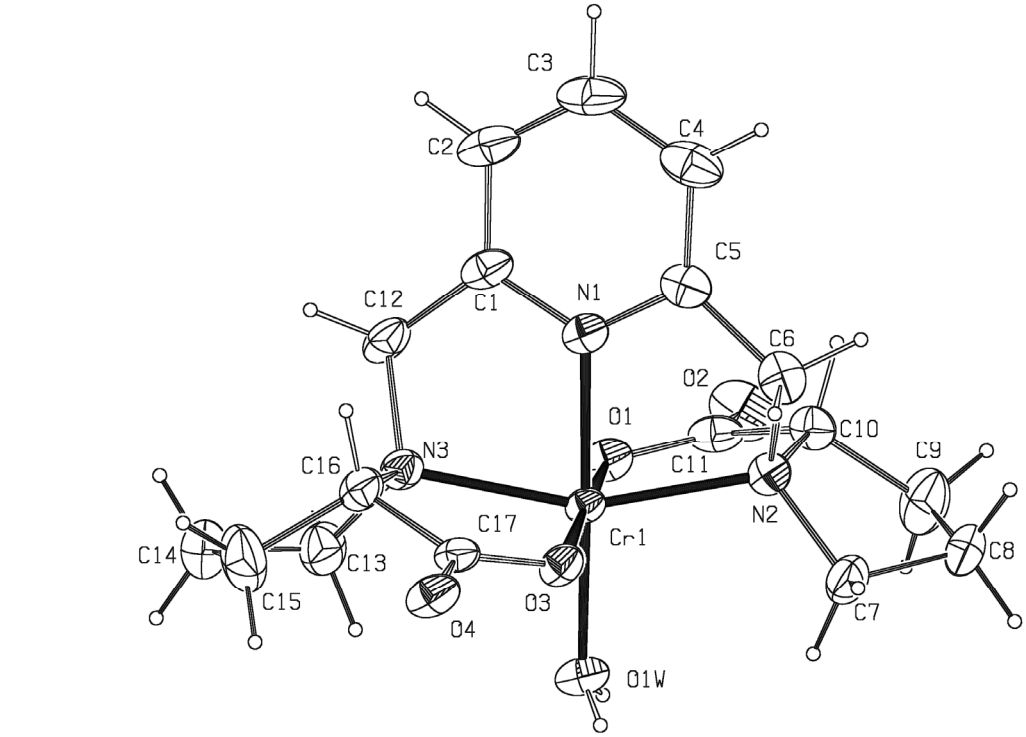

(a)

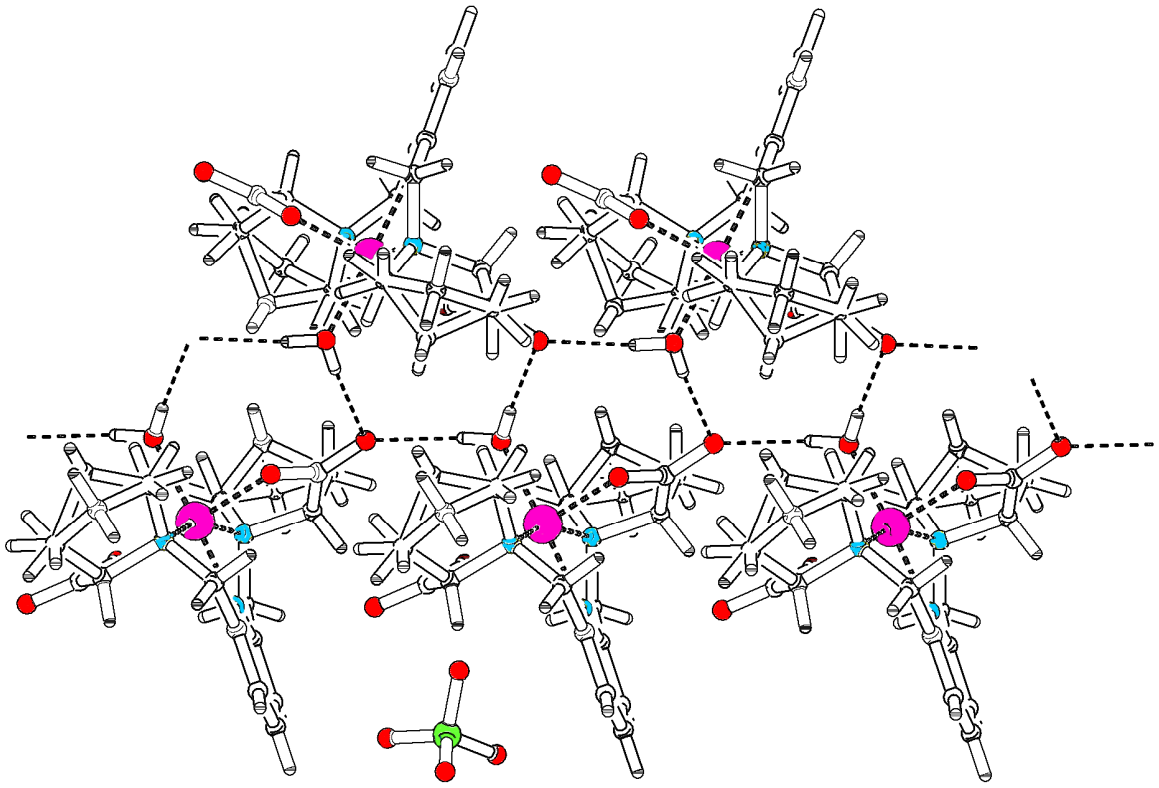

(b)

Fig. 4-1. *X-ray structure of Λ-[Cr^{III}((S,S)-promp)H$_2$O]ClO$_4$.* a) *Single cation and* b) *crystal packing.* Crystal water is not represented. Images generated by [13]. Crystallographic data, see §7.1.2 in the appendix.

4.2.2 Acid base properties

Several titration methods have been used to determine the acidity constant of $[Cr^{III}((S,S)\text{-promp})H_2O]^+$. Potentiometric and polarimetric [14a] titrations (Fig. 4-2) have yielded very similar pK_a values (6.94 vs. 6.95) whereas calculations based the absorption and ellipticity change versus pH [14a] have led to very widespread results.

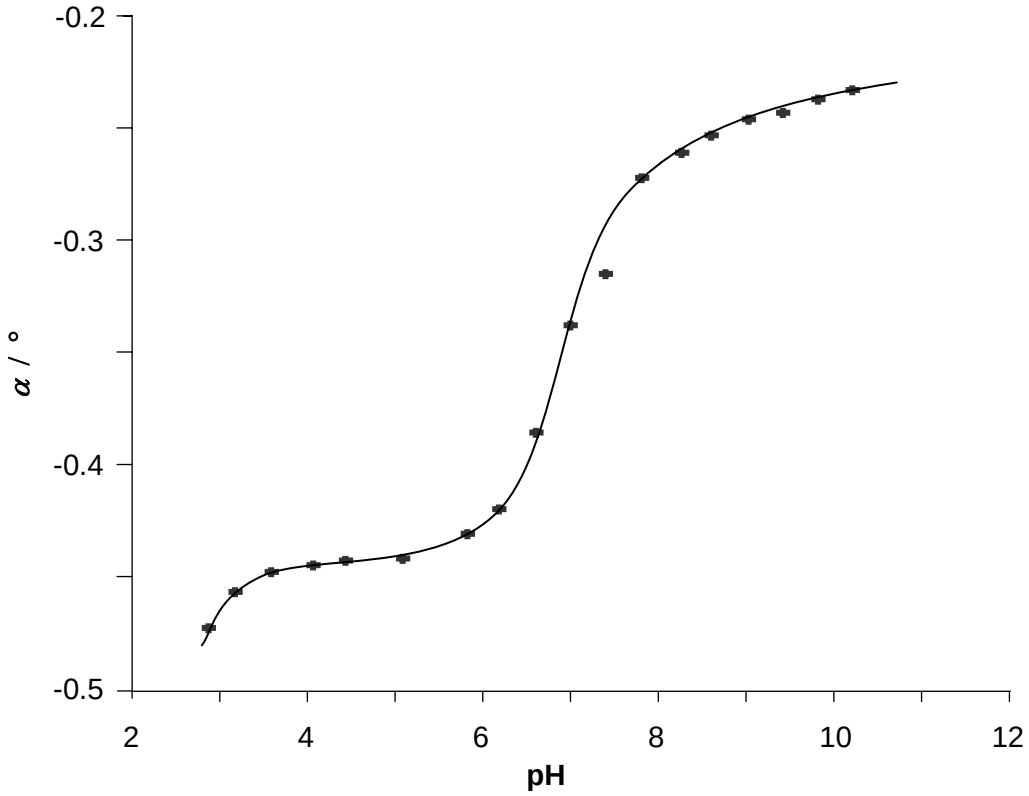

Fig. 4-2. *Polarimetric titration of* $[Cr^{III}((S,S)\text{-promp})H_2O]^+$ 10^{-2} *M*. Change of the optical rotation vs. pH at λ = 436 nm in a 10.0 cm cell.

4.2.3 Electrochemical properties

Cyclovoltammetric measurements of a $[Cr^{III}((S,S)\text{-promp})H_2O]^+$ solution at pH 7.0 (an almost equimolar mixture of $[Cr^{III}((S,S)\text{-promp})H_2O]^+$ and $[Cr^{III}((S,S)\text{-promp})OH]$) showed, at the considered scan speed, a slightly irreversible behaviour [14a]. The half wave potential of $[Cr^{III}((S,S)\text{-promp})H_2O]^+$ is -1.02 V *vs.* SHE at pH 7.0; it is notably lower than for the chromium complex with the more planar tetradentate ligand 1,4,8,12-tetraazacyclopentadecane

(15-aneN$_4$) [15][1]) used by Sykes and al. in cytochrome *c* reduction. As explained in the next section, the [Cr^{II}(promp)H$_2$O] so formed is likely to be re-oxidized rapidly by the water protons, so that the chromium(II) concentration is always very small. As a consequence, the voltammetric wave occurs at a mixed potential, which means that the actual standard potential is still more negative.

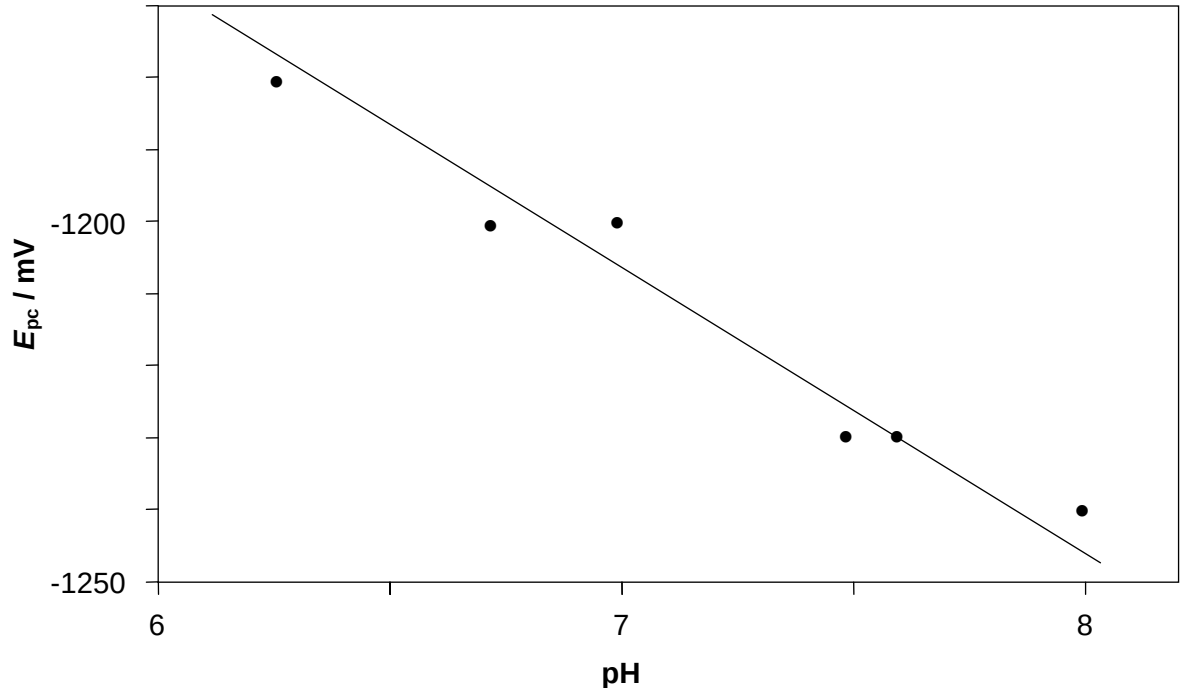

Fig. 4-3. *Evolution of the cathodic peak potential vs. pH of [Cr^{III}((*S,S*)-promp)H$_2$O]$^+$ / [Cr^{III}((*S,S*)-promp)OH] 10^{-3}M in 0.1M phosphate buffer.* According to [14a].

4.2.4 Chiroptical properties

ORD and CD spectra of the aqua-, hydroxy- and chlorocomplex of [Cr^{III}((*S,S*)-promp)X] are compared on Fig. 4-4 and Fig. 4-5. The shape of the ORD spectrum of the aqua-complex seems to be very different to that of the corresponding hydroxy-complex. The apparently opposite Cotton effects at the zero angle points near 500 nm are due to a hypsochromic shift of

[1]) $E_{\frac{1}{2}}$ = -0.58 V for [Cr^{III}(15-aneN$_4$)(H$_2$O)$_2$]$^{3+}$ *vs.* SHE in (15-aneN$_4$) 0.4M H$^+$. By extrapolation of the diagram on Fig. 4-3, $E_{\frac{1}{2}}$ = -0.81 V for [Cr^{III}((*S,S*)-promp)H$_2$O]$^+$ *vs.* SHE under the same conditions. A peak separation of 0.04 V (the same as at pH 7.0) has been supposed at pH 0.4.

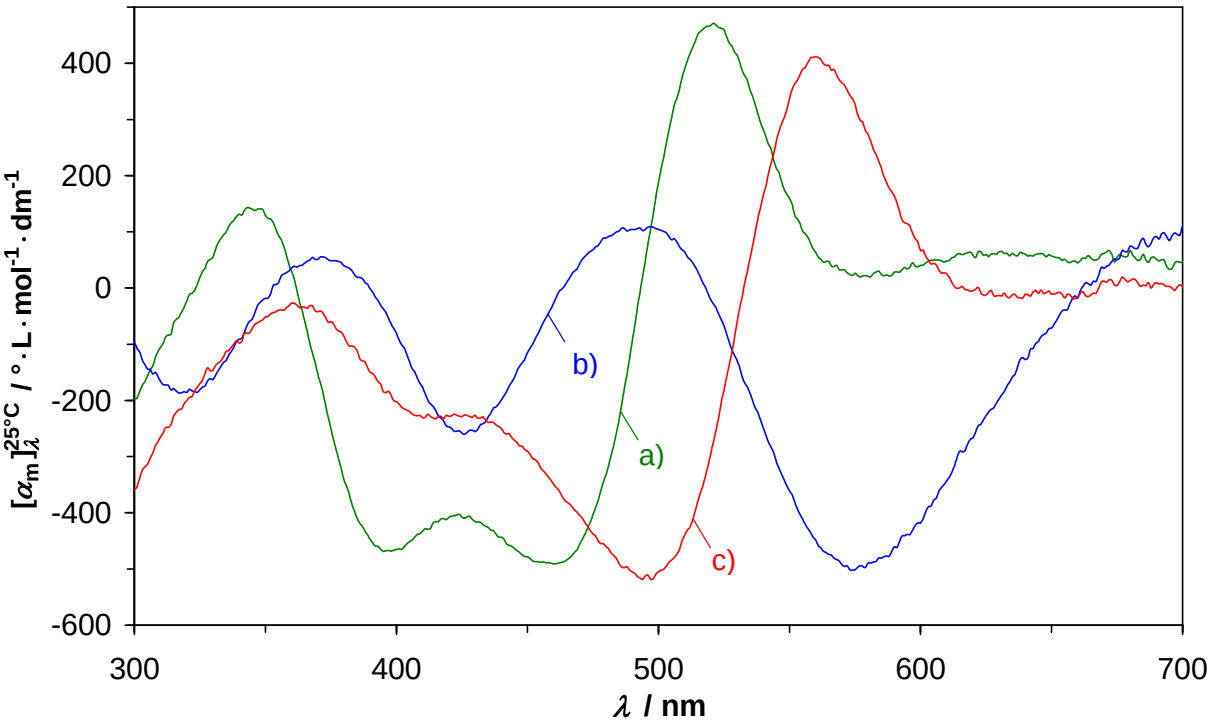

Fig. 4-4. *Normalised ORD spectra of* a) *$[Cr^{III}((S,S)\text{-}promp)H_2O]^+$ at pH 3.8* (——), b) *$[Cr^{III}((S,S)\text{-}promp)OH]$ at pH 9.1* (——), c) *$[Cr^{III}((S,S)\text{-}promp)Cl]$* (——). The original spectra were recorded with $3\cdot10^{-3}$M solutions in a 1 cm cell [16].

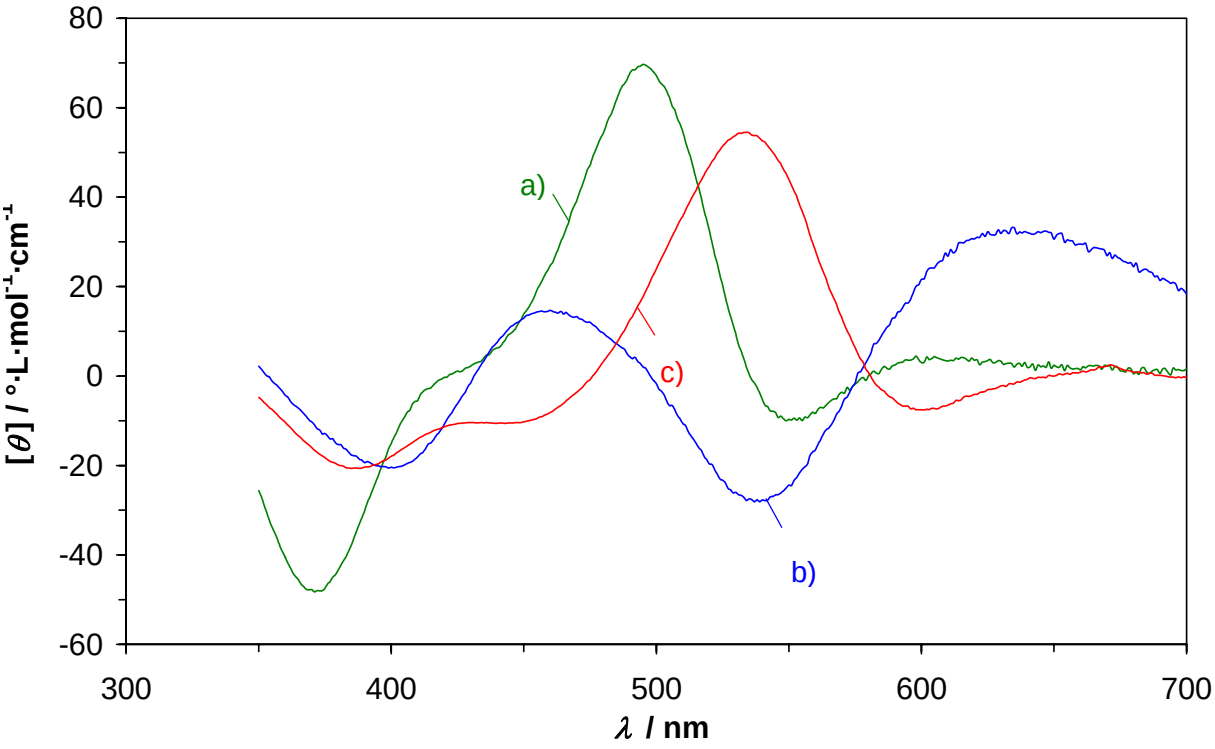

Fig. 4-5. *Normalised CD spectra. (a and b) and a 5 cm cell (c).* a) *$[Cr^{III}((S,S)\text{-}promp)H_2O]^+$ at pH 4.0* (——), b) *$[Cr^{III}((S,S)\text{-}promp)OH]$ at pH 8.2* (——), c) *$[Cr^{III}((S,S)\text{-}promp)Cl]$* (——). Data from [14b]. The original spectra were recorded with $1.0\cdot10^{-3}$M solutions in a 1 cm cell.

the hydroxy-complex in the considered spectral range and not to inverse absolute configurations of both complexes at their coordination centres. This assertion is confirmed by the CD spectra of these compounds (Fig. 4-5): Both of them exhibit a (-,+,-,+) pattern in the visible region, which is an indication for an identical chiral arrangement of the N_3O_3 chromophore around the chromium centre.

The ORD spectrum of the corresponding chloro-complex has a similar shape as the one of the aqua-complex, so that an identical absolute configuration at the metal centre can be asserted. The different chromophore system (N_3O_2Cl) shifts the CD spectrum to higher wavelengths but does not modify its pattern.

4.3 Electrochemical generation of an optically active chromium(II) complex

4.3.1 Instrumentation

Electrochemical reduction is a heterogeneous synthesis method that allows transformation without introduction of an additional reagent so that, ideally, no secondary products are generated. The installation schematised on Fig. 4-6 has been used for electrolytic reduction.

A large mercury pool cathode was used as electroactive surface. A silver rod in a 3M KCl solution served as anode. The correct operation had been previously checked by the methylviologen system ($E^{\circ\prime}$ = -0.436 V at pH 7.0 [17]) that generates a deep blue radical species upon reduction:

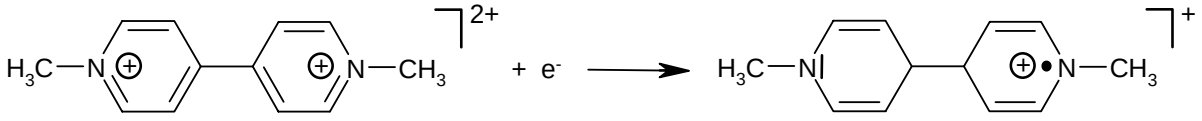

A 10^{-3}M solution of $[Cr^{III}((S,S)\text{-promp})H_2O]^+$ in 0.1M phosphate buffer at pH 7.5 or 8.5[1]) has been in rigorous air free-conditions [14]:

[1]) In order to limit the phosphate concentration, the buffer solution has been replaced in further experiments by solid sodium hydrogen phosphate that was added just in the necessary amount to reach the desired pH.

$[Cr^{III}((S,S)\text{-promp})H_2O]^+ + e^- \rightarrow [Cr^{II}((S,S)\text{-promp})H_2O]$

The applied potential of -1.30 V vs. Ag/AgCl was slightly more negative than the cathodic peak potential of the cyclic voltammogram recorded in the same conditions.

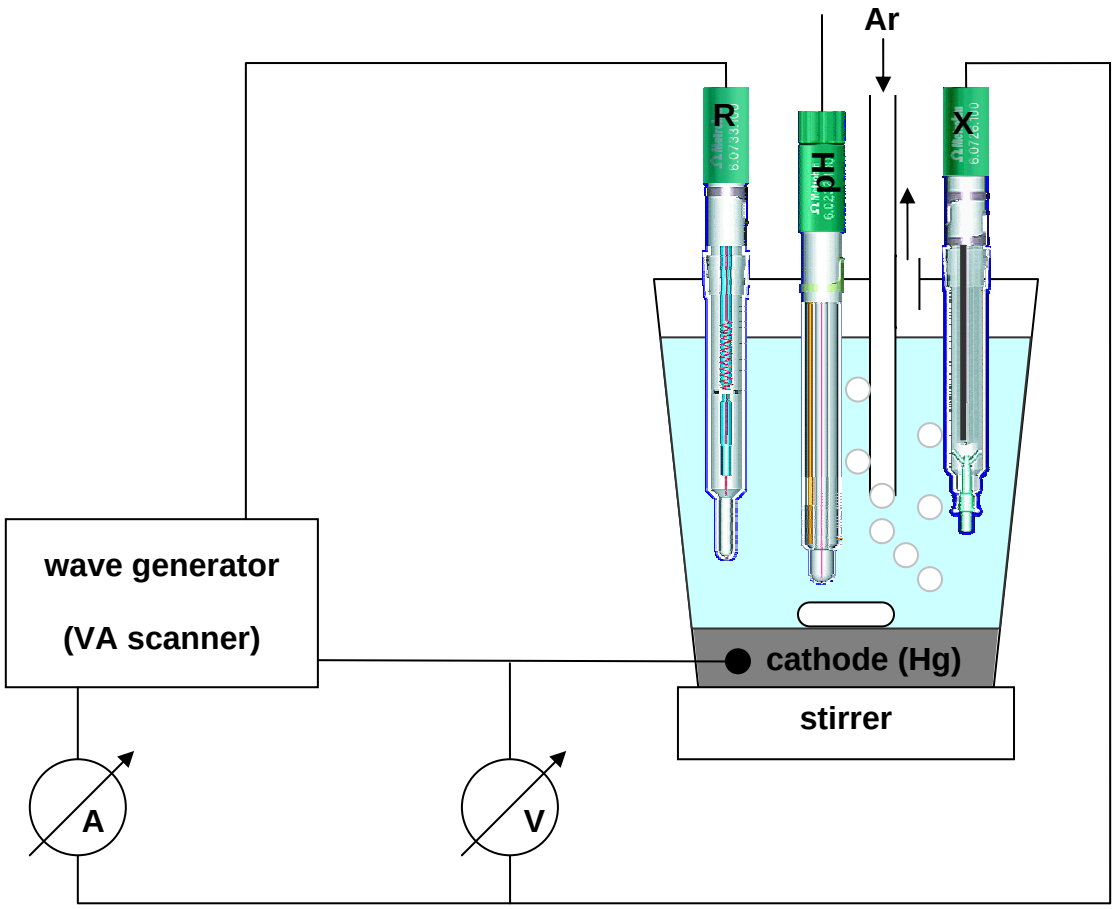

Fig. 4-6. *Electric scheme for the electrolytic reduction of chromium(III) to chromium(II).* Electrode pictures from [18]. A: ammeter; R: reference electrode Ag/AgCl; V: voltmeter; X: auxiliary electrode Ag/AgCl.

4.3.2 Identification of a short-lived chromium(II) species

The formation of a chromium(II) complex can often be recognized by its characteristic deep blue colour. Nevertheless, if its lifetime is short, it has to be trapped in order to transform it into an identifiable compound. The method we use is based on Taube's investigations [19] of the electron transfer reaction between the high spin and labile $[Cr(H_2O)_6]^{2+}$ and the low spin and inert $[Co(NH_3)_5Cl]^{2+}$:

$$[Cr^{II}(H_2O)_6]^{2+} + [Co^{III}(NH_3)_5Cl]^{2+} + 5\ H_3O^+ \rightarrow [Cr^{III}(H_2O)_5Cl]^{2+} + [Co^{II}(H_2O)_6]^{2+} + 5\ NH_4^+$$

Whereas the labile cobalt(II) was found exclusively as aqua-complex at the end of the reaction, almost all the chromium(III) was present under the form of $[Cr^{III}(H_2O)_5Cl]^{2+}$. As chromium(II) is labile and chromium(III) inert, it can be concluded that the electron and the chloride transfer take place simultaneously (in opposite directions). Hence, this reaction follows an inner sphere mechanism in which the chloride acts as bridging ligand.

Analogously, we chose to use $[Co(NH_3)_5Cl]^{2+}$ in our system to trap the electrochemically formed $[Cr^{II}(promp)H_2O]$:

$$[Cr^{II}(promp)H_2O] + [Co^{III}(NH_3)_5Cl]^{2+} + 5\ H_3O^+ \rightarrow [Cr^{III}(promp)Cl] + [Co^{II}(H_2O)_6]^{2+} + 5\ NH_4^+$$

The possible formation of [Cr(promp)Cl] could be followed by UV and CD spectrometry (see Fig. 4-5) and in this way demonstrate the former presence of the chromium(II) complex.

For further details, see §4.8.

Results and discussion

The UV and CD spectra of $[Cr((S,S)\text{-promp})H_2O]^+$ neither change nor decrease in their signal intensities during the supposed reaction [14b]; this means *a priori* that both, the promp and the aqua ligand, remain on the chromium centre. A subsequent column chromatography on a cation exchange resin did not reveal any neutral fraction that was coloured so that the formation of the chloro-complex, even in minor amounts, can be excluded. As a current is detected during the electrolysis of $[Cr^{III}(promp)H_2O]^+$, it might be explained by H_2 formation due to the reduction of water protons by $[Cr^{II}(promp)H_2O]$.

In order to find an evidence for this hypothesis, we carried out another ligand exchange experiment, using zinc instead of a mercury cathode as electron donor.

4.4 Ligand exchange on an optically active chromium(II) complex

4.4.1 $cdta^{4-}$ as competing ligand

The optically active chromium(III) complex is reduced by amalgamated zinc in the presence of $Hcdta^{3-}$ (prevailing species at pH 7.5). The high stability of cdta chelates – the stability constant of the homologous compound $[Co^{II}(cdta)]^{2-}$ is almost four orders of magnitude higher than that of $[Co^{II}(promp)H_2O]$[1]) – should favour the ligand exchange at the labile chromium(II) centre:

$$2\,[Cr^{III}(promp)H_2O]^{+} + Zn(Hg) + 2\,Hcdta^{3-} + 6\,H_2O \rightarrow 2\,[Cr^{II}(cdta)]^{2-} + 2\,H_2promp + [Zn(H_2O)_6]^{2+} + 2\,OH^{-}$$

Furthermore, an excess of chelating ligand lowers the redox potential of zinc by the complexation of the oxidized form:

$$[Zn(H_2O)_6]^{2+} + Hcdta^{3-} \rightarrow [Zn(cdta)]^{2-} + H_3O^{+} + 5\,H_2O$$

$$[Zn(H_2O)_6]^{2+} + H_2promp \rightarrow [Zn(promp)H_2O] + 2\,H_3O^{+} + 3\,H_2O$$

$$E' = E°(Zn^{2+}/Zn) + \frac{RT}{nF}\cdot\ln[Zn^{2+}] = E°(Zn^{2+}/Zn) + \frac{RT}{nF}\cdot\ln\frac{[ZnL]}{\beta_{ZnL}\cdot[L]}$$

Since the system is heterogeneous and diffusion controlled – the reaction cell was briefly shaken at regular time intervals – only qualitative and semi-quantitative interpretations are given afterwards.

The UV-VIS spectra of different mixtures of $[Cr^{III}(promp)H_2O]^{+}$ and $[Cr^{II}(cdta)]^{2-}$ on Fig. 4-7 simulate the evolution of the absorbance during the reaction if the expected ligand exchange takes place. The actual absorption spectra of the reaction plotted as a function of time are similar to the simulated spectra with respect to bathochromic shift of the absorption maximum in the red region from 605 to 544 nm. Nevertheless, the presence of zinc and zinc hydroxide particles in suspension produce important wavelength dependent and irreproducible baseline shifts so that the isosbestic points are not visible. CD spectroscopy is a more suitable tool to

[1]) see table 7-10 (appendix)

visualize the ligand exchange because, due to the differential nature of the signal, the turbidity of the medium influences only the resolution of the signal but not its average intensity.

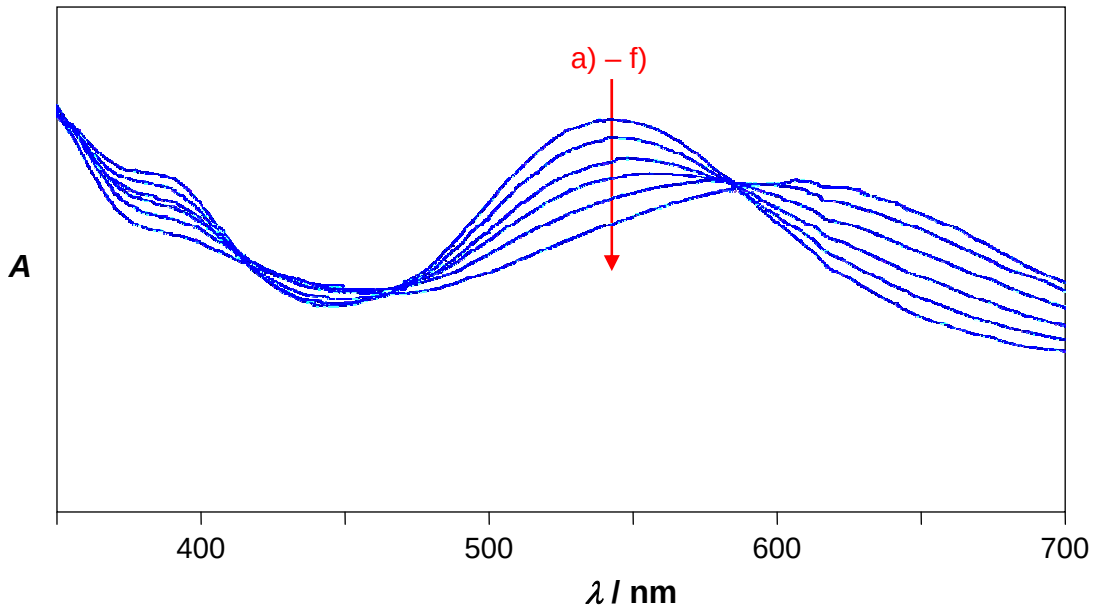

Fig. 4-7. *UV-VIS spectra of* a) *$[Cr^{III}(promp)H_2O]^+$*, f) *$[Cr^{III}(cdta)H_2O]^-$ and mixtures of both complexes at various ratios:* b) *4:1*, c) *3:2*, d) *2:3 and* e) *1:4.* Aqueous solutions at pH 7.5. [20]

Results and discussion

Fig. 4-8 confirms by the decrease of the ellipticity that the ligand exchange takes place indeed if and only if zinc is present in the system. The final ellipticity, ψ_f, corresponds to the residual $[Cr^{III}(promp)H_2O]^+$ whose amount is conditioned by the equilibrium between both chromium(II) complexes, "frozen" at the inert chromium(III) state:

$$[Cr^{III}((S,S)\text{-promp})H_2O^+] = \frac{\psi_f}{33000 \cdot \Delta\varepsilon_{[Cr^{III}((S,S)\text{-promp})H_2O]^+} \cdot l}$$

$$= [Cr^{III}(cdta)^-] \cdot \frac{\beta'_{[Cr^{II}((S,S)\text{-promp})H_2O]}}{\beta'_{[Cr^{II}(cdta)^{2-}]}} \cdot \frac{[(S,S)\text{-promp}^{2-}]}{[cdta^{4-}]}$$

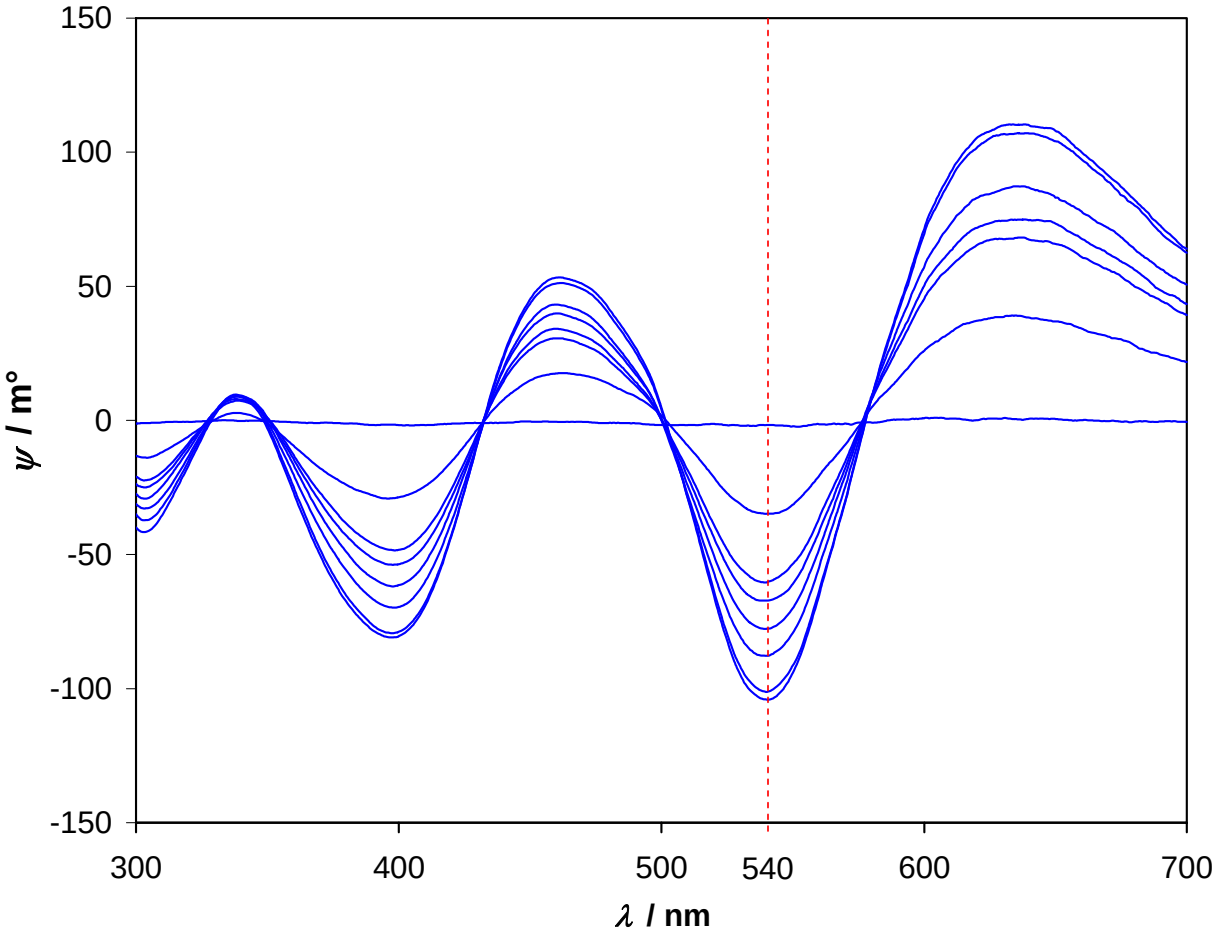

Fig. 4-8. *CD spectra during the reaction between 3.2·10^{-3}M [Cr^{III}((S,S)-promp)H$_2$O]$^+$ and amalgamated zinc (129 eq.) in presence of H$_2$cdta^{2-} (51 eq.) at pH 7.8,* μ *= 0.1 (Tris-HCl buffer) and r.t.* Spectra recorded before mixing and 1, 11, 21, 31, 41, 100 min and 4 d after mixing.

A mechanistic proposition of the ligand exchange is given on Fig. 4-9: During the induction phase, ①, the reduction of [Cr^{III}(promp)H$_2$O]$^+$ on the active zinc surface is the rate limiting step. In step ②, the promp^{2-} ligand is exchanged against the competing ligand and the formed Cr^{II} complex is immediately oxidized by another [Cr^{III}(promp)H$_2$O]$^+$ ion (③). Due to the increasing [Cr^{II}(promp)H$_2$O] concentration, the global reaction rate becomes (ideally) independent of the active zinc surface and increases notably until a steady state is set up. In this stage, step ③ occurs at the same rate than step ②; so that the concentrations of both Cr^{II} complexes remain constant as it would be the case for a catalyst. However, the Cr^{II} species are continually formed and consumed so that we can speak of pseudo-catalysis. Besides, both chromium(II) species are also oxidized by the solvent protons (④). An excess of zinc is thus necessary to compensate this side reaction. Observations in the further experiments described below confirm this mechanism hypothesis.

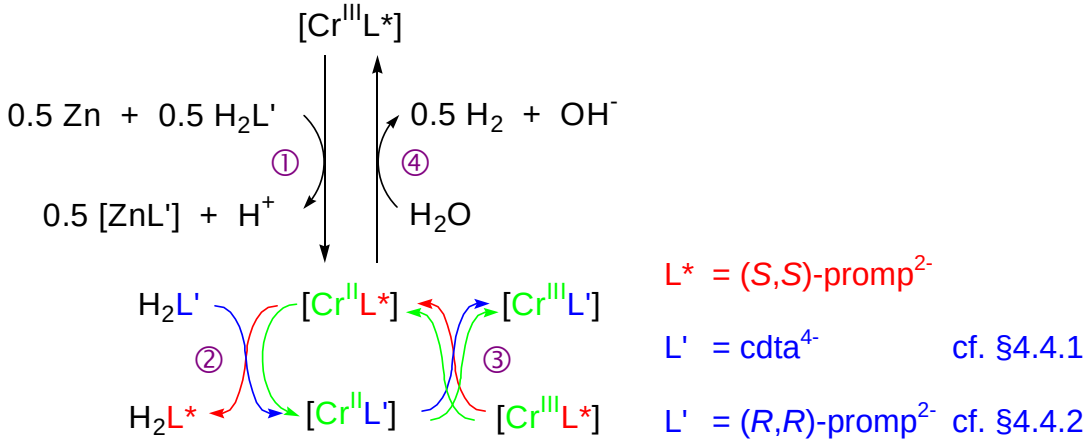

Fig. 4-9. *Catalysis-like cycle ("α-loop ") for the ligand exchange on the chromium centre.* Green arrows indicate the chromium pathway, blue and red arrows the ligands' pathway inside the α-loop. Reaction steps ① to ④ are explained in the text. Charges and aqua ligands omitted.

Based on this mechanism proposal, the following set of kinetic equations can be established:

$$[Cr^{III}L]^{+}(\sigma) + e^{-}(\sigma) \xrightarrow{k_0} [Cr^{II}L]^{+}$$

$$[Cr^{II}L] + H_2O \xrightarrow{k_{-0}} [Cr^{III}L]^{+} + \tfrac{1}{2}H_2 + OH^{-}$$

$$[Cr^{II}L] + L' \underset{k_{-1}}{\overset{k_1}{\rightleftharpoons}} [Cr^{II}L'] + L$$

$$[Cr^{II}L'] + H_2O \xrightarrow{k_2} [Cr^{III}L']^{+} + \tfrac{1}{2}H_2 + OH^{-}$$

$$[Cr^{II}L'] + [Cr^{III}L]^{+} \xrightarrow{k_3} [Cr^{III}L']^{+} + [Cr^{II}L]$$

The following hypotheses are formulated:

a) During the initial phase, the concentration of $Cr^{III}L'$ is so small that it reduction on the zinc surface does not occur:

$$v = +\frac{d[Cr^{III}L'^{+}]}{dt} = k_2[Cr^{II}L'] + k_3[Cr^{II}L'][Cr^{III}L'^{+}]$$

b) A steady state is reached:

$$\frac{d[\mathrm{Cr^{II}L}]}{dt} = 0 \quad \Rightarrow k_0[\mathrm{Cr^{III}L^+}]_\sigma + k_{-1}[\mathrm{Cr^{II}L'}][\mathrm{L}] = k_{-0}[\mathrm{Cr^{II}L}] + k_1[\mathrm{Cr^{II}L}][\mathrm{L'}]$$

$$\frac{d[\mathrm{Cr^{II}L'}]}{dt} = 0 \quad \Rightarrow k_1[\mathrm{Cr^{II}L}][\mathrm{L'}] = k_{-1}[\mathrm{Cr^{II}L'}][\mathrm{L}] + \left(k_2 + k_3[\mathrm{Cr^{III}L}]\right)[\mathrm{Cr^{II}L'}]$$

The global reaction rate is deduced from this equation system:

$$v = k_0 k_1 [\mathrm{Cr^{III}L^+}]_\sigma [\mathrm{L'}] \frac{k_2 + k_3[\mathrm{Cr^{III}L^+}]}{k_{-0}k_{-1}[\mathrm{L}] + k_{-0}k_2 + k_{-0}k_3[\mathrm{Cr^{III}L^+}] + k_1 k_2 [\mathrm{L'}]}$$

The equilibrium constants K_i are defined by $K_i = \frac{k_i}{k_{-i}}$

We consider four limiting cases:

a) $k_{-0}k_2 + k_{-0}k_3[\mathrm{Cr^{III}L}] >> k_{-0}k_{-1}[\mathrm{L}] + k_1 k_2 [\mathrm{L'}]$

The oxidations of both chromium(II) complexes represent the fastest reactions.

$\Rightarrow \quad v = K_0 k_1 [\mathrm{Cr^{III}L^+}]_\sigma [\mathrm{L'}]$

Given that the concentration change of $[\mathrm{Cr^{III}L}]^+$ at the zinc surface is very slow, the global reaction rate depends only on the ever decreasing concentration of the competing ligand L'.

b) $k_1 k_2 [\mathrm{L'}] >> k_{-0}k_{-1}[\mathrm{L}] + k_{-0}k_2 + k_{-0}k_3[\mathrm{Cr^{III}L}]$ and $k_2 >> k_3[\mathrm{Cr^{III}L}]$

The ligand exchange is faster than the electron transfer reactions.

$\Rightarrow \quad v = k_0 [\mathrm{Cr^{III}L^+}]_\sigma$

The reduction on the zinc surface becomes the rate determining step.

c) $k_{-0}k_{-1}[\mathrm{L}] >> k_1 k_2 [\mathrm{L'}] + k_{-0}k_2 + k_{-0}k_3[\mathrm{Cr^{III}L}]$

$$\Rightarrow \quad v = K_0 K_1 [\mathrm{Cr^{III}L^+}]_\sigma \frac{[\mathrm{L'}]}{[\mathrm{L}]} \left(k_2 + k_3[\mathrm{Cr^{III}L^+}]\right)$$

The electron transfer at the zinc surface and the ligand exchange are in rapid equilibrium. The global reaction rate decreases strongly during the reaction. This case is improbable, given that [L] = 0 in the beginning of the reaction, which does not meet the simplification condition.

d) $k_{-0}k_3[Cr^{III}L^+] >> k_{-0}k_{-1}[L] + k_1k_2[L'] + k_{-0}k_2$ and $k_3[Cr^{III}L^+] >> k_2$

This condition is fulfilled only at higher $[Cr^{III}L^+]$ concentrations.

$$v = K_0 k_1 [Cr^{III}L^+]_\sigma [L']$$

The global reaction rate depends on the concentration of $[Cr^{III}L]^+$ at the zinc surface and of the competing ligand.

Furthermore, nine intermediate cases can be considered in which two respectively three of the summands are significant. In some of these cases, the global reaction rate decreases with increasing concentration of free L (product inhibition).

Measurements at different pH values (4.5, 7.5 and 9.0) and with different amounts of competing ligand (1, 10 and 50 eq.) yielded mainly two observations:

a) At pH 4.5, the rate of ligand exchange (and the final ellipticity if the reaction is finished within the considered timescale) does not seem to depend on the concentration of the competing ligand. This may be due to the absence of deprotonated ligand at this pH so that, independently of the analytical cdta concentration, the amount of $[Zn(cdta)]^{2-}$ remains weak.

b) The global reaction rate is considerably higher at pH 4.5 than at pH 7.5 and 9.0 (see Fig. 4-10). Besides, the reaction rate decreases slightly at every shaking, as expected for a heterogeneous reaction with kinetics of positive order. Conversely, an induction phase is observed at pH 9.0 (the situation at pH 7.5 is similar) and the kinetic trace is typical for a consecutive reaction. This behaviour can be explained by the fact that at pH 4.5 the zinc surface is always active and continuously renewed by acid attack. The catalytically active chromium(II) complex is thus formed instantaneously. This is not the case in neutral and slightly basic medium where the zinc surface is covered by a zinc hydroxide layer so that the generation of chromium(II) species is the rate determining step until this intermediate is present in a sufficient amount. Another possible reason for the lower reaction rate in neutral and basic medium is the electrostatic repulsion between the reacting species $[Cr^{II}((S,S)\text{-promp})OH]^-$ and $Hcdta^{3-}$.

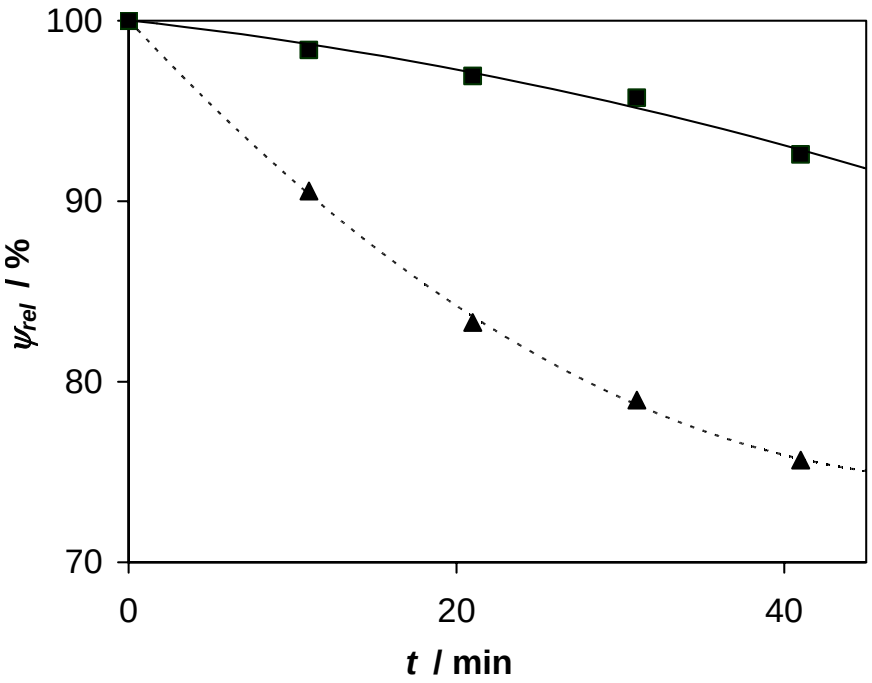

Fig. 4-10. *Decrease of the CD signal (relative ellipticity vs. the initial value) during the reaction between 3.2·10^{-3}M [Cr^{III}((S,S)-promp)H$_2$O]$^+$ and amalgamated zinc in presence of 10 eq. H$_2$cdta^{2-} in μ = 0.1 buffer solution at r.t.* (---▲---) Relative ellipticity at 371 nm, pH 4.4 (acetate buffer), 66 eq. Zn. (—■—) Relative ellipticity at 535 nm, pH 9.1 (Tris-HCl buffer), 109 eq. Zn.

4.4.2 (*R*,*R*)-promp^{2-} as competing ligand (self-exchange)

In the next step, the reduction of [Cr^{III}((*S*,*S*)-promp)H$_2$O]$^+$ has been carried out in presence of H$_2$(*R*,*R*)-promp and followed by UV-VIS as well as by CD measurement.

Results and discussion

Fig. 4-11 shows that the CD signals are inversed during the reaction; although they do not reach exactly the opposite ellipticity. The main reason is the equilibrium situation according to the part of the chromium(III) remaining complexed by the (*S*,*S*) ligand. The UV-VIS spectra that are expected to remain constant in these experiences exhibit two opposite effects: During the reaction, the background absorption of the reaction mixture increases over the whole considered wavelength range as a consequence of sample turbidity due to the appearing zinc hydroxide precipitate (see Fig. 4-12b). When limiting the amount of zinc to 20 eq., these side effects are reduced so that the obtained UV spectra remain nearly identical during several hours.

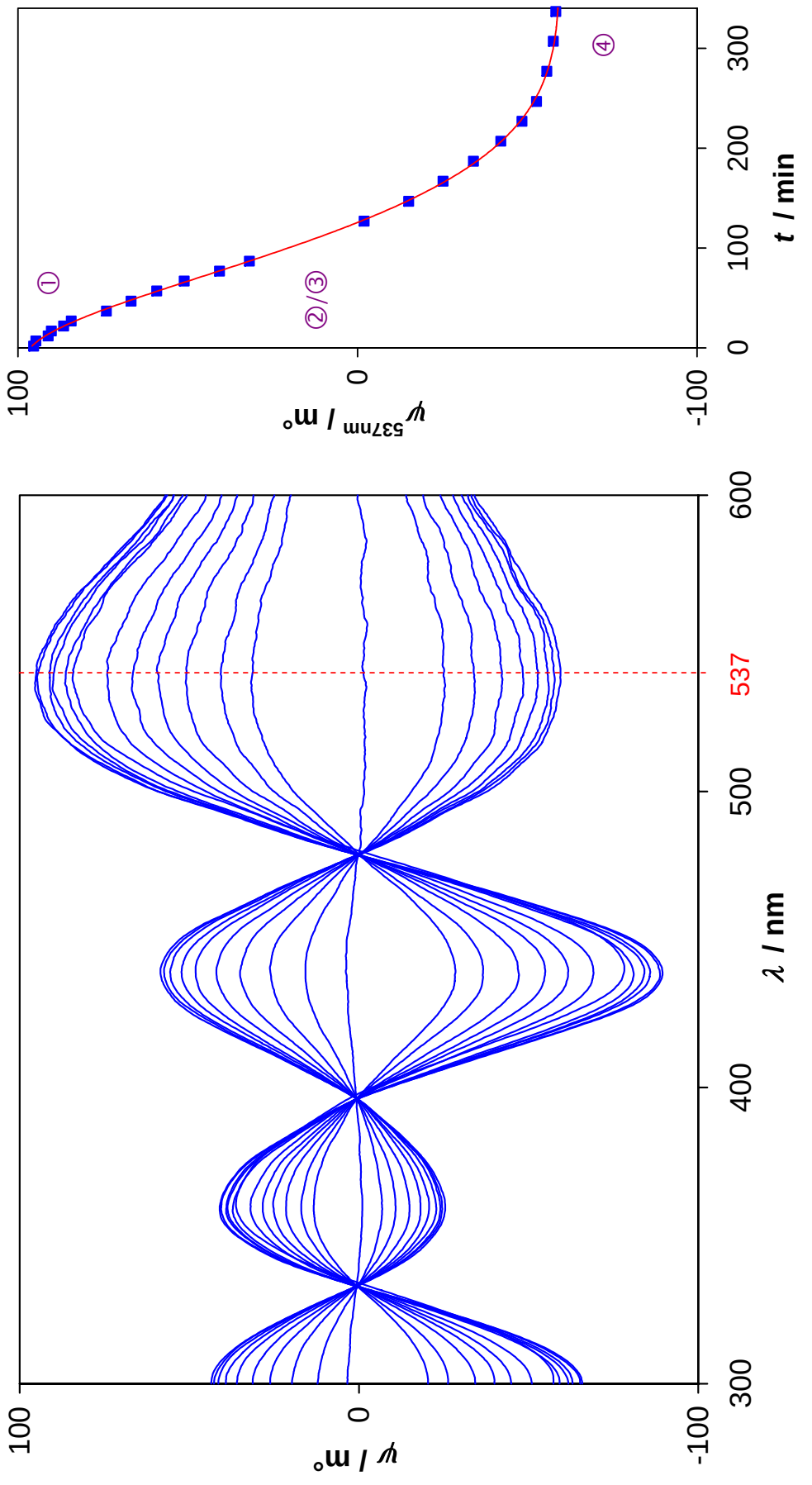

Fig. 4-11. *Evolution of the CD signal during the self exchange on [Cr^{II}(promp)H$_2$O].* [Cr^{III}((*S*,*S*)-promp)H$_2$O] = $2.81 \cdot 10^{-3}$ molL^{-1}, [H$_2$(*R*,*R*)-promp] = $1.44 \cdot 10^{-2}$ mol·L^{-1} (5.1 eq.), Zn/Hg: 7.8 eq., pH = 7.7, Θ = 29.2°C. a). *CD spectra at different reaction stages,* b) *time-resolved evolution of ellipticity at* λ_{max} = *537 nm.*

The time-resolved CD spectra of the self-exchange reactions (Fig. 4-11b) reveal mainly sigmoid shapes and thus confirm the mechanistic model described on Fig. 4-9: The induction phase ① is followed by a ligand exchange ②/③ until the equilibrium state is reached (⑤).

Compared to the ligand exchange with CDTA, the reaction rate is less sensitive towards pH. Below pH 9, the major part of the competing ligand is electrically neutral (see pK_a values in §7.2 of the appendix) so that almost no repulsive interactions with the partially negatively charged chromium(II) complexes occur.

These results underline that, even if chromium(II) is a labile metal centre, the self-exchange involving the promp ligand remains slow, as it had already been stated for the corresponding copper(II) complex [21].

At longer reaction times, the optical activity decreases again: For instance, after 3 days with 490 eq. of zinc at pH 4, the CD spectrum has the same pattern as $[Cr^{III}((R,R)\text{-promp})(H_2O)]^+$) but its intensity has dropped to 2% of its initial value. The UV spectrum corresponds to that of a $[Cr(H_2O)_6]^{3+}$ - $[Cr^{III}(promp)H_2O]^+$ mixture at a 9:1 ratio (see Fig. 4-12). This could lead to the interpretation that, under the given conditions, self-exchange is kinetically favoured while aquation would be thermodynamically favoured; an assumption that seems absurd in view of the strong chelate effect of the pentadentate $promp^{2-}$ ligand. Another explanation is that part of the chromium(III) might have been reduced to metallic chromium by zinc. After complete consumption of Zn°, the metallic chromium is then re-oxidized to $[Cr(H_2O)_6]^{3+}$ in acid medium but the complexation of this inert complex by $promp^{2-}$ does not occur without heating so that the CD signal decreases. The potential difference between both metals is weak: $\Delta E° = +0.018$ V for the reaction $2\ Cr^{3+}(aq) + 3\ Zn° \rightarrow 2\ Cr° + 3\ Zn^{2+}(aq)$ [1] which corresponds to an equilibrium constant of $10^{1.8}$. Since the stoichiometric factor of chromium is lower than that of zinc, chromium reduction is favoured at low concentrations of both aqua ions. This condition is assured by the presence of the chelating promp ligand. A third explanation would be that once the excess of free ligand has been consumed by the complexation of the formed Zn^{2+} ions, the excess zinc aqua-complex undergoes ligand exchange with the labile $[Cr^{II}(promp)H_2O]$. The formed $[Cr(H_2O)_6]^{2+}$ is then oxidized by air or remaining $[Cr^{III}(promp)H_2O]^+$ to $[Cr(H_2O)_6]^{3+}$.

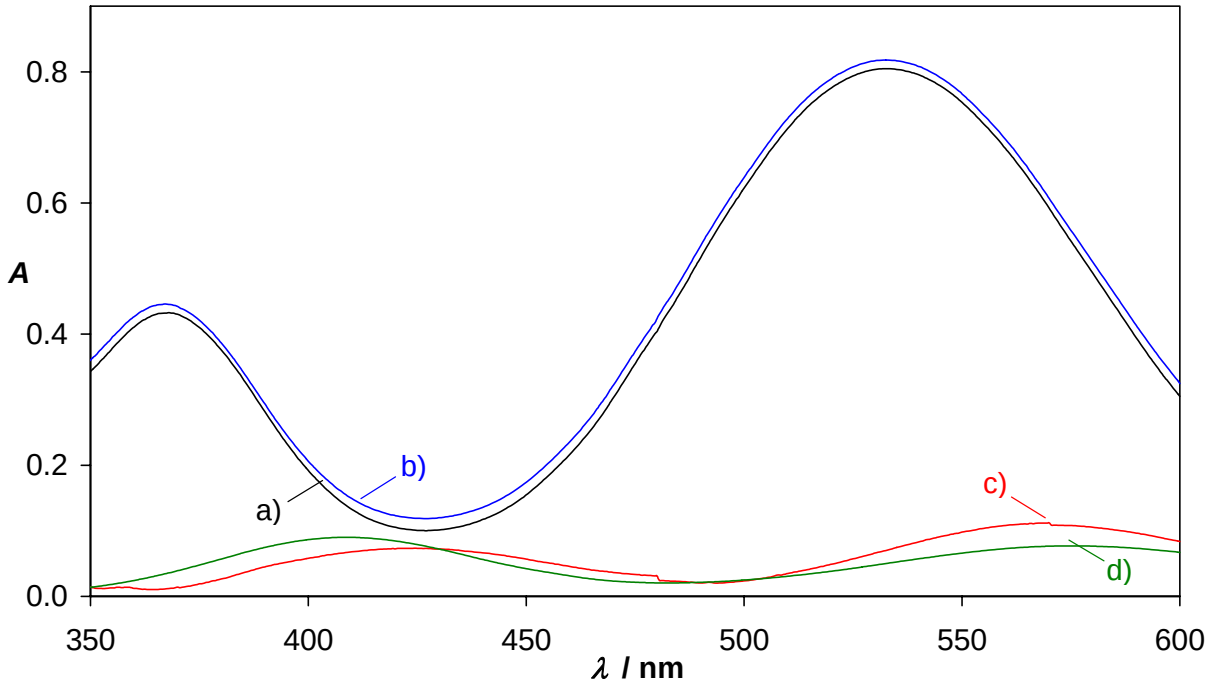

Fig. 4-12. *Evolution of the UV spectra during the reaction between* $[Cr^{III}((S,S)\text{-promp})H_2O]^+$ $5.5\cdot10^{-3}$M, H_2(R,R)*-promp (4 eq.) and zinc amalgam (490 eq.).*
a) *0 h* (——), b) *1 h* (——), c) *65 h, background turbidity corrected* (——), d) *spectrum of* $[Cr(H_2O)_6]^{3+}$ $5.5\cdot10^{-3}$M *for comparison* (——).

4.5 Electron transfer involving cytochrome *c* catalysed by an optically active chromium(III) complex

The aim of the previous experiments with chromium(III) complexes described in §4.3 and §4.4 was to investigate whether or not chromium(II) species could be used as stereoselectivity probes in electron transfer reactions involving metalloproteins. As the results have shown that such species with the pentadentate aminocarboxylate ligand used are not stable in aqueous solution, but can react *in situ*, this technique has been applied to ferricytochrome *c* reduction, according to the equation

$$\text{cyt c–Fe}^{III}\text{(aq)} + \text{Zn(s)} + L^{2-}\text{(aq)} \xrightarrow{cat.\ [Cr^{III/II}L(H_2O)]} 2\ \text{cyt c–Fe}^{III}\text{(aq)} + \text{[ZnL](aq)}$$

L^{2-} = (*S*,*S*)-promp^{2-}

The reduction of ferricytochrome *c* to ferrocytochrome *c* was carried out as described in chapter 3 but instead of a cobalt(II) complex, zinc amalgam was used as reducing agent this

time. The influence of the initial chromium(III) complex and the free ligand concentrations has been studied.

Results and discussion

In presence of the chromium(III) complex, a strong increase of the reaction rate has been observed (see Fig. 4-13). This demonstrates clearly the catalytic effect of the chromium(II) complex formed *in situ*. Two mechanistic possibilities of the reaction can be considered: Either the Cr^{II} complex formed at the metallic surface is sufficiently stable to pass into the solution and undergoes reoxidation by ferricytochrome *c* in a homogeneous reaction or the Cr^{II} species is unstable in solution and reacts with ferricytochrome *c* only at the metallic surface immediately after having been formed. It seems that the latter possibility is more likely because all attempts to isolate or to identify electrochemically produced chromium(II) species (by trapping with $[Co(NH_3)_4Cl]^{2+}$, see §4.3.2) had failed.

Fig. 4-13 shows that the temperature and pH effects on reaction rates are rather weak for both, the uncatalysed and the catalysed reaction.

As shown by Fig. 4-13 a-c, the reaction is slightly faster at 53°C than at 26 or 41°C. However, the situation at 54°C is not comparable to those at lower temperatures because the protein undergoes a conformation change at 53°C [22]. On the other hand, no temperature effect is perceivable between 26 and 41°C either for the uncatalysed or for the catalysed reductions. Consequently, the determining factor of the reaction rate is not the activation energy. As the system of the uncatalysed reaction is heterogeneous, the stay time on the zinc surface – obviously temperature independent – seems to determine the overall reaction rate. In presence of the chromium(III) complex, the reaction proceeds faster because it follows a different mechanism.

The main differences in the reaction medium at pH 9 compared to pH 7.6 are:

1. The conditional stability constant of the $[Zn(promp)H_2O]$ complex is increased, so that the redox potential of zinc is more negative and the equilibrium is shifted towards chromium(II) formation.
2. The concentration the hydroxy-complex $[Cr^{II}(promp)OH]^-$ is higher. The approach to the positively charged protein surface is facilitated.

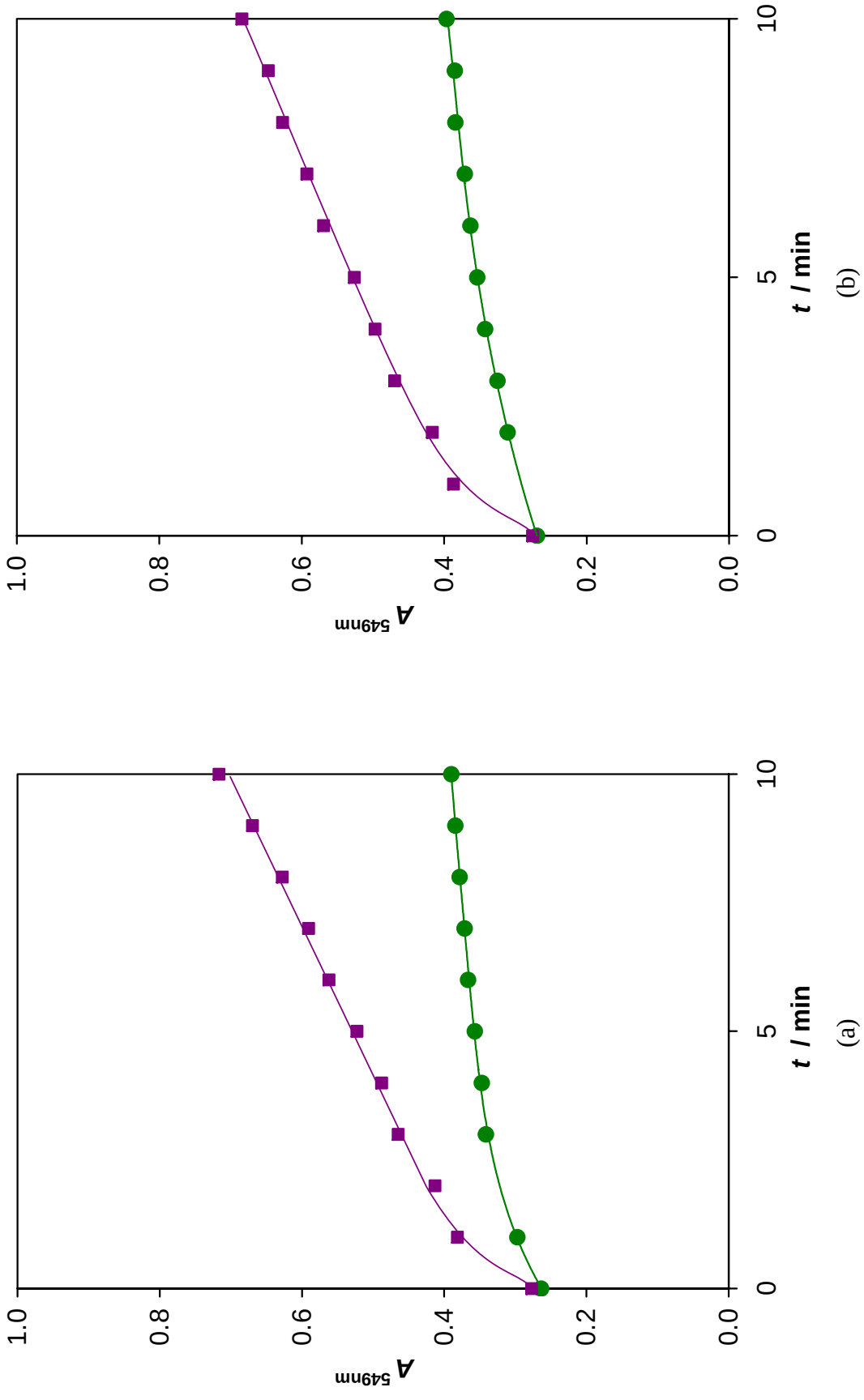

Fig. 4-13 a-b. *Time-resolved absorbance of horse-heart cytochrome c during the reduction by amalgamated zinc at 549 nm.* [cyt *c*] = $3.65 \cdot 10^{-5}$ molL^{-1}. a) *pH = 7.7, Θ = 26°C, Zn/Hg: 2300 eq., [H$_2$(S,S)-prompJ: 91 eq.,* b) *pH = 7.6, Θ = 41°C, Zn/Hg: 2000 eq., [H$_2$(S,S)-promp]: 100 eq.* (—●—) without, (—■—) with 19 eq. [Cr^{III}((*S,S*)-promp)H_2O]$^+$; for better comparison, the absorbance of the Cr^{III} complex has been deduced.

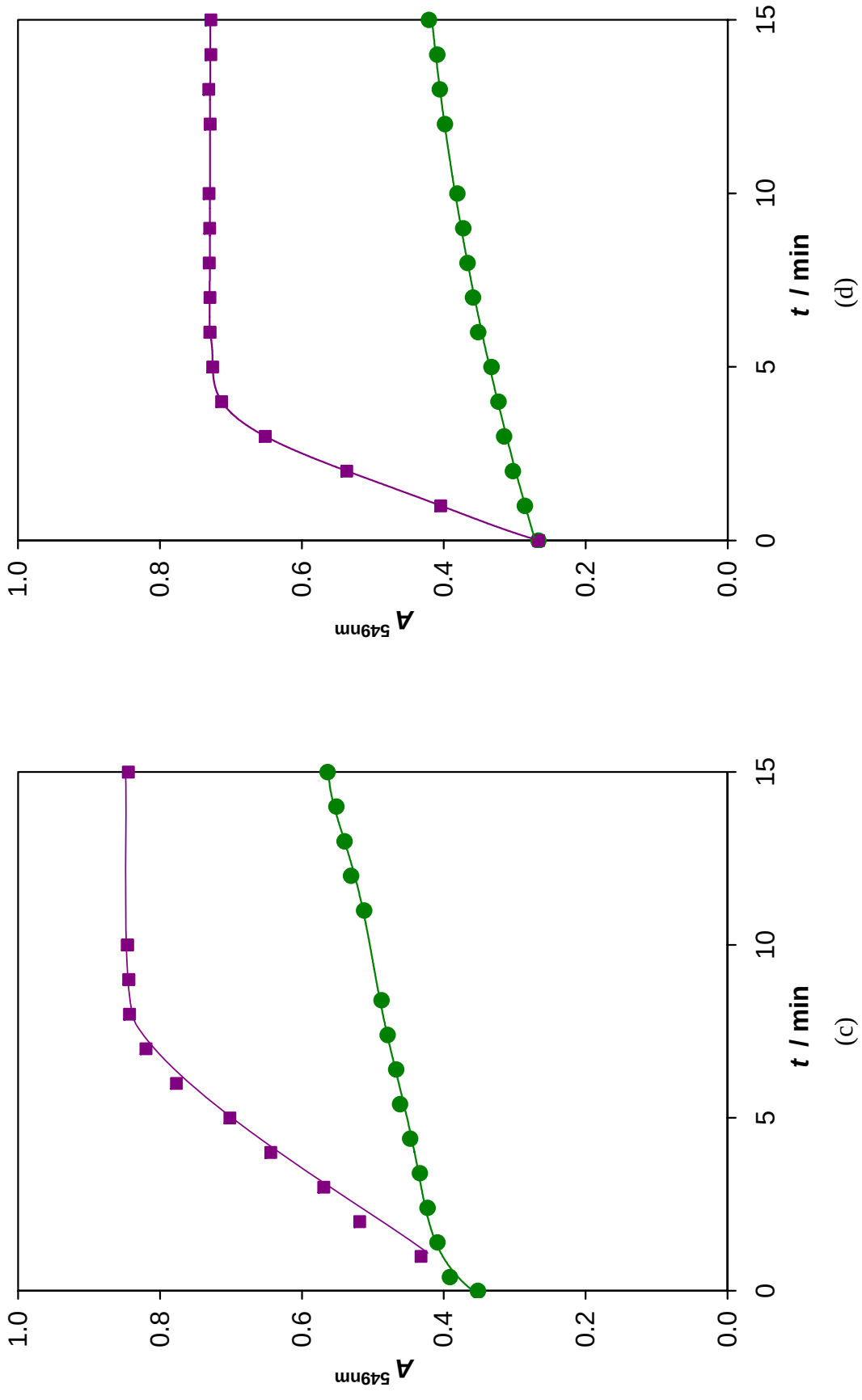

Fig. 4-13 c-d. *Time-resolved absorbance of horse-heart cytochrome c during the reduction by amalgamated zinc at 549 nm.* [cyt *c*] = $3.65 \cdot 10^{-5}$ molL^{-1}, Zn/Hg: 2000 eq. c) *pH* = *7.6*, *Θ* = *54°C*, *[H₂(S,S)-promp]: 100 eq.*, d) *pH* = *9.0*, *Θ* = *54°C*, *[H₂(S,S)-promp]: 108 eq.* (—●—) without, (—■—) with 20 eq. $[Cr^{III}((S,S)\text{-promp})H_2O]^+$; for better comparison, Cr^{III} absorbance has been deduced.

50% of the ferricytochrome *c* is present under its basic form, which has a slightly lower reduction potential. The reaction rate should be increased for both, the catalysed and the uncatalysed reaction, which is indeed the case. These differences are only relevant for the global reaction rate if the latter depends on the concentration of Cr^{III} or ferricytochrome *c*. But the features of the kinetic traces suggest that the rate determining step is of zero order kinetics, most likely its rate is limited by the extent of metallic surface and thus independent of the species in solution.

At 54°C, the uncatalysed and the catalysed reactions are both about two times faster at pH 9.0 than at pH 7.6, as shown by Fig. 4-13 c and d. This weak pH effect can hardly be considered as significant.

4.6 Fixation assay

As reported for the analogous cobalt(II) complexes in §3.3.4 and 3.4.3, the possible fixation of $[Cr^{III}((S,S)\text{-promp})H_2O]^+$ on ferrocytochrome *c* mediated by the electron transfer was equally checked. Since only one enantiomer of the chromium complex was available, the CD spectra of dialyzed cytochrome c after reduction with zinc amalgam in presence and in absence of $[Cr^{III}((S,S)\text{-promp})H_2O]^+$ were compared.

Results and discussion

At pH 8.2 and 40°C no significant difference was observed between the two CD spectra in the visible region. That means that no permanent binding had occurred under the chosen conditions. In §4.4 this behaviour was explained for the analogous cobalt complex by the large and flat promp ligand that cannot penetrate deeply into the protein. Nevertheless, *Ghizdavu* [23] had observed an electron-transfer mediated binding of $[Co^{III}((S,S)\text{-promp})H_2O]^+$ on His 83 of azurin between pH 6 and 9. The fixation rate increased with pH and with temperature. If the same tendency is true for the system considered here – which is possible provided that similar binding sites are involved for chromium(II) and cobalt(II) compounds – the chosen conditions should be mostly favourable for a fixation. So the absence of covalent binding to an imidazole group can rather been explained by the lower affinity of chromium(II) towards nitrogen coor-

dination and the well known difficulty in the substitution of the sixth coordination site on the chromium(II) centre.

4.7 Outlook

The first results observed in the cytochrome *c* reduction by an optically active chromium(II) complex are promising. It would be worth studying the behaviour of the (*R*,*R*) enantiomer of the complex in order to see whether there is some stereoselectivity. Nevertheless, with the chosen heterogeneous system, a quantitative analysis of the reaction kinetics is difficult. Another possibility might be given by the electrolytic reduction of cytochrome c in presence of the optically active chromium(III) complex. The latter could act as a mediator that increases the cathodic current ("catalytic current") under the condition that the protein is faster reduced by the chromium(II) complex than by the electrons on the cathodic surface. This system is very versatile thanks to the choice of the electrode material and of the current density. An alternative could be the use of an aprotic solvent such as DMSO but this induces important modifications in the protein structure (loss of hydrogen bonding etc.) so that its behaviour is too different from that of native ferricytochrome *c*. A more promising way to investigate the stereoselective interaction with the protein surface is the use of another ligand system that yields complexes with less negative reduction potentials. In this way, the electron transfer can be carried out in a homogeneous aqueous medium. One way to raise the reduction potential is a stabilisation of the chromium(II) state of the complex, according to the *Nernst* equation:

$$E = E°(Cr^{3+}/Cr^{2+}) + \frac{R \cdot T}{n \cdot F} \cdot \ln \frac{\beta([Cr^{II}L])}{\beta([Cr^{III}L])}$$

$$= -0.407\ V + 0.059 \cdot \ln \frac{\beta([Cr^{II}L])}{\beta([Cr^{III}L])}$$

As the Cr^{2+} radius is about 40% larger than the one of Cr^{3+} [1], the chromium(II) state of the complex can be stabilized by a ligand with a more spacious coordination cavity. A dependence of the reduction potential on size of the coordination cavity has already been observed for other metal centres, such as europium [24].The *alamp* ligand is less constraining for the metallic centre than the *promp* ligand because the amino- and carboxylate functions are not

linked by a cyclic backbone. Nevertheless, the expected effect should be rather small. Therefore, we prepared a new ligand based on a β amino acid and thus giving rise to a system of two six-membered aminocarboxylate coordination cycles instead of the five-membered cycles in the complexes with alamp and promp (see chapter 5).

4.8 Experimental part

4.8.1 General

4.8.1.1 Reagents, solvents and buffer solutions

see §2.2.1. pH 9 buffer with ionic force μ = 0.2 has been prepared from 1.0M hydrochloric acid, solid Tris and NaCl (0.15M). Though the solution is at the upper limit of the TRIS buffer domain, no significant pH shift has been observed during the reaction.

4.8.1.2 Sample handling

All samples were freed from dissolved O_2 by gently bubbling Ar for at least 15 min and handled in an inert atmosphere. Small volumes were measured with micropipettes or weighed.

4.8.2 Electrochemical measurements

According to [14].

In an electrolysis cell with mercury pool (see Fig. 4-6), solid Na_2HPO_4 was added to $[Cr^{III}(S,S)\text{-promp}(H_2O)]ClO_4$ 0.01M (50 mL) until the desired pH (7.5 or 8.5) was reached. A CD spectrum was recorded. A potential of -1.45 V vs. Ag/AgCl was applied for 150 min. The time resolved electrolytic current varied between 280 and 800 mA and was visualized by the ScopeView® software on a PC interfaced to a METEX M-3660D multimeter purchased from Westfalia, Hagen (DE). After the current was stopped, $[Co^{III}(NH_3)_5Cl]Cl_2$ 0.014M (4.5 mL, 1.3 eq.) was injected. The solution was removed immediately from the mercury pool and a

CD spectrum was recorded. 0.5M HCl was added until a pH of 2.5 and the solution was passed through an ion exchange column (SP Sephadex C-25) to remove any charged species.

4.8.3 Ligand exchange on an optically active chromium(II) intermediate

$[Cr^{III}L(H_2O)]ClO_4$ = $[Cr^{III}$(S,S)-promp$(H_2O)]ClO_4$ (M_r = 500.8)

H_nL' = H_4cdta ·H_2O (M_r = 364.35) or H_2(R,R)-$promp^{2-}$ xHCl (M_r = 333.39 + x·36.45)

To 2.5 g of a buffer solution (μ = 0.1) containing $[Cr^{III}L(H_2O)]ClO_4$ ($3.5\cdot10^{-3}$ g, $7.0\cdot10^{-6}$ mol), H_2L' (0.035 mol, 5 eq. vs. Cr^{III}) in a 1.00 cm closable cell, amalgamated zinc ($4.6\cdot10^{-3}$ g, $7\cdot10^{-5}$ mol, 10 eq. vs. Cr^{III}) was added. CD spectra between 300 and 600 nm (scan speed: 100 nm/min) towards μ = 0.1 buffer were recorded before the zinc addition and at regular intervals after the zinc addition. The evolution of the total chromium(III) concentration was followed by absorbance measurements in the same spectral range. The sample was vigorously shaken before each spectroscopic measurement.

4.8.4 Preparation of amalgamated zinc

Zinc powder is stirred in 1% mercuric chloride solution during 10 min.

4.8.5 Cyt c reduction with zinc catalysed by an optically active chromium(III) complex

$[Cr^{III}L(H_2O)]ClO_4$ = $[Cr^{III}$(S,S)-promp$(H_2O)]ClO_4$ (M_r = 500.8)

H_2L = H_2(*S*,*S*)-promp·*x*HCl (M_r = 462)

Amalgamated zinc ($4.8\cdot10^{-3}$ g, $7.30\cdot10^{-3}$ mol, 500 eq. vs. cyt *c*) and 0.5 mL of H_2L in water ($7.30\cdot10^{-3}$M, 100 eq. vs. cyt *c*, neutralized by some drops of NaOH 0.5M) were introduced into one compartment of a 2x0.475 cm tandem cell. A freshly prepared solution (0.5 mL) containing cytochrome c $7.30\cdot10^{-5}$M, $[Cr^{III}L(H_2O)]ClO_4$ $1.46\cdot10^{-3}$M (20 eq. vs. cyt *c*) and μ = 0.2 Tris-HCl buffer (pH 7.5 or 9.0) was introduced into the second compartment, then the cell

was thermostated at the desired temperature. Absorption spectra between 500 and 570 nm (scan speed: 100 nm·min^{-1}) towards μ = 0.1 buffer were recorded before mixing and at regular intervals after mixing. The sample was vigorously shaken before each absorbance measurement.

4.8.6 Fixation assay

A solution (2.5 g) containing $3.65 \cdot 10^{-4}$M freshly defrosted ferricytochrome *c* and 0.04M H_2(*S*,*S*)-promp, 0.02M Tris-HCl buffer and 0.08 M NaCl was divided into two parts. To the first part, $[Cr^{III}L(H_2O)]ClO_4$ (4.2 mg, $6.7 \cdot 10^{-3}$M, 18 eq vs. cyt *c*) was added. To both parts, amalgamated zinc (45 mg, 18 eq vs. cyt *c*) was added and the samples were left at 40°C during 30 min (part 1) and 90 min (part 2).

At the end of the reaction, both suspensions were introduced into a dialysis sack which was gently stirred in a μ = 0.1 buffer solution for 17h. Each sack content was diluted to exactly 2 g and a CD spectrum between 300 and 700 nm (scan speed: 20 nm·min^{-1}) towards μ = 0.1 buffer was recorded.

4.9 References

[1] Numerical values from: Handbook of Chemistry and Physics, 72nd edition, CRC-Press, Boca Raton, 1991.

[2] I.K. Kofi Adazamli, R. A. Henderson, J.D. Sinclair-Day, A.G. Sykes, *Inorg. Chem.* **1984**, *23*, 3069 and references therein.

[3] D.G. Holah, J.P. Fackler Jr., in 'Inorganic Syntheses', Ed., ,1969, Vol. 10, p. 26.

[4] J.C. Bailar, H.J. Emeléus, R. Nyholm. A.F. Trotman-Dickenson, 'Comprehensive Inorganic Chemistry', Pergammon Press, Oxford, 1973, Vol.3, p. 657.

[5] a) Skov, K. Olsen, U. Christensen, O. Farver, *Inorg. Chem.* **1993**, *32*, 4762-4765; b) O. Farver, I. Pecht, *Coord. Chem. Rev.* **1989**, *94*, 17.

[6] O. Farver, I. Pecht, *Proc. Nat. Acad. Sci.* **1981**, *78*, 4190.

[7] A. Kowalsky, *J. Biol. Chem.* **1969**, *244*, *6619*

[8] C.J. Grimes, D. Piszkiewicz, E.B. Fleischer, *Proc. Nat. Acad. Sci.* **1974**, *71*, 1408.

[9] R.L. Petersen, R.K. Gupta, *FEBS Letters 1979*, *107*, 427.

[10] J.W. Dawson, H.B. Gray, R.A. Holwerda, E.W. Westhead, *Proc. Natl. Acad. Sci. U.S.A.* **1972**, *69*, 30.

[11] J.K. Yandell, D.P. Fay, N. Sutin, *J. Am. Chem. Soc.* **1973**, *95*, 1131.

[12] J.J. Sauvain, Ph.D. Thesis, Université de Neuchâtel, 1990.

[13] a) A.L. Spek, 'PLATON/PLUTON', Program for Representation of Crystal Structures, Universiteit Utrecht, Utrecht, The Netherlands, 1980-2003; b) A.L.Spek, *J.Appl.Cryst.* **2003**, *36*, *7*; c) H. Stoeckli-Evans, Report of X-Ray structure determination, Université de Neuchâtel, 1998; d) Thomas Knoll et al., 'Adobe® Photoshop®', version 6.0, Program for Image Editing, Adobe Systems Inc., San Jose, United States of America, 2001.

[14] a) G. Gasser, Advanced practical work in Inorganic Chemistry, Université de Neuchâtel, 1998; b) L.A. Leuthold, Advanced practical work in Inorganic Chemistry, Université de Neuchâtel, 1998.

[15] D.J. Samuel, J.H. Espenson, *Inorg. Chem* **1979**, 18, 2587.

[16] N. Charbonnet, G. Pitarella, Advanced practical work in Inorganic Chemistry, Ecole d'ingénieurs et d'architectes de Fribourg, 2003.

[17] W. Sung Jeon, H.J. Kim, C. Lee, K. Kim, *Chem. Comm.* **2002**, 1828.

[18] Electrode catalogue, Metrohm AG, CH-Herisau, 2003 on www.metrohm.ch. Accessories catalogue, Metrohm AG, CH-Herisau, 2003 on www.metrohm.ch.

[19] a) H. Taube, H. Myers, R.R. Rich, *J. Am. Chem. Soc.* **1953**, *75*, 4118; b) M.L. Tobe, 'Reaktionsmechanismen der Anorganischen Chemie', Verlag Chemie, Weinheim, 1972; c) H. Taube, 'Electron Transfer Reactions of Complex Ions in Solution', Academic Press, New York, 1970.

[20] T. Vauthier, Travail de Certificat (bachelor thesis), Université de Neuchâtel, 2002.

[21] K. Bernauer, M.F. Gilet, *Chem. Comm.* **1997**, 1287-1288.

[22] Y.P. Myer, *Biochemistry* **1968**, 7, 765.

[23] a) K. Bernauer, S. Ghizdavu, L. Verardo, *Coord. Chem. Rev.* **1999**, *190-192*, 357; b) S. Ghizdavu, PhD Thesis, Université de Neuchâtel, 2000.

[24] a) O.A. Gansow, A.R. Kausar, K.M. Triplett, M.J. Weaver, E.L. Yee, *J. Am. Chem. Soc.* **1977**, *99*, 7087. E.L. Yee; b) O.A. Gansow, M.J. Weaver, *J. Am. Chem. Soc.* **1980**, *102*, 2278.

CHAPTER 5:

STRUCTURE AND ISOMERISATION OF COBALT(III) COMPLEXES WITH A NEW BIS(*β*-AMINOCARBOXYLATE)PYRIDINE LIGAND

5.1 Structure and isomerism of $[Co(b3amp)(H_2O)]^+$

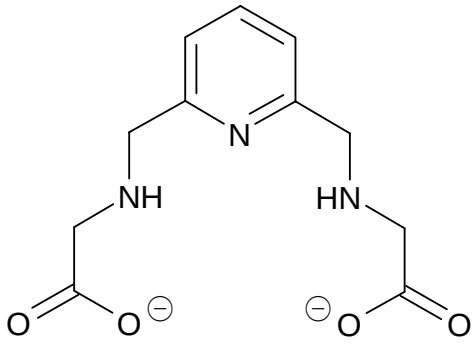

(**I**)

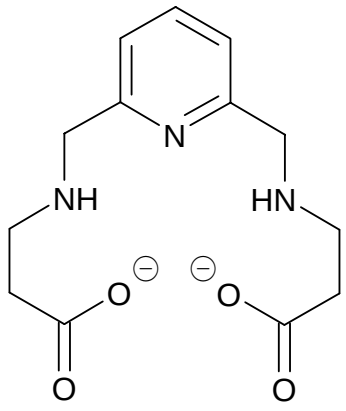

(**II**)

As mentioned in chapter 1, chiral pentadentate bis[*β*-aminocarboxylate]pyridine ligands forming two five and two six-membered chelate rings (framework **II**) have not yet been described in the literature. On the other hand, Cr^{III}/Cr^{II} complexes with this type of ligands are expected to exhibit less negative reduction potentials than the corresponding complexes with the type **I** ligands (see §4.7) so that they could act as stereoselective electron donors for metalloproteins without being oxidized by the water protons. We therefore decided to synthesise the new ligand 2,6-bis[3-carboxymethyl-2-azabutyl]pyridine, b3amp (**3**).

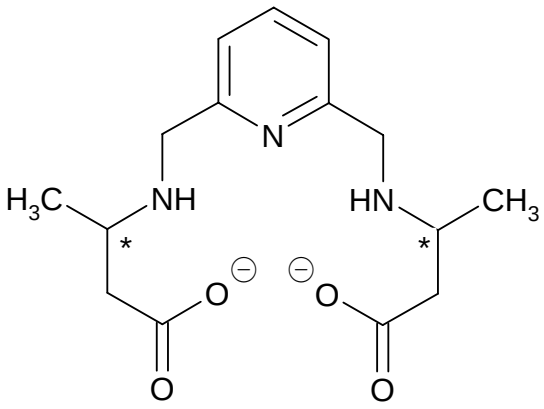

(**3**)

The replacement of the α- by the β-amino-acid unit forming two six-membered rings for the lateral chelation should have two consequences:

a) Six-membered rings show higher flexibility and therefore allow structural arrangements that are not possible with the corresponding five-membered rings.

b) Six-membered rings leave more space for the coordination centre and therefore should stabilise lower oxidation states, which means that the redox potential of Fe, Co and Cr complexes should be shifted to more positive values.

The notable consequence of the higher flexibility is to allow, whatever might be the absolute configuration of the asymmetric carbon atoms, Δ- and Λ-configuration of the complex and therefore the *R*- and *S*-configuration of the aliphatic nitrogen atoms, leading for the ligand with (*S*,*S*)-chirality to the two C_2-symmetric isomers **A1-1** and **A1-2**. Furthermore, with at least one six-membered chelate ring, the arrangement of two joint chelate rings can be facial as well as meridional. Whereas in the facial arrangement the configuration of the aliphatic nitrogen atoms is determined by the chirality of the complex – (*S*,*S*) for Δ and (*R*,*R*) for Λ in the C_2-symmetric arrangement *fac-mer-fac* (A-type, see fig. 1-2 and Table 5-1) – this is no longer the case in the unsymmetrical B-type arrangement. As in the meridional arrangement, the secondary nitrogen atom can easily assume *R*- or *S*-chirality as well, four different diasteroisomers, **B1-1**, **B1-2**, **B2-1** and **B2-2** must be expected for the unsymmetrical arrangement. Even by excluding the geometries C and D because of the facial arrangement of the inner chelate rings 2 and 3 (see Fig. 1-2) whose Baeyer strain would be too high for the central pyridine unit, 6 isomers are theoretically possible for the optically pure form of the ligand. When the synthesis is done with the racemic 3-aminobutyric acid, the free ligand can exist as the two enantiomers (*R*,*R*) and (*S*,*S*) and as the meso-form (*R*,*S*). In this case, the number of theoretically possible isomers of octahedral complexes amounts to 22. The structural features of the possible isomers for the optically active ligand with (*S*,*S*)-configuration and their schematic structures are given in Table 5-1.

Despite the large number of possible isomers, we started the exploration of cobalt(III) complexes using a mixture of the racemic and the meso-form of the ligand, essentially due to the experimental difficulties to prepare optically pure 3-aminobutyric acid (see §2.1.1, §2.3.8). Ion exchange chromatography on *SP-Sephadex C-25* of the reaction mixture yielded several red and red-brown fractions. After longer standing of the neutral solutions, the separated red and red-brown fractions could again be separated into a red and a red-brown compound revealing the reversible transformation and the equilibrium between the two forms.

Table 5-1. *Possible isomers of the complex [Co(*S,S*)-b3amp(H_2O)]$^+$.*

Coordination mode	Absolute configuration [a])			Axis with highest symmetry	Short name [c])
	N(*fac*)	N(*mer*)	Co		
fac-mer-fac (A type)	*S,S*	---	Δ	C_2	**A1-1**
	R,R	---	Λ	C_2	**A2-1**
fac-mer-mer (B type)	*S*	*S*	Λ[b])	C_1	**B1-1**
	S	*R*	Λ[b])	C_1	**B1-2**
	R	*R*	Δ[b])	C_1	**B2-1**
	R	*S*	Δ[b])	C_1	**B2-2**

[a]) all asymmetric carbon atoms have *S* configuration

[b]) with respect to the aminocarboxylate rings

[c]) for the purpose of simplification, the salts of these cations bear the same name

Charges omitted on the structures, X = H_2O

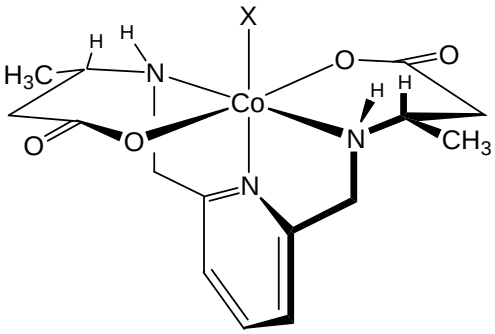

(**A1-1**)

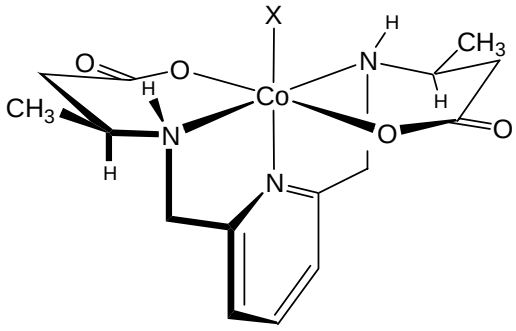

(**A2-1**)

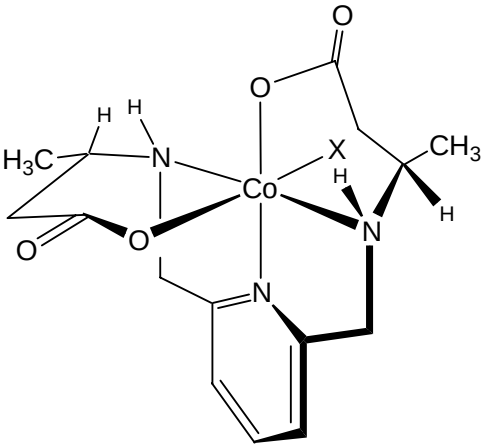

(**B1-1**)

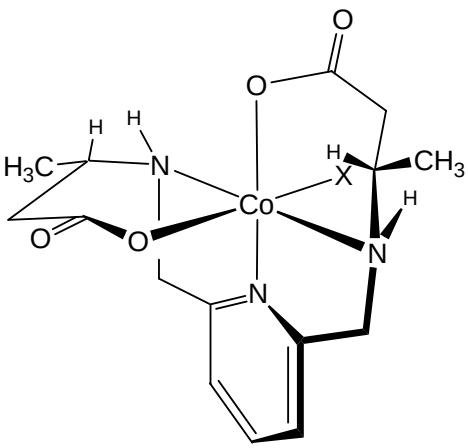

(**B1-2**)

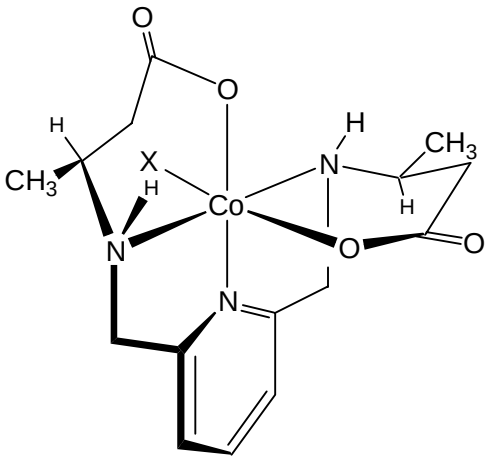

(**B2-1**)

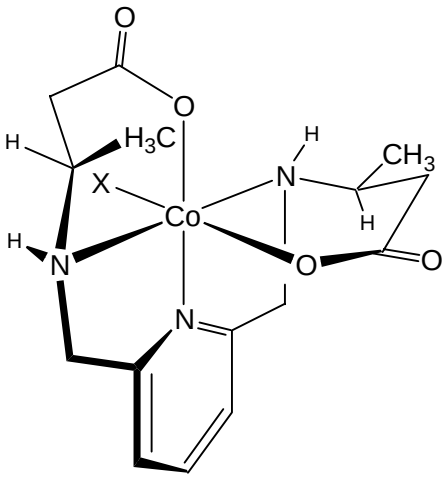

(**B2-2**)

The compound of one of the main red bands could be isolated as the solid perchlorate salt and the X-ray structure for the Δ enantiomer of the racemic compound is represented in Fig. 5-1. Corresponding to the isomer **A1-1**, its chirality pattern is Δ-(S_C,S_C)(S_N,S_N). As shown by Fig. 5-2, the substituents in **A1-1** are found in an equatorial position, orientated slightly towards the pyridine ring. This orientation differs from analogous compounds with five-membered aminocarboxylate chelate rings, as for example the Δ-[Co(*R*,*R*)-alamp(buim)]$^+$ (Fig. 5-3), where *Δ*-configuration of the coordination centre is imposed by *R*-chirality at the carbon centres and locates the substituents in an *exo* position, pointing away from the pyridine ring. As shown in Fig. 5-4, the twisted half-chair conformation of the aminocarboxylate rings and the equatorial position of the methyl groups in **A1-1** induce an almost homogeneous flat surface of the N,O,N,O-plane containing the metal centre, the chirality of which is therefore only weakly expressed. Stereoselectivity of bimolecular reactions, like electron- or metal ion-transfer, involving this type of compounds might therefore be rather small.

Based on the X-ray structure and the visible absorption spectra of the compound **A1-1** compared to the corresponding complexes of type **I** ligands (see §1.2), we attribute tentatively the C_2 symmetric structure (A-isomers) to all the red and the unsymmetrical structure (B-isomers) to all the red-brown compounds. This attribution is also confirmed by the observation that in the related red/red-brown couples the retention volume of the red-brown compound is about 50% greater, indicating a higher affinity to the ion exchanger due to its higher polarity.

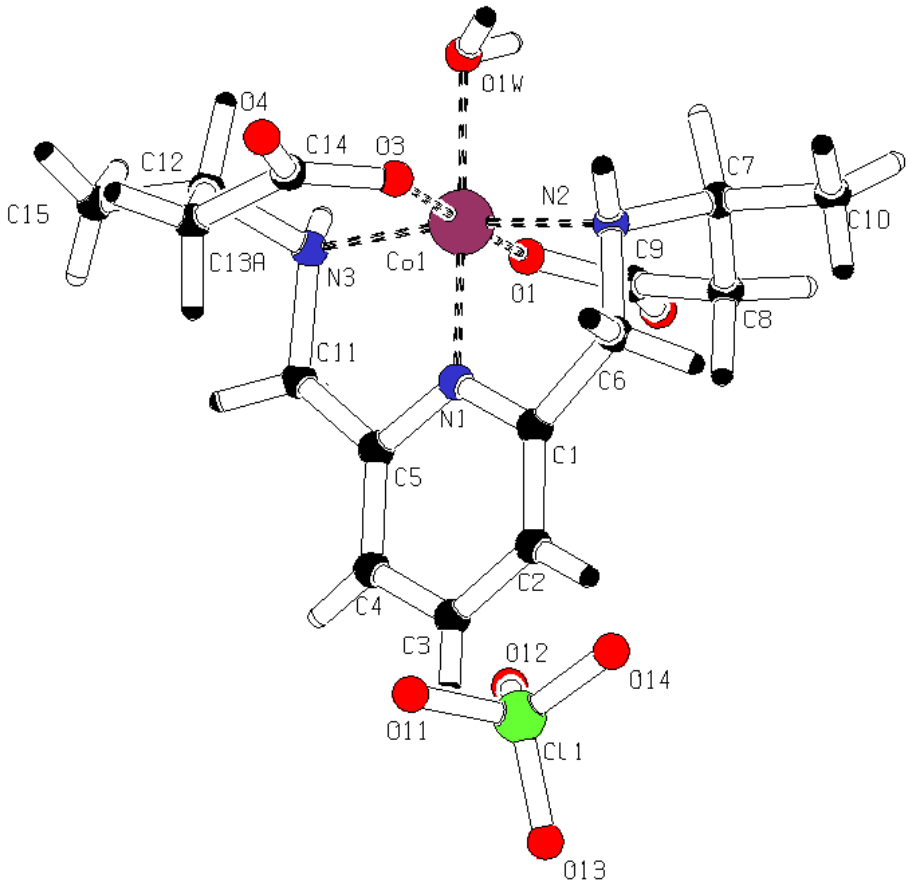

Fig. 5-1. *X-ray structure of Δ-[Co*(S_C,S_C)(S_N,S_N)*-b3amp]ClO_4 (**A1-1**).* Image generated by [1].

In order to get more information on the stereochemistry of the existing isomers, we prepared in the following the optically active cobalt(III) complexes using the ligand synthesised with pure (*3S*)-3-aminobutyric acid. The crude reaction mixture exhibited nearly no CD signal because the spectra of the formed isomers compensate each other (see Fig. 5-5). The chromatographic separation on a *SP Sephadex C-25* cation exchange column yielded mainly three fractions, two red complexes and a red-brown one. Whereas clear separation of the red-brown fraction occurred, the separation between the two red fractions remained only partial, even at a column length of 120 cm. For the analysis therefore only the head and tail fractions showing identical UV/CD intensity ratios were used. Whereas the UV/VIS spectra (Fig. 5-4) of the two red fractions are almost identical in the visible range of the spectrum, the CD (Fig. 5-5) shows (+,-,-,+) pattern for the first but (+,-,+,-) pattern for the second. That means clear inversion of the spectrum in low-energy transitions. Assuming that the chirality of these transitions is determined by the chiral arrangement of the N_3O_3 chromophore around the coordination centre and that the contribution of vicinal effects due to the substituents only change the intensity of the bands (what has been confirmed for all C_2 symmetric complexes of type **I** ligands), the

Δ-(S_C,S_C)(S_N,S_N) (**A1-1**) structure is attributed to the first band and the Λ-(S_C,S_C)(R_N,R_N) (**A2-1**) structure to the second (see Scheme 5-1).

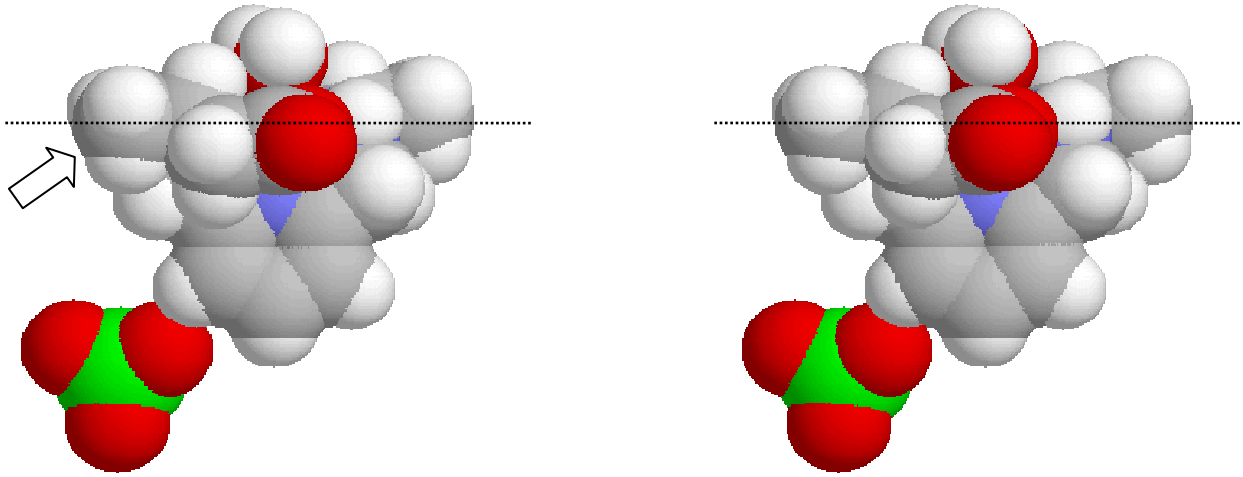

Fig. 5-2. *Stereo-view of the space-filling model of* ***A1-1,*** *based on van-der-Waals radii and the X-ray structure.* The equatorial ligand on the asymmetric carbon atom points is orientated in the (horizontal) N-Co-N axis (arrow). The methyl protons have no steric interaction with the methylene protons next to the pyridine ring. Image generated by [2].

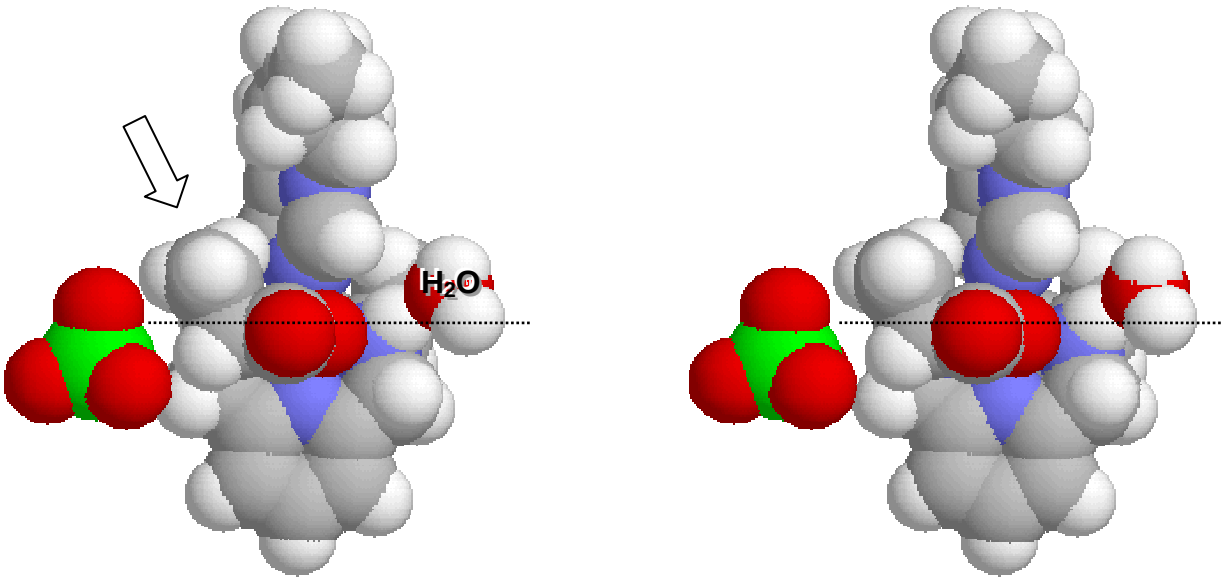

Fig. 5-3. *Stereo-view of the space-filling model of Δ-[Co((*R_C,R_C*)(*S_N,S_N*)-alamp)buim]*$ClO_4 \cdot H_2O$*, based on the van-der-Waals radii and X-ray structure [3].* Steric interaction between the methylene protons next to the pyridine ring and the methyl group force the latter into an axial type (exo) position (arrow). Image generated by [2]

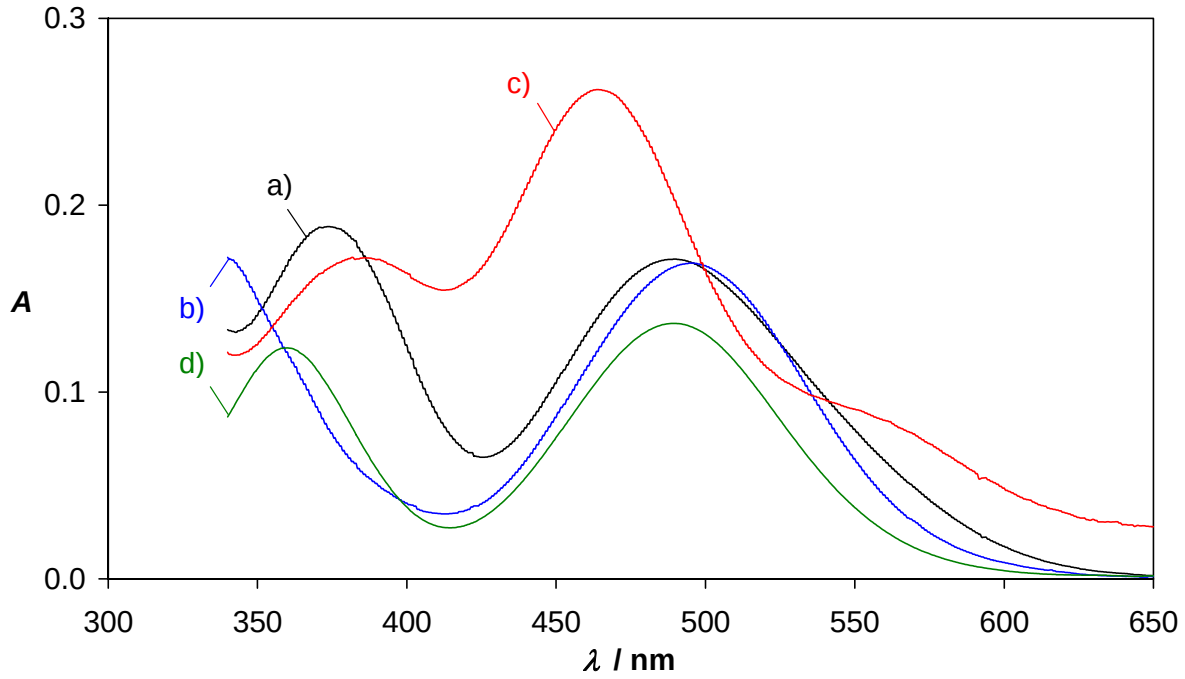

Fig. 5-4. *UV spectra at approximately $2 \cdot 10^{-4}$M, pH = 4.6 ($HClO_4$) and r.t. of the main products in the reaction between optically pure (*S,S*)-b3amp^{2-} ligand and cobalt(III).*

a) ***A1-1*** (——), b) ***A2-1*** (——), c) ***B1-1*** (——), d) *Δ-[Co(*R,R*)-alamp]$^{+}$ $2 \cdot 10^{-4}$M given for comparison* (——).

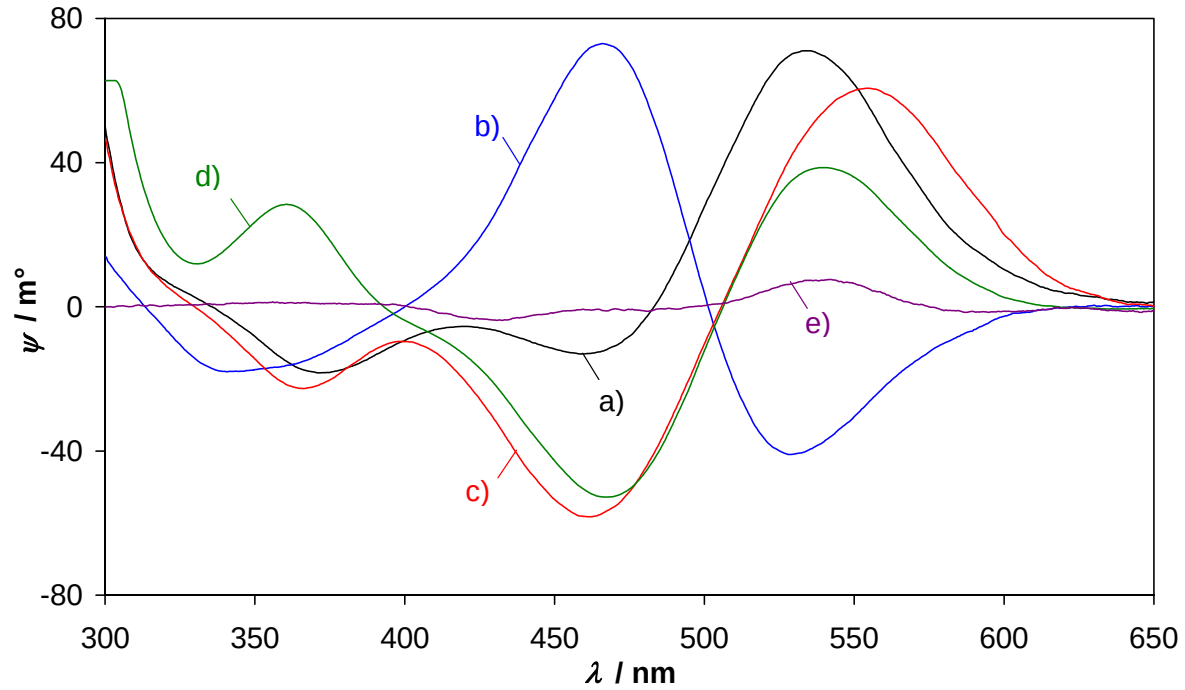

Fig. 5-5. *CD spectra at approximately $2 \cdot 10^{-4}$M, pH = 4.6 ($HClO_4$) and r.t. of the main products in the reaction between optically pure (S,S)-b3amp^{2-} ligand and cobalt(III).*

a) ***A1-1*** (——), b) ***A2-1*** (——), c) ***B1-1*** (——), d) *crude mixture of all isomers as they are formed during the cobalt(III) complexation by (S,S)-b3amp^{2-} (after 72h of reaction, concentration uncorrected, details see §2.3.9)* (——), e) *Δ-[Co(*R,R*)-alamp]$^{+}$ $2 \cdot 10^{-4}$M given for comparison* (——).

For cobalt(III) complexes there is no unsymmetrical reference compound known and the structural type of the single optically active compound of the red-brown fraction must therefore be achieved in a different way. This is described in the following section.

Scheme 5-1. *Observed equilibria between $[Co^{III}((S,S)\text{-}b3amp)H_2O]^+$ isomers.*

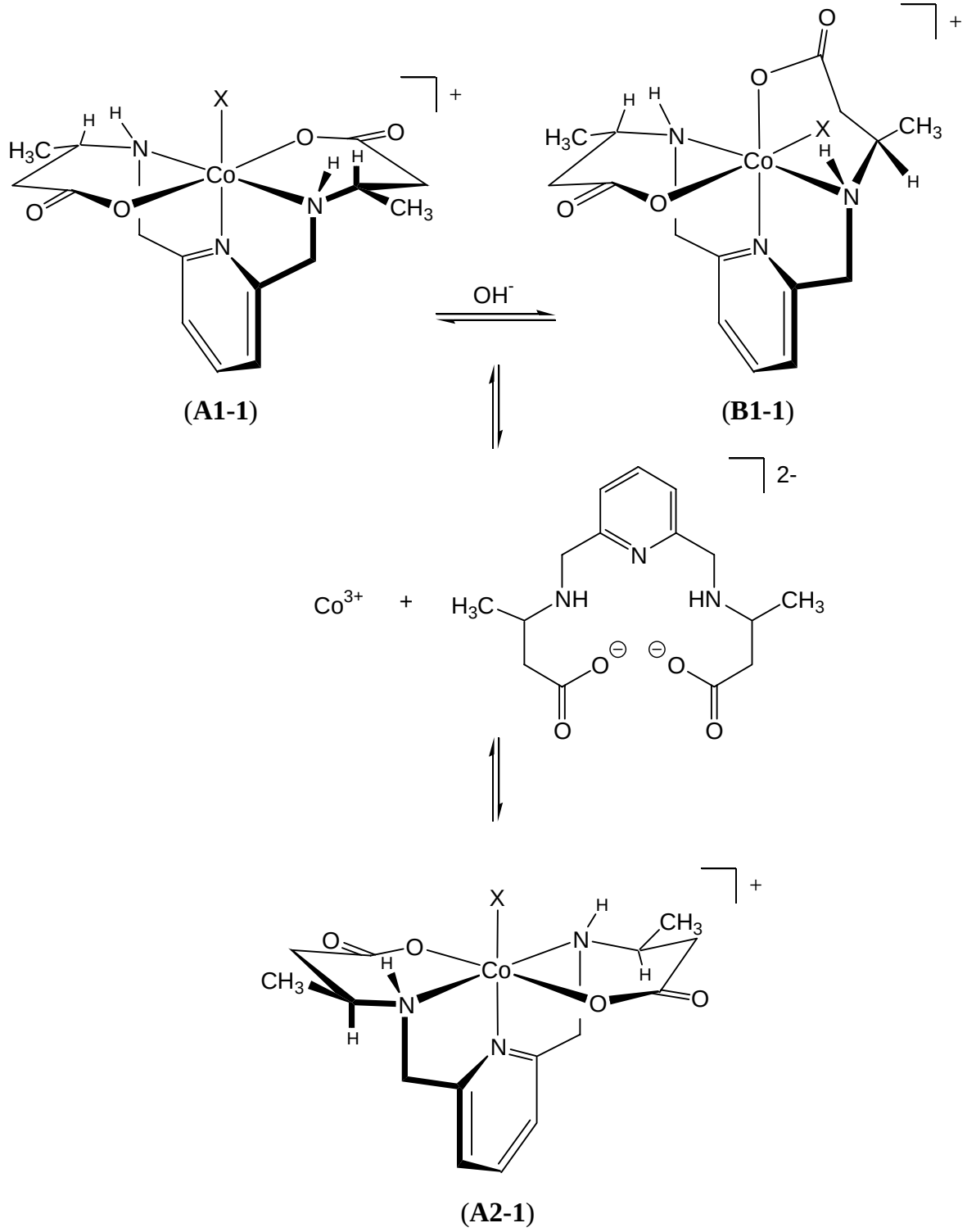

(**A1-1**) (**B1-1**)

(**A2-1**)

5.2 Isomerisation of Δ-[Co(*S*$_C$,*S*$_C$)(*S*$_N$,*S*$_N$)-b3amp)H$_2$O]$^+$ (A1-1)

As previously mentioned, red and red-brown isomers are interconvertible. Preliminary experiments with the isolated racemic form, the molecular structure of which had been determined by X-ray diffraction, revealed that the isomerisation is base catalysed and that, according to Scheme 5-2, the equilibrium is shifted to the red compound at pH < 8 and to the red-brown compound at pH > 8.

This behaviour shows, that the unsymmetrical isomers are stabilised in the *trans* position to the carboxylate group by the negatively charged OH$^-$ group, a ligand exhibiting strong trans effect. With the coordinated water molecule, *trans* effects are weaker and the symmetric structure becomes slightly more stable.

Scheme 5-2. *Hypothesis of equilibria between the A and the B type isomers of [Co(b3amp)H$_2$O]$^+$*

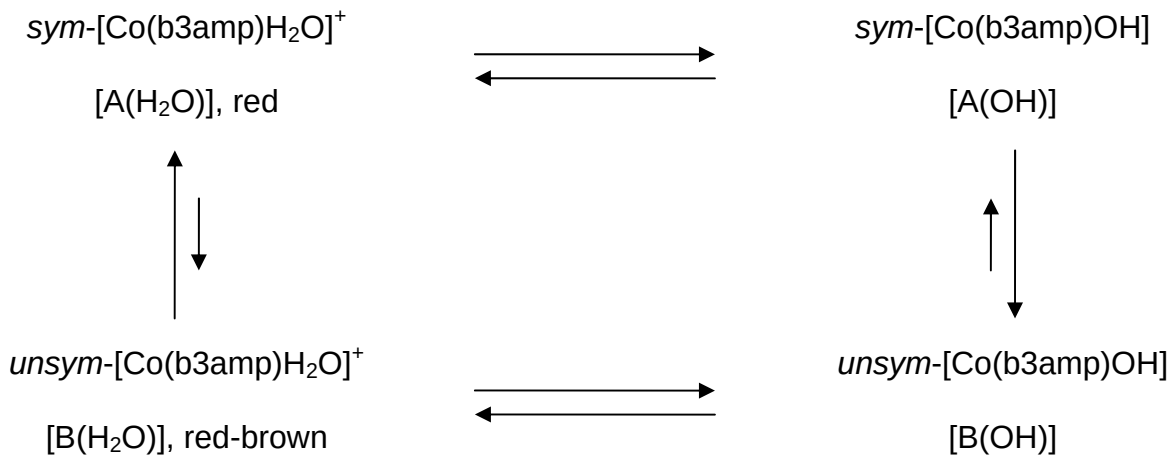

Five different possibilities for the mechanism of the isomerisation can be considered, which are in agreement with the observations mentioned above.

a) Solvent assisted dissociation of the carboxylate group and intramolecular rearrangement with ring closure of the carboxylate group in the trans-pyridine position.

b) Intermolecular substitution by OH$^-$ and ring closure of the carboxylate group in the trans-pyridine position.

c) Deprotonation of the coordinated water molecule in the apical position followed by intramolecular substitution of the carboxylate group by the coordinated OH-group with simultaneous ring closure of the carboxylate group in the trans-pyridine position.

d) Deprotonation at the coordinated amino group before ring opening. Substitution of the carboxylate group by the solvent and subsequent deprotonation and ring closure in trans-pyridine position.

e) Deprotonation of the coordinated water molecule and dissociation of the aminocarboxylate moiety followed by intramolecular rearrangement.

Mechanisms a), b) and c) occur with retention at the coordinated nitrogen atom and allow only the formation of the two B1 isomers. With mechanisms d) and e) inversion of the secondary nitrogen atom is possible and the mechanism can therefore lead to all the four B-isomers. Mechanism a) is pH independent, whereas mechanisms b) should show a linear relationship with the OH^- concentration of the solution over the whole pH domain of the solvent. As the pK_a values of coordinated secondary amines lies outside the pH domain of the solvent water, the same linear [OH^-] dependence of the reaction rate must be expected for mechanism d). The reaction rate for mechanisms b) and e) is proportional to the concentration of the deprotonated complex. The log k_{obs} varies therefore in a linear way with pH in the pH area below the pK_a value of the complex and becomes pH-independent when pH > pK_a.

Preliminary experiments [4] indicated that the reaction rate increased by a factor of 15 between pH 5.5 and 8.2 but remained almost constant in the pH ranges 4.0–5.5 and 8.2–9.6, a behaviour suggesting the existence of at least two different mechanisms. Mechanism a) is in agreement with the behaviour in slightly acidic solution and mechanism c) with the behaviour in alkaline solution, the pK_a the red isomer of $[Co(b3amp)H_2O]^+$ being 8.2. Interestingly, the same mechanism involving the intramolecular rearrangement following the deprotonation of a coordinated water molecule has been observed in the racemisation of optically enriched $[Co(sarmp)H_2O]^+$ [5]. Nevertheless, the reaction with a half-life of 800 hours at 40°C was so much slower than the isomerisation of $[Co(b3amp)H_2O]^+$ that mechanism e) can be excluded for the latter. Mechanism b) and d) are not in agreement with a pH independent rate at higher pH values. From these results it is expected that the isomerisation takes place under retention of the configuration of the nitrogen atoms and that only the unsymmetrical isomers with iden-

tical chirality at both nitrogen atoms are obtained, "Λ"-**B1-1** from Δ-**A1-1** and "Δ"-**B1-2** from Λ-**A1-2**.

Fig. 5-6 and Fig. 5-7 show the change in the visible and the CD spectrum during the isomerisation of the optically active **A1-1** fraction. The reaction was performed in slightly alkaline solution (pH = 7-8) in order to force the equilibrium on the side of the unsymmetrical complex, but the measurements were done at pH 4-5 by switching the pH between the two ranges for each measurement by adding HCl, respectively NaOH. The spectra in Fig. 5-6 and Fig. 5-7 are corrected for the volume change due to the additions of acid and base. It is clearly seen that the UV and the CD spectra of the **A1-1** fraction evolve towards the spectra of the separated **B1-1** fraction. The comparison with the spectra of the **B1-1** fraction, the concentration of which is not known, is done by adjusting the isosbestic and isodichroic points. The change of the A to the B isomer is not complete, indication that at the end of the reaction both forms still exist in the equilibrium but that the B isomer is predominant.

From these results it seems evident that the separated red-brown fraction exhibits the structure of the, *unsym*-"Λ"-$[Co(C_SC_S)(N_SN_S)$-b3amp$)H_2O]^+$ compound.[1])

When the same experiment is performed with the A1-2 fraction, no significant modification in the UV/VIS and CD spectra is observed. This can be due either to a to small isomerisation rate or to an equilibrium situation which is unfavourable for the corresponding B1-2 isomer. This might be the reason why this isomer has not been found in the reaction mixture of the synthesised cobalt(III) complexes with the optically active ligand.

[1]) It should be noted that the attribution of "Λ"-chirality to the unsymmetrical B1-1 isomer is a tentative attribution based only on the chirality of the aminocarboxylate ring pair. The change from Δ to "Λ" during the isomerisation therefore does **not** mean an inversion of the chirality at the coordination centre as clearly demonstrated by the similar pattern of the two CD spectra.

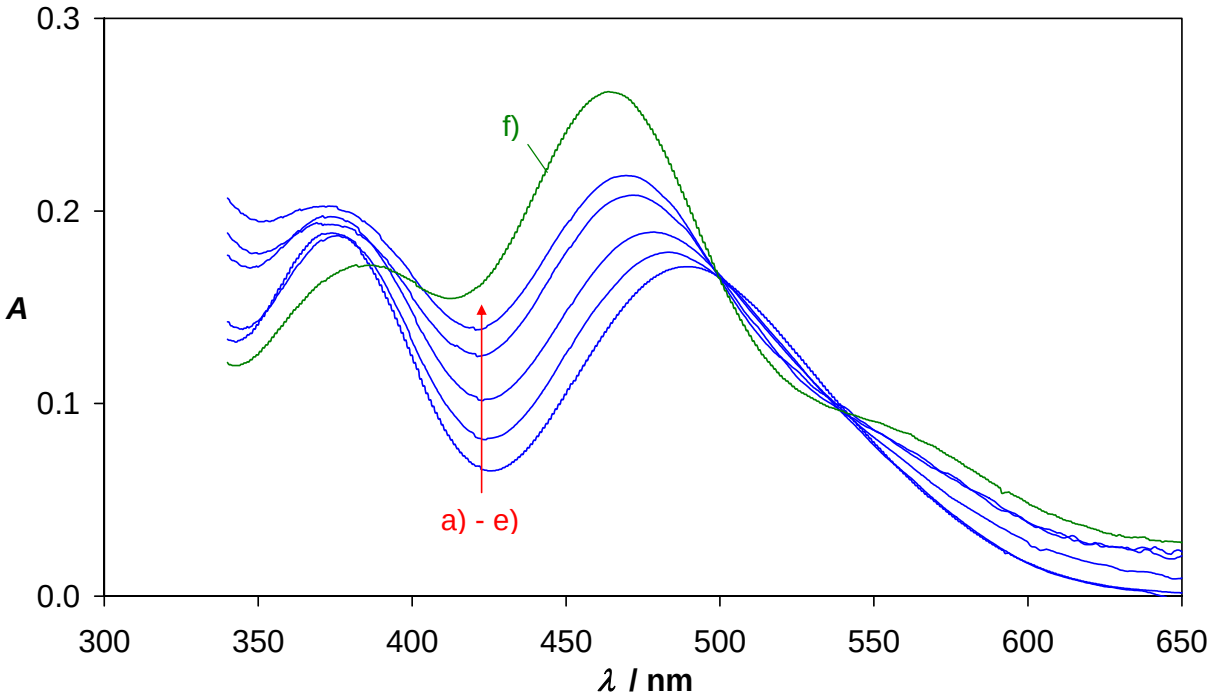

Fig. 5-6. *Transformation of* ***A1-1*** *at unknown concentration, pH 7-8 (NaOH) and r.t. as a function of time.* a)-e) *UV spectra recorded at pH = 3.2-3.7($HClO_4$) after 0 h (pH 4.5), 16 h, 46 h, 176 h and 318 h with hypsochromic shift between 450 and 500 nm* (——), f) ***B1-1*** *given for comparison* (——). Baseline and / or concentration corrections have been applied to certain spectra.

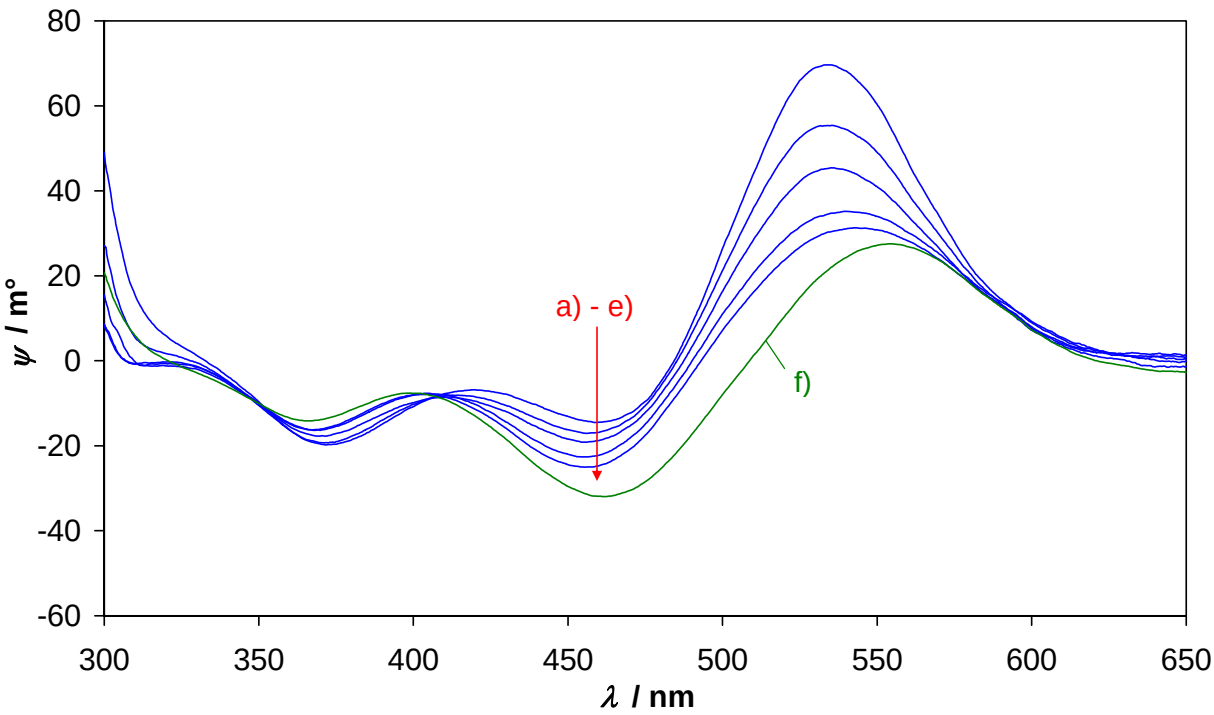

Fig. 5-7. *Transformation of* ***A1-1*** *at unknown concentration, pH 7-8(NaOH) and r.t. as a function of time.* a)-e) *CD spectra recorded at pH = 3.2-3.7($HClO_4$) after 0 h (pH 4.5), 16 h, 46 h, 176 h and 318 h with hypsochromic shift between 450 and 500 nm* (——), f) ***B1-1*** *given for comparison* (——). Baseline and / or concentration corrections have been applied to certain spectra.

5.3 Conclusions

The investigation of the coordination behaviour of the optically active type **II** ligand (*S*,*S*)-b3amp in inert cobalt(III) complexes showed that at least three isomers can be formed in similar amounts. Besides at least one unsymmetrical isomer, two isomers with C_2 symmetry and opposite chirality at the coordination centre are obtained. The initially planned use of type **II** ligands in stereoselective electron transfer reactions needs labile complexes, carrying redox-active metal centres like Cr^{II}, Fe^{II} or Co^{II} with a single, predetermined chirality. This condition, perfectly fulfilled with most of the type **I** ligands, is obviously not realised with type **II** ligands. Even if a single isomer would react in a stereoselective way despite the rather flat arrangement of the ligand in the N,O,N,O plane, the stereoselectivities would be opposite and therefore cancel each other for the two symmetric isomers. Furthermore, the relative concentrations of the different isomers of metal complexes with labile metal ions cannot be determined. A possible stereoselectivity could therefore not be put in relation to a definite structure of the reagent.

For all these reasons, the idea to study stereoselectivity in electro-transfer reactions using ligands with six-membered aminocarboxylate chelate rings has been abandoned.

5.4 Experimental part

5.4.1 Reagents and solvent

Ligands, complexes and water have been prepared as described in chapter 2. All other reagents were of analytical grade.

5.4.2 Buffer solutions

Buffers in the pH range from 4.0 to 6.0 with ionic force μ = 0.5 have been prepared from solid sodium acetate and concentrated acetic acid (pK_a = 4.75 at 25°C and μ = 0.1).

Buffers in the pH range from 7.0 to 9.0 with ionic force μ = 0.5 have been prepared from 1.0M hydrochloric acid and solid Tris (pK_a = 8.09 at 25°C and μ = 0.1).

Buffers in the pH range from 9.0 to 10.0 with ionic force μ = 0.2 have been prepared from 1.0M sodium hydroxide and solid boric acid (pK_a = 9.20 at 25°C and μ = 0.1).

5.4.3 Isomerisation rate of $[Co^{III}(b3amp)H_2O]^+$

The samples consisted of a diluted mixture of a freshly prepared $[Co^{III}(b3amp)H_2O]ClO_4$ stock solution and the corresponding buffer concentrate. Absorption spectra between 340 and 740 nm (scan speed: 100 nm/min) towards μ = 0.1 buffer were recorded at regular intervals. The *in situ* concentrations of cobalt(III) complex were $2 \cdot 10^{-3}$M at a ionic force of μ = 0.1. Measurements were made at various pH values and temperatures.

5.5 References

[1] a) A.L. Spek, PLATON99, Program for Representation of Crystal Structures, Universiteit Utrecht, Utrecht, The Netherlands, 1980-2003; b) A.L. Spek, *J. Appl. Cryst.* **2003**, *36*, *7*. H. Stoeckli-Evans, Université de Neuchâtel, 2001.

[2] 'MDL® Chime', version 2.6 SP6, Browser plug-in for the three-dimensional visualisation of chemical structures, Elsevier MDL, San Ramon, United States of America, 2004.

[3] L. Verardo, Ph.D. Thesis, Université de Neuchâtel, 1996.

[4] J. Lenoble, Advanced practical work in Inorganic Chemistry, Université de Neuchâtel, 2001.

[5] C. Vichard, Diploma work, Université de Neuchâtel, 1997.

CHAPTER 6:
SUMMARIES

6.1 Summary

Keywords: cytochrome *c*, cobalt(II) complexes, chromium(II) complexes, enantioselectivity, kinetics, circular dichroism.

According to the aim of this work, the structural and redox properties of some optically active cobalt(III) and chromium(III) complexes and the use of corresponding Co^{II} and Cr^{II} compounds as chiral probes in electron transfer to cytochrome *c* have been studied.

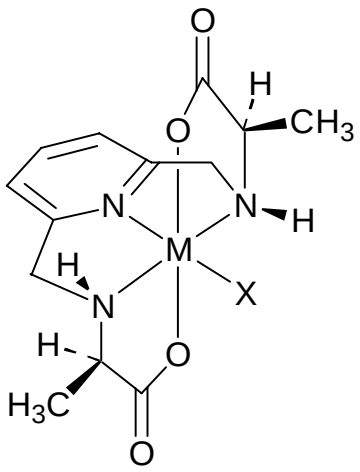

Δ-[M((*R*,*R*)-alamp)X]

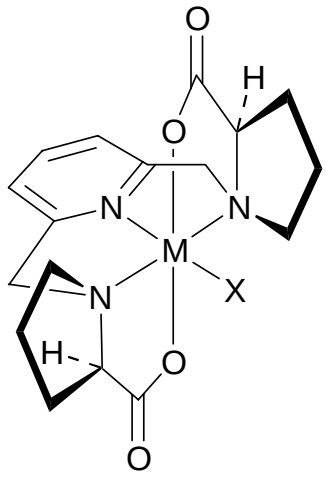

Δ-[M((*R*,*R*)-promp)X]

[Co^{II}(alamp)H_2O] and [Co^{II}(promp)H_2O] have been used as reducing agents in the electron-transfer reaction involving horse heart cytochrome *c*. The rate constants are three to four orders of magnitude lower than in the reductions employing the analogous iron(II) compounds, which is mainly due to much more negative activation entropies. The corresponding cobalt(III) species of both enantiomers of [Co^{II}(alamp)] are partly attached to the protein during electron transfer, which proves that the latter has passed, at least partially, by an inner sphere mechanism using the His 26 or His 33 imidazole as bridging ligand. No covalent binding of the [Co^{III}(promp)]-unit has been observed in the chosen reaction conditions. Whereas the overall reaction with both complexes, [Co^{II}(alamp)H_2O] and [Co^{II}(promp)H_2O], shows rather

low stereoselectivity, the latter is - with a mean k_{RR}/k_{SS} ratio of 2.9 - fairly high with $[Co^{II}(alamp)H_2O]$ for the inner-sphere part. As the stereoselectivity observed for the overall reaction is the result of both, the inner and outer-sphere part, both reaction mechanisms seem to exhibit significant but opposite stereoselectivity.

The new complex $[Cr^{III}(S,S)\text{-promp})H_2O]^+$ shows electrochemical activity at a potential of -1.0 V vs. SHE at pH 7, most probably due to the catalytic decomposition of water. The short-lived existence of the corresponding chiral Cr^{II} species was demonstrated by electron-transfer mediated ligand exchange. In the reduction of ferricytochrome *c* by zinc, $[Cr^{III}(S,S)\text{-promp})H_2O]^+$ involving a Cr^{II} intermediate at the metal surface, has a remarkable catalytic effect, but no chromium (III) species seems to be permanently bound to the protein after the electron transfer.

The new complex $[Co^{III}(S,S)\text{-b3amp}]H_2O]^+$ contains two six-membered aminocarboxylate chelate rings. The existence of at least three diastereoisomers, two symmetrical and one unsymmetrical, and the isomerisation equilibrium between two of them in basic medium has been shown by spectrophotometric and spectropolarimetric analyses. Due to the existence of this isomerisation equilibrium, the complexes with this new ligand b3amp have been considered as unsuitable for stereochemical investigations related to electron-transfer reactions. Therefore, the part of the project employing this type of complexes for chiral recognition in electron-transfer reactions has been discarded.

The combined use of spectrophotometry and circular dichroism has once again proved to be a powerful and essential tool for the structure investigation of optically active complexes in solution as well as for the study of reaction kinetics and mechanisms.

6.2 Résumé

Le résumé français se trouve à la page VIII, en préambule à ce document.

6.3 Zusammenfassung

Schlagwörter: Cytochrom *c*, Kobalt(II)-Komplexe, Chrom(II)-Komplexe, Enantioselektivität, Kinetik, Cirkulardichroismus.

Ziel dieser Arbeit war es, die Strukturen und Redox-Eigenschaften von einigen optisch aktiven Kobalt(III)- und Chrom(III)-Komplexen, sowie den Gebrauch entsprechender Co^{II}- und Cr^{II}-Verbindungen als chirale Sonden in Elektronenübertragungs-Reaktionen mit Cytochrom *c* zu untersuchen.

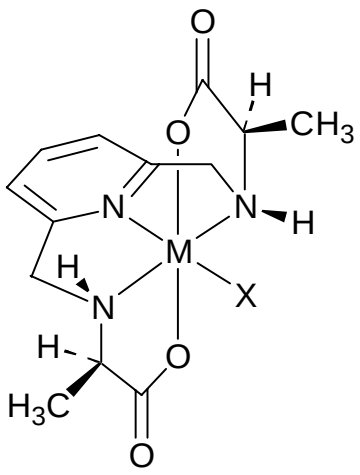

Δ-[M((*R*,*R*)-alamp)X]

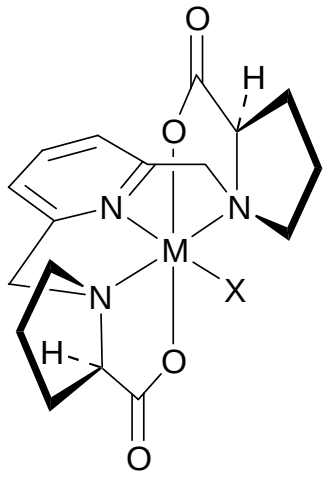

Δ-[M((*R*,*R*)-promp)X]

$[Co^{II}(alamp)H_2O]$ und $[Co^{II}(promp)H_2O]$ wurden als Reduktionsmittel für Ferricytochrom *c* eingesetzt. Die Geschwindigkeitskonstanten sind etwa drei bis vier Grössenordnungen kleiner als bei den Reduktionen mit den analogen Eisen(II)-Komplexen, was in erster Linie auf eine wesentlich negativere Aktivierungs-Entropie zurückzuführen ist. Die aus den beiden $[Co^{II}(alamp)]$-Enantiomeren entstehenden Kobalt(III)-Spezies werden zum Teil während der Elektronenübertragung an das Protein gebunden. Das zeigt, dass dieser Transfer zumindest teilweise in der inneren Koordinationssphäre das Kobalt abläuft, wobei die Histidin-Gruppen 26 oder 33 des Proteins als Brückenligand benutzt werden. Unter den gewählten Reaktionsbedingungen konnte keine koordinative Bindung der $[Co^{III}(promp)]$-Einheit festgestellt werden. Die Gesamt-Reaktion zeigt zwar bei beiden Enantiomeren-Paaren eine ziemlich geringe Stereoselektivität, diese ist aber für jenen Anteil der Reduktion mit $[Co^{II}(alamp)H_2O]$, der gemäss eines *inner-sphere*-Mechanismus abläuft, mit einem durchschnittlichen Verhältnis k_{RR}/k_{SS} von 2.9 wesentlich höher. Da die Stereoselektivität der Gesamtreaktion sich aus denen

der jeweiligen Anteile, die in der inneren und äusseren Sphäre ablaufen, zusammensetzt, scheinen beide Reaktionswege signifikante aber entgegengesetzte Stereoselektivitäten aufzuweisen.

Der neue Komplex $[Cr^{III}(S,S\text{-promp})H_2O]^+$ ist bei pH 7 und einem Potential von -1.0 V in Bezug auf die Standard-Wasserstoff-Elektrode elektrochemisch aktiv, sehr wahrscheinlich verursacht er die katalytische Zersetzung des Wassers. Die Existenz des entsprechenden Cr^{II}-Spezies ist zwar nur von kurzer Dauer, wurde aber durch Redox-Substitution des fünfzähnigen Liganden eindeutig nachgewiesen. In der Reduktion des Ferricytochrom *c* durch metallisches Zink zeigt $[Cr^{III}(promp)H_2O]^+$, im Zusammenspiel mit einem Cr^{II}-Zwischenprodukt an der Metalloberfläche, einen beachtlichen Katalyse-Effekt; bei der Elektronenübertragung scheint das gebildete Cr^{III}-Spezies jedoch nicht bleibend an das Protein gebunden zu werden.

Der neue Komplex $[Co^{III}(S,S\text{-b3amp})H_2O]^+$ enthält zwei sechsgliedrige Aminocarboxylat-Chelatringe. Das Vorhandensein von mindestens drei Diastereoisomeren, zwei symmetrischen und einem unsymmetrischen, sowie das Isomerisations-Gleichgewicht, das im basischen Milieu zwischen zwei von ihnen besteht, wurden durch spektrofotometrische und spektropolarimetrische Analysen nachgewiesen. Aufgrund dieses Isomerisations-Gleichgewichtes halten wir die Komplexe mit dem neuen b3amp-Liganden zur stereochemischen Untersuchung von Elektronenübertragungs-Reaktionen für ungeeignet. Deshalb wurde der Teil des Projektes, der den Gebrauch solcher Komplexe zur chiralen Erkennung in Elektronenübertragungs-Reaktionen vorgesehen hatte, nicht weiter verfolgt.

Die Kombination von Spektrofotometrie und Cirkulardichroismus erwies sich erneut als ein leistungsfähiges und wichtiges Instrument zur Untersuchung von Komplexstrukturen in Lösung, sowie von Reaktionskinetiken und –mechanismen.

6.4 Riassunto

Parole chiave: citocromo *c*, complessi di cobalto(II), complessi di cromo(II), enantioselettività, cinetica, dicroismo circolare.

Lo scopo di questo lavoro era di esplorare le proprietà strutturali e d'ossidoriduzione di alcuni complessi di cobalto(III) e cromo(III) nonché l'impiego di specie correlate di cobalto(II) e cromo(II) come sonde chirali nel trasferimento di elettroni implicando il citocromo *c*.

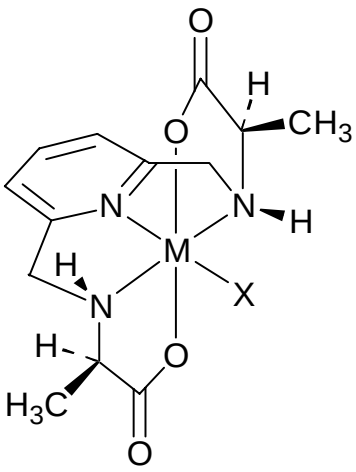

Δ-[M((*R*,*R*)-alamp)X]

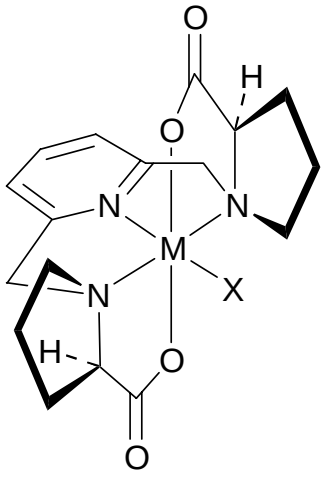

Δ-[M((*R*,*R*)-promp)X]

[Co^{II}(alamp)H_2O] e [Co^{II}(promp)H_2O] sono stati impiegati nella riduzione del ferricitocromo *c*. Le velocità specifiche (costanti cinetiche) sono di tre a quattro ordini di grandezza inferiori a quelle osservate nella riduzione con i complessi di ferro(II) corrispondenti, una differenza in maggior parte dovuta a delle entropie d'attivazione più negative. Le specie correlate di cobalto(III) di [Co^{II}(alamp)] sono parzialmente legate alla proteina durante il trasferimento elettronico. Questo conferma che la reazione si è compiuta, almeno in parte, seguendo un meccanismo di sfera interna, usando l'imidazolo dell'istidina 26 o 33 come legante a ponte. Nessun legame covalente dell'unità [Co^{III}(promp)] è stato osservato nelle condizioni di reazione scelte. Mentre la stereoselettività complessiva nella reazione con ambedue i complessi, [Co^{II}(alamp)H_2O] e [Co^{II}(promp)H_2O], è abbastanza debole, quella di [Co^{II}(alamp)H_2O] è piuttosto alta per quanto riguarda la parte della reazione svoltatisi secondo un meccanismo di sfera interna, visto che il rapporto medio k_{RR}/k_{SS} vale 2.9. Siccome la stereoselettività complessiva risulta delle due parti della reazione, quella di sfera interna e quella di sfera esterna,

ambedue i meccanismi di reazione sembrano presentare delle stereoselettività significative ma opposte.

Il nuovo complesso $[Cr^{III}(S,S)\text{-promp})H_2O]^+$ mostra un'attività elettrochimica ad un potenziale di -1.0 V a pH 7 (riferito all'elettrodo a idrogeno standard), probabilmente dovuta alla decomposizione catalitica dell'acqua. L'esistenza a breve durata della specie chirale correlata di Cr^{II} è evidenziata tramite un cambiamento di leganti, collegato ad un trasferimento elettronico. $[Cr^{III}(promp)H_2O]^+$ mostra un'attività catalitica considerabile nella riduzione del ferricitocromo *c* con lo zinco – formando un composto di cromo(II) alla superficie metallica – ma nessuna specie di cromo(III) sembra essere legata alla proteina durante il trasferimento elettronico.

Il nuovo complesso $[Co^{III}(S,S)\text{-b3amp})H_2O]^+$ contiene due cicli chelati d'amminocarbossilato a sei membri. L'esistenza di almeno tre diastereoisomeri, due simmetrici e uno non simmetrico, e l'equilibrio d'isomerizzazione fra due di loro in ambiente alcalino sono stati evidenziati tramite analizzi di spettrofotometria d'assorbimento e di dicroismo circolare (spettropolarimetria). A causa di quest'equilibrio d'isomerizzazione, i complessi con il nuovo legante b3amp sono stati valutati inadatti alle investigazioni delle interazioni stereochimiche collegate alle reazioni di trasferimento elettronico. Per questa ragione, la parte del progetto che implica questo tipo di complessi per il riconoscimento chirale, durante le reazioni di trasferimento elettronico, è stata scartata.

L'impiego combinato della spettrofotometria di assorbimento e di dicroismo circolare si è verificato una volta ancora essere uno strumento potente e sostanziale per l'esplorazione della struttura di complessi otticamente attivi in soluzione nonché per lo studio della cinetica e dei meccanismi di reazione.

CHAPTER 7:
APPENDICES

7.1 Crystallographic data of some transition metal complexes prepared in this work

All crystallographic data has been compiled and resolved by the group of Helen Stoeckli-Evans, Université de Neuchâtel (CH). The images were generated by [1].

7.1.1 Definitions

The atomic coordinates are indicated in fractions of the corresponding unit cell edge. The equivalent isotropic displacement U_{eq} is defined as $\frac{1}{3}$ of the trace of the orthogonalized U_{ij} tensor. It can be interpreted as a mean square amplitude of the vibration of the atom [2].

Uncertainties on the last digit(s) of all values are indicated in parentheses.

In the particular case of the metal complexes, 1W indicates the coordinated water and 2W the water of crystallisation.

7.1.2 Λ-Aqua[2,6- bis[((*S*)-2-carboxypyrrolidin-1-yl)methyl]pyridine]chromium(III) perchlorate ([Cr^{III}((*S*,*S*)-promp)H_2O]ClO_4, (*S*,*S*)-**12**)

Table 7-1. *Crystal data table for* ***12***

Crystal shape:	rod
Crystal colour:	purple
Crystal dimensions:	0.50 mm x 0.30 mm x 0.13 mm
Empirical formula:	$C_{17}H_{23.50}ClCrN_3O_{9.25}$
Molecular formula:	$[C_{17}H_{23}Cr\ N_3O_5]ClO_4 \cdot 0.25H_2O$
Formula weight:	505.34 $g \cdot mol^{-1}$
Density (calculated):	1.661 $g \cdot cm^{-3}$
Linear absorption coeff.:	0.758 mm^{-1}

Table 7-1 (continued)

Temperature:	223(2) K		
Crystal system:	monoclinic		
Space group:	P 2_1		
Unit cell dimensions:	a = 1.19726(12) nm	b = 0.73331(5) nm	c = 1.19787(12) nm
Unit cell angles:	α = 90°	β = 106.081(12)°	γ = 90°
Unit cell volume:	1.01053(16) nm^3		
Atoms per unit cell:	2		

Table 7-2. *Atomic coordinates and U_{eq} values for [Cr^{III}((S,S)-promp)H_2O]ClO_4.*. Relative occupancies for the alternative positions of C(8) and C(14): C(8A) = 0.657, C(8B) = 0.343, C(14A) = 0.491, C(14B) = 0.509.

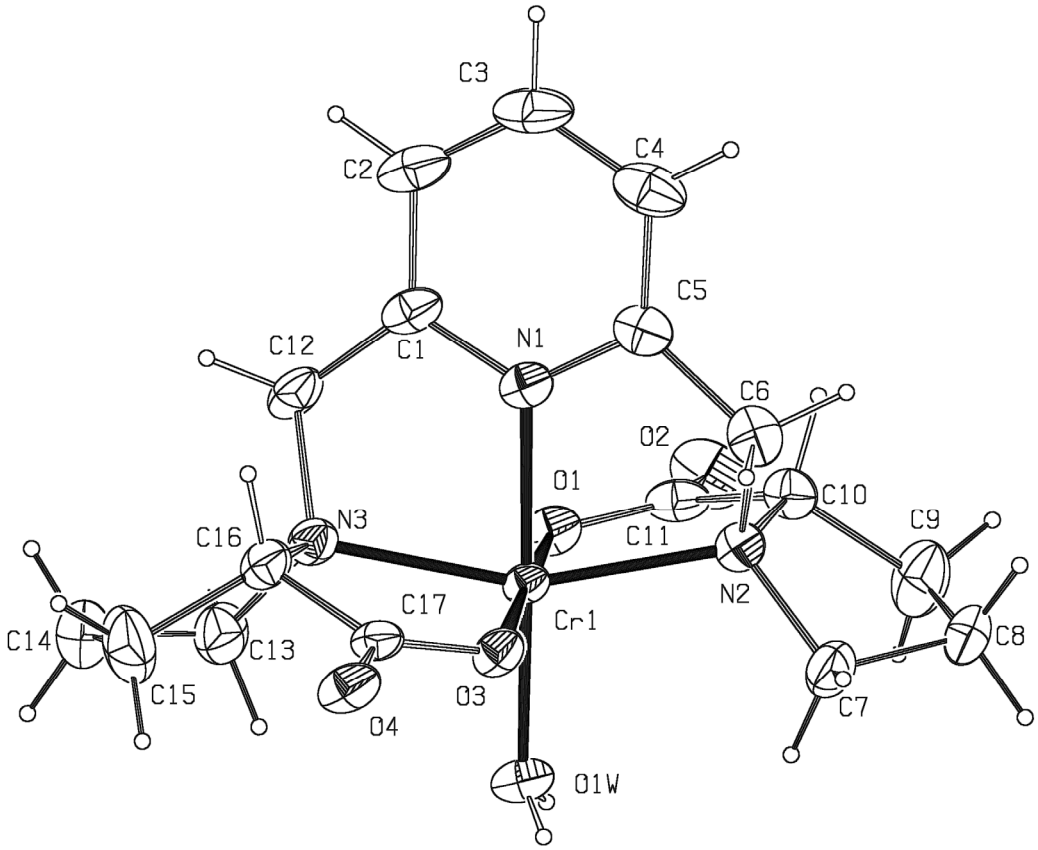

Atom	x / a	y / b	z / c	U_{eq} / pm^2
C(1)	0.9119(2)	1.1332(3)	0.3347(2)	260(10)
C(2)	0.9864(2)	1.1946(4)	0.4383(2)	350(10)
C(3)	0.9439(2)	1.2091(4)	0.5338(2)	410(10)
C(4)	0.8300(2)	1.1623(3)	0.5276(2)	360(10)
C(5)	0.7598(2)	1.0990(3)	0.4228(2)	260(10)

Table 7-2 (continued)

Atom	*x* / *a*	*y* / *b*	*z* / *c*	U_{eq} / pm^2
C(6)	0.6355(2)	1.0391(3)	0.3958(2)	290(10)
C(7)	0.4877(2)	0.8509(4)	0.2583(2)	330(10)
C(8A)	0.4649(3)	0.7051(6)	0.3394(3)	350(10)
C(8B)	0.4710(6)	0.6626(11)	0.2400(8)	430(20)
C(9)	0.5686(2)	0.5808(4)	0.3546(3)	430(10)
C(10)	0.6698(2)	0.7129(3)	0.3608(2)	250(10)
C(11)	0.7594(2)	0.6404(3)	0.3036(2)	260(10)
C(12)	0.9412(2)	1.1033(3)	0.2227(2)	290(10)
C(13)	0.8532(2)	1.0254(4)	0.0166(2)	350(10)
C(14A)	0.7873(5)	1.1490(9)	-0.0796(4)	450(20)
C(14B)	0.8963(5)	1.1794(9)	-0.0408(5)	480(20)
C(15)	0.8137(3)	1.3376(5)	-0.0232(2)	480(10)
C(16)	0.7899(2)	1.2979(3)	0.0937(2)	260(10)
C(17)	0.6620(2)	1.3189(3)	0.0902(2)	220(10)
Cl(1)	0.7309(1)	0.7191(1)	0.7111(1)	370(10)
Cr(1)	0.7056(1)	0.9700(1)	0.1866(1)	180(10)
N(1)	0.8026(1)	1.0855(3)	0.3310(2)	220(10)
N(2)	0.6155(2)	0.8898(2)	0.3057(2)	220(10)
N(3)	0.8314(1)	1.1032(3)	0.1249(1)	230(10)
O(1)	0.7896(1)	0.7445(2)	0.2290(1)	250(10)
O(2)	0.8015(2)	0.4897(3)	0.3316(1)	410(10)
O(3)	0.6144(1)	1.1884(2)	0.1320(1)	230(10)
O(4)	0.6081(1)	1.4574(3)	0.0481(1)	300(10)
O(11)	0.6228(2)	0.7539(4)	0.6280(2)	750(10)
O(12)	0.7718(2)	0.5456(4)	0.6892(3)	780(10)
O(13)	0.7094(4)	0.7203(5)	0.8207(2)	1090(10)
O(14)	0.8096(2)	0.8574(4)	0.7004(4)	1000(10)
O(1W)	0.6141(2)	0.8453(3)	0.0409(1)	270(10)
O(2W)	1.0007(8)	11104(17)	-0.1827(9)	700(30)

Crystal packing: see Fig.4-1b

7.1.3 Δ-Aqua[2,6-bis[(2*S*,3*S*)-3-carboxymethyl-2-azabutyl]pyridine]cobalt(III) perchlorate ($S_C S_C R_N R_N$)-[Co^{III}((*S*,*S*)-b3amp)H_2O]ClO_4, **A1-1**)

Table 7-3. *Crystal data table for **A1-1***

Crystal shape:	rod		
Crystal colour:	red bordeaux		
Crystal dimensions:	0.50 mm x 0.25 mm x 0.20 mm		
Empirical formula:	$C_{15}H_{23}ClCoN_3O_9$		
Formula weight:	483.74 $g \cdot mol^{-1}$		
Density (calculated):	1.747 $g \cdot cm^{-3}$		
Linear absorption coeff.:	1.136 mm^{-1}		
Temperature:	153(2) K		
Crystal system:	monoclinic		
Space group:	P 2_1/n		
Unit cell dimensions:	a = 1.06514(12) nm	b = 0.73305(5) nm	c = 2.3783(3) nm
Unit cell angles:	α = 90°	β = 97.830(13)°	γ = 90°
Unit cell volume:	1.8397(3) nm^3		
Atoms per unit cell:	4		

Table 7-4. *Atomic coordinates and U_{eq} values for* ***A1-1***

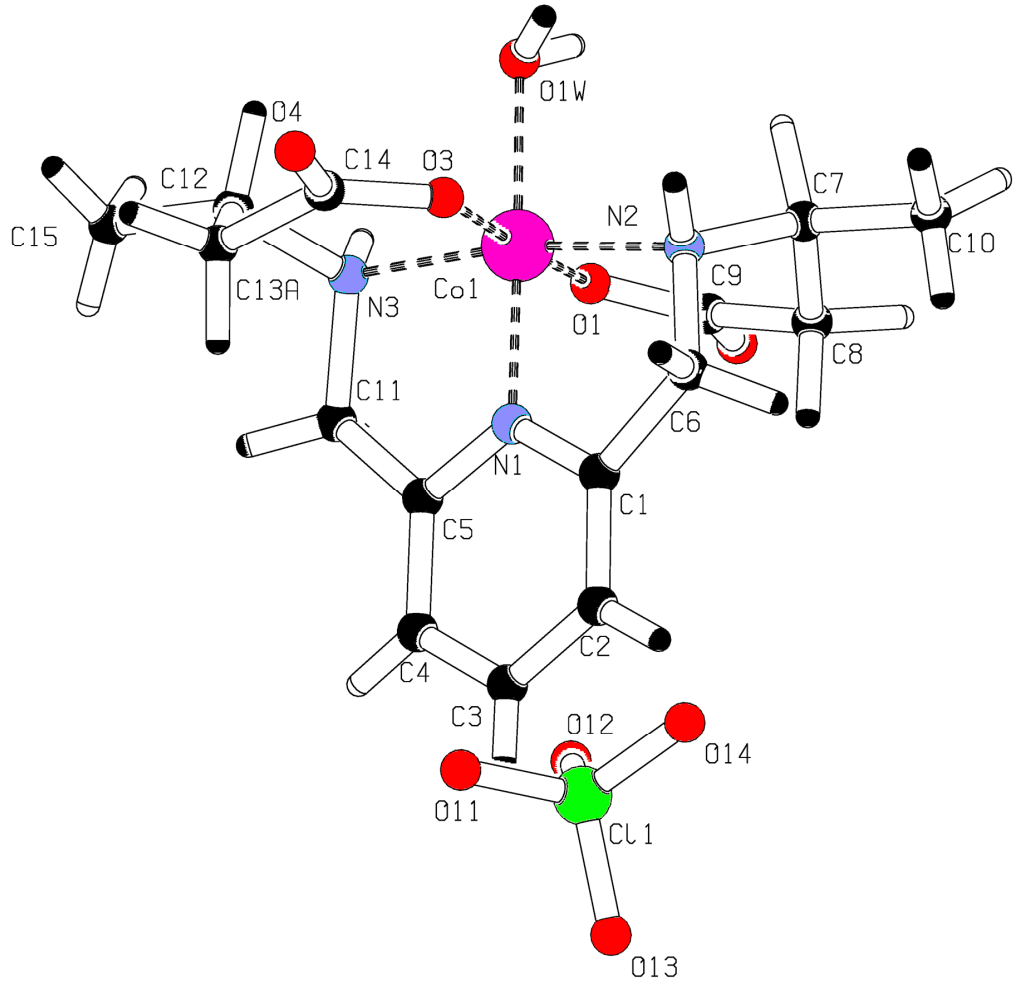

Atom	*x* / *a*	*y* / *b*	*z* / *c*	U_{eq} / pm^2
C(1)	0.5350(5)	0.8073(8)	0.1238(2)	200(10)
C(2)	0.6182(6)	0.7404(9)	0.0897(3)	240(10)
C(3)	0.5773(6)	0.7140(9)	0.0326(3)	270(10)
C(4)	0.4536(6)	0.7508(8)	0.0099(3)	230(10)
C(5)	0.3733(6)	0.8174(8)	0.0459(2)	210(10)
C(6)	0.5589(6)	0.8464(10)	0.1861(3)	250(10)
C(7)	0.4932(7)	1.1618(9)	0.2161(3)	320(10)
C(8)	0.5165(7)	1.2568(10)	0.1626(3)	380(10)
C(9)	0.4017(7)	1.2898(8)	0.1194(2)	280(10)
C(10)	0.6071(9)	1.1781(13)	0.2633(4)	470(10)
C(11)	0.2367(6)	0.8687(10)	0.0299(3)	270(10)
C(12)	0.0792(7)	0.7488(10)	0.0930(3)	390(10)
C(13A)	0.1400(7)	0.5758(10)	0.1112(3)	150(10)
C(13B)	0.0810(20)	0.6590(40)	0.1386(9)	310(10)

Table 7-4 (continued)

Atom	*x* / *a*	*y* / *b*	*z* / *c*	U_{eq} / pm^2
C(14)	0.2156(6)	0.5798(8)	0.1704(2)	230(10)
C(15)	-0.0278(7)	0.7319(11)	0.0440(3)	320(10)
Cl(1)	0.8741(1)	0.2057(2)	0.1294(1)	230(10)
Co(1)	0.3054(1)	0.9386(1)	0.1468(1)	160(10)
N(1)	0.4154(4)	0.8437(6)	0.1008(2)	150(10)
N(2)	0.4571(4)	0.9655(7)	0.2036(2)	200(10)
N(3)	0.1725(5)	0.8908(7)	0.0822(2)	210(10)
O(1)	0.3157(4)	1.1675(6)	0.1118(2)	240(10)
O(2)	0.3964(5)	1.4274(6)	0.0902(2)	340(10)
O(3)	0.2882(3)	0.7125(5)	0.1845(1)	170(10)
O(4)	0.2154(4)	0.4433(6)	0.2024(2)	250(10)
O(11)	0.8004(6)	0.0432(8)	0.1273(3)	670(10)
O(12)	0.7972(5)	0.3528(8)	0.1060(2)	500(10)
O(13)	0.9754(4)	0.1790(7)	0.0959(2)	330(10)
O(14)	0.9249(6)	0.2451(9)	0.1860(2)	600(10)
O(1W)	0.1857(4)	1.0404(6)	0.1930(2)	220(10)

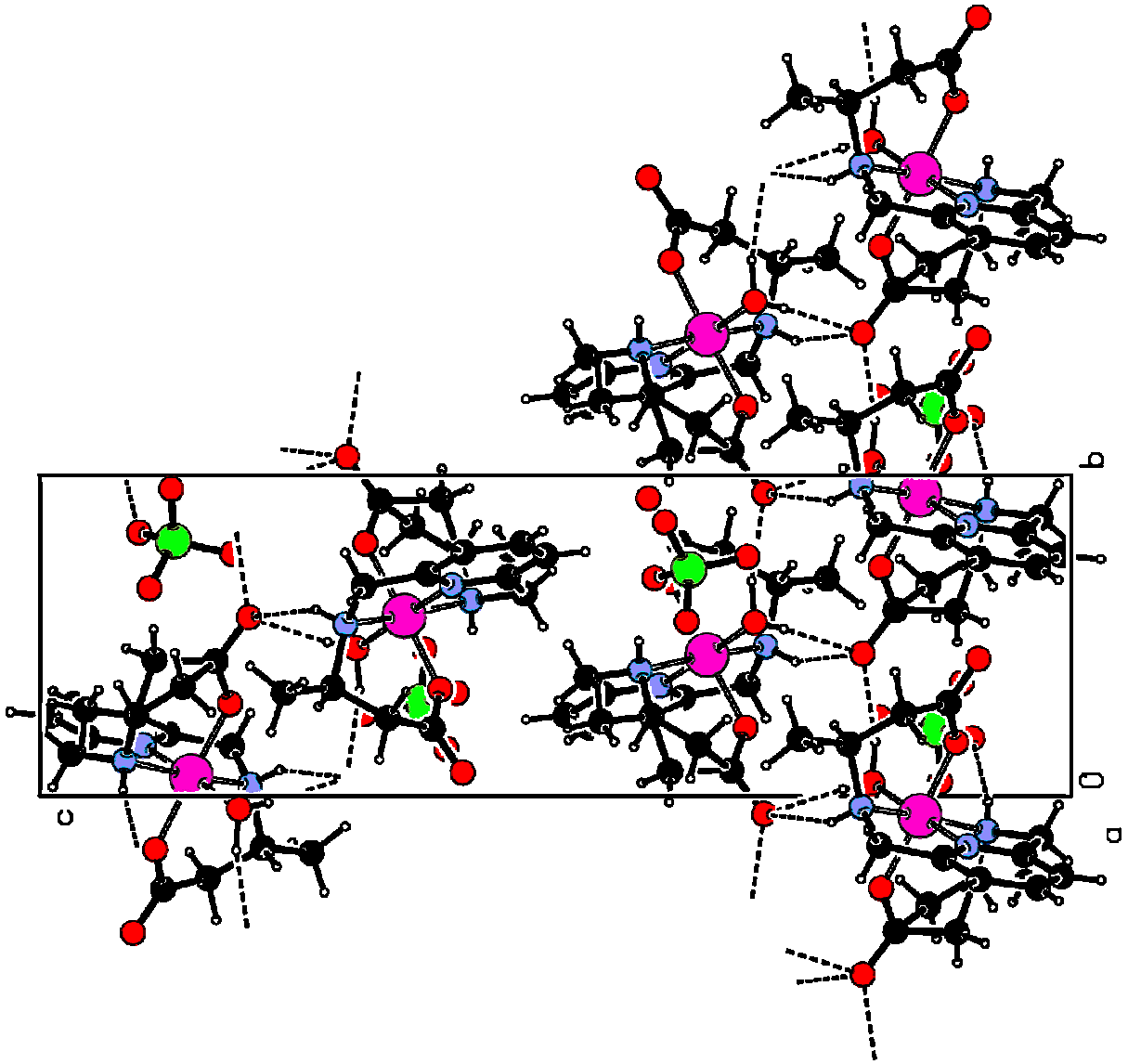

Fig. 7-1. *Crystal packing of* ***A1-1***

7.1.4 2-((3*R*)-*N*-(2'-(6'-((3"*R*)-3"-carboxymethyl-2"-azabutyl)pyridyl)methyl)-3-carboxymethyl-2-azabutyl)-6-((3*R*)-3-carboxymethyl-2-azabutyl)pyridine cobalt(III) ((*R*,*R*,*R*)-**25**))

Table 7-5. *Crystal data table for* ***25***

Crystal shape:	block
Crystal colour:	dark red
Crystal dimensions:	0.50 mm x 0.50 mm x 0.30 mm
Empirical formula:	$C_{24}H_{32}ClCoN_5O_8 \cdot 1.5\ H_2O$

Table 7-5 (continued)

Formula weight:	639.95 g·mol^{-1}		
Density (calculated):	1.621 g·cm^{-3}		
Linear absorption coeff.:	0.823 mm^{-1}		
Temperature:	153(2) K		
Crystal system:	monoclinic		
Space group:	P 2_1/n		
Unit cell dimensions:	a = 0.80067(5) nm	b = 2.79560(16) nm	c = 11.7563(8) nm
Unit cell angles:	α = 90°	β = 97.830(13)°	γ = 90°
Unit cell volume:	2.6215(3) nm^3		
Atoms per unit cell:	4		

Table 7-6. *Atomic coordinates and U_{eq} values for* ***25****. H on N2 is not represented but required to meet electroneutrality.*

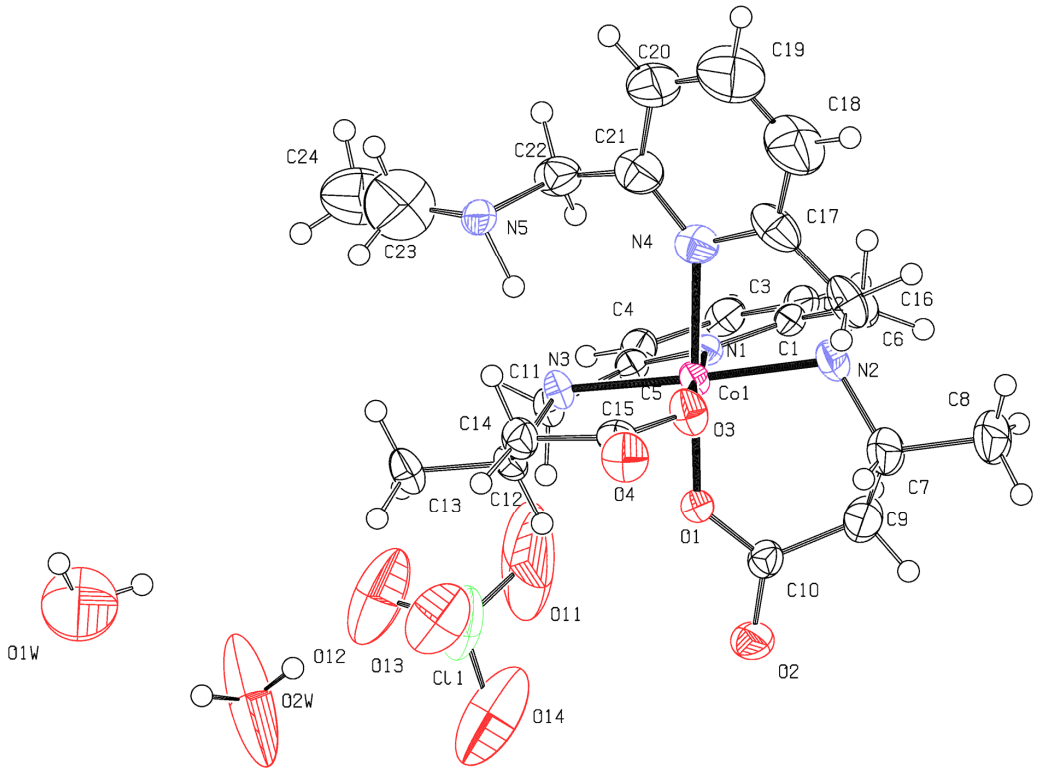

Atom	x / a	y / b	z / c	U_{eq} / pm^2
C(1)	0.1276(5)	0.3563(2)	0.1754(4)	270(10)
C(2)	-0.0233(5)	0.3327(2)	0.1527(4)	320(10)
C(3)	-0.0527(5)	0.2917(2)	0.2140(4)	320(10)
C(4)	0.0684(5)	0.2740(2)	0.2960(4)	300(10)

Table 7-6 (continued)

Atom	*x* / *a*	*y* / *b*	*z* / *c*	U_{eq} / pm^2
C(5)	0.2182(5)	0.2981(1)	0.3132(4)	250(10)
C(6)	0.1813(6)	0.4015(2)	0.1222(4)	340(10)
C(7)	0.4623(7)	0.3948(2)	0.0369(5)	480(10)
C(8)	0.4079(8)	0.4261(2)	-0.0669(5)	560(20)
C(9)	0.4452(7)	0.3432(2)	0.0078(4)	450(10)
C(10)	0.5366(5)	0.3088(2)	0.0897(4)	290(10)
C(11)	0.3707(5)	0.2830(2)	0.3888(4)	270(10)
C(12)	0.6664(5)	0.3099(2)	0.4316(4)	290(10)
C(13)	0.6881(6)	0.2751(2)	0.5316(4)	380(10)
C(14)	0.7751(6)	0.3539(2)	0.4566(4)	330(10)
C(15)	0.7871(5)	0.3906(2)	0.3630(4)	300(10)
C(16)	0.4147(7)	0.4570(2)	0.1752(5)	440(10)
C(17)	0.3676(7)	0.4644(2)	0.2928(5)	460(10)
C(18)	0.3317(10)	0.5096(2)	0.3282(7)	770(20)
C(19)	0.2757(13)	0.5152(3)	0.4332(8)	930(30)
C(20)	0.2520(9)	0.4766(2)	0.4985(6)	620(20)
C(21)	0.2874(7)	0.4305(2)	0.4562(5)	450(10)
C(22)	0.2412(6)	0.3887(2)	0.5260(5)	420(10)
C(23)	0.3359(15)	0.3412(4)	0.6772(10)	1190(40)
C(24)	0.2115(11)	0.3016(3)	0.7048(9)	910(30)
Cl(1)	0.3848(2)	0.1311(1)	0.3215(2)	770(10)
Co(1)	0.4478(1)	0.3682(1)	0.2768(1)	230(10)
N(1)	0.2423(4)	0.3385(1)	0.2541(3)	230(10)
N(2)	0.3706(5)	0.4070(1)	0.1408(3)	320(10)
N(3)	0.4870(4)	0.3250(1)	0.4089(3)	250(10)
N(4)	0.3550(5)	0.4244(1)	0.3570(3)	340(10)
N(5)	0.3852(5)	0.3732(1)	0.5971(3)	320(10)
O(1)	0.5408(4)	0.3176(1)	0.1962(3)	320(10)
O(2)	0.5961(4)	0.2718(1)	0.0534(3)	410(10)
O(3)	0.6602(4)	0.3988(1)	0.2908(3)	350(10)
O(4)	0.9181(4)	0.4139(1)	0.3608(3)	420(10)
O(11)	0.2491(11)	0.1563(7)	0.2801(8)	2620(90)
O(12)	0.3267(9)	0.1036(3)	0.4140(5)	1230(30)
O(13)	0.5222(8)	0.1588(2)	0.3698(5)	920(20)
O(14)	0.4405(10)	0.1011(3)	0.2335(5)	1300(30)
O(1W)	0.3720(11)	0.0079(2)	0.7119(6)	1240(30)
O(2W)	0.3890(30)	0.0151(4)	0.4760(14)	1870(110)

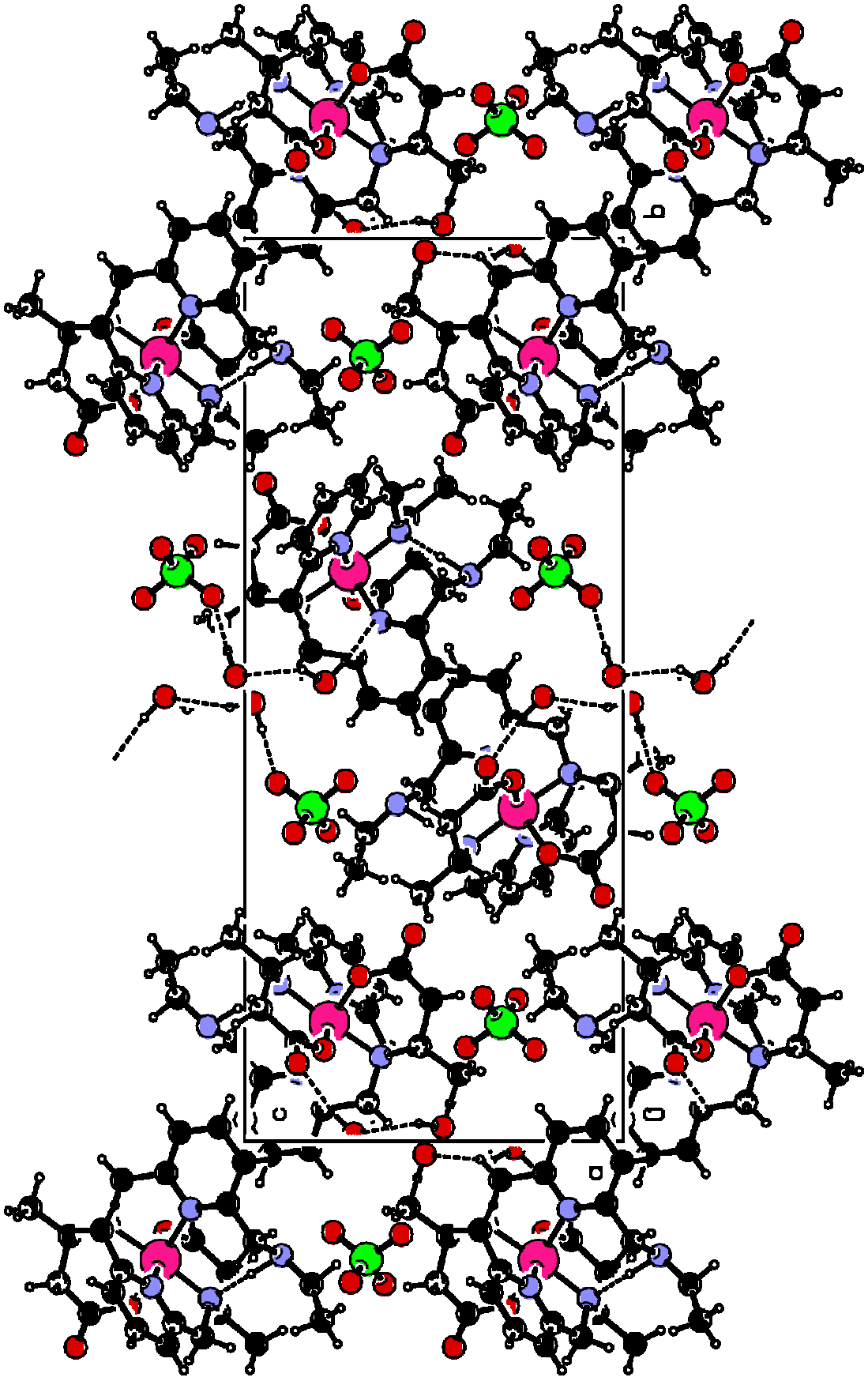

Fig. 7-2. *Crystal packing of* ***25***

7.1.5 (2*S*,3*R*,11*R*)-3,11,17,18-tetraaza-3,11-bis[(*R*)-1-methylcarboxyethyl]-2-methyltricyclo[11.3.1.1^{5,9}]octadeca-5,7,9(18),13(17),14,16-hexaene cobalt(III) perchlorate hydrate (**26**)

Table 7-7. *Crystal data table for* ***26***

Crystal shape:	rod		
Crystal colour:	red		
Crystal dimensions:	0.30 mm x 0.15 mm x 0.10 mm		
Empirical formula:	$C_{23}H_{30}Cl_2CoN_4NaO_{13}$		
Molecular formula:	$[C_{23}H_{28}CoN_4]ClO_4 \cdot H_2O \cdot NaClO_4$		
Formula weight:	723.33 g·mol^{-1}		
Density (calculated):	1.716 g·cm^{-3}		
Linear absorption coeff.:	0.895 mm^{-1}		
Temperature:	293(2) K		
Crystal system:	triclinic		
Space group:	P -1		
Unit cell dimensions:	a = 1.14627(14) nm	b = 1.15406(14) nm	c = 1.16207(14) nm
Unit cell angles:	α = 81.608(14)°	β = 83.094(15)°	γ = 67.372(13)°
Unit cell volume:	1.4003(3) nm^3		
Atoms per unit cell:	2		

Table 7-8. *Atomic coordinates and U_{eq} values of* ***26***

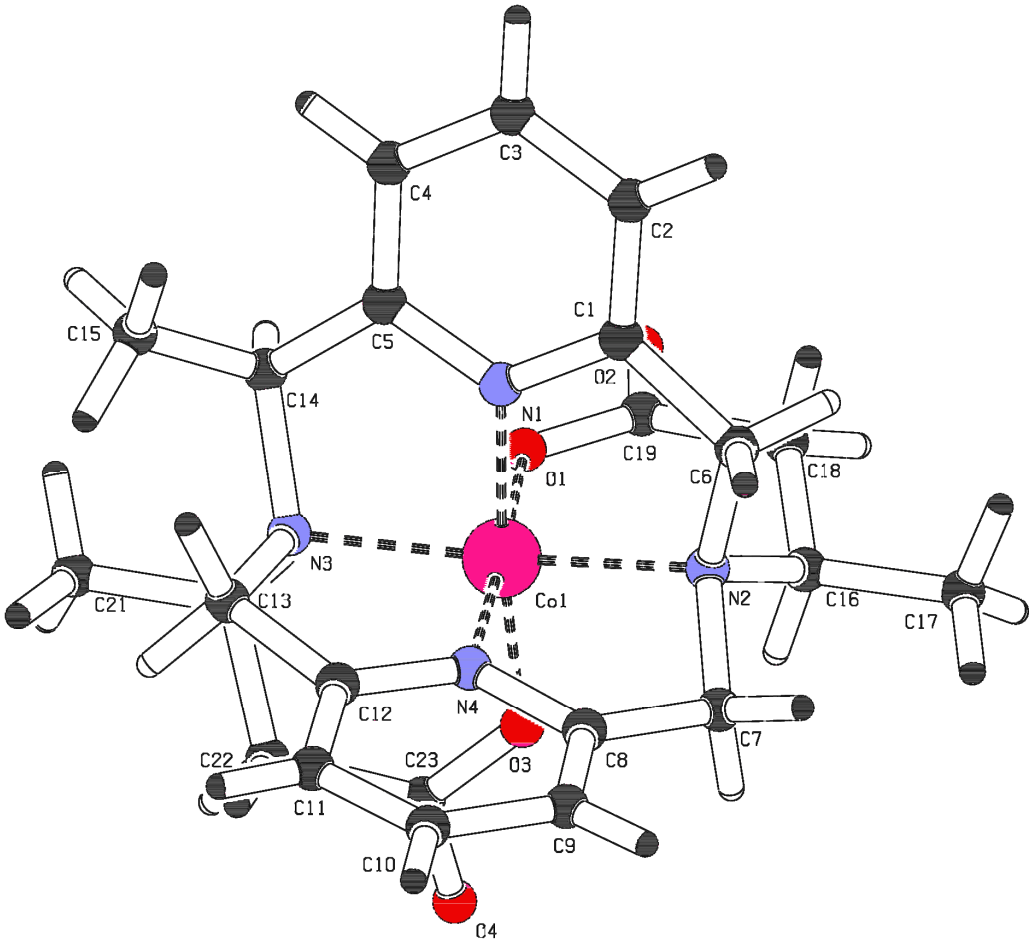

Atom	*x* / *a*	*y* / *b*	*z* / *c*	U_{eq} / pm^2
C(1)	0.9479(5)	0.8716(5)	0.7551(5)	460(10)
C(2)	1.0268(6)	0.9141(6)	0.8023(5)	590(20)
C(3)	1.0465(6)	0.8813(6)	0.9185(6)	660(20)
C(4)	0.9879(6)	0.8099(6)	0.9867(5)	620(20)
C(5)	0.9104(5)	0.7673(5)	0.9357(5)	520(10)
C(6)	0.9163(5)	0.8962(5)	0.6314(5)	510(10)
C(7)	0.7375(5)	0.8783(5)	0.5467(4)	410(10)
C(8)	0.6373(5)	0.9299(5)	0.6407(4)	380(10)
C(9)	0.5294(5)	1.0348(5)	0.6325(4)	430(10)
C(10)	0.4401(5)	1.0588(5)	0.7277(5)	490(10)
C(11)	0.4638(5)	0.9766(5)	0.8292(5)	450(10)
C(12)	0.5778(5)	0.8780(5)	0.8357(4)	380(10)
C(13)	0.6256(5)	0.7862(5)	0.9421(4)	500(10)

Table 7-8 (continued)

Atom	*x* / *a*	*y* / *b*	*z* / *c*	U_{eq} / pm^2
C(14)	0.8496(5)	0.6777(5)	0.9928(4)	510(10)
C(15)	0.7982(4)	0.7131(4)	1.1041(3)	270(10)
C(16)	0.9504(5)	0.7087(5)	0.5248(4)	500(10)
C(17)	0.9824(6)	0.7662(6)	0.4041(5)	660(20)
C(18)	1.0673(6)	0.6253(6)	0.5807(5)	630(20)
C(19)	1.0584(6)	0.5390(6)	0.6920(4)	480(10)
C(20)	0.7335(6)	0.5546(6)	0.9252(4)	550(20)
C(21)	0.7001(7)	0.5048(7)	1.0476(5)	830(20)
C(22)	0.6408(6)	0.5564(6)	0.8398(4)	610(20)
C(23)	0.6849(5)	0.5609(5)	0.7114(4)	460(10)
Cl(1)	0.3367(2)	0.7455(2)	0.6292(1)	610(10)
Cl(2)	0.6942(2)	1.1824(1)	0.0060(1)	600(10)
Co(1)	0.8126(1)	0.7190(1)	0.7522(1)	350(10)
N(1)	0.8936(4)	0.8000(4)	08221(3).	420(10)
N(2)	0.8620(4)	0.8044(4)	0.6025(3)	360(10)
N(3)	0.7477(4)	0.6812(4)	0.9149(3)	410(10)
N(4)	0.6606(4)	0.8557(4)	0.7436(3)	340(10)
Na(1)	0.5471(3)	0.3789(2)	0.6338(2)	730(10)
O(1)	0.9635(3)	0.5737(3)	0.7669(3)	430(10)
O(2)	1.1494(4)	0.4391(4)	0.7111(3)	710(10)
O(3)	0.7490(3)	0.6293(3)	0.6700(3)	390(10)
O(4)	0.6572(4)	0.5012(4)	0.6472(3)	610(10)
O(11)	0.3808(5)	0.6375(5)	0.5645(5)	1030(20)
O(12)	0.4369(5)	0.7887(5)	0.6307(5)	910(20)
O(13)	0.2333(5)	0.8416(5)	0.5746(5)	1110(20)
O(14)	0.2983(6	0.7052(6)	0.7399(4)	1270(20)
O(21)	0.7236(7)	1.1618(6)	0.7153(5)	1030(20)
O(22)	0.5704(5)	1.2741(5)	0.8343(5)	910(20)
O(23)	0.7000(5)	1.0654(4)	0.9013(4)	1110(20)
O(24A)	0.7922(7)	1.0654(4)	0.8548(8)	1270(20)
O(24B)	0.6740(30)	1.2421(17)	0.9530(20)	1270(20)
O(1W)	0.6247(3)	0.6528(4)	0.4179(3)	560(10)

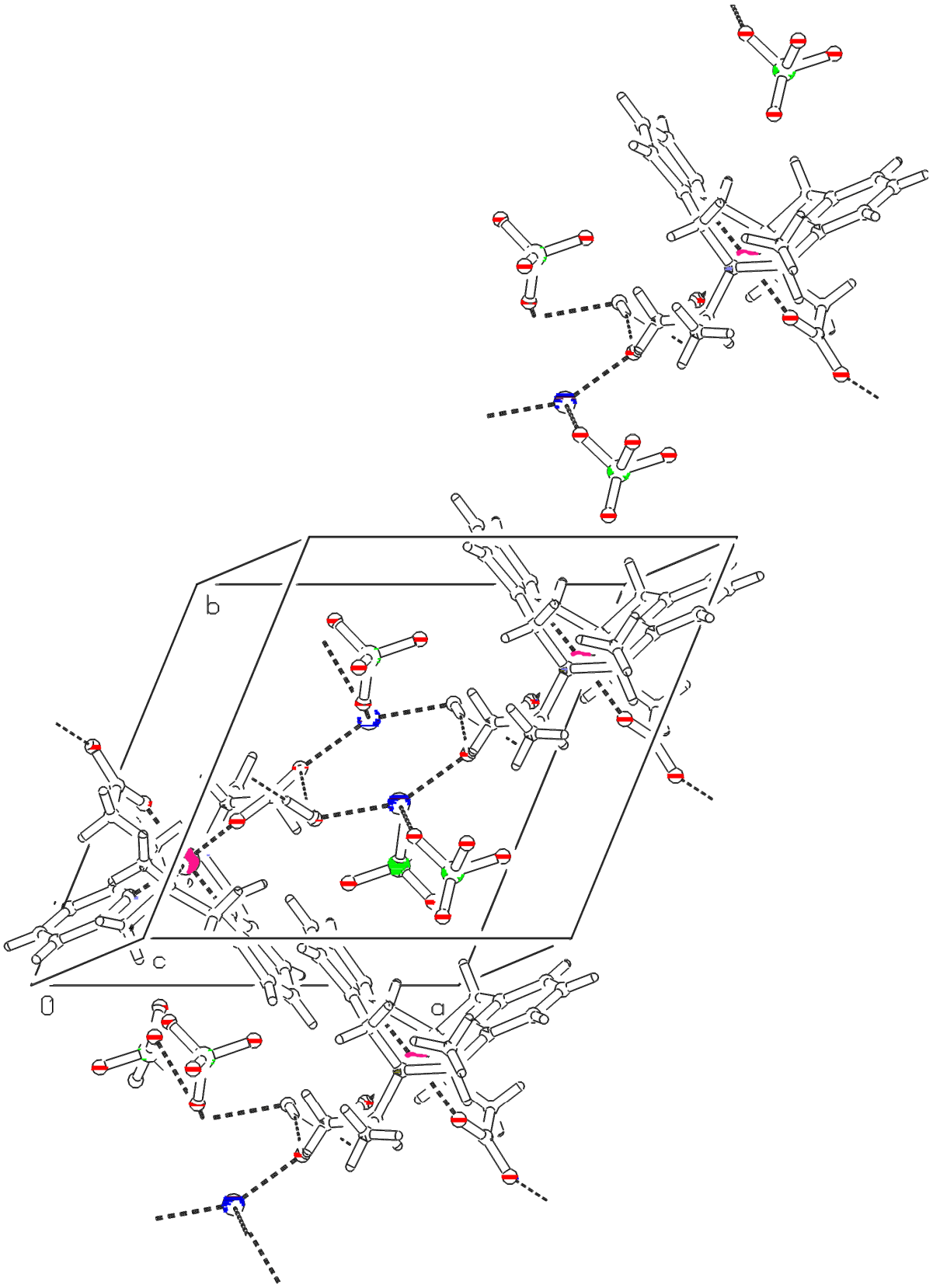

Fig. 7-3. Crystal packing of 26

7.2 Equilibrium constants of different compounds used in the present work

Table 7-9. *Acid-dissociation constants (pK_a) at 25°C and* I = *0.1.*

Compound	pK_{a1}	pK_{a2}	pK_{a3}	pK_{a4}	References
H_4cdta	2.56±0.02	3.53±0.01	6.09±0.01	12.30	[3]
H_2alamp	8.23±0.02	9.02±0.02	–	–	[4]
H_2promp	9.33±0.03	10.02±0.04	–	–	[5]
$[Cr^{III}(promp)H_2O]^+$	6.95±0.02	–	–	–	This work

Table 7-10. *Complex-formation constants (log* K_{ML}*) at 25°C and* I = *0.1.*

Ligand (L)	$Co^{II}L$	$Cr^{III}L$	$Zn^{II}L$	References
$cdta^{4-}$	18.92±0.06	22	18.67±0.06	[6][7]
$alamp^{2-}$	11.70±0.03		20.0±0.1	[4][8]
$promp^{2-}$	15.01±0.07			[5]

7.3 Nomenclature rules for pluricycles

According to [9]

During the synthesis of Co^{III} complexes with ligands based on a β-amino-acid, unsymmetrical pluricyclic systems were formed (see chapter 2). So, it is useful to report the method of naming them. We illustrate these rules by two examples, the first of which stems from this thesis.

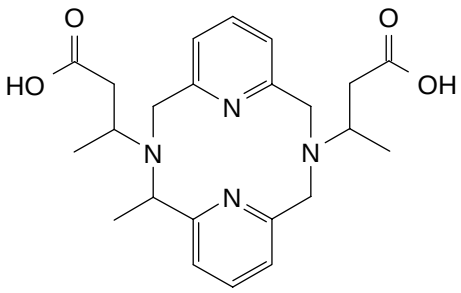

Example 1

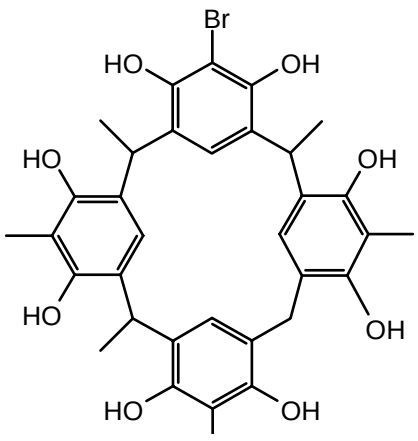

Example 2

1. Find the total number of cycles and the total number of atoms participating in the cycle system.

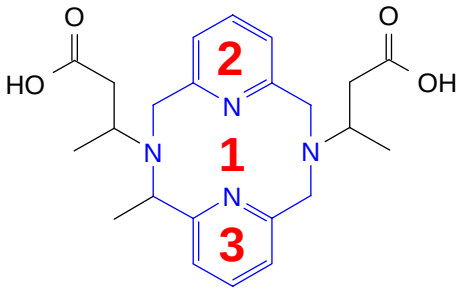

18 cycle atoms

Example 1

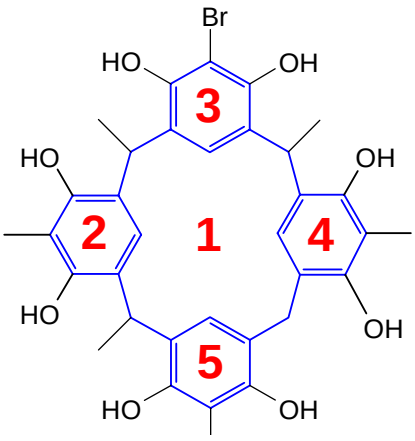

28 cycle atoms

Example 2

2. **Number the atoms** of the "large outer cycle" in such way that the atom number 1 is a bridged atom and that the heteroatoms and /or substituted atoms get the lowest possible numbers.

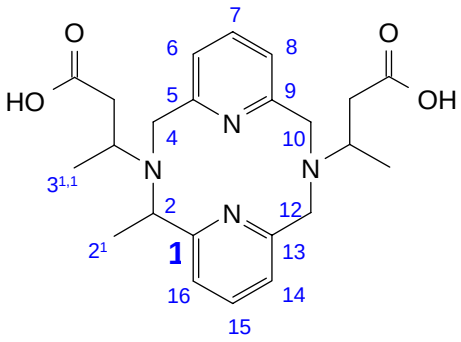

Example 1

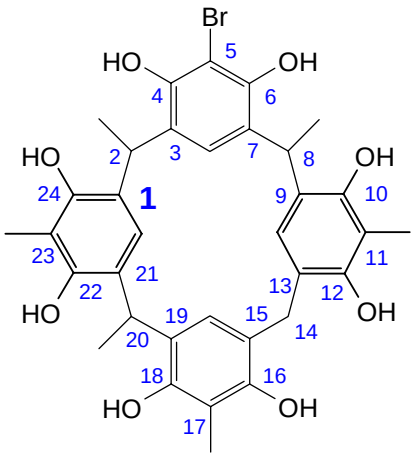

Example 2

3. **Number the atoms that are bridging** two atoms of the "large outer cycle". The nearest atom to atom 1 gets the lowest number.

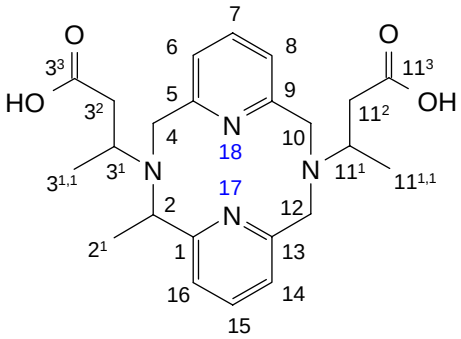

Example 1

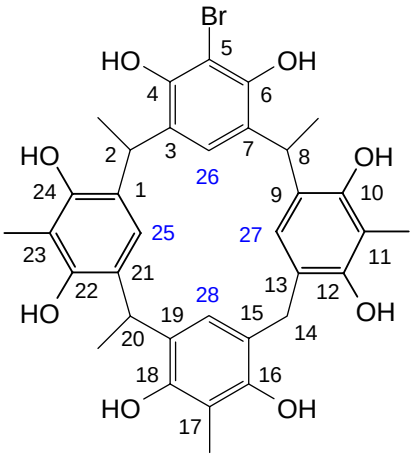

Example 2

4. Count the **number of atoms that link the first to the last bridged atom** of the large outer cycle.

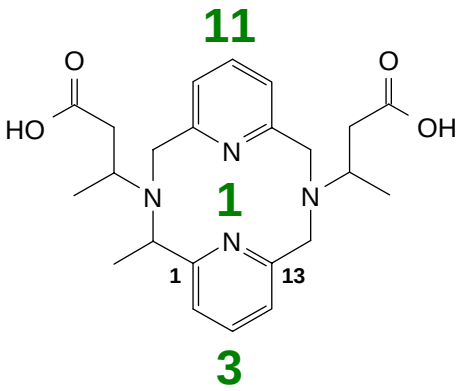

Example 1

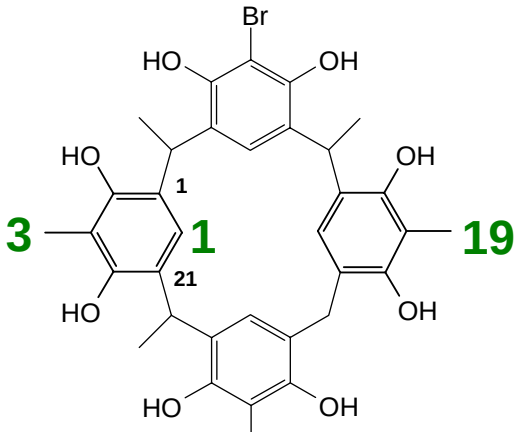

Example 2

5. Count the **number of bridging atoms that are not linked directly to the first or to the last bridged atom** of the large outer cycle. Indicate the **number of the bridged atoms** in superscript.

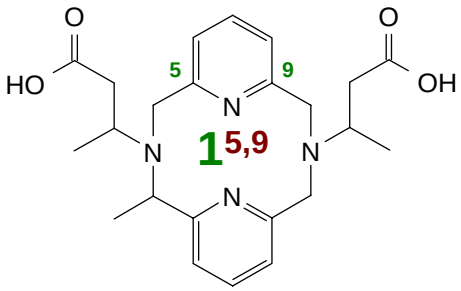

Example 1

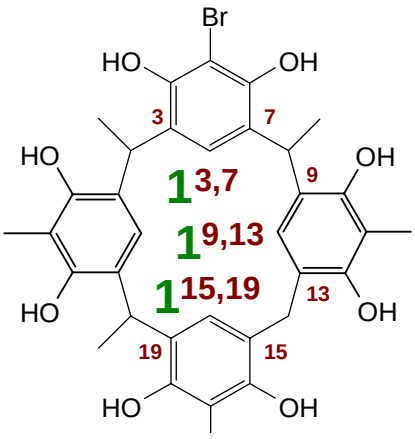

Example 2

6. The global name of the compound is based on the **number of cycles** and the **total number of all atoms** in the cycle system and the. The **bridge lengths** and **positions** are indicated in square brackets. The **heteroatoms**, **multiple bonds** and **substituents** and are mentioned according to the classic rules and the numbering mentioned above. If a double bond is not contained in the cycle, the **number of the second atom participating in the double bond** is added in round brackets:

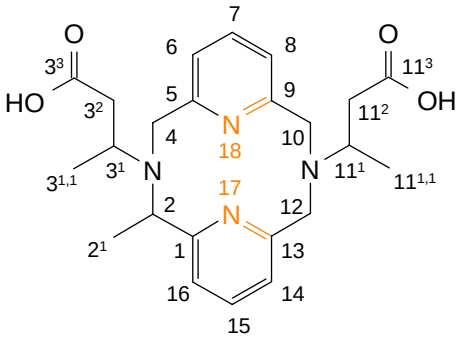

Example 1:

3,11,17,18-tetraaza-3,11-bis[1-methylcarboxyethyl]-2-methyltricyclo[11.3.1.1^{5,9}]octadeca-5,7,9(18),13(17),14,16-hexaene

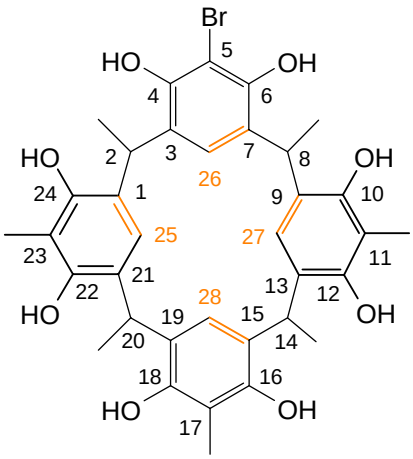

Example 2:

5-bromo-2,8,11,17,20,23-hexamethyl pentacyclo[19.3.1.1^{3,7}.1^{9,13}.1^{15,19}]octacosa-1(25),3,5,7(26),9,11,13(27),15,17,19(28),21,23-dodecaene-4,6,10,12,16,22,24-octol

7.4 CPK colour scheme

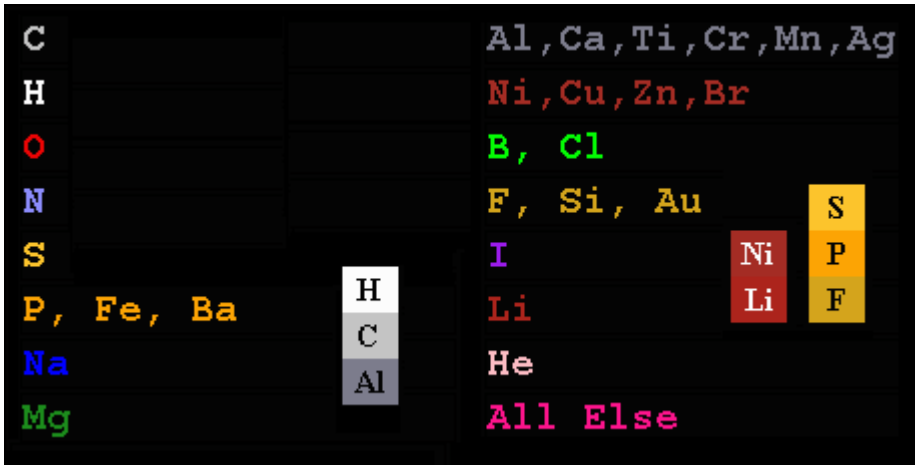

Fig. 7-4. *CPK colour scheme used for images generated by [10] and [11]*

7.5 Introduction to chiroptical methods

Based on [12]

Light is composed by an electric field vector and a magnetic field vector that form a right angle. The moduli and orientations of both vectors vary as a function of time, depending on the light wavelength, propagation rate in the considered medium and intensity. On Fig. 7-5a, we consider only the electric field vector $\vec{E}$. In non-polarised light, the directions of $\vec{E}$ are ran

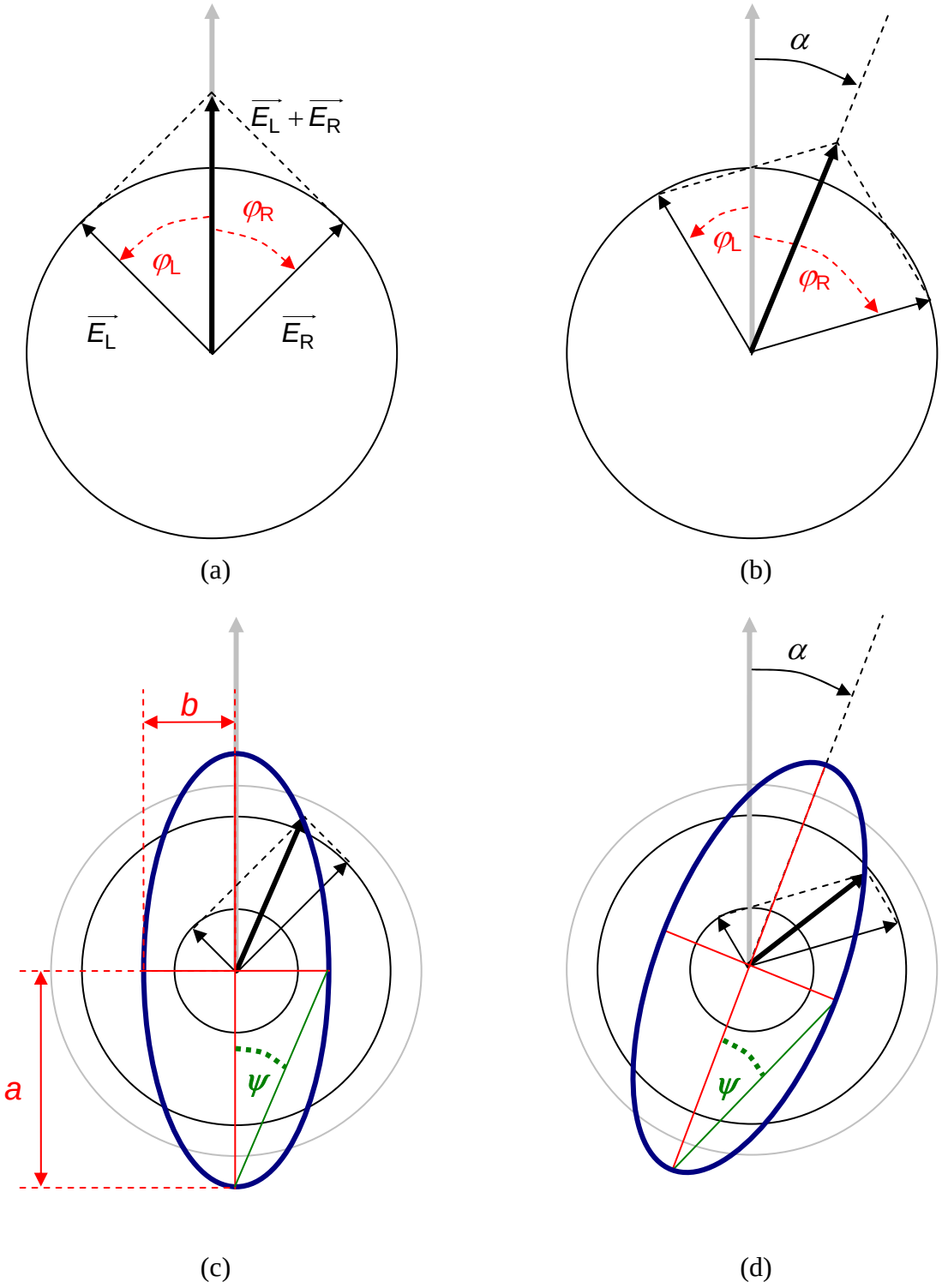

Fig. 7-5. *Modification of the electric field vectors of (initially) linear polarised monochromatic light with time after having passed through a medium.* The initial resultants are traced in grey. Four cases are considered:

a) *The medium is achiral ($\omega_L = \omega_R$) and does not absorb the light of the given wavelength.*

b) *The medium is chiral and does not absorb the light of the given wavelength.* In this case, $\omega_L < \omega_R$.

c) *The medium is chiral and light absorbing but its [α] = 0 at the given wavelength ($\omega_L = \omega_R$).*

d) *The medium is chiral and light absorbing at the given wavelength ($\omega_L < \omega_R$).*

domly distributed whereas in linearly polarised light all $\vec{E}$ vectors are oriented in parallel to one axis. This axis and the propagation axis form the *polarisation plane*. Linearly polarised light can be regarded as the superposition of two circularly polarised components $\overrightarrow{E_L}$ and $\overrightarrow{E_R}$ (called left hand and right hand polarised components) whose moduli are equal and whose resultant is contained in the polarisation plane. These components are counter-rotating at equal angular rates ω_L and ω_R.

After passing through an achiral non-absorbing medium, both angular rates vary in the same way so that, after a certain time *t*, the angle $\varphi_L(t) = \omega_L \cdot t$ is exactly the opposite of $\varphi_R(t)$ and the corresponding polarisation plane remains unchanged (Fig. 7-5a).

In the case of an achiral and absorbing medium, $\left\|\overrightarrow{E_L}\right\|$ and $\left\|\overrightarrow{E_R}\right\|$ decrease equally, depending on the molar absorption coefficient ε which is the same for both components.

When a linear polarized light beam passes through an optically active (chiral and enantiomerically enriched) but non absorbing medium (Fig. 7-5b) it becomes *plane polarized*: ω_L and ω_R vary differently so that $\varphi_L(t) \neq -\varphi_R(t)$ and the polarization plane is deviated by an angle α, called optical rotation. The normalized values *molar rotation*, $[\alpha_m]$, and *specific rotation* $[\alpha]$ are defined analogously to Beer-Lambert's law:

$$[\alpha_m]_\lambda^\theta = \frac{\alpha}{c \cdot d}$$

$$[\alpha]_\lambda^\theta = \frac{\alpha}{c' \cdot d} = \frac{100 \cdot \alpha}{w \cdot d} = [\alpha_m]_\lambda^\theta \cdot M$$

c = molar concentration [mol·L^{-1}][1]), c' = mass concentration [kg·L^{-1}][1]), w = weight percentage [g·(100 mL)$^{-1}$], d = optical path length [**dm**], M = molar mass [g·mol^{-1}], θ = relative temperature [°C][2]), λ = wavelength [nm].

[1]) The non IUPAC units dag·cm^{-3} (= 10 g·cm^{-3}) and dmol·cm^{-3} are still widely used for the concentration; in this way, different values and calculation modes are obtained for $[\alpha_m]$, $[\alpha]$ and $[\theta]$.

The variation of the rotation towards the wavelength of the incident light is called optical rotary dispersion (ORD). For a non-absorbing substance the absolute values of $[\alpha]_\lambda$ decrease asymptotically with increasing λ (normal ORD) according to the relation:

$$\alpha = 180 \cdot \frac{d}{\lambda} \cdot \left(n_{\mathrm{L}} - n_{\mathrm{R}} \right)$$

n = refractive index of the circular polarized light components; d and λ have identical units.

If the medium is optically active and, in addition, absorbs light at the considered wavelength, the left- and right-hand polarized components are absorbed with different molar absorption coefficients. The difference of both is called *molar circular dichroic absorption coefficient* $\Delta\varepsilon$:

$$\Delta\varepsilon = \varepsilon_{\mathrm{L}} - \varepsilon_{\mathrm{R}} = \frac{A_{\mathrm{L}} - A_{\mathrm{R}}}{c \cdot l}$$

l = optical path length [**cm**]

The radiant power and thus the moduli of the electric field vectors of the emergent light beam become different for the $\overrightarrow{E_{\mathrm{L}}}$ and $\overrightarrow{E_{\mathrm{R}}}$ components (see Fig. 7-5c and d). Furthermore, the polarisation of the emergent beam is no more planar but elliptic. Indeed, the moving end of the resultant does not describe any more a line as a function of time (as for linear and plane polarized light) but an ellipse, characterised by a major axis of length 2a

$$a = \left\| \overrightarrow{E_{\mathrm{L}}} \right\| + \left\| \overrightarrow{E_{\mathrm{R}}} \right\|$$

and a minor axis of length 2b

$$b = \left\| \overrightarrow{E_{\mathrm{L}}} \right\| - \left\| \overrightarrow{E_{\mathrm{R}}} \right\|$$

---

[2]) For traditional reasons, temperature is still indicated in °C, which leads to a double use of the letter θ for relative temperature and molar ellipticity.

The average position of the polarisation plane contains the main axis of the ellipse; the angle it forms with the initial polarisation plane is the rotation α (Fig. 7-5d).

Ellipticity (ψ) is the smallest angle formed between the major axis and a secant of the ellipsis that links two vertices that are located respectively on the major and the minor axis:

$$\psi = \arctan\left(\frac{b}{a}\right)$$

This relation is true when the arc secant is nearly equal to the arc length i.e. for small angles. Indeed, the numerical values of ψ are in general very small (the ellipsis on Fig. 7-5c would appear as line when using real numerical values), for this reason ψ is mainly given in m°:

$$\psi[\mathrm{m°}] = \frac{360 \cdot 10^3\,\mathrm{m°}}{2\pi} \cdot \arctan\left(\frac{b}{a}\right)$$

Ellipticity is directly proportional to the circular dichroic absorption:

$$\psi[\mathrm{m°}] = \frac{360 \cdot 10^3\,\mathrm{m°}}{2\pi} \cdot \frac{\ln 10}{4} \cdot \left(A_L - A_R\right) = 33000\,\mathrm{m°} \cdot \left(A_L - A_R\right)$$

Molar ellipticity [θ] in is defined as:

$$\left[\theta\right]_\lambda^\theta = \frac{\psi}{c \cdot l}$$

The ambiguous term "circular dichroism" for a measured value may either designate the ellipticity ψ or the absorption difference A_L - A_R.

The α vs. λ plot of a *single* chiral chromophore gives raise to a so called anomalous ORD. The sign of the first derivative of the anomalous ORD spectrum - the so called *Cotton effect* - is equal to sign of the CD signal at the same wavelength. It provides information about configurational similarities. A zero angle point on the anomalous ORD spectrum corresponds to an extremum on the CD spectrum and to a maximum on the normal absorption spectrum. The entire ORD, spectrum is a sum of all normal and anomalous ORD signals provided by the chiral centres of the molecule.

7.6 Processing methods of the kinetic data

7.6.1 The initial rate method [13]

The kinetic law of a first-order transformation A → B is expressed by

$$v = -\frac{d[\mathrm{A}]}{dt} = +\frac{d[\mathrm{B}]}{dt} = k[\mathrm{A}]$$

As shown on *Fig. 7-6*, the tangent to the [A] towards time plot in the initial point crosses the abscissa (or the asymptote of the curve $[A]_\infty$ if the transformation is reversible) at t_0. t_0 is the theoretical time the reaction would take to complete if its rate remained equal to the initial rate v_0 during the whole transformation. Since the slope of the tangent is equal to v_0, the first order constant k can be easily determined:

$$k = \frac{v_0}{[\mathrm{A}]_0} = \frac{1}{[\mathrm{A}]_0} \cdot \left(-\frac{\Delta[\mathrm{A}]}{\Delta t} \right) = \frac{1}{[\mathrm{A}]_0} \cdot \left(-\frac{0 - [\mathrm{A}]_0}{t_0} \right) = \frac{1}{t_0}$$

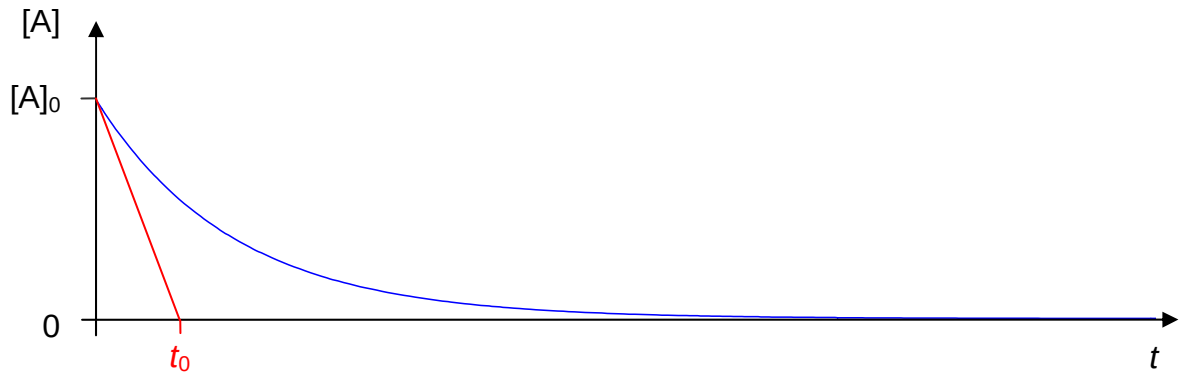

Fig. 7-6. *First-order transformation: Evolution of the reactant concentration as a function of time.*

Due to the tangent construction, the initial rate method is less precise than a logarithmic plot that takes into account all measurements. Nevertheless, it is useful to determine the rate of the first step in consecutive or reversible reaction systems.

7.6.2 Bimolecular reactions with pre-equilibrium [14]

The electron-transfer reactions from and to cytochrome *c* is supposed to proceed according to a bimolecular mechanism with a pre-equilibrium consisting in the association of both redox partners and, in several cases, a post-equilibrium for dissociation:

$$\text{A(red)} + \text{B(ox)} \overset{K_{AB}}{\rightleftharpoons} \text{A(red)B(ox)} \xrightarrow{k_{et}} \text{A(ox)B(red)} \overset{K_{dis}}{\rightleftharpoons} \text{A(ox)} + \text{B(red)}$$

The last step, if it takes place, is very rapid and product favoured; thus, it has no influence on the reaction kinetics. So, we focus on the two initial steps that can be formulated in a more general manner:

$$\text{A} + \text{B} \underset{k_{-1}}{\overset{k_1}{\rightleftharpoons}} \text{AB} \xrightarrow{k_{et}} \text{C}$$

A steady state situation of this system is defined by - $\frac{d[\text{AB}]}{dt} = 0$ or

$k_1[\text{A}][\text{B}] = k_{-1}[\text{AB}] + k_{et}[\text{AB}]$

The corresponding equilibrium constant is

$$K_{AB} = \frac{[\text{AB}]}{[\text{A}][\text{B}]} = \frac{k_1}{k_{-1} + k_{et}}$$

$$\Rightarrow [\text{AB}] = K_{AB}[\text{A}][\text{B}] \qquad (7\text{-}1)$$

In our case, the reducing agent is in a large excess with respect to the protein (global concentrations: $c_A << c_B$):

$[\text{A}] \simeq c_A - [\text{AB}]$ and $[\text{B}] \simeq c_B$

Under these conditions (7-1) becomes,

$$k_1 \cdot c_B \left(c_A - [\text{AB}]\right) = k_{-1}[\text{AB}] + k_{et}[\text{AB}]$$

$$\Rightarrow [\text{AB}] = K_{AB}c_A c_B - K_{AB}c_B[\text{AB}]$$

$$\Rightarrow [\text{AB}] = \frac{K_{AB}c_A c_B}{1 + K_{AB}c_B}$$

The rate law of the reduction is

$$v = -\frac{d[\mathrm{A}]}{dt} = +\frac{d[\mathrm{C}]}{dt} = k_{\mathrm{et}}[\mathrm{AB}] = \frac{k_{\mathrm{et}} K_{\mathrm{AB}} c_{\mathrm{A}} c_{\mathrm{B}}}{1 + K_{\mathrm{AB}} c_{\mathrm{B}}}$$

Three particular cases of this rate law are discussed in §3.2.3.

7.6.3 Calculation of inner- and outer-sphere stereoselectivities in the electron transfer from cobalt(II) complexes to cytochrome *c*

The electron transfer between the cobalt(II) complexes, $[Co^{II}(L)]$, can proceed according to an inner-sphere (IS) or an outer-sphere mechanism (OS). Both partial reactions progress with their specific rate constants k_{IS} and k_{OS} (second order constants, in this case). To simplify, it is supposed that all the cobalt(III) complexes formed after an inner-sphere electron transfer remain permanently bound to the protein :

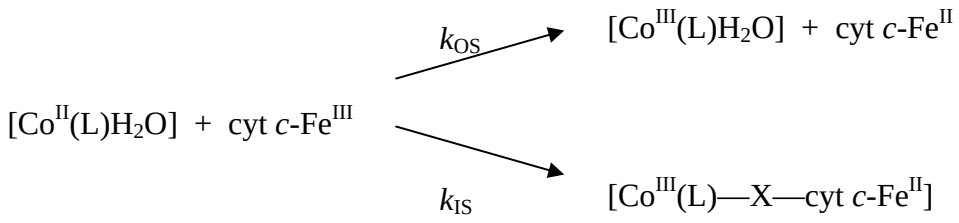

This means that the binding rate *b* (in percent) indicates directly the part of the conversion that proceeds along with an inner-sphere mechanism. On the other hand, the overall rate constant *k* is determined by the absorbance variation (see §3.3.2) and represents the sum of k_{IS} and k_{OS} :

$$k_{\mathrm{IS}} = \frac{b}{100} \cdot k$$

$$k_{\mathrm{OS}} = k - k_{\mathrm{IS}} = k \cdot \left(1 - \frac{b}{100}\right)$$

These constants are calculated separately for both enantiomers of a complex, then the inner- and outer-sphere stereoselectivities are given by

$$\frac{k_{\mathrm{IS},\,\Delta}}{k_{\mathrm{IS},\,\Lambda}} \quad \text{and} \quad \frac{k_{\mathrm{OS},\,\Delta}}{k_{\mathrm{OS},\,\Lambda}}$$

7.7 References

[1] a) A.L. Spek, 'PLATON/PLUTON', Program for Representation of Crystal Structures, Universiteit Utrecht, Utrecht, The Netherlands, 1980-2003; b) A.L.Spek, *J.Appl.Cryst.* **2003**, *36*, *7*; c) Thomas Knoll et al., 'Adobe® Photoshop®', version 6.0, Program for Image Editing, Adobe Systems Inc., San Jose, United States of America, 2001.

[2] W. Clegg, 'Crystal Structure Determination', Oxford University Press, Oxford, 1998.

[3] R. Delgado, M. do Carmo Figueira, S. Quintino, *Talanta* **1997**, *45*, 451 and references therein.

[4] K. Bernauer, P. Pousaz, J. Porret, A. Jeanguenat, *Helv. Chim. Acta* **1988**, *71*, 1339.

[5] K. Bernauer, H. Stoeckli-Evans, D. Hugi-Cleary, H.J. Hilgers, H. Abd-el-Khalek, J. Porret, J.J. Sauvain, *Helv. Chim. Acta* **1992**, *75*, 2327.

[6] A.R. Selmer-Olsen, *Anal. Chim. Acta* **1962**, *26*, 482.

[7] a) G. Schwarzenbach, H. Ackermann, *Helv. Chim. Acta* **1949**, *32*, 1682; b) G. Schwarzenbach, R. Gut, G. Anderegg, *Helv Chim. Acta* **1954**, *37*, 937.

[8] D. Berdat, Travail avancé en chimie inorganique, Université de Neuchâtel, 2000.

[9] a) G.P. Moss, *Pure Appl. Chem.* **1999**, *71*, 513 and references therein; b) J.M. Bourgeois, (Department of Industrial Technologies, University of Applied Sciences Fribourg), personal communication.

[10] Eric Martz, 'Protein Explorer 1.982', Program for the visualisation of pdb data files, University of Massachusetts at Amherst, United States of America, 2002.

[11] MDL Information Systems, Chemscape Chime 2.6 SP4, Program for the Three-Dimensional Representation of Molecules from pdb files, San Leandro CA, United States of America, 2001.

[12] a) International Union of Pure and Applied Chemistry (IUPAC), 'Grössen, Einheiten und Symbole in der Physikalischen Chemie', VCH, Weinheim, 1996; b) P.W. Atkins, 'Physical Chemistry', Oxford University Press, Oxford, 1994; c) H.A. Staab, 'Einführung in die theoretische organische Chemie', Verlag Chemie, Weinheim, 1964. d) G. Snatzke, *Chemie in unserer Zeit* **1981**, *3*, 78; 'Jasco J-710/720 CD·ORD

Measurement Manual', Japan Spectroscopic Co., Tokyo, 1990; e) F.A. Cotton, G. Wilkinson, 'Advanced Inorganic Chemistry', John Wiley Interscience, New York, 1972.

[13] C. Capellos, B.H. Bielski, 'Kinetic Systems', John Wiley, New York, 1972.

[14] a) L. Stryer, 'Biochemie', Spektrum der Wissenschaft, Heidelberg, 1990;
b) K. Bernauer, 'Cours de cinétique chimique', Université de Neuchâtel, 1993.